

THE UNIVERSITY OF ADELAIDE

DOCTORAL THESIS

GABA regulation of gas exchange in
barley (*Hordeum vulgare*)

Author:
Na SAI

Supervisors:
Prof. Matthew GILLIHAM
Dr. Bo XU
Dr. Nathan WATSON-HAIGH

*A thesis submitted in fulfillment of the requirements
for the degree of Doctor of Philosophy*

in the

ARC COE Plant Energy Biology
School of Agriculture, Food and Wine
Faculty of Science

June 10, 2022

CONTENTS

	Page
Abstract	v
Declaration of Authorship	vii
Acknowledgments	xi
List of Tables	xiii
List of Figures	xv
1 Introduction	1
1.1 Stress and crop production: the big battlefield in agriculture	3
1.2 Stomata and stress response: the signal from environment to plants . .	3
1.3 GABA regulation: from <i>Arabidopsis</i> to barley	4
References	6
2 Literature review	9
2.1 GABA shunt is a substitute for particular steps of the TCA cycle	11
2.2 GABA: from a stress metabolite to a signaling molecule	13
2.2.1 GABA is a guard cell signal regulating plant water loss	13
2.2.2 Communication between glutamate and GABA signals in plants	17
2.2.3 Cross talk between GABA and plant hormones	19
References	22
3 GABA responses of barley stomata	33
3.1 Results	35
3.1.1 Light/dark transition: the everyday signal controlling stomatal movement	35
3.1.1.1 Stomatal assay on epidermal peels	35
3.1.1.2 Leaf gas exchange	36

3.1.2	GABA-ABA interaction: when water related stress signals meet GABA	40
3.1.2.1	Stomatal response with GABA and ABA treatment	40
3.1.2.2	Water loss measurement with GABA and/or ABA supplements	41
3.2	Discussion	43
3.2.1	Low-dose of GABA suppresses stomatal movement in response to a signal	43
3.2.2	Candidate aluminum-activated malate transporters (ALMTs) participate stomatal movement and regulated by GABA	46
3.3	Material and Methods	49
3.3.1	Plant material	49
3.3.2	Stomatal assay	49
3.3.2.1	Light/Dark transition in the presence of GABA	49
3.3.2.2	ABA treatment in the presence of GABA	50
3.3.3	Leaf feeding assay	50
3.3.4	Gas exchange measurement	51
	References	52
4	Guard cell complex specific transcriptional response of barley to GABA	55
4.1	Results	57
4.1.1	Data quality and post alignment processing	57
4.1.2	Differential gene expression	58
4.1.3	Gene Ontology (GO) enrichment	60
4.1.4	KEGG pathway enrichment	61
4.2	Discussion	63
4.3	Material and Methods	70
4.3.1	Plants material and RNA-Seq data	70
4.3.2	Bioinformatics workflow	70
	References	72
5	Transcriptional profiling of GABA deficient <i>Arabidopsis thaliana</i>	79
5.1	Results	81
5.1.1	Data quality and post alignment processing	81
5.1.2	Differential gene expression analysis	81
5.1.3	Gene Ontology (GO) enrichment	85
5.1.4	KEGG pathway enrichment	94
5.2	Discussion	96

5.2.1	Stress sensitivity increased with GABA deficiency	96
5.2.2	<i>gad1</i> mutant and leaf senescence	98
5.2.3	<i>gad2-1</i> maybe pre-prepared for hypoxia	98
5.2.4	<i>gad1245</i> could have altered cold/freezing tolerance and has relationship to starch degradation	99
5.2.5	Potential candidate genes in <i>gad1245</i> that may restore a wildtype-like stomatal phenotype	100
5.2.5.1	Genes in <i>gad1245</i> restore the Col-0-like expression . . .	100
5.2.5.2	Genes with the additive effect of <i>gad</i> mutations	100
5.2.5.3	Genes in <i>gad1245</i> behave uniquely to Col-0 and <i>gad2-1</i>	102
5.3	Material and Methods	103
5.3.1	Plant material and RNA-Seq data	103
5.3.2	Bioinformatics workflow	103
	References	105
6	SAI: Fast automated quantification of stomatal parameters from microscope images	111
	Abstract	115
	Introduction	115
	Results	117
	Discussion	122
	Method	124
	Acknowledgement	128
	Author Contribution	128
	References	129
7	General discussion	133
7.1	GABA act as a signal in stomata regulation	135
7.2	Interactions of GABA and plant signals at the transcriptional level . . .	136
7.2.1	GABA and the MAPK signalling pathway	136
7.2.2	GABA and ROS production	137
7.2.3	GABA deficiency leads to disruption of the circadian clock	137
7.3	SAI is a reliable and time-saving solution for stomata measuring	138
7.4	Conclusion	139
	References	141
	Appendices	145
A	Published articles	145

A.1	The emerging role of GABA as a transport regulator and physiological signal	147
A.2	GABA signalling modulates stomatal opening to enhance plant water use efficiency and drought resilience	163
B	Supplementary data of physiological experiments	221
B.1	Response speed determination of GABA treatment	223
B.2	Pilot study of GABA leaf feeding	224
B.3	Individual experiments of GABA/ABA stomata assay	225
B.4	Individual experiments of GABA/ABA water loss assay	227
B.5	ALMT protein sequence of wheat, barley and Arabidopsis	228
B.6	Hydroponic system	230
C	Supplementary data of guard cell enriched transcriptional response of GABA in barley	231
C.1	R session information	233
C.2	Data cross-validation with published data	235
C.3	Summary of enriched DE genes of MAPK signalling pathway	236
C.4	GABA induced photorespiration and carbon fixation associated genes	238
	References	239
D	Supplementary data of transcriptional profiling of GABA deficient mutants in <i>Arabidopsis thaliana</i>	241
D.1	R session information	243
D.2	Summary of nutrient starvation directly related DE genes in <i>gad1</i> -Col-0 comparison with its other GO functions	245
D.3	Direct related gene ontology of DE genes in <i>gad1245-gad2-1</i> comparison	247
E	Supplementary data of SAI	249
E.1	Supplementary data of Average-Human/Machine Test	251
E.2	Supplementary data of human processed datasets	256
E.3	Default Training Procedure	257
E.4	Batch Size	258
E.5	Keypoint Head Complexity	259
E.6	Keypoint and Mask Head Pooler Resolution	260
E.7	Image Resolution	262
E.8	Keypoint Head Complexity at Higher Resolution	263
E.9	Final Schema	264
E.10	Pseudocode	265

ABSTRACT

Stomatal guard cells are the primary gatekeepers for gas exchange between plants and the atmosphere, and therefore, modulate the rate of photosynthesis (i.e. plant energy production) and transpiration (i.e. plant water loss). It is well known that carbon gain and water loss through stomatal regulation is critical to plant growth and development, which is impacted by the diurnal cycle and stress. During stress, rapid accumulation of GABA (γ -aminobutyric acid) can occur through the GABA shunt, which bypasses two stress-inhibited reactions of the mitochondrial based TCA cycle. This observation makes GABA well known as a stress metabolite in plants. Far beyond this, evidence in the literature is emerging that GABA may act as a signal to impact stomatal regulation was demonstrated in multiple dicot plants to enhance plant water use efficiency and drought resilience. However, the interaction of GABA in regulating the stomata of cereal monocots such as barley, which provides a large proportion of food worldwide, has been less well explored. Considering the economic importance of barley in Australia and preventing yield loss from more frequent environmental challenges due to climate change, studying GABA signalling in barley stomatal regulation would be a meaningful topic to the agriculture industry.

Here, it was found through physiological assays GABA inhibited light-induced stomatal opening of barley on both epidermal strips and reduced gas exchange in intact leaves. In contrast, GABA inhibition of dark-induced stomatal closure was only seen on epidermal peels. Like darkness-induced closure, GABA reduced the ABA sensitivity of stomatal response in epidermal strips but did not reduce water loss from leaves during steady state conditions. The inconsistent results between experimental systems suggests mesophyll cells may contribute to GABA regulation of stomatal pore movement.

Transcriptionally, gene expression profiling was explored following manipulation of GABA. With the external application of GABA and ABA on barley guard cell samples, the expression pattern of differentially expressed genes (DE genes) were distinct between GABA and ABA treatment with distinct Gene Ontology (GO) and Kyoto Encyclopedia of Genes and Genomes (KEGG) pathways highlighted for the different treatments. Alternatively, in the leaf samples from GABA deficient Arabidopsis mutants, many stress defence signals related GO terms were commonly down-regulated across mutants due to the absence of GABA. The results indicated that GABA could interact with other signals transcriptionally, and suggests that it may contribute to stress defence. Interestingly, the convergence point for the defence-signalling network – the MAPK signalling pathway was shown as enriched regardless of GABA deficiency or external application. The MAPK signalling pathway could be a point of interaction of

GABA with other signals including ABA.

Stomatal assays, such as those reported above, represent a significant bottleneck in research pipelines, adding much time as a large repetitive workload for researchers. StomataAI (SAI) was developed as a reliable and user-friendly tool that is able to measure the stomatal pore aperture of the model plant *Arabidopsis* (dicot) and the crop plant barley (monocot) via the application of deep computer vision. The reliability of predicted measurements was examined with the designed Average-Human/Machine Test. Throughout the test, SAI was capable of producing measurements in line with human experts and reproducing conclusions of published datasets in a fraction of the time taken manually. Hence, SAI boosts the number of images that biologists could evaluate at one time to obtain more accurate measurements.

Overall, this thesis illustrated that GABA is likely to act as a signal at both physiological and transcriptional level. SAI provide a reliable, efficient and high-throughput solution for stomatal pore measurement. The above biological outcomes contribute to further knowledge base on GABA regulation of stomata, particularly in the monocot barley. We highlight future areas that now can be explored including GABA dose-dependency effects and GABA-ALMT interaction.

DECLARATION OF AUTHORSHIP

I Na SAI, certify that this work contains no material which has been accepted for the award of any other degree or diploma in my name, in any university or other tertiary institution and, to the best of my knowledge and belief, contains no material previously published or written by another person, except where due reference has been made in the text. In addition, I certify that no part of this work will, in the future, be used in a submission in my name, for any other degree or diploma in any university or other tertiary institution without the prior approval of the University of Adelaide and where applicable, any partner institution responsible for the joint-award of this degree.

I acknowledge that copyright of published works contained within this thesis resides with the copyright holder(s) of those works.

I also give permission for the digital version of my thesis to be made available on the web, via the University's digital research repository, the Library Search and also through web search engines, unless permission has been granted by the University to restrict access for a period of time.

I acknowledge the support I have received for my research through the provision of an Australian Government Research Training Program Scholarship.

Signed:

Date:

“Life can be full of surprises.”

— Julia Maddon

ACKNOWLEDGMENTS

Doing PhD is never a solo journey. Mine started with the question "Charlotte, why do you want to do a PhD?" asked by my wise principle supervisor – Matthew Gilliam. I feel lucky and honoured to be his student during my master and PhD, and have Bo Xu (Weasley) during my PhD as co-supervisor. I appreciated the guidance with full of patient, knowledge and insightful advice. Not to mention the freedom and support they offered in exploring my project and SAI development. I would also like to show my appreciation to my bioinformatics supervisor Nathan Watson-Haigh, and my mentor, Stephen Pederson. It would not be possible to make me get my hands full with bioinformatic skills like today without Steve, Nathan and Bioinformatics Hub.

I would also like to sincerely thank everyone who helped me throughout this project. Particularly, I would like to thank Johannes Herrmann, Andrés Zhou Tsang, Adriane Piechatzek and Xueying Feng for their help with experiments, Jiaen Qiu for emotional care; and Rebecca Vandeleur and Wendy Sullivan for their professional support. In addition, it is my honour to take my research with GRDC/ARC COE Plant Energy Biology Scholarship at the University of Adelaide; and I appreciated the additional financial support from Matt towards the end of my PhD.

I feel grateful to have my PhD buddies: Pei Qin (Sabrina) Ng, Ying Meng and Nhi Hin for sharing coffee, laughter and tears. It is joyful to see we become a better us in these years through learning from each other, and I appreciated this friendship. A special thanks to my genius collaborator James Paul Bockman. Thank you for building SAI with me and bringing my whimsical idea into reality.

Last but not least, thanks to my parents for supporting me to study overseas and raising me as a decent young lady when the year I came to Australia. I love you, and my heart will always be with you wherever I am.

LIST OF TABLES

TABLE	Page
3.1 Summary of significant treatment response time point of ABA and GABA+ABA	42
4.1 Summary of DE gene enriched Gene Ontologies	61
4.2 Summary of ABA and GABA treatment enriched KEGG pathway	63
4.3 Potential candidate genes that regulated by both GABA and ABA	68
4.4 Summary of DE gene commonly induced by GABA and ABA in MAPK signaling pathway	69
5.1 Shared GO terms between <i>gad1</i> , <i>gad2-1</i> and <i>gad1245</i> compared to Col-0 . .	87
5.2 GO terms uniquely enriched in comparison <i>gad1245</i> -Col-0	90
5.3 Uniquely enriched GO terms found when comparing <i>gad1</i> or <i>gad2-1</i> with Col-0	92
5.4 Shared KEGG pathways between <i>gad1</i> , <i>gad2-1</i> and <i>gad1245</i> compared to Col-0	95
5.5 Uniquely enriched KEGG pathway in <i>gad1</i> , <i>gad2-1</i> and <i>gad1245</i> compared to Col-0	95
5.6 <i>gad1245-gad2-1</i> DE genes direct matched KEGG pathways	96
6.1 Summary metrics for stomatal pore dataset used in model training and evaluation	125
6.2 Summary of Average-Human/Machine Test dataset	127
6.3 Summary of the experimental design	127
B.1 Summary of slope calculation (response speed) and analysis of co-variance (ANCOVA)	223
B.2 Goodness of fit of ABA dose-response curve with GABA present	226
B.3 Composition of Hoagland's solution	230
C.1 Amount of DE genes matched with published GCSC transcriptome data . .	235
E.1 Summary of measured stomata in number and mean value of corresponding measuring feature	255

LIST OF TABLES

E.2	Model prediction scores when training with the default strategy outlined in section E.3 for various input batch sizes	258
E.3	Comparison of limiting keypoint head depth and width	259
E.4	Trails highlighting the impact of keypoint head pooler resolution on model performance	260
E.5	Experiments isolating mask head pooler resolution’s effect on task performance	261
E.6	Quantifying the impact of training crop resolution on final model predictive power	262
E.7	Comparison of keypoint head depth and width with increased pooler and input resolutions	263

LIST OF FIGURES

FIGURE	Page
2.1 The illustration of the GABA shunt and its regulation in plants	11
2.2 Proposed model of GABA-improved water use efficiency in plants	15
3.1 GABA inhibits stomatal movement during a light-to-dark and dark-to-light transition	35
3.2 Time-resolved net CO ₂ assimilation, stomatal conductance and transpiration rate during a light-to-dark transition	37
3.3 Time-resolved net CO ₂ assimilation, stomatal conductance and transpiration rate during a dark-to-light transition	38
3.4 Transpiration rate and stomatal conductance fitted with a linear regression following light-to-dark or dark-to-light transition between control and GABA fed leaves from individual experiments	39
3.5 Leaf water use efficiency (WUE _l) and intrinsic water use efficiency (iWUE) during a dark-to-light transition	40
3.6 ABA dose-response curve with GABA present	41
3.7 Water loss assay in response to 10 nM ABA with 1 mM GABA	42
3.8 Exogenous GABA antagonises stomatal movement triggered by light, darkness or ABA in <i>Arabidopsis</i>	44
3.9 Stomatal conductance and transpiration rate in <i>Arabidopsis</i> with presence and absent of GABA	45
3.10 Evolutionary relationship of ALMTs between <i>Arabidopsis</i> , wheat and barley and its GABA-binding motif	48
3.11 Demonstration of leaf sample preparation for the stomata assay	49
3.12 Demonstration of leaf preparation for the gas exchange measurement	51
4.1 Multidimensional scaling plot of distances between gene expression profiles	57
4.2 Volcano plot of ABA and GABA induced differentially expressed genes	58
4.3 Gene expression profiling of ABA and GABA induced differentially expressed genes compared to control	59

LIST OF FIGURES

4.4	DE gene enriched Gene ontologies	60
4.5	DE genes enriched KEGG pathway	62
5.1	Multidimensional scaling plot of distances between gene expression profiles	81
5.2	Volcano plot of differentially expressed genes in GABA deficient mutants compared to baseline control	82
5.3	The expression level of GADs in Col-0, <i>gad1 gad2-1</i> and <i>gad1245</i>	83
5.4	Number of shared DE genes with the <i>gad2-1</i> and <i>gad1245</i> mutations compared to their baseline control	83
5.5	The expression level of selected DE genes in Col-0, <i>gad2-1</i> and <i>gad1245</i> . .	84
5.6	Mutation induced up- and down-regulated DE gene enriched gene ontology	86
5.7	The log2 fold change of mutation induced DE gene enriched for the GO cold acclimation (GO:0009631)	88
5.8	The hierarchical relationship of GO terms associated with hypoxia and log2 fold change of DE genes enriched	89
5.9	The hierarchical relationship of GO terms associated with starch degradation in <i>gad1245</i>	91
5.10	The hierarchical relationship of GO terms associated with nutrients starvation	93
5.11	KEGG pathways enriched following DE gene analysis of <i>gad</i> mutants and Col-0	94
5.12	KEGG pathway visualisation of DE genes matched on the plant MAPK signaling pathway	97
5.13	KEGG pathway visualisation of DE genes mapped on circadian rhythm – plant	101
6.1	The stomata of <i>Arabidopsis thaliana</i> and barley (<i>Hordeum vulgare</i>	116
6.2	SAI prediction vs average <i>human-level</i> reference set in <i>Arabidopsis</i> and barley stomatal width	119
6.3	SAI predicted measurements are consistent with outcomes obtained by human researchers	120
6.4	Wall clock time measured when processing a single microscope image using SAI	121
6.5	Annotation examples of <i>Arabidopsis</i> and barley stomata	125
B.1	Water loss assay in response to 2 mM, 4 mM and 8 mM GABA	224
B.2	Individual stomatal assay of GABA/ABA interaction	225
B.3	Water loss assay in response to 25 nM and 100 nM ABA with 1 mM GABA .	227

E.1	SAI prediction vs human-level reference set for Arabidopsis and barley stomatal length, area and width/length ratio	251
E.2	Individual human measurements vs <i>human-level</i> reference set for Arabidopsis and barley with corresponding relative error of stomatal width, length, area and width/length ratio	253
E.3	Measurement comparison of stomatal width, length, area and width/length ratio in Arabidopsis and barley	254
E.4	Mean of stomatal width and measurement distribution illustration	256

INTRODUCTION

Barley (*Hordeum vulgare*), an annual monocotyledon crop from the grass (*Poaceae*) family, is one of the world's most widely grown and consumed cereals. Barley is predominantly grown in temperate climates globally and is a major source of animal feed, but it is also used for human nutrition. In some developing country, barley is the primary carbohydrate source. Another major use of barley is the production of malt, which is a key ingredient in beer and whisky production (Lee et al., 2020).

Australia produces high-quality 2-row barley from southern Queensland through to Western Australia, averaging over 10 million tonnes of annual production (FAOSTAT, 2020a). According to the Food and Agriculture Organization of United Nations, Australia is the world 4th largest barley producer in terms of tonnage in 2018, the second-highest net production value producer after France in 2016 and the world biggest barley exporter in 2017 (FAOSTAT, 2018, 2019, 2020b). Barley, therefore, is a significantly important cereal crop for both local and export markets of Australia. Besides, barley is an important model monocot species with the barley genome sequence having been recently completed and annotated (Mascher, 2019). As such, new tools are available for enhancing physiological and genetic investigation of barley, and for breeding. Furthermore, knowledge gained from barley research can be transferred to research on other crop species, such as wheat, rye, rice or oats.

1.1 Stress and crop production: the big battlefield in agriculture

According to the Intergovernmental Panel on Climate Change (IPCC) special report in 2017, the human-induced global warming has already gone 1 °C above the level during the pre-industrial period (1850–1900) (Allen et al., 2018). If the trend follows the current warming rate, human-induced global warming will reach 1.5 °C around 2040 (Allen et al., 2018). Temperature rises are predicted to result in a series of alterations to natural systems, such as more frequent droughts, floods, heatwaves or other types of extreme weather, sea-level rises and even loss of biodiversity (Allen et al., 2018; Mittler and Blumwald, 2010; Mysiak et al., 2016). These changes cause severe threats to agricultural regions with significant yield loss.

Differences in yield performance can be often explained by exposure to unfavourable environmental conditions which can trigger a series of stress responses from crops ranging from gene expression and cellular metabolism alteration to growth rate and crop productivity changes (Shao et al., 2008). Abiotic stresses such as heat, drought, cold, flooding and salinity are serious threats to agriculture and can result in yield losses for major crops by more than 50% (Wang et al., 2003). Water shortages limit rain-fed cereal production, which frequently reduces yield potential by about 30-50% (Mueller et al., 2012). Crop plants also have to protect themselves from pest and pathogens (biotic stress) including bacteria, viruses, fungi or herbivorous insects, and following abiotic stress susceptibility to biotic stresses can increase (Atkinson and Urwin, 2012). To prevent damage and ensure survival, plants employ a complicated cellular and molecular defence response system, but this results in a reduced growth or yield as a trade-off (Bechtold et al., 2010; Herms and Mattson, 1992; Smith and Stitt, 2007).

1.2 Stomata and stress response: the signal from environment to plants

Heat, drought or water-logging (anoxia) are primary limiters of Australian crop productivity and food production (Turrall et al., 2011). Anoxia reduces cereal yield by, in part, preventing the opening of stomata (the pores on leaves that control gas exchange between plants and the atmosphere), which limits carbon gain and productivity (Sojka, 1992). In pea and maize, seed abortion in response to drought and heat stress is, in part, the consequence of the carbon starvation (Guilioni et al., 2003; McLaughlin and Boyer, 2004a,b). These observations suggest that carbon supply is a critical factor linking plant

growth and productivity (Smith and Stitt, 2007). In order to have sufficient carbon intake from the environment, the plant's stomata, as the main pathway of carbon gain, has become an area of extensive research activity.

Stomatal guard cells are a specific type of cell found in aerial plant tissues that regulate the size of the stomatal pore. They play a crucial role in modulating the rate of CO₂ entry into leaves as the substrate of photosynthesis (plant energy production), and the rate at which plants move water through the plant (transpiration). CO₂ gain and water loss are regulated by mediating the degree of stomatal opening in response to environmental changes, such as atmospheric humidity, CO₂ concentration and light including daily rhythms with stomata closing at night in C3 and C4 crops (Hetherington and Woodward, 2003; Kim et al., 2010; Roelfsema and Hedrich, 2005). Likewise, abiotic stress such as heat, drought or water-logging (anoxia) also has an affect upon stomatal aperture. Some plants survive during excessive heat by keeping stomata open to cool down leaves via water evaporation, and close stomata to prevent water loss when facing drought stress (Rizhsky et al., 2004). Therefore, the gas exchange and water use efficiency are controlled by stomata.

1.3 GABA regulation: from *Arabidopsis* to barley

The stresses that are predicted to increase in frequency related to global warming are all known to increase GABA (γ -aminobutyric acid) content in plants (Kinnersley and Turano, 2000; Turrall et al., 2011). Recently, it has been discovered that both exogenously applied and endogenously manipulated GABA can change stomatal aperture. It has been proposed that GABA acts as a brake on stomatal pore movement stimulated by other signals (Xu et al., 2021a). When the year of this PhD work started, unpublished data was obtained by our lab on the impact of GABA on the stomata of *Arabidopsis thaliana*, a dicotyledonous plant, with no knowledge of GABA's impact on the cereal monocots that produce the majority of the world's staple foods.

Understanding if GABA has a role in the control of stomatal aperture in barley, and especially during the critical stresses such as drought, heat or anoxia would provide a meaningful advance. This knowledge is also highly desired to provide new insights to the industry devising breeding and management strategies for yield improvement, especially under sub-optimal conditions, which might lead to higher yields under a variable climate. Improving water use efficiency of crops grow in water limited conditions is known to improve yield for crops such as barley (Condon et al., 2002; Hatfield and Dold,

2019). Besides, 40% of calories are grown under irrigated agriculture worldwide (Turrall et al., 2011). Finding new ways to limit water loss and improve water use efficiency through influencing plant gas exchange may reduce environmental impacts and costs associated with irrigation of agricultural crops.

In this thesis, the role of GABA as a regulator of stomatal aperture control, GABA's relationship to the amino acid glutamate and its associated signalling roles, and, the potential cross talk with hormonal signals is reviewed in Chapter 2 (this is an abridged version of a published paper (Xu et al., 2021b) which is included as Publication I in Appendix A to this thesis). The question of whether GABA regulates the aperture of barley stomata is examined in Chapter 3. Some of the results in Chapter 3 on the regulation of barley stomata by GABA were included in the publication (Xu et al., 2021a,b; Appendix A). Chapter 4 is an attempt to understand the potential mechanisms of barley stomatal control via transcriptional analysis of barley guard cell enriched RNA-Seq data performed to examine GABA and abscisic acid (ABA) induced changes and the potential intersection between the two signals. RNA-Seq data of Arabidopsis GABA deficient mutants was examined in Chapter 5 to explore the transcriptional changes that occurred in response to reduced GABA content to obtain several candidate genes that possibly contribute to GABA related stomatal phenotypes. In Chapter 6, a new software tool was developed to accelerate the data retrieval for stomatal assays.

References

- M. Allen, O. Dube, W. Solecki, F. Aragón-Durand, W. Cramer, S. Humphreys, M. Kainuma, J. Kala, N. Mahowald, Y. Mulugetta, R. Perez, M. Wairiu, and K. Zickfeld. *Global Warming of 1.5°C. An IPCC Special Report on the impacts of global warming of 1.5°C above pre-industrial levels and related global greenhouse gas emission pathways, in the context of strengthening the global response to the threat of climate change, sustainable development, and efforts to eradicate poverty*, chapter Framing and Context. Intergovernmental Panel on Climate Change, 2018.
- N. J. Atkinson and P. E. Urwin. The interaction of plant biotic and abiotic stresses: from genes to the field. *Journal of Experimental Botany*, 63(10):3523–3543, 2012.
- U. Bechtold, T. Lawson, J. Mejia-Carranza, R. C. Meyer, I. R. Brown, T. Altmann, J. Ton, and P. M. Mullineaux. Constitutive salicylic acid defences do not compromise seed yield, drought tolerance and water productivity in the Arabidopsis accession C24. *Plant, Cell & Environment*, 33(11):1959–1973, 2010.
- A. G. Condon, R. A. Richards, G. J. Rebetzke, and G. D. Farquhar. Improving intrinsic water-use efficiency and crop yield. *Crop Science*, 42(1):122–131, 2002.
- FAOSTAT. Value of agricultural production, 2018. URL <http://www.fao.org/faostat/en/#data/QV>.
- FAOSTAT. Crops and livestock products, 2019. URL <http://www.fao.org/faostat/en/#data/TP>.
- FAOSTAT. Commodities by country, 2020a. URL https://www.fao.org/faostat/en/#rankings/commodities_by_country.
- FAOSTAT. Crops, 2020b. URL <http://www.fao.org/faostat/en/#data/QV>.
- L. Guilioni, J. Wéry, and J. Lecoeur. High temperature and water deficit may reduce seed number in field pea purely by decreasing plant growth rate. *Functional Plant Biology*, 30(11):1151, 2003.
- J. L. Hatfield and C. Dold. Water-use efficiency: advances and challenges in a changing climate. *Frontiers in Plant Science*, 10:103, 2019.
- D. A. Herms and W. J. Mattson. The dilemma of plants: To grow or defend. *The Quarterly Review of Biology*, 67(3):283–335, 1992.
- A. M. Hetherington and F. I. Woodward. The role of stomata in sensing and driving environmental change. *Nature*, 424(6951):901–908, 2003.

- T. H. Kim, M. Böhmer, H. Hu, N. Nishimura, and J. I. Schroeder. Guard cell signal transduction network: Advances in understanding abscisic acid, CO₂, and Ca²⁺ signaling. *Annual Review of Plant Biology*, 61(1):561–591, 2010.
- A. M. Kinnersley and F. J. Turano. Gamma aminobutyric acid (GABA) and plant responses to stress. *Critical Reviews in Plant Sciences*, 19(6):479–509, 2000.
- S. Lee, T. Lee, S. Yang, and I. Lee. BarleyNet: A network-based functional omics analysis server for cultivated barley, *Hordeum vulgare* L. *Frontiers in Plant Science*, 11:98, 2020.
- M. Mascher. Pseudomolecules and annotation of the second version of the reference genome sequence assembly of barley cv. Morex [Morex V2], 2019.
- J. E. McLaughlin and J. S. Boyer. Sugar-responsive gene expression, invertase activity, and senescence in aborting maize ovaries at low water potentials. *Annals of Botany*, 94(5):675–689, 2004a.
- J. E. McLaughlin and J. S. Boyer. Glucose localization in maize ovaries when kernel number decreases at low water potential and sucrose is fed to the stems. *Annals of Botany*, 94(1):75–86, 2004b.
- R. Mittler and E. Blumwald. Genetic engineering for modern agriculture: Challenges and perspectives. *Annual Review of Plant Biology*, 61(1):443–462, 2010.
- N. D. Mueller, J. S. Gerber, M. Johnston, D. K. Ray, N. Ramankutty, and J. A. Foley. Closing yield gaps through nutrient and water management. *Nature*, 490(7419):254–257, 2012.
- J. Mysiak, S. Surminski, A. Thieken, R. Mechler, and J. Aerts. Brief communication: Sendai framework for disaster risk reduction – success or warning sign for paris? *Natural Hazards and Earth System Sciences*, 16(10):2189–2193, 2016.
- L. Rizhsky, H. Liang, J. Shuman, V. Shulaev, S. Davletova, and R. Mittler. When defense pathways collide. the response of arabidopsis to a combination of drought and heat stress. *Plant Physiology*, 134(4):1683–1696, 2004.
- M. R. G. Roelfsema and R. Hedrich. In the light of stomatal opening: new insights into ‘the Watergate’. *New Phytologist*, 167(3):665–691, 2005.
- H. B. Shao, L. Y. Chu, C. A. Jaleel, and C.-X. Zhao. Water-deficit stress-induced anatomical changes in higher plants. *Comptes Rendus Biologies*, 331(3):215 – 225, 2008.

- A. M. Smith and M. Stitt. Coordination of carbon supply and plant growth. *Plant, Cell & Environment*, 30(9):1126–1149, 2007.
- R. E. Sojka. Stomatal closure in oxygen-stressed plants. *Soil Science*, 154(4):269–280, 1992.
- H. Turrall, J. Burke, and J.-M. Faurès. Climate change, water and food security. *FAO*, 2011.
- W. Wang, B. Vinocur, and A. Altman. Plant responses to drought, salinity and extreme temperatures: towards genetic engineering for stress tolerance. *Planta*, 218(1):1–14, 2003.
- B. Xu, Y. Long, X. Feng, X. Zhu, N. Sai, L. Chirkova, A. Betts, J. Herrmann, E. J. Edwards, M. Okamoto, R. Hedrich, and M. Gilliam. GABA signalling modulates stomatal opening to enhance plant water use efficiency and drought resilience. *Nature Communications*, 12(1):1–15, 2021a.
- B. Xu, N. Sai, and M. Gilliam. The emerging role of GABA as a transport regulator and physiological signal. *Plant Physiology*, 187(4):2005–2016, 2021b.

LITERATURE REVIEW

The non-proteinogenic amino acid γ -aminobutyric acid (GABA) has been proposed to be an agent of cellular communication that emerged very early in evolution, being conserved across modern animals and plants (Ben-Ari et al., 2007; Ramesh et al., 2016; Shelp et al., 2006; Žárský, 2015). GABA is primarily synthesized from glutamate by glutamate decarboxylase (GAD) in the cytosol, and is degraded by GABA transaminase (GABA-T) into succinic semialdehyde (SSA) in mitochondria, bypassing two stress-inhibited reactions of the mitochondrial-based tricarboxylic acid (TCA) cycle (Bouché et al., 2003; Bown and Shelp, 2016). Polyamine derived GABA synthesis can also have a significant impact on plant function under certain scenarios (Zarei et al., 2016). GABA synthesis in plants is stimulated by stress and its known or proposed roles – as a metabolite in plants – were traditionally thought to be confined to processes such as pH regulation, redox status and carbon-nitrogen balance (Batushansky et al., 2014; Bor and Turkan, 2019; Bouché and Fromm, 2004; Shelp et al., 1999). Beyond the above physiological role, GABA was proposed to play a signalling role in plants, and here we explore the ways in which it may interact with other known signals to modulate plant physiology.

2.1 GABA shunt is a substitute for particular steps of the TCA cycle

Cellular GABA metabolism (synthesis and catabolism) predominantly occurs via the GABA shunt pathway and is enacted by orthologous key enzymes in animals and plants (Bouché et al., 2003; Bown and Shelp, 2016). The three main steps of the GABA shunt are catalyzed by glutamate decarboxylase (GAD), GABA transaminase (GABA-T) and succinic semialdehyde dehydrogenase (SSADH) shown in Figure 2.1.

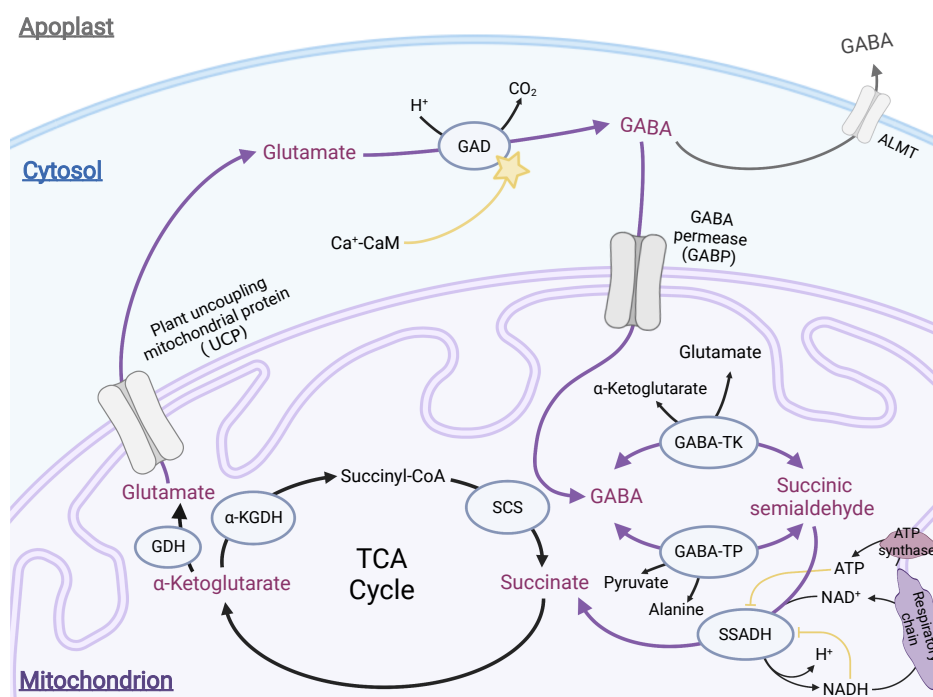


Figure 2.1. The illustration of the GABA shunt and its regulation in plants. The GABA shunt is connected with darker purple arrows and important metabolites/transporters in the GABA shunt are marked in lighter purple. Glutamate decarboxylase (GAD) is regulated (yellow) by the Ca^{2+} -calmodulin (CaM) complex indicated as a star. ATP and NADH can inhibit (yellow) the activity of SSADH. GDH, Glutamate Dehydrogenase; GAD, Glutamate Decarboxylase; GABA-T, GABA-Transaminase; SSADH, Succinic Semialdehyde Dehydrogenase; α -KGDH, α -Ketoglutarate Dehydrogenase; SCS, Succinyl-CoA Synthetase; ALMT, Aluminium-Activated Malate Transporters. This figure was generated through Biorender.

The first step of the GABA shunt is to convert glutamate that from α -ketoglutarate to GABA through the irreversible α -decarboxylation by GAD in the cytosol. GAD is a cytosolic enzyme that is specific for L-glutamate and is pyridoxal-5'-phosphate-dependent (Bown and Shelp, 1997). Initially, studies with *petunia* GAD showed the enzyme has a

calmodulin (CaM) binding domain and later on it was found that GAD activity from extracts in many plant species such as rice, soybean, Arabidopsis, and tobacco is modulated by Ca^{2+} -CaM (Aurisano et al., 1995; Baum et al., 1993; Snedden et al., 1995; Yun and Oh, 1998). Moreover, detailed molecular analysis and characterization of the CaM-binding domain in *petunia* GAD provided one possible theory to explain the rapid GABA accumulation under various stress situations, which is that the stress elicited cytosolic Ca^{2+} concentration changes stimulate GAD activity (Arazi et al., 1995; Snedden et al., 1996). The demonstration that GAD activity is stimulated in response to anoxia provides supporting evidence that this process involves Ca^{2+} -CaM. GAD has an acidic pH optimum around 5.8 and has up to 40% of its maximal activity around pH 7 (Bown and Shelp, 1997). Therefore, apart from Ca^{2+} -CaM, reduced cytosolic pH by anoxia can stimulate GAD activity. Evidence showed that stress-induced GABA synthesis due to cytosolic acidosis induced GAD activation demonstrating an increase of H^+ precedes GABA accumulation (Crawford et al., 1994; Snedden et al., 1992). Moreover, in a detailed study which investigated the role of Ca^{2+} -CaM in cold shock induced GABA accumulation, stress-induced GABA synthesis was inhibited by Ca^{2+} channel blockers or CaM antagonists, but cytosolic acidification stimulated GABA synthesis was not inhibited (Cholewa et al., 1997). Thus, both Ca^{2+} and H^+ appear sufficient for GAD activation but may occur independently and result rapid GABA accumulation under stress.

The second step is of the GABA shunt is the reversible conversion of GABA to succinic semialdehyde in mitochondria, which relies on GABA transport into the mitochondria via GABA permease (Michaeli et al., 2011). This conversion catalysed by GABA-T used either pyruvate (GABA-TP) or α -ketoglutarate (GABA-TK) as amino acceptor. GABA-T activity appears to prefer pyruvate rather than α -ketoglutarate *in vitro* (Bouché and Fromm, 2004; Shelp et al., 1995; Van Cauwenberghe and Shelp, 1999). In mammals, only GABA-TK seems to be present while both GABA-TP and GABA-TK can be detected in crude plants extracts (Bouché and Fromm, 2004; Shelp et al., 1999). Arabidopsis knockouts which are disrupted GABA-T (*pop2-1*), result in a 113-fold and 23-fold GABA content increase in flowers and leaves compared to the wild-type plants (Palanivelu et al., 2003). This result confirmed that GABA-TP is the functional enzyme in the GABA shunt *in vivo*.

The last step involved in the GABA shunt pathway is catalysed by SSADH, which irreversibly converts succinic semialdehyde (SSA) to succinate by oxidization, which then feeds into the TCA cycle. SSADH is localised in mitochondria with an alkaline pH optimum around 9 (Bouché and Fromm, 2004; Shelp et al., 1999). *In vitro* analysis

revealed SSADH is specific to succinate and uses NAD^+ to produce NADH exclusively. Succinate and NADH are the substrates of the respiratory chain in mitochondria that produces ATP as final product, and negatively regulate SSADH activity (Bouché and Fromm, 2004). Interestingly, the negative regulation of SSADH activity by ATP indicates a tight feedback control on substrates produced from GABA.

2.2 GABA: from a stress metabolite to a signaling molecule

2.2.1 GABA is a guard cell signal regulating plant water loss

Stomatal guard cells delineate the stomatal pores on plant aerial surfaces and respond to environmental signals by regulating the stomatal pore aperture to modulate plant water loss and carbon assimilation (Hetherington and Woodward, 2003; Kim et al., 2010; Murata et al., 2015; Xu et al., 2021a). It has been shown numerous times that water loss was minimised from a variety of plants when GABA was applied as a treatment (Farooq et al., 2017; Krishnan et al., 2013; Li et al., 2016; Razik et al., 2020). *GAD1* and *GAD2* are the major *GAD* isoforms in roots and leaves of *Arabidopsis thaliana* respectively, and their knockout leads to negligible GABA concentrations in tissues; further, it was proposed that depletion of GABA concentration in *gad1/gad2* leaves led to plants that were more drought prone (Mekonnen et al., 2016).

The greater stomatal conductance and drought sensitivity of *gad1/gad2* mutants was initially attributed to their more open stomatal phenotype and greater stomatal density (Mekonnen et al., 2016). The minor developmental phenotype of *gad1/gad2* is likely to be due to the smaller leaves of the line tested compared to wildtype, as other *GAD* mutants do not share this feature (Xu et al., 2021a), so it is unlikely that GABA plays a significant role in stomatal development. The greater stomatal aperture of *gad1/gad2* was proposed to be due to H^+ -ATPases mediating a greater proton (H^+) efflux across the plasma membrane leading to greater pore opening and inhibition of stomatal closure; this was inferred after it was observed that *gad1/gad2* roots had a greater acidification capacity of the surrounding media (Mekonnen et al., 2016). Interestingly, when direct microelectrode-based measurements of *gad1/gad2* roots were made, it was found that their H^+ efflux capacity was diminished compared to wildtype plants, but was increased in GABA overaccumulating mutants, and that the membrane potential was relatively depolarised in *gad1/gad2* roots when exposed to 100 mM NaCl (Su et al., 2019). It was suggested that GABA inhibited NaCl stimulated K^+ -efflux from

roots and that this was correlated to a greater ability to quench reactive oxygen species (ROS), whereas *gad1/gad2* had greater K⁺-efflux, which was proposed to occur via GORK (Guard cell outwardly rectifying K⁺ channel; Su et al. 2019). GABA has previously been implicated in activating transcription of 14-3-3 proteins, which are known activators of H⁺-ATPases and GORK (Alsterfjord et al., 2004; Lancien and Roberts, 2006; van Kleeff et al., 2018). Furthermore, GORK has been shown to be activated by ROS (Demidchik et al., 2010; Wang et al., 2016), and GABA has been implicated in ROS detoxification through an unidentified mechanism (Wu et al., 2021). In a further study, 10 mM GABA was shown to activate K⁺-efflux from roots in a GORK-dependent manner, and it was argued that GORK shared the same putative GABA sensitive motif found in ALMTs (Adem et al., 2020; Wu et al., 2021).

In Ramesh et al. (2015) it was proposed that negative regulation of anion efflux via ALMT would indirectly reduce the activity of the plasma membrane H⁺-ATPase. ALMT activity is a prime candidate for contributing to the short circuit (equal and opposite charge exchange) that maintains H⁺-ATPase activity by preventing it stalling at extremely hyperpolarised membrane potentials. This hypothesis is compatible with the above observations of altered membrane potential, and is a possible explanation for the inconsistencies observed for K⁺ and H⁺-fluxes between studies if the H⁺-ATPase and K⁺ channels are not direct targets of GABA. The hypothesis that GABA regulation of ALMT constituted a physiological signal was furthered in Xu et al. (2021a) using the stomatal guard cell as an experimental system.

Similar to *gad1/gad2* mutants, *gad2* mutants exhibited high stomatal conductance and drought sensitivity; however, *gad2* mutants do not share the developmental differences of *gad1/gad2* when compared to wildtype plants e.g. smaller rosettes or higher stomatal densities (Mekonnen et al., 2016; Xu et al., 2021a). Furthermore, the high stomatal conductance and drought sensitivity of *gad2* plants was complemented by the additional loss of *ALMT9* (Xu et al., 2021a). *ALMT9* is a tonoplast localised anion transporter that catalyses malate and chloride (Cl⁻) uptake across the vacuolar membrane of the guard cell to contribute to the osmotic increase that is required for stomatal opening (De Angeli et al., 2013; Kovermann et al., 2007). The loss of *ALMT9* impairs light-induced stomatal opening and led to *almt9* mutants being more drought tolerant (De Angeli et al., 2013); ablation of *ALMT9* also abolished the ability of GABA to inhibit stomatal opening, which was restored by native *ALMT9* complementation (Xu et al., 2021a). This signifies that GABA inhibits stomatal opening via acting on *ALMT9* (Figure 2.2). Attempted complementation of *almt9* plants with *ALMT9*^{F243C/Y245C} (containing mutations within the putative GABA interacting motif first characterised in the wheat

(*Triticum aestivum*) TaALMT1 (Long et al., 2020; Ramesh et al., 2015, 2016) failed to restore the sensitivity of stomatal opening to GABA, but instead phenocopied the higher stomatal conductance of the *gad2* mutant (Xu et al., 2021a). These data are consistent with ALMT9 being the predominant ‘GABA receptor’ in guard cells and when GABA synthesis is inhibited, ALMT9 is deregulated resulting in increased opening and pore aperture, and an increase in drought sensitivity of the plant (Figure 2.2, Xu et al. 2021a). It is noted that a range of candidates for interaction with GABA were nominated by Ramesh et al. (2016) based on the presence of a putative GABA binding site within a number of plant proteins, with none of these other candidates yet being examined *in planta*.

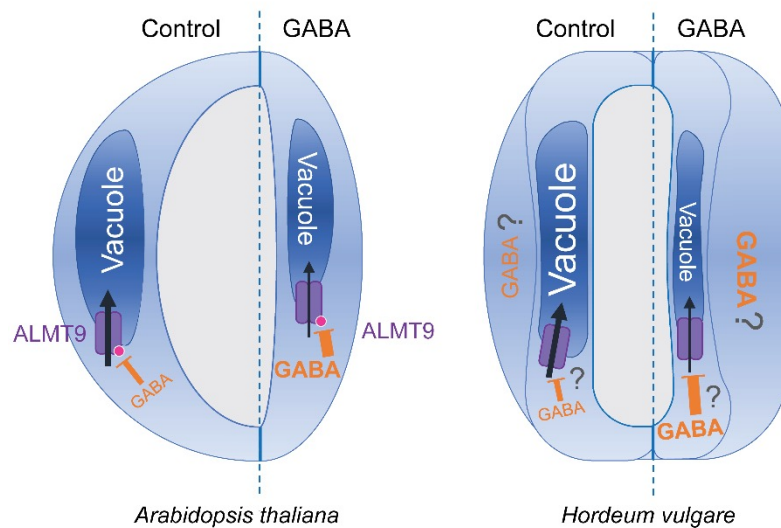


Figure 2.2. Proposed model of GABA-improved water use efficiency in plants. *Left:* A proposed model of GABA supplementation reducing stomatal opening in dicots *A. thaliana*. Increases in cellular GABA have an inhibitory effect on anion uptake through tonoplast ALMT9 into guard-cell vacuoles, reducing stomatal opening and water loss through stomatal pores. *Right:* A proposed model of GABA-enhanced water-use efficiency in monocot *H. vulgare*. GABA may be associated with negative regulation of anion uptake through unidentified anion channels, perhaps e.g. tonoplast-localised HvALMT(s) in guard cells to reduce opening extent of stomatal pores; however it is unknown whether GABA acts in subsidiary cells in this regulation, as stomatal opening of barley plants is modulated by ionic influx into guard cells and efflux from subsidiary cells Chen et al. (2017). Figure was adapted from (Xu et al., 2021b)

There were a number of other significant observations in regard to the nature of GABA as a signal stemming from Xu et al. (2021a). Firstly, overproduction of GABA in

wildtype plants improved water use efficiency and led to an improvement in drought resilience (Xu et al., 2021a). This suggests that GABA metabolism can be manipulated to improve stress tolerance in plants over and above wildtype levels. Secondly, Xu et al. (2021a) showed supplementation to epidermal peels of GABA or muscimol (a GABA analogue) suppressed stomatal movement in response to multiple opening (e.g. light and coronatine; Melotto et al., 2006; Shimazaki et al., 2007; Susmilch et al., 2019) or closing signals (e.g. dark, low-dose ABA and H₂O₂; Shimazaki et al. 2007; Susmilch et al. 2019). This differentiates it from many of the more well-defined guard-cell signals, such as abscisic acid (ABA), hydrogen peroxide (H₂O₂) and calcium (Ca²⁺) (Kim et al., 2010; Murata et al., 2015), as GABA itself does not stimulate stomatal movement when its treatment falls within the physiological range (i.e. under non-stressed and stressed conditions e.g. 1 μmol g⁻¹ fresh weight (FW) and 2 μmol g⁻¹ FW, equivalent to 1 – 2 mM respectively) (Deng et al., 2020; Ramesh et al., 2015, 2018; Xu et al., 2021a). When GABA was fed to leaves through the petiole to corroborate the findings in epidermal peels it was found that GABA only impacted stomatal opening, not closure (Xu et al., 2021a), indicating the loss of the mesophyll in epidermal peels impairs the ability to reproduce the standard physiological response of intact plants (Lawson et al., 2008, 2014; Lee and Bowling, 1992). This finding also suggests that GABA does not regulate stomatal closure, nor activate GORK under the conditions tested. The physiological conditions where GABA impacts closure *in planta* are yet to be determined. However, it was found that GABA was unable to inhibit, in epidermal peels, closure of knockout mutants of *ALMT12* (otherwise known as QUAC1 – quickly activated anion channel 1; (Xu et al., 2021a)) and so this is likely to represent a mechanism by which GABA could inhibit guard cell closure.

The high stomatal conductance, low water-use-efficiency (WUE) and drought sensitivity of the *gad2* mutant could be complemented to wildtype levels by guard cell specific expression of *GAD2Δ* (a constantly active form of *GAD2* with truncation of a Ca²⁺/Calmodulin (Ca²⁺/CaM) binding domain), but not by mesophyll-cell complementation of *GAD2Δ* (Akama and Takaiwa, 2007; Turano and Fang, 1998; Xu et al., 2021a; Zik et al., 1998). This suggests, on first examination, that the generation of GABA within the guard cell cytosol is sufficient to constitute a signal, and that mesophyll GABA accumulation does not overtly contribute to stomatal regulation. However, full-length *GAD2* complementation driven by a constitutive 35S promoter recovered the higher stomatal conductance of *gad2* to wildtype levels under normal conditions, whereas gain of *GAD2* in guard cells only complemented *gad2* under water-deficit stress (Xu et al., 2021a). This indicates the importance of post-translational control in shaping GABA signals, and that different cell types are likely to contribute to the nature of the signal

under different conditions.

GABA synthesis is stimulated by acidification of the cytosolic pH and Ca^{2+} /CaM-dependent activation of GAD (Carroll et al., 1994; Crawford et al., 1994; Turano and Fang, 1998; Zik et al., 1998). GABA breakdown is catalysed by GABA-T in mitochondria (Clark et al., 2009). Both synthesis and degradation elements (GADs and GABA-T respectively) have distinct expression patterns in plants (Clark et al., 2009; Renault et al., 2010; Scholz et al., 2015). It is possible, therefore, that GABA metabolomic levels may be differentially controlled in different cell types. Intracellular pH and Ca^{2+} signals, the key regulators of GAD-catalysed GABA synthesis (Zik et al., 1998) are known to be spatially and temporally regulated in response to the environment (Behera et al., 2018; Li et al., 2021). It can therefore be expected that cellular GABA signals are dynamically shaped in plant tissue, and this will need to be investigated with the application of technologies such as intensity-based GABA sensing fluorescence reporters (e.g. iGABASnFR) *in planta* (Fromm, 2020; Marvin et al., 2019).

GABA's impact on stomatal pore movement occurs across a range of crop plants and relatives, including *Vicia faba*, *Glycine max* and *Nicotiana benthamiana* (Xu et al., 2021a). In this thesis the effect of GABA on the stomata of the monocot grass barley will be examined. Initial results for the effect of GABA on barley stomata from epidermal strips were included in (Xu et al., 2021a) and are detailed in Chapter 3 – so further discussion of this is not included here.

2.2.2 Communication between glutamate and GABA signals in plants

GABA and glutamate are intimately linked through the synthesis of GABA via GAD. Not only is glutamate the substrate for GABA synthesis but also glutamate may stimulate Ca^{2+} entry into cells to activate GAD. Both glutamate and GABA have been implicated in playing a role in plant responses to wounding.

Plants generate long-distance electrical signalling in response to wounding, such as systemic surface potential changes and action potentials (APs; Farmer et al., 2020; Hedrich et al., 2016). Glutamate-dependent Ca^{2+} channels (i.e. GLR3.3 and 3.6) mediate wound-induced transient long-distance Ca^{2+} signal transduction and surface electrical changes via plasmodesmata that later stimulate distal jasmonate biosynthesis and systemic ROS propagation; this has been recently reviewed (Johns et al., 2021).

Wounding caused by the robotic caterpillar MecWorm on Arabidopsis (on leaf 8, the typical leaf for testing signal transduction to younger leaves) is also known to provoke systemic GABA accumulation in distal leaves (i.e. leaf 5, 11 and 13) (Farmer et al., 2013; Scholz et al., 2015, 2017). It is unclear whether such systemic GABA accumulation is linked to glutamate-dependent Ca^{2+} activation of GAD(s), but the role of tonoplast-localised Two Pore calcium Channel protein 1 (TPC1) in increasing cytosolic Ca^{2+} was ruled out (Scholz et al., 2017; Toyota et al., 2018). Cellular GABA metabolic status has been observed to affect stress (i.e. NaCl and hypoxia) triggered H^+ flux, membrane potential changes and ROS signalling, where greater GABA accumulation is associated with faster restoration from stress-depolarised membrane potential and less ROS production (Su et al., 2019; Wu et al., 2021). Therefore, the question arises of whether GABA can facilitate the recovery of local cell membrane potential and/or mitigation of ROS damage if both are primed by glutamate-activated (GLR-mediated) Ca^{2+} influx during wound responses (Fichman et al., 2021; Lew et al., 2020).

Similar to surface potential changes, wound-stimulated APs involves long-distance transmission (Felle and Zimmermann, 2007; Hedrich et al., 2016; Zimmermann et al., 2009). APs can be propagated in barley by the application of many substances, such as NaCl, KCl, CaCl_2 , glutamate and GABA (Felle and Zimmermann, 2007). Amongst these, glutamate and GABA were proposed to act on putative “receptors” to prime Ca^{2+} influx, Ca^{2+} -dependent Cl^- efflux and initiate APs together with transient apoplastic pH regulation (Felle and Zimmermann, 2007). Later, Hedrich et al. (2016) proposed that AP are excited by membrane depolarisation via anion efflux through R-type anion channels (e.g. ALMT12/QUAC1), followed by depolarisation-activated K^+ release through GORK and/or Shaker-like Outwardly-Rectifying K^+ channel (SKOR) to re-hyperpolarise membrane potential. Indeed, the Arabidopsis *GORK* knock-out mutant (*gork*) had impaired APs in magnitude and duration when generated by electrical stimulation (Cuin et al., 2018), and GABA-stimulated K^+ efflux was abolished in the root epidermis of *gork1* mutants (Adem et al., 2020).

Although it has been noted that both glutamate and GABA may facilitate long-distance electrical signal transmission through plants, such as APs (Felle and Zimmermann, 2007), it is unclear whether they interact to shape such signals. On one hand, intracellular Ca^{2+} signal modulated by glutamate-dependent GLR may shape GAD activity and GABA signals (Shao et al., 2020; Toyota et al., 2018; Xu et al., 2021a; Zik et al., 1998); on the other hand, GABA may be associated with apoplastic pH balance and cellular H^+ flux via ALMTs and/or H^+ -ATPases that work together with glutamate to regulate the activity of GLR-mediated Ca^{2+} influx, membrane potential changes and

ROS propagations (Kamran et al., 2020; Ramesh et al., 2018; Shao et al., 2020; Wu et al., 2021).

2.2.3 Cross talk between GABA and plant hormones

Emerging evidence suggests that GABA as a signalling molecule interacts with other signals to coordinate particular physiological processes. In terms of guard cell signalling, ABA closes stomata via activation of Open Stomata 1/Snf1-Related protein Kinase 2.6 (OST1/SnRK2.6)- and/or CPK(s)-dependent phosphorylation on SLAC1/SLAH3 and ALMT12 to release anions (Brandt et al., 2012, 2015; Geiger et al., 2011; Gutermuth et al., 2018; Imes et al., 2013; Mori et al., 2006). ABA also phosphorylates tonoplast-localised ALMT4 to activate anion release from guard cell vacuoles to facilitate stomatal closure (Eisenach et al., 2017). GABA can attenuate ABA-induced stomatal closure at low doses (2.5 μM), presumably acting via the inhibition of ALMT12, since the loss of *ALMT12* function in the *almt12* mutant reduced stomatal sensitivity to both signals (Imes et al., 2013; Meyer et al., 2010; Xu et al., 2021a). However, it is unknown whether GABA attenuates ABA's effect also via reducing ALMT4-mediated anion release from vacuoles in this process. This could play out in a physiological scenario when cellular GABA increases to reduce the sensitivity of the guard cell to low ABA concentrations. However, GABA has no impact on the effect of high concentrations of ABA (25 μM) on stomatal closure implicating that reduced anion efflux via ALMT12 by GABA may not reverse guard-cell membrane depolarisation and anion efflux through SLAC1/SLAH3 in such circumstances (Brandt et al., 2012, 2015; Geiger et al., 2011; Kollist et al., 2014; Xu et al., 2021a). Collectively, this suggests that GABA homeostasis may fine adjust tissue sensitivity to cellular signals when the stimulus is of low intensity, but not antagonise the plant response when these signals are of sufficient magnitude. Intriguingly, a high dose of ABA (25 μM) does not fully close stomata on epidermal peels of *gad2* mutants (Xu et al., 2021a). The open stomata phenotype here was proposed to be due to de-regulation of ALMT9 in *gad2* mutants as discussed in section above; as such ALMT9 appears not to be a target of ABA. This suggests that some GABA-mediated processes may be not overwritten by amplifying other signals, and therefore provides an opportunity to engineer GABA responses in plants for altered outcomes to environmental stress.

Wound or herbivory attack on leaves stimulates systemic jasmonate (JA) and GABA biosynthesis in plants, as discussed above. JA accumulation promotes biosynthesis of secondary metabolites (e.g. glucosinolates) and proteinase inhibitors to repel herbivory attack, such as the Arabidopsis herbivore *Arion lusitanicus* and rice root-feeding insects *Diabrotica balteata* and *Lissorhoptrus oryzophilus* (Falk et al., 2014;

Lu et al., 2015; Wang et al., 2019). GABA production reduces insect growth and survival (e.g. *Spodoptera littoralis* larvae), probably due to its effects on invertebrate (insect) ionotropic GABA receptors at neuromuscular junctions (Bown et al., 2006; Scholz et al., 2015, 2017; Tarkowski et al., 2020). GABA depletion (in *gad1/gad2*) or overaccumulation (in *pop2-5*) does not alter JA biosynthesis stimulated by *S. littoralis* and MecWorm feeding (Scholz et al., 2015, 2017), this implicates that endogenous GABA metabolism does not regulate of JA synthesis. But mutation in *JAsmonate Resistant 1 (JAR1)*, in *jar1*, did cause greater GABA accumulation when attacked by *S. littoralis* (Scholz et al., 2015), and *JAR1* encodes a jasmonate-amido synthetase that catalyses the formation of JA-Ile that structurally is an amino acid (Ile) conjugated JA and directly facilitates the JA-signalling core target interaction (i.e. SCF^{COI1}-JAZ1; (Katsir et al., 2008; Staswick et al., 2002)). The loss of *COI1* –the key JA-Ile receptor (in *coi1*) and lowering JA-Ile stimulation (in *cml37*) both resulted in greater susceptibility to *S. littoralis* (Scholz et al., 2014). Taken together, JA signalling may affect the levels of wound-stimulated GABA production in plants or render the plant more susceptible to insect attack, damage and consequently stimulate more production of GABA.

Exogenous application of 10 mM GABA stimulates ethylene biosynthesis in sunflower (*Helianthus annuus L.*) and the Caryophyllaceae *Stellaria longipes* via up-regulation of ethylene signalling genes – *1-aminocyclopropane-1-carboxylic acid (ACC) synthase (ACS)* and *ACC oxidase (ACO)* (Booker and DeLong, 2015; Kathiresan et al., 1997, 1998). Salt stress increased ethylene biosynthesis at 24 h and GABA production at 48 h in *Caragana intermedia* roots (Shi et al., 2010). Interestingly, 10 mM GABA supplement suppressed this early 24-h ethylene accumulation, whilst promoting ethylene production and further enhancing endogenous GABA accumulation 48 h post treatment (Shi et al., 2010). Similarly, GABA treatment has also been found to affect ethylene production in poplar (*Populus tomentosa* Carr) with a low dose of GABA (0.25 mM) enhancing ethylene synthesis, again through up regulation of ACS and ACOs (Ji et al., 2018). Together, this suggests that the GABA metabolism appears to affect ethylene synthesis response to salt stress in plants, and different plant species may vary in sensitivity to endogenous GABA in order to stimulate ethylene synthesis.

In plants, ethylene is a key hormone that controls (climacteric) fruit ripening and malate impacts fruit flavour (Alexander and Grierson, 2002; Hu et al., 2019; Liu et al., 2015; Wege, 2020). The down-regulation of ethylene biosynthesis via silencing ACS and ACO genes is associated with low ethylene production in apple (*Malus domestica*) fruits (Dandekar et al., 2004; Defilippi et al., 2004). The malate content in apple fruit is expected to be significantly reduced at 2 weeks post-harvest; however, it remains

unchanged in low-ethylene transgenic apple fruits that can be reversed by exogenous ethylene application (Dandekar et al., 2004; Defilippi et al., 2004). Exogenous GABA treatment (10 mM) increases GABA and malate contents, but lowers ethylene synthesis in apple fruit during storage up to 70 days (Han et al., 2018). Malate storage in apple and tomato (*Solanum lycopersicum*) fruit is respectively linked with *MdALMT9/MdMa1* and *SlALMT9* (Li et al., 2019; Ye et al., 2017). *MdALMT9/MdMa1*, an ortholog of *ALMT9* from Arabidopsis, encodes a tonoplast-localised channel catalysing malate uptake into the vacuoles and facilitating malate accumulation in apple fruit (Li et al., 2019)). Moreover, *MdALMT9/MdMa1* contains identical amino-acid residues (FIYPIWAGEDLH) of the GABA regulation motif within Arabidopsis *ALMT9*, in which the mutation of two aromatic residues (F243 and Y245) abolished its GABA sensitivity *in planta* (Li et al., 2019; Ramesh et al., 2016; Xu et al., 2021a), implicating that *MdALMT9* might have GABA sensitivity as well. Intriguingly, both ethylene and GABA have been demonstrated to negatively regulate malate efflux through *TaALMT1* at wheat root apices (Ramesh et al., 2015; Tian et al., 2014). Accordingly, the equilibrium between ethylene and GABA signalling may regulate fruit taste via the modulation of tonoplast-localised *ALMT*-mediated malate storage within fruit during ripening and postharvest storage. This provides a mechanistic link between GABA and ethylene that goes beyond the proposed correlation of GABA and ethylene production with malate metabolism (Defilippi et al., 2004; Han et al., 2018).

In summary, GABA can fulfil a signalling role in plants that ultimately may regulate key growth, development and stress tolerance processes. As GABA synthesis increases during stress, to sustain energy production via the TCA cycle (Bown and Shelp, 2016; Gilliham and Tyerman, 2016), GABA has the potential to modulate other signals; cross talk of GABA therefore has the potential to fine tune plant physiology rather than initiating a physiological response *per se*. This appears to the case with the interaction with known signals such as ethylene and ABA, and in the regulation of guard cell movement. Of the knowledge reviewed, several questions are remaining unanswered:

1. Considering the morphological differences in stomata between dicots and monocots, does GABA regulate stomatal pore movement along with gas exchange in barley?
2. GABA likely interacts with other hormones, what is the possible mechanism of this interaction?
3. What physiological roles does GABA fulfil to have an impact on stomatal regulation?

References

- G. D. Adem, G. Chen, L. Shabala, Z. H. Chen, and S. Shabala. GORK channel: A master switch of plant metabolism? *Trends in Plant Science*, 25(5):434–445, 2020.
- K. Akama and F. Takaiwa. C-terminal extension of rice glutamate decarboxylase (OsGAD2) functions as an autoinhibitory domain and overexpression of a truncated mutant results in the accumulation of extremely high levels of GABA in plant cells. *Journal of Experimental Botany*, 58:2699–2707, 2007.
- L. Alexander and D. Grierson. Ethylene biosynthesis and action in tomato: a model for climacteric fruit ripening. *Journal of Experimental Botany*, 53(377):2039–2055, 2002.
- M. Alsterfjord, P. C. Sehnke, A. Arkell, H. Larsson, F. Svennelid, M. Rosenquist, R. J. Ferl, M. Sommarin, and C. Larsson. Plasma membrane H⁺-atpase and 14-3-3 isoforms of arabidopsis leaves: Evidence for isoform specificity in the 14-3-3/H⁺-ATPase interaction. *Plant and Cell Physiology*, 45(9):1202–1210, 2004.
- T. Arazi, G. Baum, W. A. Snedden, B. J. Shelp, and H. Fromm. Molecular and biochemical analysis of calmodulin interactions with the calmodulin-binding domain of plant glutamate decarboxylase. *Plant Physiology*, 108(2):551–561, 1995.
- N. Aurisano, A. Bertani, and R. Reggiani. Involvement of calcium and calmodulin in protein and amino acid metabolism in rice roots under anoxia. *Plant and cell physiology*, 36(8):1525–1529, 1995.
- A. Batushansky, M. Kirma, N. Grillich, D. Toubiana, P. A. Pham, I. Balbo, H. Fromm, G. Galili, A. R. Fernie, and A. Fait. Combined transcriptomics and metabolomics of *Arabidopsis thaliana* seedlings exposed to exogenous GABA suggest its role in plants is predominantly metabolic. *Molecular Plant*, 7(6):1065–1068, 2014.
- G. Baum, Y. Chen, T. Arazi, H. Takatsuji, and H. Fromm. A plant glutamate decarboxylase containing a calmodulin binding domain. cloning, sequence, and functional analysis. *The Journal of Biological Chemistry*, 268(26):19610–19617, 1993.
- S. Behera, Z. Xu, L. Luoni, M. C. Bonza, F. G. Doccula, M. I. D. Michelis, R. J. Morris, M. Schwarzländer, and A. Costa. Cellular Ca²⁺ signals generate defined pH signatures in plants. *The Plant Cell*, 30(11):2704–2719, 2018.
- Y. Ben-Ari, J.-L. Gaiarsa, R. Tyzio, and R. Khazipov. GABA: A pioneer transmitter that excites immature neurons and generates primitive oscillations. *Physiological Reviews*, 87(4):1215–1284, 2007.

- M. A. Booker and A. DeLong. Producing the ethylene signal: Regulation and diversification of ethylene biosynthetic enzymes. *Plant Physiology*, 169(1):42–50, 2015.
- M. Bor and I. Turkan. Is there a room for GABA in ROS and RNS signalling? *Environmental and Experimental Botany*, 161:67–73, 2019.
- N. Bouché and H. Fromm. GABA in plants: just a metabolite? *Trends in Plant Science*, 9(3):110–115, 2004.
- N. Bouché, B. Lacombe, and H. Fromm. GABA signaling: a conserved and ubiquitous mechanism. *Trends in Cell Biology*, 13(12):607–610, 2003.
- A. Bown and B. Shelp. The metabolism and functions of γ -aminobutyric acid. *Plant Physiology*, 115(1):1–5, 1997.
- A. W. Bown and B. J. Shelp. Plant GABA: Not just a metabolite. *Trends in Plant Science*, 21(10):811–813, 2016.
- A. W. Bown, K. B. MacGregor, and B. J. Shelp. Gamma-aminobutyrate: defense against invertebrate pests? *Trends in Plant Science*, 11(9):424–427, 2006.
- B. Brandt, D. Brodsky, S. Xue, J. Negi, K. Iba, J. Kangasjärvi, M. Ghassemian, A. Stephan, H. Hu, and J. Schroeder. Reconstitution of abscisic acid activation of SLAC1 anion channel by CPK6 and OST1 kinases and branched ABI1 PP2C phosphatase action. *Proceedings of the National Academy of Sciences*, 109(26):10593–10598, 2012.
- B. Brandt, S. Munemasa, C. Wang, D. Nguyen, T. Yong, P. G. Yang, E. Poretsky, T. F. Belknap, R. Waadt, F. Alemán, and J. I. Schroeder. Calcium specificity signaling mechanisms in abscisic acid signal transduction in arabidopsis guard cells. *eLife*, 4:e03599, 2015.
- A. D. Carroll, G. G. Fox, S. Laurie, R. Phillips, R. G. Ratcliffe, and G. R. Stewart. Ammonium assimilation and the role of γ -aminobutyric acid in pH homeostasis in carrot cell suspensions. *Plant Physiology*, 106(2):513–520, 1994.
- Z. H. Chen, G. Chen, F. Dai, Y. Wang, A. Hills, Y. L. Ruan, G. Zhang, P. J. Franks, E. Nevo, and M. R. Blatt. Molecular evolution of grass stomata. *Trends in Plant Science*, 22(2):124–139, 2017.
- E. Cholewa, A. W. Bown, A. J. Cholewinski, B. J. Shelp, and W. A. Snedden. Cold-shock-stimulated γ -aminobutyric acid synthesis is mediated by an increase in cytosolic Ca^{2+} , not by an increase in cytosolic H^{+} . *Canadian Journal of Botany*, 75(3):375–382, 1997.

- S. M. Clark, R. Di Leo, P. K. Dhanoa, O. R. Van Cauwenberghe, R. T. Mullen, and B. J. Shelp. Biochemical characterization, mitochondrial localization, expression, and potential functions for an *Arabidopsis* γ -aminobutyrate transaminase that utilizes both pyruvate and glyoxylate. *Journal of Experimental Botany*, 60(6):1743–1757, 2009.
- L. A. Crawford, A. W. Bown, K. E. Breitzkreuz, and F. C. Guinel. The synthesis of γ -aminobutyric acid in response to treatments reducing cytosolic pH. *Plant Physiology*, 104(3):865–871, 1994.
- T. Cuin, I. Dreyer, and E. Michard. The role of potassium channels in *Arabidopsis thaliana* long distance electrical signalling: AKT2 modulates tissue excitability while GORK shapes action potentials. *International Journal of Molecular Sciences*, 19(4): 926, 2018.
- A. M. Dandekar, G. Teo, B. G. Defilippi, S. L. Uratsu, A. J. Passey, A. A. Kader, J. R. Stow, R. J. Colgan, and D. J. James. Effect of down-regulation of ethylene biosynthesis on fruit flavor complex in apple fruit. *Transgenic Research*, 13(4):373–384, 2004.
- A. De Angeli, J. Zhang, S. Meyer, and E. Martinoia. AtALMT9 is a malate-activated vacuolar chloride channel required for stomatal opening in *Arabidopsis*. *Nature Communications*, 4(1):1–10, 2013.
- B. G. Defilippi, A. M. Dandekar, and A. A. Kader. Impact of suppression of ethylene action or biosynthesis on flavor metabolites in apple (*Malus domestica* borkh) fruits. *Journal of agricultural and food chemistry*, 52(18):5694–5701, 2004.
- V. Demidchik, T. A. Cuin, D. Svistunenko, S. J. Smith, A. J. Miller, S. Shabala, A. Sokolik, and V. Yurin. *Arabidopsis* root K^+ -efflux conductance activated by hydroxyl radicals: single-channel properties, genetic basis and involvement in stress-induced cell death. *Journal of Cell Science*, 123(9):1468–1479, 2010.
- X. Deng, X. Xu, Y. Liu, Y. Zhang, L. Yang, S. Zhang, and J. Xu. Induction of γ -aminobutyric acid plays a positive role to *Arabidopsis* resistance against *Pseudomonas syringae*. *Journal of Integrative Plant Biology*, 62(11):1797–1812, 2020.
- C. Eisenach, U. Baetz, N. V. Huck, J. Zhang, A. De Angeli, G. J. Beckers, and E. Martinoia. ABA-induced stomatal closure involves ALMT4, a phosphorylation-dependent vacuolar anion channel of *Arabidopsis*. *The Plant Cell*, 29(10):2552–2569, 2017.
- K. L. Falk, J. Kästner, N. Bodenhausen, K. Schramm, C. Paetz, D. G. Vassão, M. Reichelt, D. von Knorre, J. Bergelson, M. Erb, J. Gershenzon, and S. Meldau. The role of

- glucosinolates and the jasmonic acid pathway in resistance of *Arabidopsis thaliana* against molluscan herbivores. *Molecular Ecology*, 23(5):1188–1203, 2014.
- E. Farmer, E. Farmer, S. Mousavi, and A. Lenglet. Leaf numbering for experiments on long distance signalling in *Arabidopsis*. *Protocol Exchange*, 2013.
- E. E. Farmer, Y. Q. Gao, G. Lenzoni, J. L. Wolfender, and Q. Wu. Wound- and mechanostimulated electrical signals control hormone responses. *New Phytologist*, 227(4):1037–1050, 2020.
- M. Farooq, A. Nawaz, M. A. M. Chaudhry, R. Indrasti, and A. Rehman. Improving resistance against terminal drought in bread wheat by exogenous application of proline and gamma-aminobutyric acid. *Journal of Agronomy and Crop Science*, 203(6):464–472, 2017.
- H. H. Felle and M. R. Zimmermann. Systemic signalling in barley through action potentials. *Planta*, 226(1):203–214, 2007.
- Y. Fichman, R. J. Myers Jr, D. G. Grant, and R. Mittler. Plasmodesmata-localized proteins and ROS orchestrate light-induced rapid systemic signaling in *Arabidopsis*. *Science Signaling*, 14(671):eabf0322, 2021.
- H. Fromm. GABA signaling in plants: targeting the missing pieces of the puzzle. *Journal of Experimental Botany*, 71(20):6238–6245, 2020.
- D. Geiger, T. Maierhofer, K. A. S. AL-Rasheid, S. Scherzer, P. Mumm, A. Liese, P. Ache, C. Wellmann, I. Marten, E. Grill, T. Romeis, and R. Hedrich. Stomatal closure by fast abscisic acid signaling is mediated by the guard cell anion channel SLAH3 and the receptor RCAR1. *Science Signaling*, 4(173):ra32, 2011.
- M. Gilliam and S. D. Tyerman. Linking metabolism to membrane signaling: the GABA–Malate connection. *Trends in Plant Science*, 21(4):295–301, 2016.
- T. Gutermuth, S. Herbell, R. Lassig, M. Brosché, T. Romeis, J. A. Feijó, R. Hedrich, and K. R. Konrad. Tip-localized Ca^{2+} -permeable channels control pollen tube growth via kinase-dependent R- and S-type anion channel regulation. *New Phytologist*, 218(3):1089–1105, 2018.
- S. Han, Y. Nan, W. Qu, Y. He, Q. Ban, Y. Lv, and J. Rao. Exogenous γ -aminobutyric acid treatment that contributes to regulation of malate metabolism and ethylene synthesis in apple fruit during storage. *Journal of agricultural and food chemistry*, 66(51):13473–13482, 2018.

- R. Hedrich, V. Salvador-Recatalà, and I. Dreyer. Electrical wiring and long-distance plant communication. *Trends in Plant Science*, 21(5):376–387, 2016.
- A. M. Hetherington and F. I. Woodward. The role of stomata in sensing and driving environmental change. *Nature*, 424(6951):901–908, 2003.
- B. Hu, D.-W. Sun, H. Pu, and Q. Wei. Recent advances in detecting and regulating ethylene concentrations for shelf-life extension and maturity control of fruit: A review. *Trends in Food Science & Technology*, 91:66–82, 2019.
- D. Imes, P. Mumm, J. Böhm, K. A. S. Al-Rasheid, I. Marten, D. Geiger, and R. Hedrich. Open stomata 1 (OST1) kinase controls R-type anion channel QUAC1 in Arabidopsis guard cells. *The Plant Journal*, 74(3):372–382, 2013.
- J. Ji, J. Yue, T. Xie, W. Chen, C. Du, E. Chang, L. Chen, Z. Jiang, and S. Shi. Roles of γ -aminobutyric acid on salinity-responsive genes at transcriptomic level in poplar: involving in abscisic acid and ethylene-signalling pathways. *Planta*, 248(3):675–690, 2018.
- S. Johns, T. Hagihara, M. Toyota, and S. Gilroy. The fast and the furious: rapid long-range signaling in plants. *Plant Physiology*, 185(3):694–706, 2021.
- M. Kamran, S. A. Ramesh, M. Gilliam, S. D. Tyerman, and J. Bose. Role of TaALMT1 malate-GABA transporter in alkaline pH tolerance of wheat. *Plant, Cell & Environment*, 43(10):2443–2459, 2020.
- A. Kathiresan, P. Tung, C. C. Chinnappa, and D. M. Reid. γ -aminobutyric acid stimulates ethylene biosynthesis in sunflower. *Plant Physiology*, 115(1):129–135, 1997.
- A. Kathiresan, J. Miranda, C. Chinnappa, and D. Reid. γ -aminobutyric acid promotes stem elongation in *Stellaria longipes*: The role of ethylene. *Plant Growth Regulation*, 26(2):131–137, 1998.
- L. Katsir, H. S. Chung, A. J. Koo, and G. A. Howe. Jasmonate signaling: a conserved mechanism of hormone sensing. *Current Opinion in Plant Biology*, 11(4):428–435, 2008.
- T. H. Kim, M. Böhmer, H. Hu, N. Nishimura, and J. I. Schroeder. Guard cell signal transduction network: Advances in understanding abscisic acid, CO₂, and Ca²⁺ signaling. *Annual Review of Plant Biology*, 61(1):561–591, 2010.
- H. Kollist, M. Nuhkat, and M. R. G. Roelfsema. Closing gaps: linking elements that control stomatal movement. *New Phytologist*, 203(1):44–62, 2014.

- P. Kovermann, S. Meyer, S. Hörtensteiner, C. Picco, J. Scholz-Starke, S. Ravera, Y. Lee, and E. Martinoia. The *Arabidopsis* vacuolar malate channel is a member of the ALMT family. *The Plant Journal*, 52(6):1169–1180, 2007.
- S. Krishnan, K. Laskowski, V. Shukla, and E. B. Merewitz. Mitigation of drought stress damage by exogenous application of a non-protein amino acid γ -aminobutyric acid on perennial ryegrass. *Journal of the American Society for Horticultural Science*, 138(5):358–366, 2013.
- M. Lancien and M. R. Roberts. Regulation of *Arabidopsis thaliana* 14-3-3 gene expression by γ -aminobutyric acid. *Plant, Cell & Environment*, 29(7):1430–1436, 2006.
- T. Lawson, S. Lefebvre, N. R. Baker, J. I. L. Morison, and C. A. Raines. Reductions in mesophyll and guard cell photosynthesis impact on the control of stomatal responses to light and CO₂. *Journal of Experimental Botany*, 59(13):3609–3619, 2008.
- T. Lawson, A. J. Simkin, G. Kelly, and D. Granot. Mesophyll photosynthesis and guard cell metabolism impacts on stomatal behaviour. *New Phytologist*, 203(4):1064–1081, 2014.
- J. Lee and D. J. F. Bowling. Effect of the mesophyll on stomatal opening in *commelina communis*. *Journal of Experimental Botany*, 43(7):951–957, 1992.
- T. T. S. Lew, V. B. Koman, K. S. Silmore, J. S. Seo, P. Gordiichuk, S. Y. Kwak, M. Park, M. C. Y. Ang, D. T. Khong, M. A. Lee, M. B. Chan-Park, N. H. Chua, and M. S. Strano. Real-time detection of wound-induced H₂O₂ signalling waves in plants with optical nanosensors. *Nature Plants*, 6(4):404–415, 2020.
- C. Li, L. Dougherty, A. E. Coluccio, D. Meng, I. El-Sharkawy, E. Borejsza-Wysocka, D. Liang, M. A. Piñeros, K. Xu, and L. Cheng. Apple ALMT9 requires a conserved C-terminal domain for malate transport underlying fruit acidity. *Plant Physiology*, 182(2):992–1006, 2019.
- K. Li, J. Prada, D. S. C. Damineli, A. Liese, T. Romeis, T. Dandekar, J. A. Feijó, R. Hedrich, and K. R. Konrad. An optimized genetically encoded dual reporter for simultaneous ratio imaging of Ca²⁺ and H⁺ reveals new insights into ion signaling in plants. *New Phytologist*, 230(6):2292–2310, 2021.
- Z. Li, Y. Peng, and B. Huang. Physiological effects of γ -aminobutyric acid application on improving heat and drought tolerance in creeping bentgrass. *Journal of the American Society for Horticultural Science*, 141(1):76–84, 2016.

- M. Liu, J. Pirrello, C. Chervin, J. P. Roustan, and M. Bouzayen. Ethylene control of fruit ripening: revisiting the complex network of transcriptional regulation. *Plant Physiology*, 169(4):2380–2390, 2015.
- Y. Long, S. D. Tyerman, and M. Gilliam. Cytosolic GABA inhibits anion transport by wheat ALMT1. *New Phytologist*, 225(2):671–678, 2020.
- J. Lu, C. A. M. Robert, M. Riemann, M. Cosme, L. Mène-Saffrané, J. Massana, M. J. Stout, Y. Lou, J. Gershenzon, and M. Erb. Induced jasmonate signaling leads to contrasting effects on root damage and herbivore performance. *Plant Physiology*, 167(3):1100–1116, 2015.
- J. S. Marvin, Y. Shimoda, V. Magloire, M. Leite, T. Kawashima, T. P. Jensen, I. Kolb, E. L. Knott, O. Novak, K. Podgorski, N. J. Leidenheimer, D. A. Rusakov, M. B. Ahrens, D. M. Kullmann, and L. L. Looger. A genetically encoded fluorescent sensor for in vivo imaging of GABA. *Nature Methods*, 16(8):763–770, 2019.
- D. W. Mekonnen, U. I. Flügge, and F. Ludewig. Gamma-aminobutyric acid depletion affects stomata closure and drought tolerance of *Arabidopsis thaliana*. *Plant Science*, 245:25–34, 2016.
- M. Melotto, W. Underwood, J. Koczan, K. Nomura, and S. Y. He. Plant stomata function in innate immunity against bacterial invasion. *Cell*, 126(5):969–980, 2006.
- S. Meyer, P. Mumm, D. Imes, A. Endler, B. Weder, K. A. Al-Rasheid, D. Geiger, I. Marten, E. Martinoia, and R. Hedrich. AtALMT12 represents an R-type anion channel required for stomatal movement in *Arabidopsis* guard cells. *The Plant Journal*, 63(6):1054–1062, 2010.
- S. Michaeli, A. Fait, K. Lagor, A. Nunes-Nesi, N. Grillich, A. Yellin, D. Bar, M. Khan, A. R. Fernie, F. J. Turano, and H. Fromm. A mitochondrial GABA permease connects the GABA shunt and the TCA cycle, and is essential for normal carbon metabolism. *The Plant Journal: for Cell and Molecular Biology*, 67(3):485–498, 2011.
- I. C. Mori, Y. Murata, Y. Yang, S. Munemasa, Y.-F. Wang, S. Andreoli, H. Tiriatic, J. M. Alonso, J. F. Harper, J. R. Ecker, J. M. Kwak, and J. I. Schroeder. CDPKs CPK6 and CPK3 function in ABA regulation of guard cell S-Type anion- and Ca^{2+} - permeable channels and stomatal closure. *PLoS Biology*, 4(10):e327, 2006.
- Y. Murata, I. C. Mori, and S. Munemasa. Diverse stomatal signaling and the signal integration mechanism. *Annual Review of Plant Biology*, 66(1):369–392, 2015.

- R. Palanivelu, L. Brass, A. F. Edlund, and D. Preuss. Pollen tube growth and guidance is regulated by POP2, an Arabidopsis gene that controls GABA levels. *Cell*, 114(1): 47–59, 2003.
- S. A. Ramesh, S. D. Tyerman, B. Xu, J. Bose, S. Kaur, V. Conn, P. Domingos, S. Ullah, S. Wege, S. Shabala, J. A. Feijó, P. R. Ryan, and M. Gilliam. GABA signalling modulates plant growth by directly regulating the activity of plant-specific anion transporters. *Nature Communications*, 6(1):1–10, 2015.
- S. A. Ramesh, S. D. Tyerman, M. Gilliam, and B. Xu. γ -aminobutyric acid (GABA) signalling in plants. *Cellular and Molecular Life Sciences*, 74(9):1577–1603, 2016.
- S. A. Ramesh, M. Kamran, W. Sullivan, L. Chirkova, M. Okamoto, F. Degryse, M. McLaughlin, M. Gilliam, and S. D. Tyerman. Aluminum-activated malate transporters can facilitate GABA transport. *The Plant Cell*, 30(5):1147–1164, 2018.
- E. S. A. Razik, B. M. Alharbi, T. B. Pirzadah, G. S. H. Alnusairi, M. H. Soliman, and K. R. Hakeem. γ -Aminobutyric acid (GABA) mitigates drought and heat stress in sunflower (*Helianthus annuus* L.) by regulating its physiological, biochemical and molecular pathways. *Physiologia Plantarum*, 172(2):505–527, 2020.
- H. Renault, V. Roussel, A. E. Amrani, M. Arzel, D. Renault, A. Bouchereau, and C. Deleu. The arabidopsis *pop2-1* mutant reveals the involvement of GABA transaminase in salt stress tolerance. *BMC Plant Biology*, 10(1):1–16, 2010.
- S. S. Scholz, J. Vadassery, M. Heyer, M. Reichelt, K. W. Bender, W. A. Snedden, W. Boland, and A. Mithöfer. Mutation of the Arabidopsis calmodulin-like protein CML37 deregulates the jasmonate pathway and enhances susceptibility to herbivory. *Molecular Plant*, 7(12):1712–1726, 2014.
- S. S. Scholz, M. Reichelt, D. W. Mekonnen, F. Ludewig, and A. Mithöfer. Insect herbivory-elicited GABA accumulation in plants is a wound-induced, direct, systemic, and jasmonate-independent defense response. *Frontiers in Plant Science*, 6:1128, 2015.
- S. S. Scholz, J. Malabarba, M. Reichelt, M. Heyer, F. Ludewig, and A. Mithöfer. Evidence for GABA-induced systemic GABA accumulation in Arabidopsis upon wounding. *Frontiers in Plant Science*, 8:388, 2017.
- Q. Shao, Q. Gao, D. Lhamo, H. Zhang, and S. Luan. Two glutamate- and pH-regulated Ca^{2+} channels are required for systemic wound signaling in Arabidopsis. *Science Signaling*, 13(640):eaba1453, 2020.

- B. Shelp, A. Bown, and M. McLean. Metabolism and functions of gamma-aminobutyric acid. *Trends in Plant Science*, 4(11):446–452, 1999.
- B. J. Shelp, C. S. Walton, W. A. Snedden, L. G. Tuin, I. J. Oresnik, and D. B. Layzell. GABA shunt in developing soybean seeds is associated with hypoxia. *Physiologia Plantarum*, 94(2):219–228, 1995.
- B. J. Shelp, A. W. Bown, and D. Faure. Extracellular γ -aminobutyrate mediates communication between plants and other organisms. *Plant Physiology*, 142(4):1350–1352, 2006.
- S. Q. Shi, Z. Shi, Z. P. Jiang, L. W. Qi, X. M. Sun, C. X. Li, J. F. Liu, W. F. Xiao, and S. G. Zhang. Effects of exogenous GABA on gene expression of *Caragana intermedia* roots under NaCl stress: regulatory roles for H₂O₂ and ethylene production. *Plant, Cell & Environment*, 33(2):149–162, 2010.
- K. Shimazaki, M. Doi, S. M. Assmann, and T. Kinoshita. Light regulation of stomatal movement. *Annual Review of Plant Biology*, 58(1):219–247, 2007.
- W. A. Snedden, I. Chung, R. H. Pauls, and A. W. Bown. Proton/L-glutamate symport and the regulation of intracellular pH in isolated mesophyll cells. *Plant Physiology*, 99(2):665–671, 1992.
- W. A. Snedden, T. Arazi, H. Fromm, and B. J. Shelp. Calcium/calmodulin activation of soybean glutamate decarboxylase. *Plant Physiology*, 108(2):543–549, 1995.
- W. A. Snedden, N. Koutsia, G. Baum, and H. Fromm. Activation of a recombinant petunia glutamate decarboxylase by calcium/calmodulin or by a monoclonal antibody which recognizes the calmodulin binding domain. *The Journal of Biological Chemistry*, 271(8):4148–4153, 1996.
- P. E. Staswick, I. Tiryaki, and M. L. Rowe. Jasmonate response locus *JAR1* and several related Arabidopsis genes encode enzymes of the firefly luciferase superfamily that show activity on jasmonic, salicylic, and indole-3-acetic acids in an assay for adenylation. *The Plant Cell*, 14(6):1405–1415, 2002.
- N. Su, Q. Wu, J. Chen, L. Shabala, A. Mithöfer, H. Wang, M. Qu, M. Yu, J. Cui, and S. Shabala. GABA operates upstream of H⁺-ATPase and improves salinity tolerance in Arabidopsis by enabling cytosolic K⁺ retention and Na⁺ exclusion. *Journal of Experimental Botany*, 70(21):6349–6361, 2019.

- F. C. Sussmilch, J. Schultz, R. Hedrich, and M. R. G. Roelfsema. Acquiring control: The evolution of stomatal signalling pathways. *Trends in Plant Science*, 24(4):342–351, 2019.
- Ł. P. Tarkowski, S. Signorelli, and M. Höfte. γ -aminobutyric acid and related amino acids in plant immune responses: emerging mechanisms of action. *Plant, Cell & Environment*, 43(5):1103–1116, 2020.
- Q. Tian, X. Zhang, S. Ramesh, M. Gilliam, S. D. Tyerman, and W. H. Zhang. Ethylene negatively regulates aluminium-induced malate efflux from wheat roots and tobacco cells transformed with TaALMT1. *Journal of Experimental Botany*, 65(9):2415–2426, 2014.
- M. Toyota, D. Spencer, S. Sawai-Toyota, W. Jiaqi, T. Zhang, A. J. Koo, G. A. Howe, and S. Gilroy. Glutamate triggers long-distance, calcium-based plant defense signaling. *Science*, 361(6407):1112–1115, 2018.
- F. J. Turano and T. K. Fang. Characterization of two glutamate decarboxylase cDNA clones from arabidopsis. *Plant Physiology*, 117(4):1411–1421, 1998.
- O. R. Van Cauwenberghe and B. J. Shelp. Biochemical characterization of partially purified GABA:pyruvate transaminase from *Nicotiana tabacum*. *Phytochemistry*, 52(4):575–581, 1999.
- P. van Kleeff, J. Gao, S. Mol, N. Zwart, H. Zhang, K. Li, and A. de Boer. The Arabidopsis GORK K^+ -channel is phosphorylated by calcium-dependent protein kinase 21 (CPK21), which in turn is activated by 14-3-3 proteins. *Plant Physiology and Biochemistry*, 125:219–231, 2018.
- F. Wang, Z. H. Chen, X. Liu, T. D. Colmer, L. Shabala, A. Salih, M. Zhou, and S. Shabala. Revealing the roles of GORK channels and NADPH oxidase in acclimation to hypoxia in Arabidopsis. *Journal of Experimental Botany*, 68(12):3191–3204, 2016.
- J. Wang, D. Wu, Y. Wang, and D. Xie. Jasmonate action in plant defense against insects. *Journal of Experimental Botany*, 70(13):3391–3400, 2019.
- S. Wege. Sweet or sour? important link between nitrate signaling and malate accumulation identified in apple. *Plant Physiology*, 183(2):439–440, 2020.
- Q. Wu, N. Su, X. Huang, J. Cui, L. Shabala, M. Zhou, M. Yu, and S. Shabala. Hypoxia-induced increase in GABA content is essential for restoration of membrane potential and preventing ros-induced disturbance to ion homeostasis. *Plant Communications*, 2(3):100188, 2021.

- B. Xu, Y. Long, X. Feng, X. Zhu, N. Sai, L. Chirkova, A. Betts, J. Herrmann, E. J. Edwards, M. Okamoto, R. Hedrich, and M. Gilliam. GABA signalling modulates stomatal opening to enhance plant water use efficiency and drought resilience. *Nature Communications*, 12(1):1–15, 2021a.
- B. Xu, N. Sai, and M. Gilliam. The emerging role of GABA as a transport regulator and physiological signal. *Plant Physiology*, 187(4):2005–2016, 2021b.
- J. Ye, X. Wang, T. Hu, F. Zhang, B. Wang, C. Li, T. Yang, H. Li, Y. Lu, J. J. Giovannoni, Y. Zhang, and Z. Ye. An indel in the promoter of *Al-ACTIVATED MALATE TRANSPORTER9* selected during tomato domestication determines fruit malate contents and aluminum tolerance. *The Plant Cell*, 29(9):2249–2268, 2017.
- S. J. Yun and S. H. Oh. Cloning and characterization of a tobacco cDNA encoding calcium/calmodulin-dependent glutamate decarboxylase. *Molecules and Cells*, 8(2): 125–129, 1998.
- A. Zarei, C. P. Trobacher, and B. J. Shelp. Arabidopsis aldehyde dehydrogenase 10 family members confer salt tolerance through putrescine-derived 4-aminobutyrate (GABA) production. *Scientific Reports*, 6(1):35115, 2016.
- V. Žárský. Signal transduction: GABA receptor found in plants. *Nature Plants*, 1(8): 1–2, 2015.
- M. Zik, T. Arazi, W. A. Snedden, and H. Fromm. Two isoforms of glutamate decarboxylase in Arabidopsis are regulated by calcium/calmodulin and differ in organ distribution. *Plant Molecular Biology*, 37(6):967–975, 1998.
- M. R. Zimmermann, H. Maischak, A. Mithöfer, W. Boland, and H. H. Felle. System potentials, a novel electrical long-distance apoplastic signal in plants, induced by wounding. *Plant Physiology*, 149(3):1593–1600, 2009.

GABA RESPONSES OF BARLEY STOMATA

Stomata are the primary gatekeepers for plant gas exchange, a process that involves the transfer of CO₂ into the plant and water vapour out. Stomatal pore movement (opening or closure) occurs in response to internal signals (e.g. plant hormones, abscisic acid (ABA)) and environmental stimuli (e.g. day/night cycles, temperature, drought and pathogens). GABA has been shown to inhibit stomatal pore movement in the dicot model plant – *Arabidopsis thaliana*, however, monocot grass crops, such as barley, have a distinct stomatal morphology from those in dicot plants. Therefore, GABA may have a differential effect on barley stomatal pore movement. Thus, investigating whether GABA regulates barley stomatal movement would provide insights into whether GABA may have an impact on crop performance.

3.1 Results

3.1.1 Light/dark transition: the everyday signal controlling stomatal movement

3.1.1.1 Stomatal assay on epidermal peels

To determine whether GABA may have a role as a physiological signal regulating stomatal pore movements in barley, a stomatal assay was performed with a light/dark transition as described in methods section 3.3.2. To give enough statistical power, over 170 stomata in each group were sampled, and the stomatal width (aperture) were measured. Under constant dark or light, exogenous GABA (1 mM) application did not elicit changes to stomatal width (Figure 3.1). In contrast, during a light to dark transition, exogenous GABA treated stomata showed a higher mean value in stomatal width compared to control ($p < 0.001$, Figure 3.1(a)). Following a dark-to-light transition,

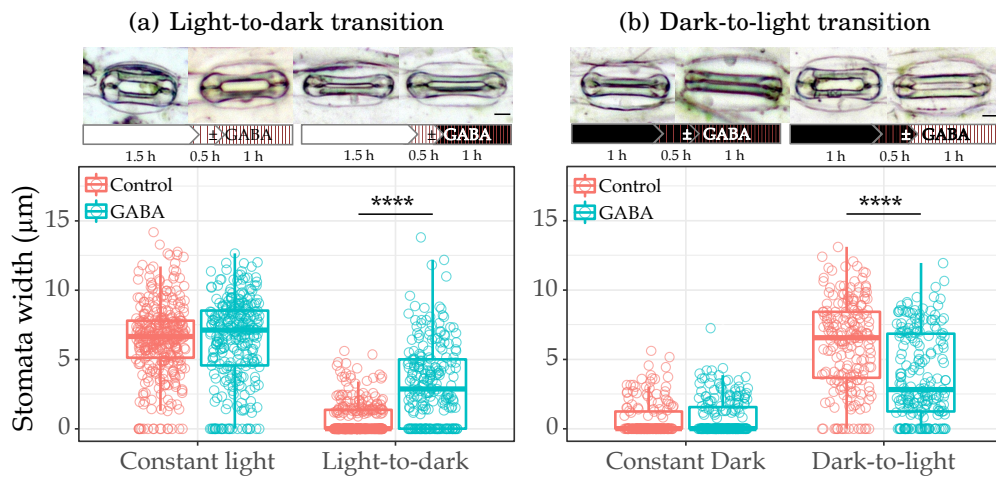


Figure 3.1. GABA inhibits stomatal pore movement during a light-to-dark (a) and dark-to-light (b) transition. (a) Epidermal strips were incubated under light for 2 hours followed by constant light or a light-to-dark transition for an additional 1 hour as illustrated by white (light) and black (dark) bars. (b) Epidermal strips were incubated under dark for 1.5 hours followed by constant dark or a dark-to-light transition for an additional 1 hour as illustrated by white (light) and black (dark) bar. The pre-treatment was applied 30 minutes before transition with or without 1 mM GABA as indicated by the red vertical line. Each stomatal image is representative of the average stomatal pore width of each group with scale bar represent 10 μm . Box plots represents second quartile, median and third quartile. A two-way ANOVA were performed with HSD test ($N > 220$ for light-to-dark and $N > 170$ for dark-to-light per sample group, **** $p < 0.0001$).

the stomatal width was narrower for the GABA treated stomata than control ($p < 0.001$, Figure 3.1(b)).

3.1.1.2 Leaf gas exchange

Stomatal aperture assays may not always represent the gas exchange responses of intact leaves to the environment, which is thought to occur due to the loss of the mesophyll layers as seen in Arabidopsis (e.g. Xu et al. 2021). The direct measurement of transpiration rate, stomatal conductance and net CO₂ assimilation from detached intact leaves is expected to better reflect plant response to treatment by putative signalling molecules than occurs via epidermal strips. For instance, aperture assays from Arabidopsis epidermal strips showed that GABA can antagonise both stomatal opening and closure, whereas in intact leaf feeding assays, it appears that GABA predominantly suppressed stomatal opening instead of closure (Xu et al., 2021). Therefore, the stomatal aperture assay was further validated in intact leaves.

Considering that the amount of GABA intake through the transpiration stream will not be directly equivalent to the GABA used for the stomata assay where guard cells are in directly contact with the buffer, and the concentration cannot easily be controlled, the pilot study explored a series of GABA concentrations (2, 4, 8 mM) through intact leaf feeding. All concentrations tested did not change the rate of water loss over 2.5 hours of recording in the constant light (for details see Appendix Section B.2). So in further experiments the highest concentration, 8 mM, was used in gas exchange experiments, as it did not itself close stomata and it would maximize the most chance of inhibiting stomatal pore movement.

Overall results of time-resolved gas exchange recording

Our light-to-dark transition recordings included 3 phases: the pre-treatment phase (45 minutes), to allow leaves to reach a steady state, which involved feeding an artificial xylem sap prior to treatment; followed by the GABA-feeding phase (60 minutes), allowing GABA uptake from the sap solution into leaves and the dark phase (45 minutes), to initiate stomatal closure to examine whether GABA had a statistically significant effect on inhibiting the stomatal closing process, as occurred for the aperture assays (Figure 3.2). No difference in the pre-treatment and GABA-feeding phase were observed between the control and 8 mM GABA treated groups in all three measurements as evidenced by the Welch two sample t-test. Stomatal conductance and transpiration rate was significantly lower with dark induced closure with GABA fed samples compared to non-GABA fed samples at later points the in dark phase (during the 127th–149th

(starts 22 minutes in dark, 82 minutes in GABA treatment) and the 130th–149th minute (starts 25 minutes in dark, 85 minutes in GABA treatment); Figure 3.2(b) and 3.2(c)).

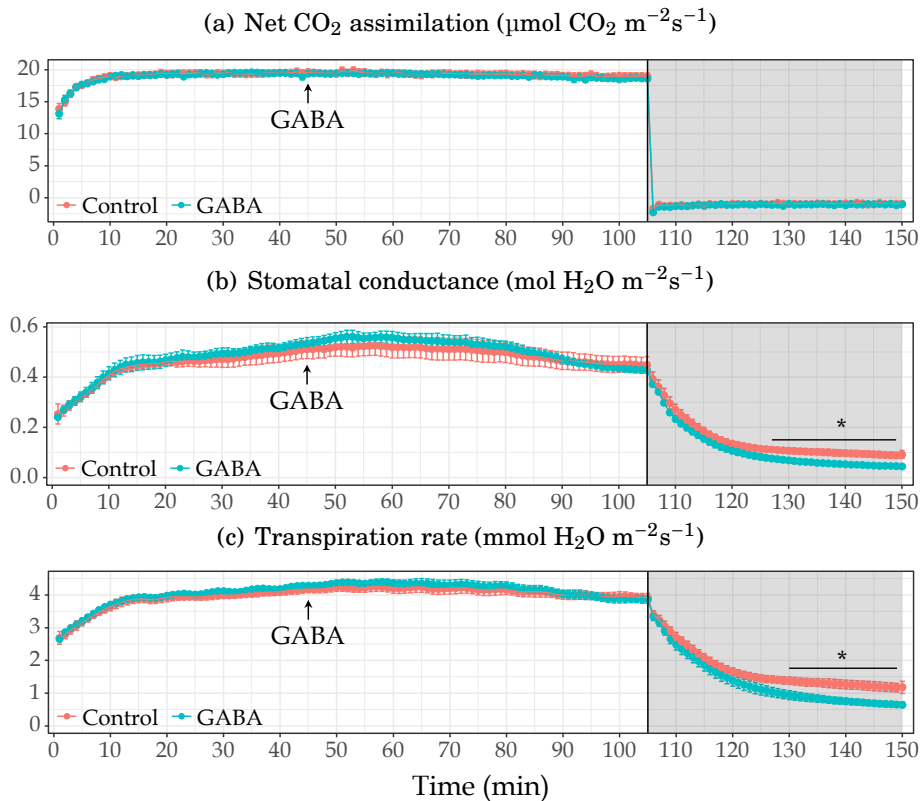


Figure 3.2. Time-resolved net CO₂ assimilation (a), stomatal conductance (b) and transpiration rate (c) during a light-to-dark transition. The whole 2.5 hours of the recording contains a pre-treatment phase (45 minutes), GABA-feeding phase (60 minutes, 8 mM GABA, indicated by an arrow) and a dark phase (45 minutes, indicated with shade). The net CO₂ assimilation (a), stomatal conductance (b) and transpiration rate (c) were recorded every minute, and statistical analysis was determined by two-sided Welch two sample t-test. Data represent the mean \pm SE with N = 4 per treatment group, * $p < 0.05$.

The dark-to-light recording was similar to the procedure described above, with an additional light phase and each phase being 30 minutes in duration. The extra light phase allowed stomata to re-open in response to light stimuli with or without GABA. The same measurement was recorded as above with three biological replicates (Figure 3.3). During the pre-treatment, GABA-feeding and dark phases, no significant difference was found in all measurements between control and GABA fed samples with a similar starting point right before entering the light phase. Stomatal conductance was significantly reduced upon light induced reopening in the presence of GABA compared to the non-GABA treated plants during the 102th–119th minute (starts 12 minutes in

light, minutes 72 in GABA treatment) while the significant reduce present during the 112th–115th minute (starts 22 minutes in light, 82 minutes in GABA treatment) in transpiration (Figure 3.3(b) and 3.3(c)).

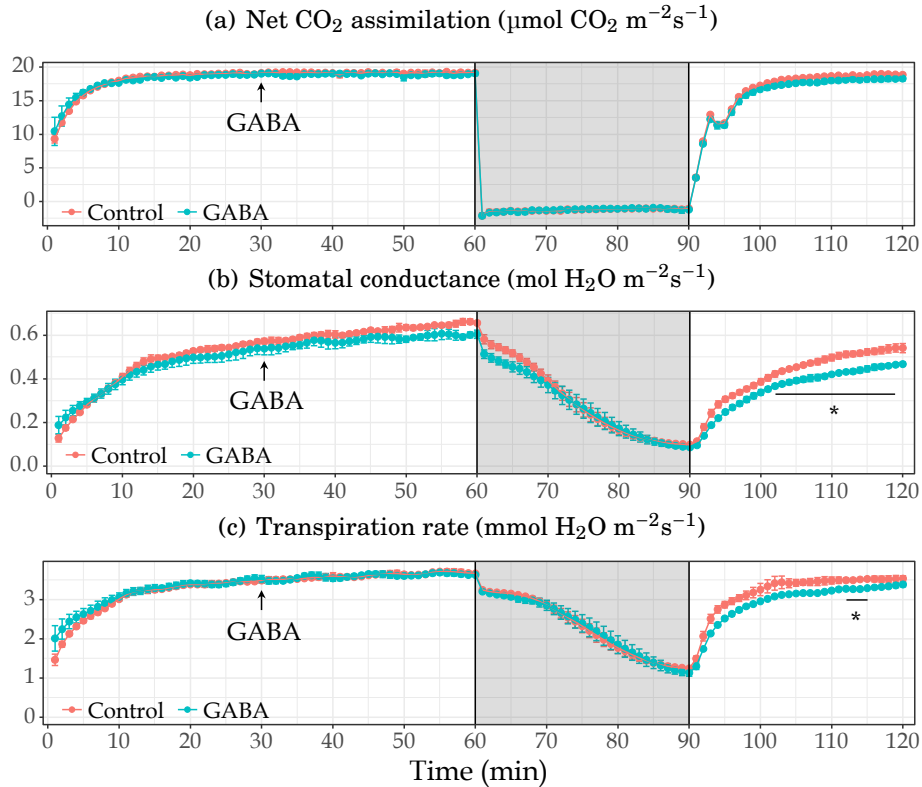


Figure 3.3. Time-resolved net CO₂ assimilation (a), stomatal conductance (b) and transpiration rate (c) during a dark-to-light transition. The whole 2 hours of the recording contains a pre-treatment phase, GABA-feeding phase (8 mM GABA, indicated by an arrow) and a dark phase (indicated with shade) and a light phase (white region, 1000 $\mu\text{mol m}^{-2}\text{s}^{-1}$) with 30 minutes duration in each phase. The net CO₂ assimilation (a), stomatal conductance (b) and transpiration rate (c) were recorded every minute, and statistical analysis was determined by two-sided Welch two sample t-test. N = 3 in each condition and presented with mean \pm SE, * $p < 0.05$.

Response speed upon GABA feeding

Beyond the impact of GABA in changing the extent of stomatal conductance and transpiration rate in response to dark/light, another approach is to impact the speed of dark or light response. A rapid response of transpiration rate and stomatal conductance in both control and GABA groups was observed within 10 minutes after entering the dark phase in light-to-dark (Figure 3.2) and 5 minutes after entering the light phase in dark-to-light transition (Figure 3.3). These periods could be fitted with a linear equation in both experiments, of which the slope was used to calculate the rate of

each process, and to determine the speed at which the stomata were impacted by GABA.

With different biological replicates, the slope in transpiration and stomatal conductance were calculated, and analysis of co-variance (ANCOVA) was applied to determine the slope difference (dark/light response speed with or without GABA) and visualised in Figure 3.4 (detailed results shown in Table B.1, <http://www.biostathandbook.com/ancova.html>). No slope difference was driven by GABA in both transpiration rate and stomatal conductance for the light-to-dark experiment, whereas the GABA effects appeared in the dark-to-light experiments (stars shown in Figure 3.4). In other words, the dark-to-light response for both transpiration rate and stomatal conductance is slower with GABA presence.

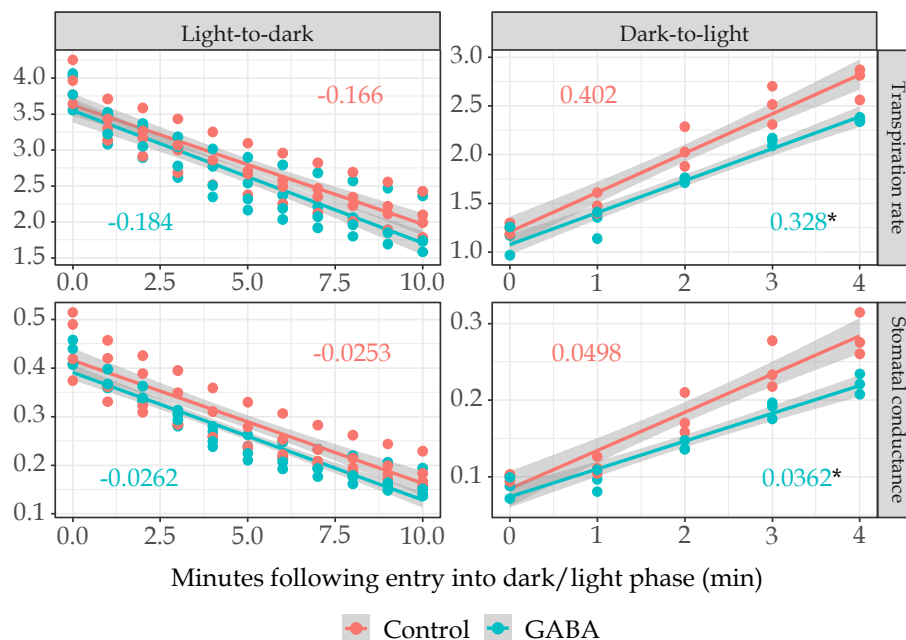


Figure 3.4. Transpiration rate and stomatal conductance fitted with a linear regression following light-to-dark or dark-to-light transition between control and GABA fed leaves from individual samples. The most linear time period of transpiration rate ($\text{mmol H}_2\text{O m}^{-2}\text{s}^{-1}$) and stomatal conductance ($\text{mol H}_2\text{O m}^{-2}\text{s}^{-1}$) was picked to perform the linear regression and the slope was calculated (shown on the figure) with R^2 . Slope difference was determined by ANCOVA (details see Table B.1). The gray ribbon represents the 95 % confidence interval of the regression line. $N=4$ in light-to-dark and $N=3$ in dark-to-light experiment, * $p < 0.05$.

Water use efficiency

Open stomata are required for CO_2 intake and are the gate for water vapour exit. There

is a trade-off between carbon gain and water loss. To understand whether GABA has an impact on the balance between CO₂ uptake and transpiration, leaf water use efficiency (WUE_l) and intrinsic water use efficiency (iWUE) were calculated with the individual samples in the dark-to-light transition experiment according to the equation 3.1 and 3.2 described in methods section 3.3.4. A two-sided Welch t-test was performed at a range that showed significant difference between control and GABA treatments in transpiration rate (3.3(c)) and stomatal conductance (Figure 3.3(b)). The significant increase of WUE_l and iWUE with average increase value at 3.79% and 12.61% were found (Figure 3.5).

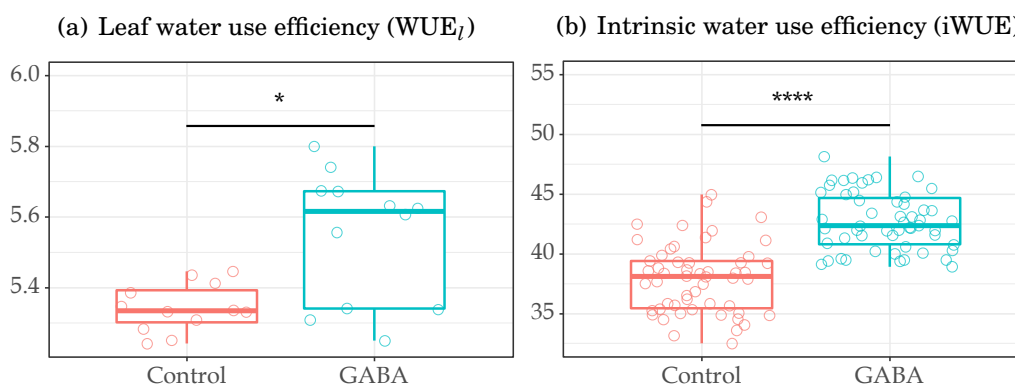


Figure 3.5. Leaf water use efficiency (WUE_l) (a) and intrinsic water use efficiency (iWUE) (b) during a dark-to-light transition. WUE_l ($\mu\text{mol CO}_2/\text{mmol H}_2\text{O}$) and iWUE ($\mu\text{mol CO}_2/\text{mol H}_2\text{O}$) were calculated as the ratio of photosynthetic rate (Figure 3.3(a)) divided by transpiration rate (Figure 3.3(c)) for WUE_l or stomatal conductance (Figure 3.3(b)) for iWUE within a range that showed significant difference between control and GABA treatments. A two-sided Welch two sample t-test performed on WUE_l (a) between the 112th minute to the 115th minutes, N = 12; and iWUE (b) between the 102th minute to the 119th minutes, N = 54. Box plot presented significant water use efficiency difference between GABA fed sample and control (* $p < 0.05$, **** $p < 0.0001$).

3.1.2 GABA-ABA interaction: when water related stress signals meet GABA

3.1.2.1 Stomatal response with GABA and ABA treatment

GABA suppressed dark-induced stomatal closure. In addition to dark, ABA is a stomatal closing signal. Here, it was investigated whether GABA also antagonised ABA-induced stomatal closure. In Arabidopsis, GABA only antagonized ABA-induced movement when ABA was supplied at low-doses (2.5 μM) rather than at high doses (25 μM) (Xu

et al., 2021). Therefore, we examined the effect of a series of ABA doses on barley stomatal closure and whether there was any change in efficacy in the presence of GABA. For barley, GABA showed both an enhancing effect on ABA induced closure, depending with presence of GABA. As shown in Figure 3.6, the dose-response curve illustrated the ABA half-maximal effective concentration (EC_{50}) at $5.533 \pm 0.53 \mu\text{M}$ with no GABA present. With the presence of 1 mM GABA, the EC_{50} shifted to $17.95 \pm 0.68 \mu\text{M}$, which indicated ABA sensitivity was reduced. 2 mM GABA presented similar ABA sensitivity as with no GABA presence at $5.58 \pm 0.41 \mu\text{M}$. Interestingly, stomatal width itself reduced by approximately 25% of the average control stomatal width with the higher concentration of GABA (2 mM) itself while 1 mM GABA did not elicit stomatal movement. Detailed individual experiment are in Appendix Figure B.2

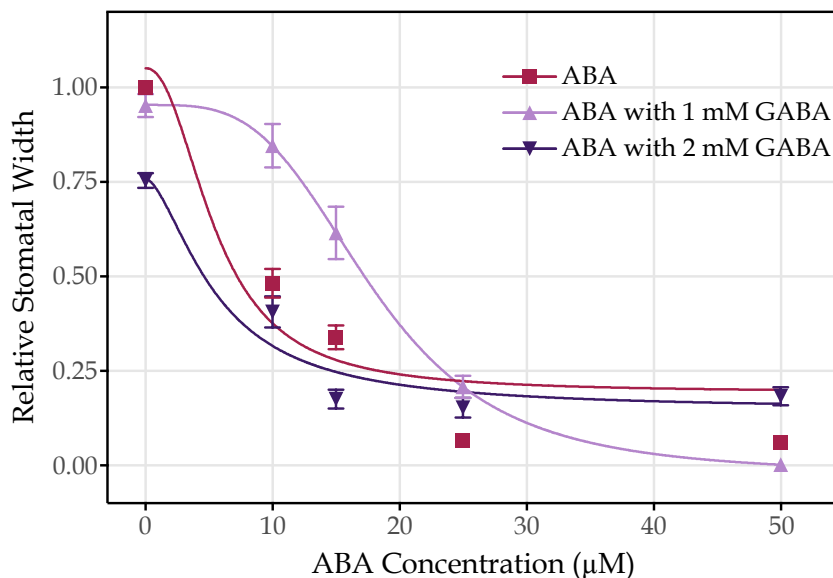


Figure 3.6. ABA dose-response curve with GABA present. Data points represent the mean of relative stomatal width normalised to control along the ABA concentration increase ($n > 150$ in each group). The half-maximal effective concentration of ABA without GABA, with 1 mM GABA and with 2 mM GABA are 5.533 ± 0.53 , 17.95 ± 0.68 and $5.58 \pm 0.41 \mu\text{M}$ respectively. Data points represent mean \pm SE. Detailed information about curve fitting is in Appendix table B.2

3.1.2.2 Water loss measurement with GABA and/or ABA supplements

Leaf feeding assays were performed to further validate the GABA and ABA interaction on stomatal regulation, as determined by aperture assays. A series of leaf feeding assays in different ABA concentrations (100 nM, 25 nM and 10 nM) with the presence and absence of 1 mM GABA were conducted – as this was the concentration that inhibited

ABA induced movement. In general, no difference was found between control and GABA treatment in water loss as shown in example Figure 3.7. ABA always effectively closed stomata regardless the presence or absence of GABA, suggesting that this system worked properly. We calculated the sampling time point where ABA+GABA significantly reduced water loss rate of detached leaves, as summarised in Table 3.1. The significant ABA response time point was increased as ABA concentration was reduced and no time point delay was observed with the inclusion of 1 mM GABA, except for 1 mM GABA with 25 nM ABA. The demonstration of time-recorded examples is shown in Figure 3.7, more details of individual experiment is in Appendix section B.4.

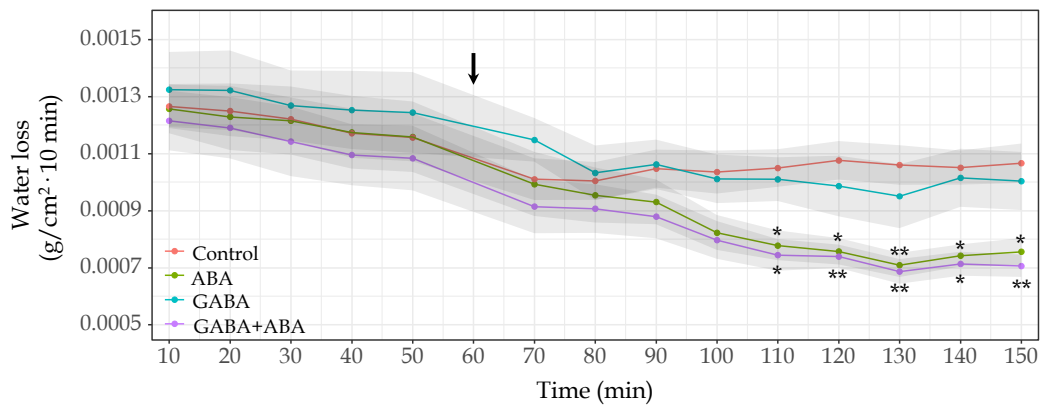


Figure 3.7. Water loss assay in response to 10 nM ABA with 1 mM GABA. All leaf samples were weighed sequentially every 10 minutes for an hours to monitor water loss stability, then transferred to its corresponding treatment (indicated by an arrow) and continue weighting for 1.5 hours. Water loss was calculated every 10 minutes and tested with one-way ANOVA. Data represent mean \pm SE (shown in gray ribbon), N = 5 in each group, * $p < 0.05$, ** $p < 0.01$ compared to control.

Table 3.1. Summary of significant treatment response time point of ABA and GABA+ABA

ABA concentration (nM)	Significant treatment respond time point (minutes after treatment)	
	ABA	GABA+ABA
100	30	30
25	30	40
10	50	50

3.2 Discussion

3.2.1 Low-dose of GABA suppresses stomatal movement in response to a signal

In section 3.1.1.1 and 3.1.2.1, 1 mM GABA, was shown for the first time to have an antagonistic affect on barley epidermal strips for both light-induced stomatal opening, and dark or low-dose ABA-induced stomatal closure. GABA itself at this concentration did not elicit a change in stomatal width. Similar results has been previously reported in dicot model species *Arabidopsis thaliana* (Figure 3.8; Xu et al., 2021). 2 mM GABA supplement does not change stomatal status and suppressed light-induced opening and dark-induced closure in *Arabidopsis* (Figure 3.8(a) and 3.8(b)), whereas 1 mM GABA in barley was enough to present its suppressive effect. Consistent with the GABA and ABA interaction observed in *Arabidopsis* aperture assays (Figure 3.8(c) and 3.8(d)), GABA antagonises the effect of low doses of ABA, but not high-doses in barley (Appendix Figure B.2), suggesting that ABA can override GABA's inhibitory effects on stomatal movement when it is of a certain sufficient magnitude (Xu et al., 2021).

It seems that barley and *Arabidopsis* have differential sensitivity to GABA. Two millimolar GABA in *Arabidopsis* inhibited the stomatal pore movement triggered by light, darkness and ABA, but such concentration was sufficient to initiate stomatal closure of barley stomata under steady light (Figure 3.8, Appendix B.3). Therefore GABA may increase barley WUE via reducing stomatal opening, this could be additionally improved by further increasing GABA biosynthesis to promote stomatal closure as it is seen that 2 mM GABA stimulates stomatal closure in Figure 3.6; while 1 mM can reduced stomatal opening (Figure 3.1). Intriguingly, GABA supplement through barley leaf petiole up to 8 mM did not stimulate stomatal closure under light, again suggesting that stomata on epidermal layer may respond differently from intact leaves. However, under a dark transition 1 mM GABA did have lower transpirational water loss in the dark (Figure 3.2(c)). Generally, the GABA concentration in *Arabidopsis thaliana* could up to 1 $\mu\text{mol g}^{-1}$ fresh weight, while in barley, the GABA concentration is 0.02 $\mu\text{mol g}^{-1}$ fresh weight (summarised table in Ramesh et al. (2016)), it is still unknown what the endogenous GABA concentrations are in barley under stress.

By closely monitoring the opening and closure process through the gas exchange, the increase of transpiration and stomatal conductance during a dark-to-light transition were reduced in GABA fed leaves compared to the leaves just fed by artificial xylem sap solution. The result is consistent with what observed with our barley stomatal assay

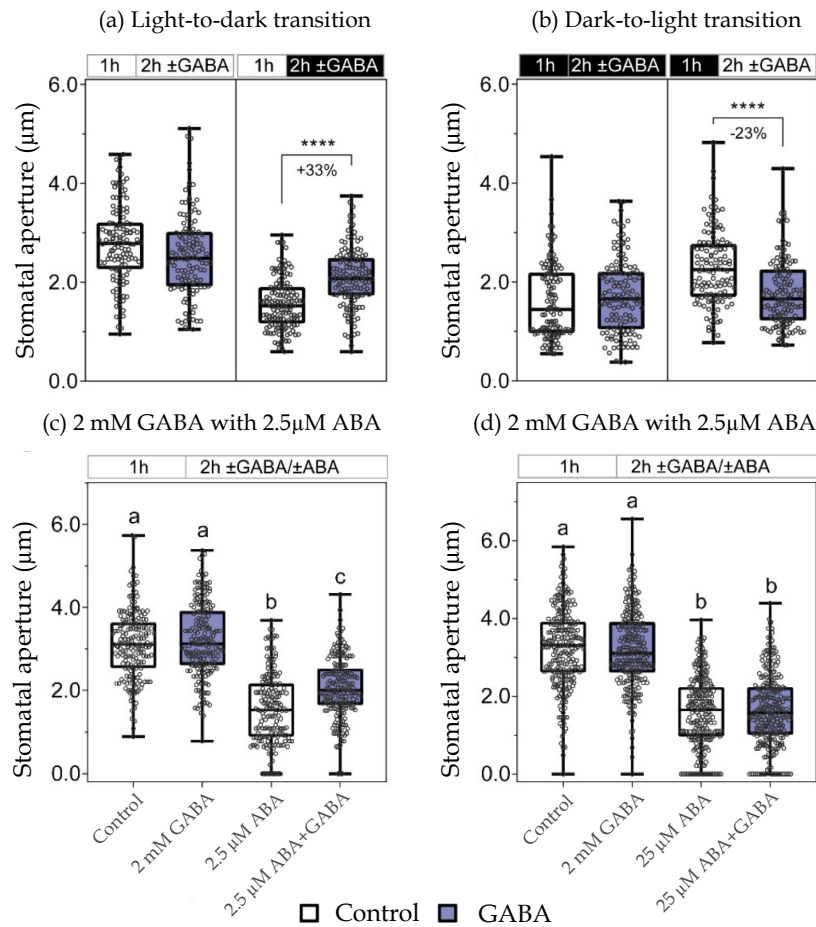


Figure 3.8. Exogenous GABA antagonises stomatal movement triggered by light, darkness or ABA in *Arabidopsis*. (a,b) Stomatal aperture of wild-type *Arabidopsis thaliana* leaves in response to light or dark. Epidermal strips were pre-incubated in stomatal measurement buffer for 1 h under light (a) or dark (b), followed by 2 h incubation under constant light (a), dark (b), light-to-dark transition (a) or dark-to-light transition (b) as indicated above graphs by black (dark) or white (light) bars, together with the application of 2 mM GABA. Data are plotted with box and whiskers plots: whiskers plot represents minimum and maximum values, and box plot represents second quartile, median and third quartile. Statistical difference was determined by two-sided Student’s t-test ($N > 120/\text{group}$; **** $p < 0.0001$). (c,d) Exogenous GABA application reduce stomatal closure in response to 2.5 µM ABA (c), but not 25 µM ABA (d). Epidermal strips were pre-incubated in stomatal pore measurement buffer for 1 h under light, followed by 2 h treatment under light with or without combination of ABA ± 2 mM GABA. Statistical difference as determined by One-Way ANOVA ($N > 170/\text{group}$; a, b and c represent groups without significant difference; $p < 0.05$). The figure is adapted from Xu et al. (2021).

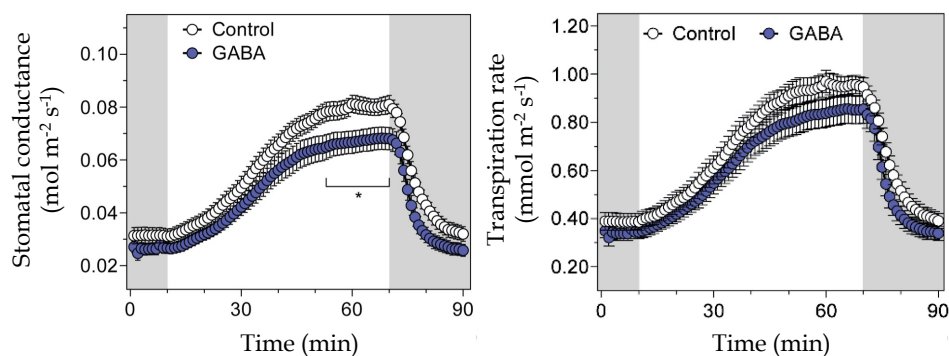


Figure 3.9. Stomatal conductance and transpiration rate in *Arabidopsis* with presence and absent of GABA. GABA-feeding reduces stomatal conductance and transpiration rate. Detached leaves from 5-6 week-old *A. thaliana* wild-type plants was used for data recording through a LiCOR LI-6400XT in response to dark (shaded region) and $200 \mu\text{mol m}^{-2}\text{s}^{-1}$ light (white region), fed with artificial xylem sap solutions $\pm 4 \text{ mM}$ GABA supplements. The figure is adapted from Xu et al. (2021).

that the extent of stomata opening was dampened (Figure 3.1(b)) and similar with the stomatal response from *Arabidopsis* (Figure 3.9). Here, the GABA antagonistic effects during a dark-to-light transition reflected not only on the reduced level of transpiration and stomatal conductance when reaching the steady phase at the re-opening light phase (Figure 3.3(c) and 3.3(b)), but also the response speed of light-induced opening derived from the fitted slope in the right side of Figure 3.4. Thus, it is confirmed that the GABA suppressive effect slows down light-induced opening and reduces transpiration and stomatal conductance in barley.

Unexpectedly, with 1 hour GABA feeding under constant light, GABA further reduces the stomatal conductance and water transpiration in the light-to-dark gas exchange experiment than the non-GABA fed samples after ~ 25 minutes of entering the dark phase (Figure 3.2(b) and 3.2(c)). With GABA feeding time halved, no such difference between GABA and non-GABA fed samples with 30 minutes of dark (duration between 30th and 90th in Figure 3.3(b) and 3.3(c)) was found. Hence, a longer GABA feeding time allows more GABA intake through the transpiration stream, and resulting a higher GABA accumulation in leaf samples. Such observations of the stomatal assay and gas exchange could lead to the assumption that a high-dose or large accumulation of GABA within tissues may trigger stomatal movement in barley.

In guard cells Potassium (K^+) and chloride (Cl^-) ions are the dominant ions present. It has been found that K^+ and Cl^- are shuttled between guard cells and subsidiary

cells in maize during the stomatal movement: K^+ and Cl^- moved from subsidiary cells to guard cells in light-induced stomata opening, then they returned from guard cells to subsidiary cells upon darkening (Raschke and Fellows, 1971). Later, Schäfer et al. (2018) determined that guard cells contain less K^+ and Cl^- in a closed stomata, while subsidiary cells exhibit higher K^+ and Cl^- in barley. Such dynamic relationship of K^+ and Cl^- content between guard cells and subsidiary cells shown in maize is expected in barley.

Recently, Adem et al. (2020) determined the K^+ channel – guard cell outwardly rectifying K^+ channel (GORK) activated by 10 mM of GABA in Arabidopsis root. As known from above, changing content of K^+ contributes to stomatal opening and closure (Raschke and Fellows, 1971; Schäfer et al., 2018). Loss function of *GORK* strongly altered darkness and ABA induced stomatal closure but no such impact upon light induced stomatal opening in Arabidopsis (Hosy et al., 2003), suggesting GORK is participating the process of stomatal closure. Besides, *in silico* analysis suggests that GORK shares a similar putative GABA-sensitive motif found in aluminum-activated malate transporter (ALMT), thereby it was speculated that GORK might be regulated by GABA too (Adem et al., 2020). Hence, the activation of GORK by GABA could possibly explain the observation of stomatal closure by GABA application from the stomatal assay and light-to-dark gas exchange experiment.

Regardless, GABA appears to antagonize stomatal movement when receiving both an opening or closing signal in both monocot and dicots, when using excised epidermal strips and in gas exchange. In the future study, a full profile of barley (and Arabidopsis) stomatal sensitivity to GABA requires a dose-dependency assay. Investigation of whether GORK is regulated by GABA is also necessary.

3.2.2 Candidate aluminum-activated malate transporters (ALMTs) participate stomatal movement and regulated by GABA

In Arabidopsis, GABA's inhibitory effect on stomatal opening and closure acts via negative regulation of tonoplast-localized ALMT9 and plasma-membrane localized ALMT12 (Xu et al., 2021), respectively, as they respectively control stomatal opening and closing process (De Angeli et al., 2013; Meyer et al., 2010). Similar to Arabidopsis, the barley genome has ALMT members with homology to ALMT9 and 12, such as HvALMT1, SL19623 and SL1251 (Figure 3.10(a)). All three barley ALMT homologs contain the 12 amino-acid residue putative GABA interaction motif when aligned with

TaALMT1 and GABA_A receptors, implicating that they might sense intracellular GABA signals (Figure 3.10(b)). Although SL19623's GABA motif does not contain aromatic amino acid phenylalanine (F) as Ramesh et al. (2015) suggested that F is important for GABA sensitivity, it doesn't fully rule out the possibility of GABA regulation on SL19623 until examine its GABA sensitivity. The only well-characterised barley ALMT – HvALMT1, is localised at the plasma membrane and is expressed in roots and guard cells Gruber et al. (2010). While its anion transport capacity was inhibited by GABA (Ramesh et al., 2015), its over-expression resulted in greater closure with no opening phenotype (Gruber et al., 2010), and RNAi knockdown resulted in diminished closure in the dark and greater water loss (Xu et al., 2015) – opposite to that observed for *almt9* (Xu et al., 2021). Here, the results elucidated the barley gas exchange response to GABA parallels the phenotype of Arabidopsis, it is entirely possible that GABA's effects are actioned through inhibition of barley tonoplast ALMTs that have a role in opening pores. Whilst a simple bioinformatic search can reveal the barley ALMTs, without functional characterisation it would not be possible to identify the correct target or indeed those present on the tonoplast (David et al., 2019).

Certainly, future research is required to determine the role of these barley ALMT candidates in GABA sensing and their modulation of stomatal regulation (Gruber et al., 2010; Ramesh et al., 2015). The barley stomatal complex is formed by dumbbell-shaped guard cells flanked by subsidiary cells and its movement is coordinated by both guard cells and subsidiary cells (Chen et al., 2017); it is possible then that GABA signals may regulate ionic flux across both barley guard cell and subsidiary cell membranes (Figure 2.2; Chen et al., 2017; Merilo et al., 2014), and this would need to be tested. So far, no ALMT has been reported to be expressed in subsidiary cells and it is still unknown whether GABA metabolism in subsidiary cells also contributes to stomatal movement and sensitivity, this is worthy further research.

To conclude, GABA modifies stomatal behaviour across many levels, not only signal-wise i.e. light/dark, ABA or other signal listed in Xu et al. (2021) but also species-wise, as mentioned above. The fine control of GABA regulation is reflected in the level of stomatal movement and signal response time, and it is concentration dependent. Further investigation to reveal the actual mechanism of GABA regulation in barley could start from characterizing the potential ALMT and GORK candidates. In addition, GABA antagonized barley stomatal closure in response to closing signals (i.e. darkness and ABA), but this could not be phenocopied in leaf feeding assays using both LiCOR and water loss measurement, again suggesting that the GABA inhibitory stomatal closure requires further research to uncover how the loss of mesophyll cells from epidermal

strips alter stomatal response or sensitivity.

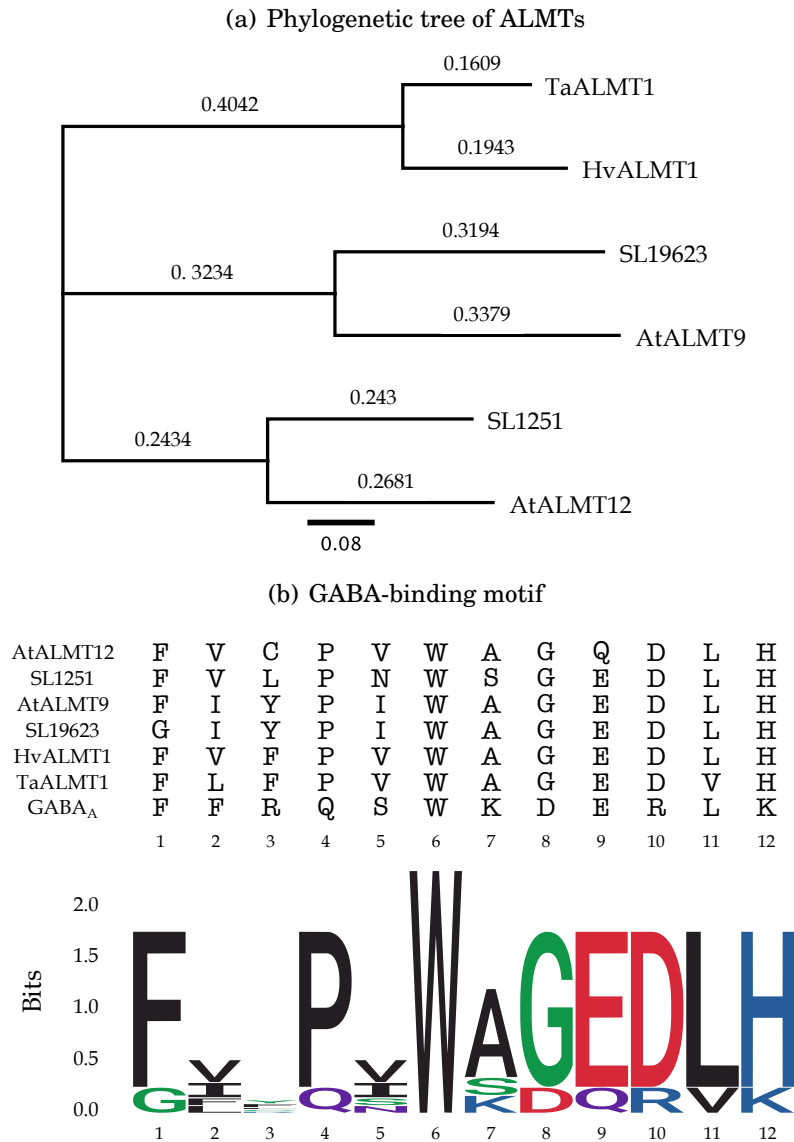


Figure 3.10. Evolutionary relationship of ALMTs between *A. thaliana*, wheat (*Triticum aestivum*) and barley (*Hordeum vulgare*) and its GABA-binding motif. (a) The phylogenetic tree was generated from protein sequence of ALMT1 in wheat (Ta), HvALMT1, SL1251, SL19623 in barley (Hv) and ALMT9, ALMT12 in *Arabidopsis* (At) using Geneious Prime with Jukes-Cantor model and neighbor-joining building method. Protein sequence is available in Appendix section B.5. (b) Residues corresponding to logo in proteins form GABA_A TaALMT1, HvALMT1, SL1251, SL19623 in barley and ALMT9, ALMT12 in *Arabidopsis*. The sub-figure is adjusted from Ramesh et al. (2015) with MEME analysis and visualised through ggseqlogo (Wagih, 2017).

3.3 Material and Methods

3.3.1 Plant material

Barley seeds (cv. Barke) were germinated on filter paper for 5-6 days and then planted in a hydroponic system in half-strength Hoagland's solution (Conn et al. 2013; Hoagland and Arnon 1950; Appendix Table B.3). Seedlings were grown for three weeks under a 16 hours photoperiod at 23 °C and a $100 \mu\text{mol m}^{-2} \text{s}^{-1}$ photosynthetic photon flux density (PPFD).

3.3.2 Stomatal assay

3.3.2.1 Light/Dark transition in the presence of GABA

Two- to three-week-old leaf samples were first detached, and about 3 centimeters of the central part of the leaf was dissected away. The leaf section was quartered as illustrated in Figure 3.11 and each section bathed in 2 ml modified measurement buffer (50 mM KCl, 10 mM MES with pH 6.1 by KOH) individually under light ($100 \mu\text{mol m}^{-2} \text{s}^{-1}$) or darkness for 1.5 hours. Pre-treated leaf sections were pre-incubated in the same buffer with or without GABA for 30 minutes, then put into continuous light/dark or light-to-dark/dark-to-light transition for an additional 1 hour as indicated in Figure 3.1.

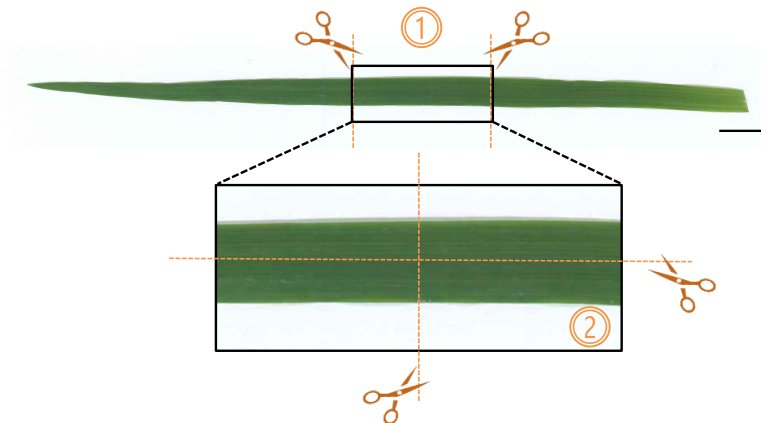


Figure 3.11. Demonstration of leaf sample preparation for the stomatal assay. Selected leaf section in middle part was cut into 4 pieces for further sample preparation. The scale bar represent 1 cm of leaf sample.

After the incubation, all the leaf sections were peeled as described in Shen et al. (2015), stuck on a glass cover slip set into the bottom of petri dish and imaged using an inverted microscope (Nikon DS-Fi3 digital camera attached to a Nikon Diaphot 200 Inverted

phase Contrast Microscope). For each leaf section, five random areas were focused upon and captured to obtain images of stomata in excess on 100 in one sample group for performing statistical analyses. Stomatal area and width were measured through Fiji ImageJ (<https://imagej.net/Fiji>).

3.3.2.2 ABA treatment in the presence of GABA

A fully expanded second leaf was first detached, quartered and bathed in modified measuring buffer as described in Figure 3.11. All leaf sections were incubated in a individual petri dish for 2 hours under light ($100 \mu\text{mol m}^{-2} \text{s}^{-1}$). The test leaf section was peeled after 2 hours under light incubation and stomatal opening status was examined under the microscope to ensure stomata were fully opened. After the stomatal opening status was determined, 2 ml modified measuring buffer (Control), ABA, GABA and GABA+ABA were applied to the corresponding leaf section with random matching (blind treatment) with additional 1 hour light incubation. When the incubation finished all leaf sections were peeled, imaged and measured as described as above.

A series of ABA concentration (10, 15, 25, 50 μM) were applied were applied together with 0 mM, 1 mM or 2 mM GABA as combinations. To compare across different concentration combinations, all treatment groups were normalized to its own non-treatment control.

3.3.3 Leaf feeding assay

A fully expanded barley 2nd leaf was detached about 16 cm from the tip, and placed into a container filled with water. A second cut was made under water to avoid under water to avoid vasculature embolism. The leaf sample was immediately transferred to a cuvette filled with 1 ml artificial xylem solution containing 1 mM KH_2PO_4 , 1mM K_2HPO_4 , 1 mM $\text{CaCl}_2 \cdot 2\text{H}_2\text{O}$, 0.1 mM $\text{MgSO}_4 \cdot 7\text{H}_2\text{O}$, 1 mM KNO_3 and 0.1mM $\text{MnSO}_4 \cdot \text{H}_2\text{O}$, pH 6.1 (KOH); and sealed with parafilm to minimize non-transpirational water loss. A total of 20 leaf samples were prepared and incubated under $100 \mu\text{mol m}^{-2} \text{s}^{-1}$ light for 1 hour. Samples were randomly assigned to the control, ABA, GABA and GABA+ABA group in equal number. The mass of each sample was acquired on a five decimal balance every 10 minutes for 1 hour; then the samples were transferred to a new cuvette that contained a corresponding treatment. Weighing continued for an additional 1.5 hours. ABA concentrations (10, 15, 100 nM) with or without 1 mM GABA were applied in combination. Grams of water lost per square centimeter of leaf area per ten minutes ($\text{g/cm}^2 \cdot 10 \text{ min}$) was calculated. Leaf area was obtained by scanning leaf samples and image size was calculated through Fiji ImageJ.

3.3.4 Gas exchange measurement

Two-to-three-week-old barley plants were used for gas exchange experiments grown in the same growth conditions described in section 3.3.1. The leaf sample preparation occurred at the 3 leaf stage, based on a method in Ceciliato et al. (2019) with minor adaptations. Briefly, a fully expanded isolated 2nd leaf of the barley seedling was obtained by cutting the stem 0.5-1 cm from its base, and first leaf along with the sheath was carefully removed. The leaf sample was placed into a container filled with water and a second cut was made on the stem underwater about 3.5 cm away from the second leaf blade to avoid xylem embolism. Immediately the leaf sample was transferred into a 2 ml microcentrifuge tube filled with artificial xylem sap solution as outlined in section 3.3.3. Four leaf samples were prepared as described above in one microcentrifuge tube and sealed with parafilm. The second leaf blades were taped together using micropore tape (3M) leaving an area in the middle of the leaf blades free to fit into the gas exchange chamber cuvette (Figure 3.12).

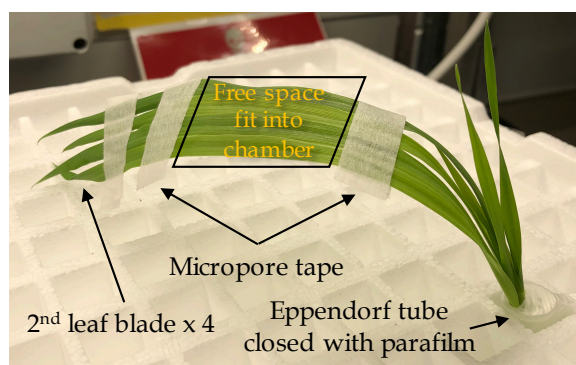


Figure 3.12. Demonstration of leaf preparation for the gas exchange measurements.

The net CO₂ assimilation (A_n), transpiration rate (T) and stomatal conductance (g_s) was measured using a LI-6400XT portable photosynthesis system (LI-COR Bioscience) attached to a 6400-02B LED light source (LI-COR Bioscience). The experiment was set with light at 1000 $\mu\text{mol m}^{-2} \text{s}^{-1}$; flow rate of 500 mmol s^{-1} (for light-to-dark) or 300 mmol s^{-1} (for dark-to-light); 400 ppm CO₂ and ~50% relative humidity at 22 °C. Transient intrinsic water use efficiency ($iWUE$) and transient leaf water use efficiency (WUE_l) were calculated by the following equation defined by Leakey et al. (2019):

$$WUE_l = \frac{A_n}{T} \quad (3.1)$$

$$iWUE = \frac{A_n}{g_s} \quad (3.2)$$

References

- G. D. Adem, G. Chen, L. Shabala, Z. H. Chen, and S. Shabala. GORK channel: A master switch of plant metabolism? *Trends in Plant Science*, 25(5):434–445, 2020.
- P. H. O. Ceciliato, J. Zhang, Q. Liu, X. Shen, H. Hu, C. Liu, A. R. Schöffner, and J. I. Schroeder. Intact leaf gas exchange provides a robust method for measuring the kinetics of stomatal conductance responses to abscisic acid and other small molecules in arabidopsis and grasses. *Plant Methods*, 15(1):1–10, 2019.
- Z. H. Chen, G. Chen, F. Dai, Y. Wang, A. Hills, Y. L. Ruan, G. Zhang, P. J. Franks, E. Nevo, and M. R. Blatt. Molecular evolution of grass stomata. *Trends in Plant Science*, 22(2):124–139, 2017.
- S. J. Conn, B. Hocking, M. Dayod, B. Xu, A. Athman, S. Henderson, L. Aukett, V. Conn, M. K. Shearer, S. Fuentes, S. D. Tyerman, and M. Gilliam. Protocol: optimising hydroponic growth systems for nutritional and physiological analysis of *Arabidopsis thaliana* and other plants. *Plant Methods*, 9(1):1–11, 2013.
- R. David, C. S. Byrt, S. D. Tyerman, M. Gilliam, and S. Wege. Roles of membrane transporters: connecting the dots from sequence to phenotype. *Annals of Botany*, 124(2):201–208, 2019.
- A. De Angeli, J. Zhang, S. Meyer, and E. Martinoia. AtALMT9 is a malate-activated vacuolar chloride channel required for stomatal opening in Arabidopsis. *Nature Communications*, 4(1):1–10, 2013.
- B. D. Gruber, P. R. Ryan, A. E. Richardson, S. D. Tyerman, S. Ramesh, D. M. Hebb, S. M. Howitt, and E. Delhaize. HvALMT1 from barley is involved in the transport of organic anions. *Journal of Experimental Botany*, 61(5):1455–1467, 2010.
- D. R. Hoagland and D. I. Arnon. The water-culture method for growing plants without soil. *Circular. California Agricultural Experiment Station*, 347(2nd edit):32, 1950.
- E. Hosy, A. Vavasseur, K. Mouline, I. Dreyer, F. Gaymard, F. Porée, J. Boucherez, A. Lebaudy, D. Bouchez, A. A. Véry, T. Simonneau, J. B. Thibaud, and H. Sentenac. The Arabidopsis outward K⁺ channel GORK is involved in regulation of stomatal movements and plant transpiration. *Proceedings of the National Academy of Sciences*, 100(9):5549–5554, 2003.
- A. D. Leakey, J. N. Ferguson, C. P. Pignou, A. Wu, Z. Jin, G. L. Hammer, and D. B. Lobell. Water use efficiency as a constraint and target for improving the resilience

- and productivity of C3 and C4 crops. *Annual Review of Plant Biology*, 70(1):781–808, 2019.
- E. Merilo, I. Jõesaar, M. Brosché, and H. Kollist. To open or to close: species-specific stomatal responses to simultaneously applied opposing environmental factors. *New Phytologist*, 202(2):499–508, 2014.
- S. Meyer, P. Mumm, D. Imes, A. Endler, B. Weder, K. A. Al-Rasheid, D. Geiger, I. Marten, E. Martinoia, and R. Hedrich. AtALMT12 represents an R-type anion channel required for stomatal movement in Arabidopsis guard cells. *The Plant Journal*, 63(6): 1054–1062, 2010.
- S. A. Ramesh, S. D. Tyerman, B. Xu, J. Bose, S. Kaur, V. Conn, P. Domingos, S. Ullah, S. Wege, S. Shabala, J. A. Feijó, P. R. Ryan, and M. Gilliam. GABA signalling modulates plant growth by directly regulating the activity of plant-specific anion transporters. *Nature Communications*, 6(1):1–10, 2015.
- S. A. Ramesh, S. D. Tyerman, M. Gilliam, and B. Xu. γ -aminobutyric acid (GABA) signalling in plants. *Cellular and Molecular Life Sciences*, 74(9):1577–1603, 2016.
- K. Raschke and M. P. Fellows. Stomatal movement in *Zea mays*: Shuttle of potassium and chloride between guard cells and subsidiary cells. *Planta*, 101(4):296–316, 1971.
- N. Schäfer, T. Maierhofer, J. Herrmann, M. E. Jørgensen, C. Lind, K. von Meyer, S. Lautner, J. Fromm, M. Felder, A. M. Hetherington, P. Ache, D. Geiger, and R. Hedrich. A tandem amino acid residue motif in guard cell SLAC1 anion channel of grasses allows for the control of stomatal aperture by nitrate. *Current Biology*, 28(9):1370 – 1379, 2018.
- L. Shen, P. Sun, V. C. Bonnell, K. J. Edwards, A. M. Hetherington, M. R. McAinsh, and M. R. Roberts. Measuring stress signaling responses of stomata in isolated epidermis of graminaceous species. *Frontiers in plant science*, 6:533, 2015.
- O. Wagih. ggseqlogo: a versatile R package for drawing sequence logos. *Bioinformatics*, 33(22):3645–3647, 2017.
- B. Xu, Y. Long, X. Feng, X. Zhu, N. Sai, L. Chirkova, A. Betts, J. Herrmann, E. J. Edwards, M. Okamoto, R. Hedrich, and M. Gilliam. GABA signalling modulates stomatal opening to enhance plant water use efficiency and drought resilience. *Nature Communications*, 12(1):1–15, 2021.

M. Xu, B. D. Gruber, E. Delhaize, R. G. White, R. A. James, J. You, Z. Yang, and P. R. Ryan. The barley anion channel, HvALMT1, has multiple roles in guard cell physiology and grain metabolism. *Physiologia Plantarum*, 153(1):183–193, 2015.

GUARD CELL COMPLEX SPECIFIC TRANSCRIPTIONAL RESPONSE OF BARLEY TO GABA

RNA-Seq is a widely used transcriptomics technology for high-throughput sequencing that reveals the presence and quantity of RNA in a biological sample. The higher coverage and greater resolution of RNA-Seq over technology such as microarray-based methods has increased its popularity and implementation since its first use in 2008 (Nagalakshmi et al., 2008; Wilhelm et al., 2008). A wide range of barley breeding, disease and stress defence, studies have benefited from the RNA-Seq techniques (Derakhshani et al., 2020; Huang et al., 2016; Tanaka et al., 2019; Tombuloglu et al., 2013). Particularly, Schäfer et al. (2018) used stomatal complex (barley guard cell and subsidiary cell; GCSC) enriched RNA-Seq to investigate the transcriptional machinery that was responsible for bringing about barley stomatal closure.

From the last chapter, it was determined that GABA can modulate the stomatal pore movement and gas exchange of barley in response to light, darkness or ABA signals. However, whether there is a transcriptomic response to GABA that might impact the mechanism of GABA response is unclear. GABA is predominantly synthesised from glutamate through GABA shunt, which bypasses two steps of mitochondrial-based tricarboxylic acid (TCA) cycle (Bouché et al., 2003; Bown and Shelp, 2016). GABA signalling regulation was previously proposed through direct regulation of a plant-specific anion transporter – aluminum-activated malate transporters (ALMTs; Ramesh et al. 2015). The 12 amino acid motif found on plants ALMTs are similar to the important motif of GABA binding site in rat GABA_A receptors (Ramesh et al., 2015, 2016). Xu et al. (2021) illustrated the negative regulation of Arabidopsis ALMT9 and ALMT12

that controls the process of stomatal opening and closing (De Angeli et al., 2013; Meyer et al., 2010). The negative regulation of ALMT9 and 12 result in inhibition of stomatal movement, hence, links GABA signaling with stomatal regulation.

The ABA signalling response in contrast, as an important part of signalling networks in stomatal regulation, is much more well studied. ABA is known to be synthesised in vascular tissues, mesophyll cells and guard cells (Askari-Khorsgani et al., 2018; Bauer et al., 2013; Boursiac et al., 2013). The endogenous ABA level is correlated with 9-*cis*-epoxycarotenoid dioxygenase (NCED) expression, which produces xanthoxin, the precursor of ABA (Schwartz et al., 2003). Xanthoxin then converted to ABA through ABA2 and abscisic aldehyde oxidase (AAO3; Chen et al. 2020).

The well-defined core of ABA signalling consists of 3 main components: 2C protein phosphatase (PP2C), pyrabactin resistance/pyrabactin resistance-like/regulatory components of the ABAreceptor (PYR/PYL/RCAR) and subclass III sucrose non-fermenting-1 (SNF1)-related protein kinase 2 (SnRK2; Cotelte and Leonhardt 2019). When ABA is absent, SnRK2s are not activated to mediate a signal because of the dephosphorylation and physical interaction with PP2C. When ABA concentrations increase, SnRK2s will be activated and phosphorylated when PP2C inhibition occurs through the formation with ABA and PYR/PYL/RCAR (Fujii et al., 2009; Ruschhaupt et al., 2019; Soon et al., 2012; Umezawa et al., 2009; Vlad et al., 2009). Once the SnRK2s are activated, it triggers signal transduction in downstream ABA-dependent targets such as slow anion channel-associated 1 (SLAC1) and quickly activating anion channel 1 (QUAC1) for stomatal closing (Eisenach et al., 2017; Hsu et al., 2021; Imes et al., 2013), and transcriptional factors that are required for activation of stress responsive genes transcriptionally (Fujii et al., 2009; Ruschhaupt et al., 2019; Sirichandra et al., 2010; Takahashi et al., 2017).

To understand what transcriptional changes GABA may invoke and the potential GABA-ABA interactions that occur on a transcriptional level, barley guard cell and subsidiary cell (GCSC) enriched RNA-Seq data was captured in control conditions, or following GABA or ABA treatment. Differentially expressed genes (DE genes) induced by GABA or ABA compared to control conditions was explored to identify potential target genes that might be involved in the interaction between GABA and ABA in the stomatal complex.

4.1 Results

4.1.1 Data quality and post alignment processing

Sequencing read quality was assessed before and after adaptor trimming. Overall average per base sequence quality score of assessed sequencing reads was greater than 30 across all bases after trimming, which indicated the good quality of sequencing reads. Due to the variety difference between Barke and the reference genome (Morex), each sample obtained ~70% of reads that uniquely aligned to genome with at least 23 million reads in total. Full report of sequencing reads and mapping quality is on GitHub (<https://github.com/CharlotteSai/BarleyGCRNASEq>). Gene counts were filtered by the filtering function *filterByExpr()* in *edgeR* to remove lowly expressed genes (i.e. cpm > 0.34 in at least 3 samples), and 24,106 genes passed the filtration. A multidimensional scaling plot was generated to examine sample clustering after filtering (Figure 4.1). Control and treatments were clearly separated on the biological coefficient of variation (BCV) distance 2, and treatments were spread along BCV distance 1. This indicated that the sample separation was strongly determined by treatment.

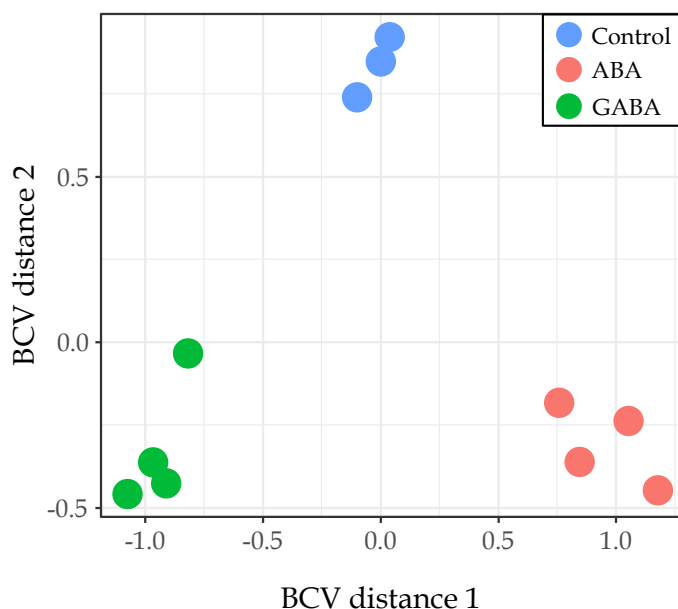


Figure 4.1. Multidimensional scaling plot of distances between gene expression profiles. The separation distance is based on the typical log₂ fold changes between the samples. Samples are colour coded by genotype.

4.1.2 Differential gene expression

In order to identify ABA or GABA induced transcriptional differences, filtered counts were fitted using a negative binomial generalized log-linear model after estimating dispersions. The differential gene expression was tested through a quasi-likelihood (QL) F-test. Among those genes that detected expression, 2042 genes following the ABA treatment had significant changes in expression compared to control, where 2743 genes were identified as differentially expressed genes (DE genes) in the GABA treated group passing the threshold adjusted p -value threshold ≤ 0.05 and $\log_2\text{FC} \geq 1$ (Figure 4.2).

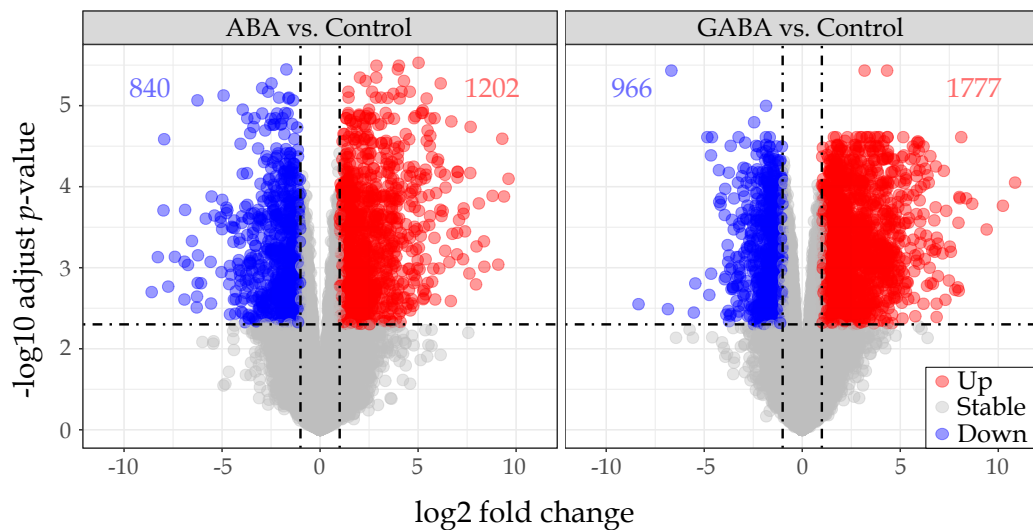


Figure 4.2. Volcano plot of ABA and GABA induced differentially expressed genes (DE genes). The horizontal line represents the p -value $-\log_{10}(0.05)$ and vertical lines indicate a \log_2 fold change of -1 and 1, the parameters chosen to define those genes considered as DE. Data points coloured in red and blue are DE genes that were counted as up or down regulated compared to control.

Gene expression profiling of ABA and GABA induced DE genes are shown in figure 4.3, and the full DE gene list is available on github repository (<https://GitHub.com/CharlotteSai/BarleyGCRNASeq>). Comparing between ABA and GABA, the treatment induced DE genes are mostly distinct which suggests that both ABA and GABA initiate changes in gene expression but, on the whole, activate and repress different sets of genes. Besides, 539 of DE genes were shared in their differential expression compared to control under the two treatments: 428 DE genes were regulated in same direction (i.e. both treatment activate and repress the same gene), whereas 111 DE genes were differentially regulated compared to control but in the opposite direction (ABA induces expression of a gene and GABA suppresses its expression and vice versa). The result

indicated that ABA and GABA could have some interactions through regulating the same gene.

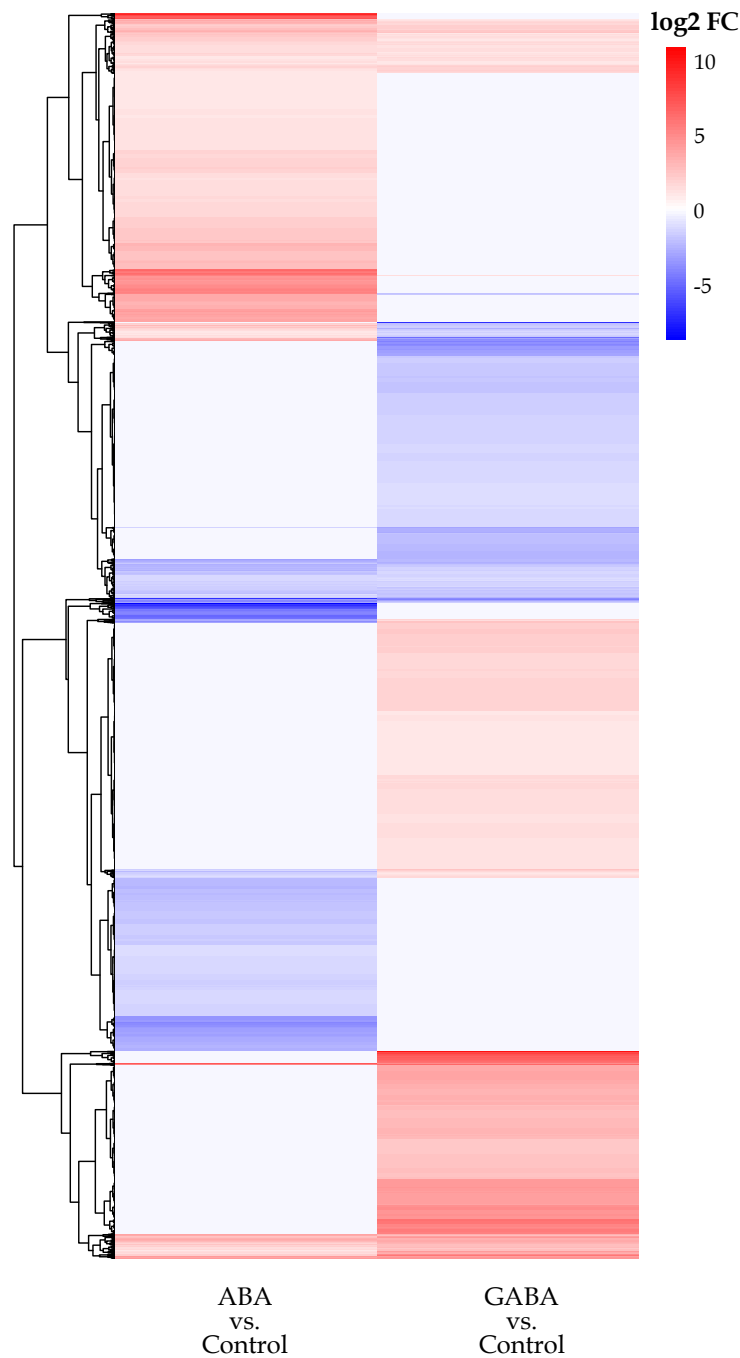


Figure 4.3. Gene expression profiling of ABA and GABA induced differentially expressed genes. Log₂ fold change of differentially expressed genes at least in one treatment group are visualised in a heatmap. Hierarchical clustering was performed with the heatmap by the default clustering method "complete" in the R package *pheatmap*. Up and down regulation of DE genes were colour coded with red and blue as showed in scale bar.

4.1.3 Gene Ontology (GO) enrichment

The GO enrichment analysis was based on Fisher's exact test to determine whether experimentally-derived genes (DE genes in this case) in a predefined GO term are present more than it could be expected (i.e. over-represented; [Agresti, 2003](#)). In our data, DE genes are split into up and down regulated in each group to test GO term over-representation (Figure 4.4). ABA and GABA induced DE genes were mostly enriched in distinct GO terms with three shared terms: hydrolase activity, hydrolyzing O-glycosyl compounds (GO:0004553), kinase activity (GO:0016301) and phosphotransferase activity, alcohol group as acceptor (GO:0016773). In addition, two of the shared GO terms were enriched in DE genes that were oppositely regulated compared to control.

Significant GO terms were mostly enriched in down regulated DE genes that were induced by ABA and up regulated DE genes induced by GABA. Apart from the mentioned

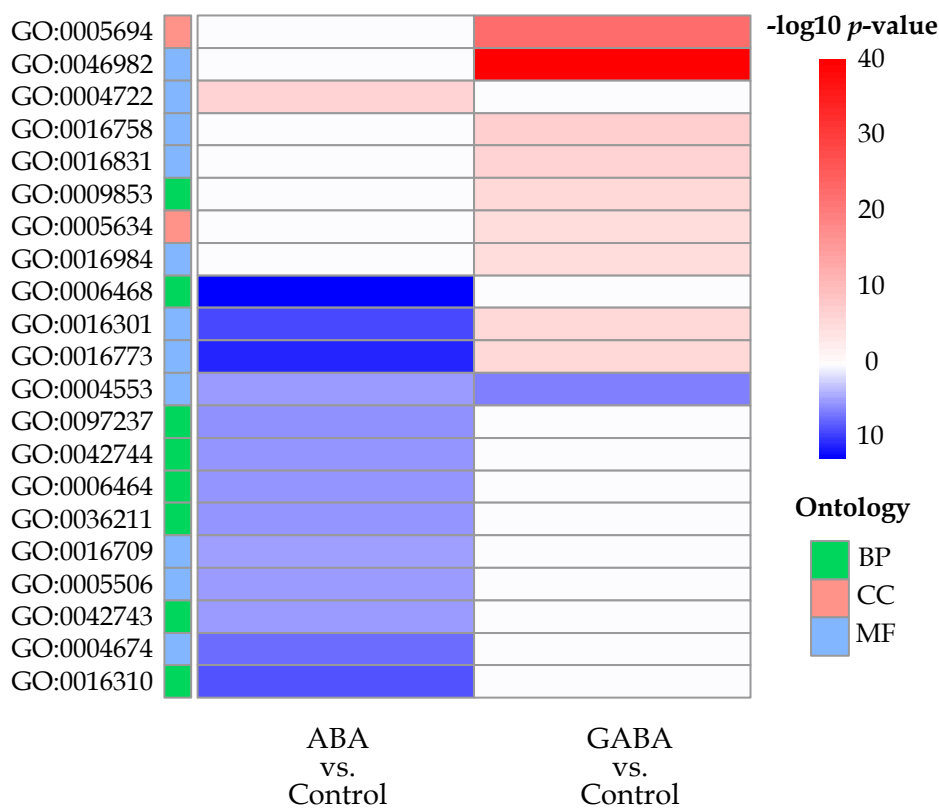


Figure 4.4. DE genes enriched Gene ontologies. Significantly enriched Gene Ontology categories separated by up regulation (red) and down regulation (blue) are displayed with $-\log_{10} p$ -value. Darker colours depict more significant enrichment. GO classifications are annotated in the category of biological process (BP), cellular component (CC) and molecular function (MF) along the side of heatmap.

shared GO terms, ABA induced down regulated DE genes were related to oxidoreductase activity, phosphorylation, iron ion binding, protein modification, hydrogen peroxide metabolic and cellular response to toxic substance enriched, and protein phosphatase activity was enriched for up regulated DE genes (Table 4.1). In contrast, GABA induced DE genes were related to carboxy-lyase (decarboxylase) activity, protein heterodimerization activity, organelle and photorespiration. In summary, GABA regulated a distinct set of GCSC transcriptional effects in terms of gene function compared to ABA.

Table 4.1. Summary of DE gene enriched Gene Ontologies

GO term	Description	Ontology*	DE gene ratio**	
			ABA	GABA
GO:0006464	Cellular protein modification process	BP	118/5862	
GO:0006468	Protein phosphorylation	BP	103/3499	
GO:0009853	Photorespiration	BP		8/34
GO:0016310	Phosphorylation	BP	116/4943	
GO:0036211	Protein modification process	BP	118/5862	
GO:0042743	Hydrogen peroxide metabolic process	BP	15/298	
GO:0042744	Hydrogen peroxide catabolic process	BP	15/287	
GO:0097237	Cellular response to toxic substance	BP	19/410	
GO:0005634	Nucleus	CC		254/6903
GO:0005694	Chromosome	CC		84/792
GO:0004553	Hydrolase activity, hydrolyzing o-glycosyl compounds	MF	30/943	36/943
GO:0004674	Protein serine/threonine kinase activity	MF	50/1655	
GO:0004722	Protein serine/threonine phosphatase activity	MF	13/121	
GO:0005506	Iron ion binding	MF	30/931	
GO:0016301	Kinase activity	MF	105/4261	173/4261
GO:0016709	Oxidoreductase activity, acting on paired donors, with incorporation or reduction of molecular oxygen, NAD(P)H as one donor, and incorporation of one atom of oxygen	MF	13/238	
GO:0016758	Transferase activity, transferring hexosyl groups	MF		63/1054
GO:0016773	Phosphotransferase activity, alcohol group as acceptor	MF	99/3669	150/3669
GO:0016831	Carboxy-lyase activity	MF		24/268
GO:0016984	Ribulose-bisphosphate carboxylase activity	MF		8/39
GO:0046982	Protein heterodimerization activity	MF		77/402

Note: * GO classifications are in the category of biological process (BP), cellular component (CC) and molecular function (MF). ** DE gene ratio is presented by number of DE genes present in a GO term divided by the total number of genes present within the GO term. The colour indicates whether the DE gene enriched GO term is up-regulated (red) or down-regulated (blue).

4.1.4 KEGG pathway enrichment

The Kyoto Encyclopedia of Genes and Genomes (KEGG) pathway analysis uses the same grounding theory as GO enrichment analysis to determine the over-representation (i.e. the enrichment) in a predefined KEGG pathway. Since the KEGG annotations for barley are not yet available, the best hit of BLASTP alignment of barley protein sequence against with the *Arabidopsis thaliana* protein sequences (TAIR10, <https://www.arabidopsis.org>) were used to assign the Arabidopsis homologous genes to barley for further enrichment analysis (Camacho et al., 2009; Schäfer et al.,

2018). The Arabidopsis homologous genes that matched with ABA and GABA induced DE genes were used in this enrichment test to examine the pathways that had significant changes.

The pattern of KEGG pathways that were enriched by ABA and GABA induced DE were mostly distinct with some sharing (Figure 4.5). Phenylpropanoid biosynthesis (ath00940) and starch and sucrose metabolism (ath00500) had similar levels of enrichment in both comparisons. MAPK signaling pathway (ath04016) and glycine, serine and threonine metabolism (ath00260) had higher levels of enrichment in ABA to control expression whereas zeatin biosynthesis (ath00908) and glycolysis/gluconeogenesis (ath00010) had higher levels of enrichment in GABA compared to control.

ABA induced DE genes had 17 uniquely enriched KEGG pathways that involved in lipid metabolism, carbohydrates metabolism, amino acid metabolism, energy metabolism, biosynthesis of other secondary metabolites, metabolism of terpenoids and polyketides,

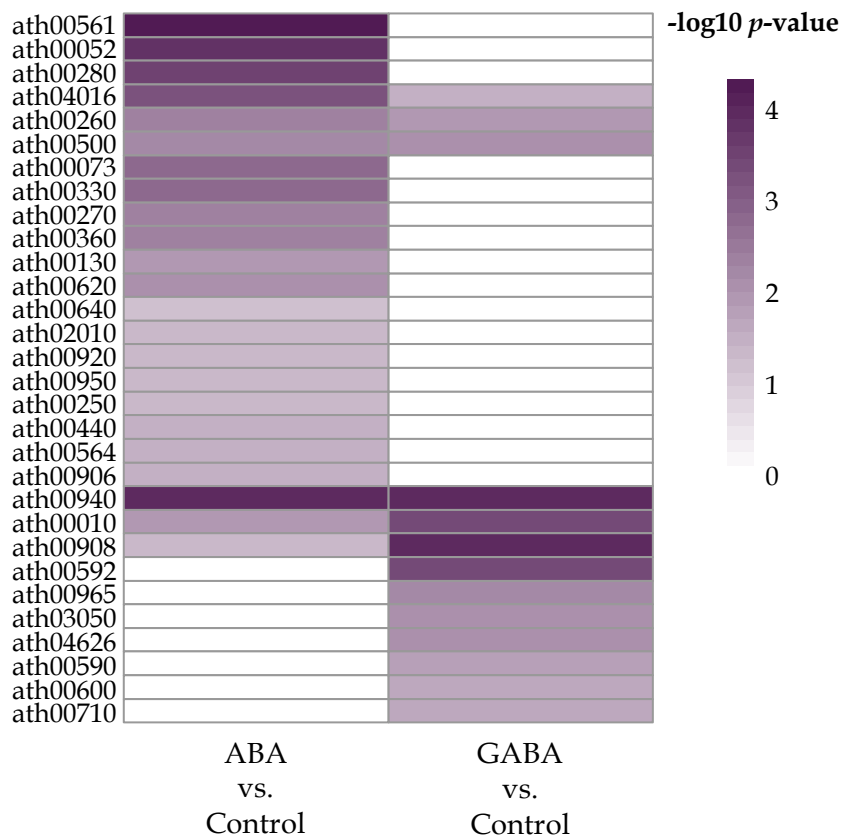


Figure 4.5. DE genes enriched KEGG pathway. Significant enrichment pattern displayed with $-\log_{10} p$ -value. Darker colour indicated more significant enrichment KEGG pathways.

membrane transport and metabolism of cofactors and vitamins (Table 4.2). On the contrary, GABA induced DE genes have 7 uniquely enriched KEGG pathways that related to lipid metabolism, energy metabolism, biosynthesis of other secondary metabolites environmental adaptation and folding, sorting and degradation.

Table 4.2. Summary of ABA and GABA treatment enriched KEGG pathway.

Class	KEGG pathway	Pathway accession	DE gene ratio*	
			ABA	GABA
Signal transduction	MAPK signaling pathway – plant	ath04016	20/139	18/139
Lipid metabolism	Glycerolipid metabolism	ath00561	14/66	
	Cutin, suberine and wax biosynthesis	ath00073	8/37	
	Glycerophospholipid metabolism	ath00564	12/98	
	Alpha-Linolenic acid metabolism	ath00592		11/43
	Arachidonic acid metabolism	ath00590		5/20
	Sphingolipid metabolism	ath00600		6/29
Carbohydrates metabolism	Starch and sucrose metabolism	ath00500	20/171	23/171
	Glycolysis/Gluconeogenesis	ath00010	15/119	21/119
	Galactose metabolism	ath00052	12/57	
	Pyruvate metabolism	ath00620	13/97	
	Propanoate metabolism	ath00640	6/43	
Amino acid metabolism	Glycine, serine and threonine metabolism	ath00260	11/70	12/70
	Valine, leucine and isoleucine degradation	ath00280	11/52	
	Arginine and proline metabolism	ath00330	10/54	
	Cysteine and methionine metabolism	ath00270	16/120	
	Phenylalanine metabolism	ath00360	7/33	
Metabolism of other amino acid	Alanine, aspartate and glutamate metabolism	ath00250	7/51	
	Phosphonate and phosphinate metabolism	ath00440	2/5	
Energy metabolism	Sulfur metabolism	ath00920	6/42	
	Carbon fixation in photosynthetic organisms	ath00710		11/69
Biosynthesis of other secondary metabolites	Phenylpropanoid biosynthesis	ath00940	25/176	29/176
	Zeatin biosynthesis	ath00908	5/32	10/32
	Isoquinoline alkaloid biosynthesis	ath00950	4/22	
	Betalain biosynthesis	ath00965		2/2
Metabolism of terpenoids and polyketides	Carotenoid biosynthesis	ath00906	5/29	
Membrane transport	ABC transporters	ath02010	5/32	
Metabolism of cofactors and vitamins	Ubiquinone and other terpenoid-quinone biosynthesis	ath00130	7/39	
Environmental adaptation	Plant-pathogen interaction	ath04626		27/204
Folding, sorting and degradation	Proteasome	ath03050		11/61

Note: * DE gene ratio is presented by number of DE genes present in a KEGG pathway divided by the total number of genes present within the KEGG pathway.

4.2 Discussion

In this chapter, the GCSC enriched RNA-Seq data was explored as an approach to examine potential GABA–ABA interactions. From the initial projection of RNA-Seq

data on MDS, we know that the ABA and GABA treated transcriptome profiling was distinct (Figure 4.1). This also reflected in the expression pattern of DE genes as most obtained were treatment specific (Figure 4.3). Compared to the barley GCSC data previously published from Schäfer et al. (2018), the majority of detected DE genes from our data are present in this published GCSC dataset, which confirms the detected DE genes are truly expressed in the stomatal complex. We also compared our ABA-induced DE genes to the published Arabidopsis guard cell microarray data with ABA treatment (Leonhardt et al., 2004) through BLASTP (Camacho et al., 2009), and 24/151 reported ABA-induced genes are matched with 38 of our ABA-induced DE genes in barley, suggests ABA and barley may share some ABA target genes. Details of these cross-validation see Appendix Section C.2. The gene expression profiling, via GO enrichment and KEGG enrichment analysis, of ABA and GABA induced DE genes both showed the same trend that these two treatments induce different pathways within stomatal complex.

In our data, two GO functions, kinase activity (GO:0016301) and phosphotransferase activity, alcohol group as acceptor (GO:0016773) were enriched in both GABA and ABA treatments, but by DE genes that were regulated in the opposite direction compared to control (Figure 4.4). Within the gene set of the 2 two GO terms, 3 of DE genes were found induce changes of expression by both ABA and GABA (see Table 4.3) and gene expression were also found in the GCSC data from Schäfer et al. (2018). It suggests that those gene listed in Table 4.3 are modulated both by ABA and GABA, however it is unclear: (1) how they are regulated by ABA and GABA together; (2) does ABA override GABA transcriptional regulation, as it does on stomatal closure?; and (3) can GABA reverse any transcriptional regulation triggered by ABA. Answering these question would be expected to inform how GABA and ABA interact at a transcriptional level.

These genes activated in their expression by GABA and ABA all have GO categories involved in kinase activity, ATP binding, phosphorylation and membrane with some other GO functions respectively according to their direct associated GO terms. Due to the limited information found for these genes, the homologous genes in Arabidopsis were explored. The Arabidopsis homology suggest that *HORVU.MOREX.r2.2HG0084420* is a receptor kinase (*AT4G21380*, *ARK3/RK3*); *HORVU.MOREX.r2.2HG0114190* is a cysteine-rich receptor-like protein kinase (*AT4G23180*, *RLK4/CRK10*) and the last one *HORVU.MOREX.r2.7HG0565210* is a concanavalin A-like lectin protein kinase family protein (*AT5G06740*, *LecRK-S.5*). These 3 genes in Arabidopsis are all related to defence responses to various stimuli. Few studies are focused on these particular receptor kinases as most of research is interested in the general features of the whole family

(Bouwmeester and Govers, 2009; Pastuglia et al., 2002; Quezada et al., 2019). *ARK3* has been mentioned to accumulate after both wounding and bacterial infection (Pastuglia et al., 2002). *CRK10 (RLK4)* is transcriptionally induced by reactive oxygen species (ROS), pathogen attack and salicylic acid (SA) application (Du and Chen, 2000; Wrzaczek et al., 2010). A virus infection study on Arabidopsis transcriptome has been suggested that *LecRK-S.5* is associated with *Tobacco Etch Virus* defence and involved in ROS signalling (Wu et al., 2017).

Using homology analysis using Arabidopsis, it is indicated that all three genes that were regulated by both GABA and ABA, have some tentative relationship with stress defence responses. During pathogen defence, plants are known to often respond by restricting pathogen entry into leaves via inhibiting stomatal opening or promoting stomatal closure. ABA signalling is known to play an important role during this process; at the same time, ROS production is induced by ABA (Cotelle and Leonhardt, 2019; Sierla et al., 2016). *LecRK-V.5*, another member of lectin protein kinase family protein was shown to be a negative regulator of stomatal immunity which inhibits ABA signalling upstream of ROS production (Theveniau et al., 2012). *LecRK-S.5*, in our case may behave similarly to *LecRK-V.5*.

In a similar case, GABA and ABA both induce changes in MAPK signalling pathways (ath04016), which are an important signaling network in stress defence (Zhang and Klessig, 2001). Within this pathway, 3 of DE genes were both induced by GABA and ABA which suggests GABA and ABA regulation may share cross points through these genes (Table 4.4 and full list of enriched DE gene in MAPK signalling pathway is in Appendix Section C.3). All three genes were found in the dataset from Schäfer et al. (2018) confirms its GCSC specific expression. Especially, *HORVU.MOREX.r2.2HG0154390* (matched to *HORVU2Hr1G094230*) is also marked as GC enriched gene that Schäfer et al. (2018) cross validated with Bauer et al. (2013).

In particular, *HORVU.MOREX.r2.1HG0045440* was oppositely regulated by GABA and ABA compared to control. The Arabidopsis homolog of this gene *AT1G10940* is the SNF1-related protein kinase 2.4 (*SnRK2.4*) that is localized in cytoplasm and nucleus (Szymańska et al., 2019). *SnRK2s* are major regulators in plants when response to osmotic stress. *SnRK2.4* has been frequently reported to be involved in salt stress responses (Boudsocq et al., 2004; Krzywińska et al., 2016; McLoughlin et al., 2012; Szymańska et al., 2019). Specifically, *SnRK2.4* modulated homeostasis of ROS through regulating the expression of several genes responsible for ROS generation (e.g. *RbohD* and *RbohF*) in Arabidopsis in response to salt stress (Szymańska et al., 2019) with

SnRK2.10. In our data, *HORVU.MOREX.r2.2HG0179990*, homologue to Arabidopsis *SnRK2.10* (*AT1G60940*) was also found down-regulated like *SnRK2.4* by GABA, where *SnRK2.6* (also known as *Open Stomata 1*; *OST1*; *AT4G33950*) is up-regulated along with *SnRK2.4* by ABA (Appendix Section C.3).

As known that ROS is generated by respiratory burst oxidases (Rboh)/NADPH oxidase enzymes (Kwak et al., 2003). From our data, 4 DE genes induced by GABA are homolog of Arabidopsis *RbohD* and *RbohF*, and were shown to be up-regulated compared to control, while 1 DE genes induced by ABA (Appendix Section C.3). In Arabidopsis, *RbohD* and *RbohF* are expressed in guard cells (Leonhardt et al., 2004) and *RbohF* is the main isoform involved in ABA-related stomatal responses (Kwak et al., 2003). ABA-induced stomatal closure is partially impaired when *AtRbohF* function is lost (Kwak et al., 2003). In *atrbohF/atrbohD*, stomatal closure is further reduced and ROS production is abolished (Kwak et al., 2003). Sirichandra et al. (2009) demonstrated that SnRK2.6 can directly interact and phosphorylate the N terminus of *AtRbohF* *in vitro*. SnRK2s is kept inactive by 2C protein phosphatase (PP2C) until ABA increases then induces inhibition of PP2C via forming a complex of ABA, ABA receptor (PYR/PYL/RCAR) and PP2C; and activated SnRK2s could further transduce downstream signals (Fujii et al., 2009; Ruschhaupt et al., 2019; Soon et al., 2012; Umezawa et al., 2009; Vlad et al., 2009). Thus, SnRK2s mediates ROS production through direct phosphorylation and activation of *AtRbohF* at Ser174 and Ser13 in a ABA-dependent manner (Sirichandra et al., 2009) and DE genes induced by ABA that are homologous to Arabidopsis *RbohF* (*AT1G64060*), *SnRK2.6* and *HAB1* (*AT1G72770*) also shown in our data under ABA treatment (Appendix Section C.3).

Above showed a clear pathway on ABA-induced ROS production, but the mechanism of how GABA interact with guard cell *RbohD* and/or *RbohF* is a different question. Based on (Szymańska et al., 2019), we know that SnRK2.4 maintain homeostasis of ROS through regulate the expression of ROS generation related genes, including *RbohD* and *RbohF*. In our data, the expression level of DE genes that are homologs to *RbohD* and *RbohF* are all up-regulated regardless of *SnRK2.4* was up or down regulated by treatment. However, the down-regulation of *SnRK2.4* possibly resulting less protein kinase been produced. Hence, less production of ROS may occur even *RbohD/F* is expressed and ready for activation.

GABA could also link to ROS through photorespiration. In our data, GO and KEGG enrichment illustrated that GABA application appears to interact with photorespiration (GO:0009853) and changed the pathway of carbon fixation in photosynthetic

organisms (ath00710; details of DE genes enriched in GO and KEGG in in Appendix Section C.4). Increased rates of photorespiration commonly occur due to a limitation of CO₂ fixation. (Araújo et al., 2014; Kozaki and Takeba, 1996). These GO and KEGG enrichment results could also be related to GABA's interactions with the photosystem I and II. Vijayakumari and Puthur (2015) found that the activity of photosystem I and II were increased significantly compared to control with 10 and 15 days of 2 mM GABA treatment in *Piper nigrum* hydroponics within the Hoagland's growth medium. The enhanced activity of the photosystem could produce more ROS, NADPH and ATP. As ROS could damage the photosynthetic apparatus, leading to photoinhibition (Kozaki and Takeba, 1996). Photorespiration functions as sink of electrons to prevent electron transport chain over-reduction and ROS accumulation (Wingler et al., 2000). Conversely, GABA itself is also suggested to be involved in reducing ROS production during stress (Ansari et al., 2021).

To summarise, ABA and GABA both have a relationship with ROS. Three of the DE gene candidates that are oppositely regulated by ABA and GABA signalling may be involved in cross-talk ROS signalling. With interactions of ROS production through *Rboh*, ABA and GABA have different approaches to the same destination, and GABA might also have alternative way of producing ROS though enhance activity of the photosystem. Further investigation, the combined treatment of GABA and ABA should be included, along with the GABA and ABA individual treatment and all possible candidate genes involves GABA-ABA interaction should validated on independent samples.

Table 4.3. Potential candidate genes that regulated by both GABA and ABA

Gene ID	logFC		Associated GO	GO description	Arabidopsis homologue	Araport 11 description
	ABA	GABA				
<i>HORVU.MOREX.r2.2HG0084420</i>	-1.300195	1.126652	GO:0000166	Nucleotide binding	<i>AT4G21380</i>	Receptor kinase 3 (ARK3/RK3)
			GO:0004672	Protein kinase activity		
			GO:0004674	Protein serine/threonine kinase activity		
			GO:0005524	ATP binding		
			GO:0005886	Plasma membrane		
			GO:0006468	Protein phosphorylation		
			GO:0016020	Membrane		
			GO:0016021	Integral component of membrane		
			GO:0016301	Kinase activity		
			GO:0016310	Phosphorylation		
			GO:0016740	Transferase activity		
GO:0048544	Recognition of pollen					
<i>HORVU.MOREX.r2.2HG0114190</i>	-1.144407	1.083231	GO:0004672	Protein kinase activity	<i>AT4G23180</i>	Cysteine-rich RLK (receptor-like protein kinase) 10 (CRK10/RLK4)
			GO:0005524	ATP binding		
			GO:0006468	Protein phosphorylation		
			GO:0016020	Membrane		
			GO:0016021	Integral component of membrane		
			GO:0016301	Kinase activity		
GO:0016310	Phosphorylation					
<i>HORVU.MOREX.r2.7HG0565210</i>	-1.694658	1.394383	GO:0000166	Nucleotide binding	<i>AT5G06740</i>	Concanavalin A-like lectin protein kinase family protein (LecRK-S.5)
			GO:0004672	Protein kinase activity		
			GO:0004674	Protein serine/threonine kinase activity		
			GO:0005524	ATP binding		
			GO:0006468	Protein phosphorylation		
			GO:0016020	Membrane		
			GO:0016021	Integral component of membrane		
			GO:0016301	Kinase activity		
			GO:0016310	Phosphorylation		
GO:0016740	Transferase activity					
GO:0030246	Carbohydrate binding					

Table 4.4. Summary of DE gene commonly induced by GABA and ABA in MAPK signaling pathway

Gene ID	logFC		Associated GO	GO description	Arabidopsis homologue	Araport 11 description
	ABA	GABA				
<i>HORVU.MOREX.r2.1HG0045440</i>	3.2155	-2.6996	GO:0004674	Protein serine/threonine kinase activity	<i>AT1G10940</i>	SNF1-related protein kinase 2. (SnRK2.4)
			GO:0016301	Kinase activity		
			GO:0006468	Protein phosphorylation		
			GO:0016310	Phosphorylation		
<i>HORVU.MOREX.r2.2HG0154390</i>	1.8517	2.4972	GO:0030170	Pyridoxal phosphate binding	<i>AT4G11280</i>	1-aminocyclopropane-1-carboxylic acid (acc) synthase 6 (ACS6)
<i>HORVU.MOREX.r2.7HG0555000</i>	-1.1415	-1.7735	GO:0005576	Extracellular region	<i>AT4G33720</i>	CAP (Cysteine-rich secretory proteins, Antigen 5, and Pathogenesis-related 1 protein) superfamily protein (ATCAPE3)

*Note: Associated gene ontology (GO) of DE genes were obtained at least 4 levels away from the root ontology categories (i.e. biological process (BP), cellular component (CC) and molecular function (MF)).

4.3 Material and Methods

4.3.1 Plants material and RNA-Seq data

Barley (*Hordeum vulgare* cv. Barke) seed (Saatzucht J. Breun GmbH & Co. KG) were germinated on filter paper 5-6 days and then planted in the hydroponics system with half-strength Hoagland's solution (Conn et al., 2013; Hoagland and Arnon, 1950) and cultivated in a growth cabinet (Percival Scientific, AR-60L) at 26/16 °C with $60 \pm 5\%$ relative humidity and 12/12 hours day/night cycle with $250 \text{ m}^{-2}\text{s}^{-1}$ photo flux density on LED light source.

About 10 to 12-day-old sample plants were sprayed with $50 \mu\text{M}$ \pm ABA or 5 mM GABA in deionized water containing 0.1% v/v Triton X-100 or mock treatment (deionized water with Triton X-100) with 4 replicates in each group and sampling 4 hours after spray. The sample preparation of RNA sequencing followed the instructions from Schäfer et al. (2018). The detached leaf samples were peeled as described in Shen et al. (2015) to prepare isolated epidermal peels. RNA was extracted from 20 epidermal peels per sample using the NucleoSpin[®] RNA Plant Kit (Macherey-Nagel, Dueren, Germany) and treated with RNase-free DNase (New England Biolabs, Ipswich, MA, USA). The sequencing library was constructed with a TruSeq RNA Sample Prep Kit v2 (Illumina, San Diego, CA, USA) and sequenced on a HiSeq 3000 (Illumina) resulting in 76bp paired-end reads. All plant material, RNA extraction and GCSC enriched RNA-Seq libraries were prepared by collaborator Johannes Herrmann from Germany.

4.3.2 Bioinformatics workflow

To process raw sequencing data to gene counts, the following steps were performed after the quality check with *FastQC* (version 0.11.8; <http://www.bioinformatics.babraham.ac.uk/projects/fastqc>):

1. *Trimmomatic* (version 0.39; Bolger et al. 2014) was used to remove adaptor sequence.
2. Trimmed reads were aligned to the barley reference genome (Morex v2; Mascher 2019) using *STAR* (version 2.7.3a; Dobin et al. 2012).
3. The number of reads aligned to each gene were summarised by *featureCounts* in *Subread* (version 1.6.4; Liao et al. 2013) with the barley (Morex v2; Mascher 2019) genome annotation.

All the above steps were managed through *Snakemake* (Köster and Rahmann, 2012) and ran on "Phoenix", the University of Adelaide's High Performance Compute (HPC) Service.

Following read counting, differential gene expression analysis was performed, followed by functional and pathway analysis using R (version 4.1.0). To identify the differentially expressed genes, *edgeR* was used. Gene Ontology analysis was performed with R packages *GO.db* and *annotate*, while pathway analysis was conducted with *KEGGREST* to determine treatment specific enrichment of gene function and pathways (Carlson, 2021; Gentleman, 2021; Robinson et al., 2009; Tenenbaum and Maintainer, 2021). Detailed parameter settings are available at Snakemake workflow and R code at <https://github.com/CharlotteSai/BarleyGCRNASeq>. R session information is available in the appendix C, section C.1.

References

- A. Agresti. *Categorical data analysis*, volume 482. John Wiley & Sons, 2003.
- M. I. Ansari, S. U. Jalil, S. A. Ansari, and M. Hasanuzzaman. GABA shunt: a key-player in mitigation of ROS during stress. *Plant Growth Regulation*, 94(2):131–149, 2021.
- W. L. Araújo, A. Nunes-Nesi, and A. R. Fernie. On the role of plant mitochondrial metabolism and its impact on photosynthesis in both optimal and sub-optimal growth conditions. *Photosynthesis Research*, 119(1):141–156, 2014.
- O. Askari-Khorsgani, F. Flores, and M. Pessaraki. Plant signaling pathways involved in stomatal movement under drought stress conditions. *Advances in Plants & Agriculture Research*, 8(3):290–297, 2018.
- H. Bauer, P. Ache, S. Lautner, J. Fromm, W. Hartung, K. A. Al-Rasheid, S. Sonnewald, U. Sonnewald, S. Kneitz, N. Lachmann, R. R. Mendel, F. Bittner, A. M. Hetherington, and R. Hedrich. The stomatal response to reduced relative humidity requires guard cell-autonomous ABA synthesis. *Current Biology*, 23:53–57, 2013.
- A. M. Bolger, M. Lohse, and B. Usadel. Trimmomatic: a flexible trimmer for Illumina sequence data. *Bioinformatics*, 30(15):2114–2120, 2014.
- N. Bouché, B. Lacombe, and H. Fromm. GABA signaling: a conserved and ubiquitous mechanism. *Trends in Cell Biology*, 13(12):607–610, 2003.
- M. Boudsocq, H. Barbier-Brygoo, and C. Laurière. Identification of nine sucrose nonfermenting 1-related protein kinases 2 activated by hyperosmotic and saline stresses in *Arabidopsis thaliana*. *Journal of Biological Chemistry*, 279(40):41758–41766, 2004.
- Y. Boursiac, S. Léran, C. Corratgé-Faillie, A. Gojon, G. Krouk, and B. Lacombe. ABA transport and transporters. *Trends in Plant Science*, 18(6):325–333, 2013.
- K. Bouwmeester and F. Govers. Arabidopsis L-type lectin receptor kinases: phylogeny, classification, and expression profiles. *Journal of Experimental Botany*, 60(15):4383–4396, 2009.
- A. W. Bown and B. J. Shelp. Plant GABA: Not just a metabolite. *Trends in Plant Science*, 21(10):811–813, 2016.
- C. Camacho, G. Coulouris, V. Avagyan, N. Ma, J. Papadopoulos, K. Bealer, and T. L. Madden. BLAST+: architecture and applications. *BMC Bioinformatics*, 10(1):1–9, 2009.

- M. Carlson. *GO.db: A set of annotation maps describing the entire Gene Ontology*, 2021.
- K. Chen, G.-J. Li, R. A. Bressan, C.-P. Song, J.-K. Zhu, and Y. Zhao. Abscisic acid dynamics, signaling, and functions in plants. *Journal of Integrative Plant Biology*, 62(1):25–54, 2020.
- S. J. Conn, B. Hocking, M. Dayod, B. Xu, A. Athman, S. Henderson, L. Aukett, V. Conn, M. K. Shearer, S. Fuentes, S. D. Tyerman, and M. Gilliam. Protocol: optimising hydroponic growth systems for nutritional and physiological analysis of *Arabidopsis thaliana* and other plants. *Plant Methods*, 9(1):1–11, 2013.
- V. Cotellet and N. Leonhardt. ABA signaling in guard cells. *Advances in Botanical Research*, 92:115–170, 2019.
- A. De Angeli, J. Zhang, S. Meyer, and E. Martinoia. AtALMT9 is a malate-activated vacuolar chloride channel required for stomatal opening in *Arabidopsis*. *Nature Communications*, 4(1):1–10, 2013.
- B. Derakhshani, H. Jafary, B. Maleki Zanjani, K. Hasanpur, K. Mishina, T. Tanaka, Y. Kawahara, and Y. Oono. Combined QTL mapping and RNA-Seq profiling reveals candidate genes associated with cadmium tolerance in barley. *Plos one*, 15(4): e0230820, 2020.
- A. Dobin, C. A. Davis, F. Schlesinger, J. Drenkow, C. Zaleski, S. Jha, P. Batut, M. Chaisson, and T. R. Gingeras. STAR: ultrafast universal RNA-seq aligner. *Bioinformatics*, 29(1):15–21, 2012.
- L. Du and Z. Chen. Identification of genes encoding receptor-like protein kinases as possible targets of pathogen- and salicylic acid-induced WRKY DNA-binding proteins in *Arabidopsis*. *The Plant Journal*, 24(6):837–847, 2000.
- C. Eisenach, U. Baetz, N. V. Huck, J. Zhang, A. De Angeli, G. J. Beckers, and E. Martinoia. ABA-induced stomatal closure involves ALMT4, a phosphorylation-dependent vacuolar anion channel of *Arabidopsis*. *The Plant Cell*, 29(10):2552–2569, 2017.
- H. Fujii, V. Chinnusamy, A. Rodrigues, S. Rubio, R. Antoni, S. Y. Park, S. R. Cutler, J. Sheen, P. L. Rodriguez, and J. K. Zhu. *In vitro* reconstitution of an abscisic acid signalling pathway. *Nature*, 462(7273):660–664, 2009.
- R. Gentleman. *annotate: Annotation for microarrays*, 2021.
- D. R. Hoagland and D. I. Arnon. The water-culture method for growing plants without soil. *Circular. California Agricultural Experiment Station*, 347(2nd edit):32, 1950.

- P.-K. Hsu, G. Dubeaux, Y. Takahashi, and J. I. Schroeder. Signaling mechanisms in abscisic acid-mediated stomatal closure. *The Plant Journal*, 105(2):307–321, 2021.
- Y. Huang, L. Li, K. P. Smith, and G. J. Muehlbauer. Differential transcriptomic responses to *Fusarium graminearum* infection in two barley quantitative trait loci associated with *Fusarium* head blight resistance. *BMC genomics*, 17(1):1–16, 2016.
- D. Imes, P. Mumm, J. Böhm, K. A. S. Al-Rasheid, I. Marten, D. Geiger, and R. Hedrich. Open stomata 1 (OST1) kinase controls R-type anion channel QUAC1 in Arabidopsis guard cells. *The Plant Journal*, 74(3):372–382, 2013.
- J. Köster and S. Rahmann. Snakemake – a scalable bioinformatics workflow engine. *Bioinformatics*, 28(19):2520–2522, 2012.
- A. Kozaki and G. Takeba. Photorespiration protects C3 plants from photooxidation. *Nature*, 384(6609):557–560, 1996.
- E. Krzywińska, M. Bucholc, A. Kulik, A. Ciesielski, M. Lichocka, J. Dębski, A. Ludwików, M. Dadlez, P. L. Rodriguez, and G. Dobrowolska. Phosphatase ABI1 and okadaic acid-sensitive phosphoprotein phosphatases inhibit salt stress-activated SnRK2.4 kinase. *BMC Plant Biology*, 16(1):1–12, 2016.
- J. M. Kwak, I. C. Mori, Z.-M. Pei, N. Leonhardt, M. A. Torres, J. L. Dangel, R. E. Bloom, S. Bodde, J. D. Jones, and J. I. Schroeder. NADPH oxidase AtrbohD and AtrbohF genes function in ROS-dependent ABA signaling in Arabidopsis. *The EMBO Journal*, 22(11):2623–2633, 2003.
- N. Leonhardt, J. M. Kwak, N. Robert, D. Waner, G. Leonhardt, and J. I. Schroeder. Microarray expression analyses of arabidopsis guard cells and isolation of a recessive abscisic acid hypersensitive protein phosphatase 2C mutant. *The Plant Cell*, 16(3):596–615, 2004.
- Y. Liao, G. K. Smyth, and W. Shi. featureCounts: an efficient general purpose program for assigning sequence reads to genomic features. *Bioinformatics*, 30(7):923–930, 2013.
- M. Mascher. Pseudomolecules and annotation of the second version of the reference genome sequence assembly of barley cv. Morex [Morex V2], 2019.
- F. McLoughlin, C. S. Galvan-Ampudia, M. M. Julkowska, L. Caarls, D. van der Does, C. Laurière, T. Munnik, M. A. Haring, and C. Testerink. The SNF1-related protein kinases SnRK2.4 and SnRK2.10 are involved in maintenance of root system architecture during salt stress. *The Plant Journal*, 72(3):436–449, 2012.

- S. Meyer, P. Mumm, D. Imes, A. Endler, B. Weder, K. A. Al-Rasheid, D. Geiger, I. Marten, E. Martinoia, and R. Hedrich. AtALMT12 represents an R-type anion channel required for stomatal movement in Arabidopsis guard cells. *The Plant Journal*, 63(6): 1054–1062, 2010.
- U. Nagalakshmi, Z. Wang, K. Waern, C. Shou, D. Raha, M. Gerstein, and M. Snyder. The transcriptional landscape of the yeast genome defined by rna sequencing. *Science*, 320(5881):1344–1349, 2008.
- M. Pastuglia, R. Swarup, A. Rocher, P. Saindrenan, D. Roby, C. Dumas, and J. Cock. Comparison of the expression patterns of two small gene families of S gene family receptor kinase genes during the defence response in *Brassica oleracea* and *Arabidopsis thaliana*. *Gene*, 282(1):215–225, 2002.
- E. H. Quezada, G. X. García, M. K. Arthikala, G. Melappa, M. Lara, and K. Nanjareddy. Cysteine-rich receptor-like kinase gene family identification in the phaseolus genome and comparative analysis of their expression profiles specific to mycorrhizal and rhizobial symbiosis. *Genes*, 10(1):59, 2019.
- S. A. Ramesh, S. D. Tyerman, B. Xu, J. Bose, S. Kaur, V. Conn, P. Domingos, S. Ullah, S. Wege, S. Shabala, J. A. Feijó, P. R. Ryan, and M. Gilliam. GABA signalling modulates plant growth by directly regulating the activity of plant-specific anion transporters. *Nature Communications*, 6(1):1–10, 2015.
- S. A. Ramesh, S. D. Tyerman, M. Gilliam, and B. Xu. γ -aminobutyric acid (GABA) signalling in plants. *Cellular and Molecular Life Sciences*, 74(9):1577–1603, 2016.
- M. D. Robinson, D. J. McCarthy, and G. K. Smyth. edgeR: a Bioconductor package for differential expression analysis of digital gene expression data. *Bioinformatics*, 26(1): 139–140, 2009.
- M. Ruschhaupt, J. Mergner, S. Mucha, M. Papacek, I. Doch, S. V. Tischer, D. Hemmler, D. Chiasson, K. H. Edel, J. Kudla, P. Schmitt-Kopplin, B. Kuster, and E. Grill. Rebuilding core abscisic acid signaling pathways of Arabidopsis in yeast. *The EMBO Journal*, 38(17):e101859, 2019.
- N. Schäfer, T. Maierhofer, J. Herrmann, M. E. Jørgensen, C. Lind, K. von Meyer, S. Lautner, J. Fromm, M. Felder, A. M. Hetherington, P. Ache, D. Geiger, and R. Hedrich. A tandem amino acid residue motif in guard cell SLAC1 anion channel of grasses allows for the control of stomatal aperture by nitrate. *Current Biology*, 28(9):1370 – 1379, 2018.

- S. H. Schwartz, X. Qin, and J. A. Zeevaart. Elucidation of the indirect pathway of abscisic acid biosynthesis by mutants, genes, and enzymes. *Plant physiology*, 131(4): 1591–1601, 2003.
- L. Shen, P. Sun, V. C. Bonnell, K. J. Edwards, A. M. Hetherington, M. R. McAinsh, and M. R. Roberts. Measuring stress signaling responses of stomata in isolated epidermis of graminaceous species. *Frontiers in plant science*, 6:533, 2015.
- M. Sierla, C. Waszczak, T. Vahisalu, and J. Kangasjärvi. Reactive oxygen species in the regulation of stomatal movements. *Plant Physiology*, 171(3):1569–1580, 2016.
- C. Sirichandra, D. Gu, H. C. Hu, M. Davanture, S. Lee, M. Djaoui, B. Valot, M. Zivy, J. Leung, S. Merlot, and J. M. Kwak. Phosphorylation of the Arabidopsis AtrbohF NADPH oxidase by OST1 protein kinase. *FEBS Letters*, 583(18):2982–2986, 2009.
- C. Sirichandra, M. Davanture, B. E. Turk, M. Zivy, B. Valot, J. Leung, and S. Merlot. The arabidopsis ABA-activated kinase OST1 phosphorylates the bZIP transcription factor ABF3 and creates a 14-3-3 binding site involved in its turnover. *PloS one*, 5(11):e13935, 2010.
- F. F. Soon, L. M. Ng, X. E. Zhou, G. M. West, A. Kovach, M. H. E. Tan, K. M. S. Powell, Y. He, Y. Xu, M. J. Chalmers, J. S. Brunzelle, H. Zhang, H. Yang, H. Jiang, J. Li, E. L. Yong, S. Cutler, J. K. Zhu, P. R. Griffin, K. Melcher, and H. E. Xu. Molecular mimicry regulates ABA signaling by SnRK2 kinases and PP2C phosphatases. *Science*, 335(6064):85–88, 2012.
- K. P. Szymańska, L. Polkowska-Kowalczyk, M. Lichočka, J. Maszkowska, and G. Dobrowolska. SNF1-related protein kinases SnRK2.4 and SnRK2.10 modulate ROS homeostasis in plant response to salt stress. *International Journal of Molecular Sciences*, 20(1):143, 2019.
- Y. Takahashi, Y. Ebisu, and K.-i. Shimazaki. Reconstitution of abscisic acid signaling from the receptor to DNA via bHLH transcription factors. *Plant physiology*, 174(2): 815–822, 2017.
- T. Tanaka, G. Ishikawa, E. Ogiso-Tanaka, T. Yanagisawa, and K. Sato. Development of genome-wide SNP markers for barley via reference-based RNA-Seq analysis. *Frontiers in plant science*, 10:577, 2019.
- D. Tenenbaum and B. P. Maintainer. *KEGGREST: Client-side REST access to the Kyoto Encyclopedia of Genes and Genomes (KEGG)*, 2021.

- M. D. Theveniau, D. Arnaud, T. Y. Huang, G. J. C. Lin, W. Y. Chen, Y. C. Lin, and L. Zimmerli. The Arabidopsis lectin receptor kinase LecRK-V.5 represses stomatal immunity induced by *Pseudomonas syringae* pv. tomato DC3000. *PLoS Pathogens*, 8(2):e1002513, 2012.
- H. Tombuloglu, G. Kekec, M. S. Sakcali, and T. Unver. Transcriptome-wide identification of R2R3-MYB transcription factors in barley with their boron responsive expression analysis. *Molecular genetics and genomics*, 288(3):141–155, 2013.
- T. Umezawa, N. Sugiyama, M. Mizoguchi, S. Hayashi, F. Myouga, K. Yamaguchi-Shinozaki, Y. Ishihama, T. Hirayama, and K. Shinozaki. Type 2C protein phosphatases directly regulate abscisic acid-activated protein kinases in Arabidopsis. *Proceedings of the National Academy of Sciences*, 106(41):17588–17593, 2009.
- K. Vijayakumari and J. T. Puthur. γ -aminobutyric acid (GABA) priming enhances the osmotic stress tolerance in *Piper nigrum* linn. plants subjected to PEG-induced stress. *Plant Growth Regulation*, 78(1):57–67, 2015.
- F. Vlad, S. Rubio, A. Rodrigues, C. Sirichandra, C. Belin, N. Robert, J. Leung, P. L. Rodriguez, C. Laurière, and S. Merlot. Protein phosphatases 2C regulate the activation of the SNF1-related kinase OST1 by abscisic acid in Arabidopsis. *The Plant Cell*, 21(10):3170–3184, 2009.
- B. T. Wilhelm, S. Marguerat, S. Watt, F. Schubert, V. Wood, I. Goodhead, C. J. Penkett, J. Rogers, and J. Bähler. Dynamic repertoire of a eukaryotic transcriptome surveyed at single-nucleotide resolution. *Nature*, 453(7199):1239–1243, 2008.
- A. Wingler, P. J. Lea, W. P. Quick, and R. C. Leegood. Photorespiration: metabolic pathways and their role in stress protection. *Philosophical Transactions of the Royal Society of London. Series B: Biological Sciences*, 355(1402):1517–1529, 2000.
- M. Wrzaczek, M. Brosché, J. Salojärvi, S. Kangasjärvi, N. Idänheimo, S. Mersmann, S. Robatzek, S. Karpiński, B. Karpińska, and J. Kangasjärvi. Transcriptional regulation of the CRK/DUF26 group of receptor-like protein kinases by ozone and plant hormones in arabidopsis. *BMC Plant Biology*, 10(1):95, 2010.
- L. Wu, X. Gao, H. Li, Z. Wu, Y. Duan, W. Liu, and F. Li. Transcription profiling analysis of genes and pathomechanisms underlying the defense response against Tobacco Etch Virus infection in *Arabidopsis thaliana*. *Russian Journal of Plant Physiology*, 64(6):930–938, 2017.

CHAPTER 4. GUARD CELL COMPLEX SPECIFIC TRANSCRIPTIONAL RESPONSE
OF BARLEY TO GABA

B. Xu, Y. Long, X. Feng, X. Zhu, N. Sai, L. Chirkova, A. Betts, J. Herrmann, E. J. Edwards, M. Okamoto, R. Hedrich, and M. Gilliam. GABA signalling modulates stomatal opening to enhance plant water use efficiency and drought resilience. *Nature Communications*, 12(1):1–15, 2021.

S. Zhang and D. F. Klessig. MAPK cascades in plant defense signaling. *Trends in Plant Science*, 6(11):520–527, 2001.

TRANSCRIPTIONAL PROFILING OF GABA DEFICIENT *Arabidopsis thaliana*

External GABA application antagonises stomatal movement in both barley and *Arabidopsis*; in contrast, GABA deficiency *in planta* can disrupt stomatal pore regulation (Chapter 3; Xu et al., 2021). Glutamic acid decarboxylase (GAD), the key enzyme responsible for synthesizing GABA from glutamate, has five homologues in *Arabidopsis* with organ specific expression. *GAD1* is the main isoform expressed in roots whereas *GAD2* is detectable in almost all organs (Bouché et al., 2004; Turano and Fang, 1998; Zik et al., 1998). *GAD3* and *GAD5* are detectable in siliques and flowers respectively (Miyashita and Good, 2008). *GAD4*, on the other hand, has weak expression in roots and shoots, but is detectable in siliques and flowers (Mekonnen et al., 2016; Scholz et al., 2015).

Lost function of one or more *GAD*(s) can cause GABA synthesis disruption in various tissue with distinct phenotypes (Bouché et al., 2004; Deng et al., 2020; Mekonnen et al., 2016; Miyashita and Good, 2008). The *gad1* mutant via T-DNA insertion drastically reduced concentrations of GABA in roots and prevents GABA accumulation in response to heat stress (Bouché et al., 2004). However, the mutation did not show visible morphological defects and or developmental abnormalities under control and hypoxia stress (Bouché et al., 2004; Miyashita and Good, 2008). With combined mutation of *GAD1* and *GAD2* (i.e. *gad1/2*), the GABA content was dramatically reduced in roots and shoots and had an enlarged stomatal aperture phenotype with higher stomatal density which contribute to drought oversensitive phenotype (Mekonnen et al., 2016). Beyond *gad1/2*, the contributed mutant *gad1245* which has been introduced with

additional mutation of *GAD4* and *GAD5* showed further decreased endogenous GABA concentration and enhanced susceptibility of *Pseudomonas syringae*, but exhibit no growth defect (Deng et al., 2020).

Recently, Xu et al. (2021) determined that *Arabidopsis gad2-1* presented an enlarged stomatal aperture compared to wildtype, which leads to lower intrinsic water use efficiency (iWUE) to become drought sensitive. Interestingly, the enlarged stomatal aperture phenotype of *gad2* knockouts does not occur in *gad1* and *gad1245*, which have wildtype like stomatal apertures (Feng, 2021). As mutation of the GADs does not always result in an obvious macro phenotype (e.g. stomatal aperture), in this chapter, two of the aspects around GABA deficient mutants were explored. First, the transcriptomic changes corresponding to GABA depletion when knocking out different *GAD* homologs through T-DNA insertion was determined. The transcriptional profiling of *gad1*, *gad2-1* and *gad1245* was investigated when compared to wildtype (Col-0). Second, the transcriptional changes that could reveal the possible reasons that *gad1245* presents a wildtype-like stomatal phenotype rather than being more *gad2-1*-like. The comparison between wildtype (Col-0), *gad2* and *gad1245* was employed.

5.1 Results

5.1.1 Data quality and post alignment processing

An average of 22 million trimmed FASTQ reads per sample was obtained with a mean sequence quality score per base higher than 30 across all bases. Each sample had more than 88% of the reads uniquely mapped to the Arabidopsis TAIR10 genome with at least 12 million reads in total. Detailed reports of reads quality and mapping are available on GitHub repository (<https://github.com/CharlotteSai/ArabidopsisSubmergence>). After filtering low expressed genes (i.e cpm > 0.55 in at least 3 samples), 18,431 genes were passed to differential gene expression analysis. The multidimensional scaling plot (MDS) showed sample replicates were clustered closely except wildtype Col-0 (Figure 5.1). The Col-0 separates from GABA mutants on biological coefficient of variation

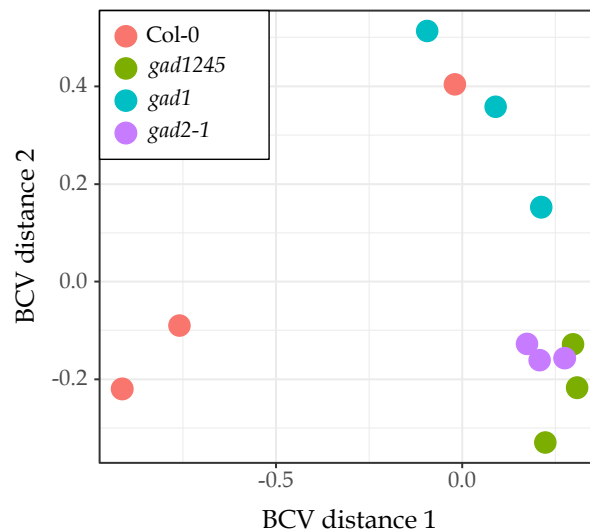


Figure 5.1. Multidimensional scaling plot of distances between gene expression profiles. The separation distance is based on the typical log₂ fold changes between the samples. Samples are colour coded by genotype.

(BCV) distance 1, except one Col-0 sample, while the three mutants separate along BCV distance 2.

5.1.2 Differential gene expression analysis

To obtain mutant specific differentially expressed genes (DE genes), all selected mutants were compared to Col-0 as a baseline control. Additionally, to investigate the difference of *gad1245* beyond the contribution from the *gad2-1* mutation, the gene

expression difference in *gad1245* compared to *gad2-1* was also included in this analysis. Filtered gene counts were fitted in a negative binomial generalized log-linear model after estimating dispersion. The full list of DE genes is available on GitHub (<https://github.com/CharlotteSai/ArabidopsisSubmergence>).

With the threshold set to a p -value ≤ 0.05 and $\log_2\text{FC} \geq 1$, 659, 1022, and 1139 DE genes were found in *gad1*, *gad2-1*, *gad1245* compared to Col-0, respectively; and 21 DE genes in *gad1245* compared to *gad2-1*. All results were obtained using a quasi-likelihood (QL) F-test and visualised in Figure 5.2. Overall, the number of DE genes were consistent with the degree of sample separation observed in Figure 5.1; the further the distance between clusters, the more DE genes were found.

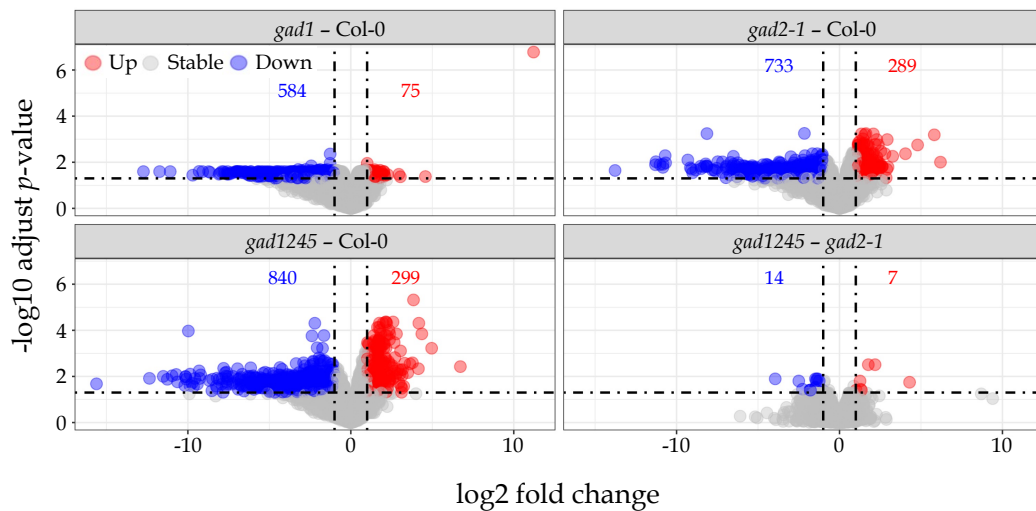


Figure 5.2. Volcano plot of differentially expressed genes (DE genes) in GABA deficient mutants compared to baseline control. The horizontal line represents the p value of $-\log_{10}(0.05)$ and vertical lines indicate a \log_2 fold change of -1 and 1, the parameters chosen to define those genes considered significantly DE. Data points coloured in red and blue are DE genes that were counted as up or down regulated compared to Col-0 or *gad2-1*.

To reveal if there were transcriptional clues as to why *gad1245* had a more wildtype-like stomatal aperture than *gad2-1*, the DE genes between Col-0, *gad2-1* and *gad1245* were compared to each other. According to stomatal conductance assay from Feng (2021) and stomatal aperture assay from Mekonnen et al. (2016), only *gad2* and *gad12* mutants showed higher stomatal conductance when *gad1* and *gad1245* presented wildtype-like behavior, which indicating that the additional *GAD4* and *GAD5* are more likely to be responsible for wildtype-like stomata phenotype. Additionally, *GAD1* has not changed its expression pattern cross the genotype (Figure 5.3) and less expressed in leaves

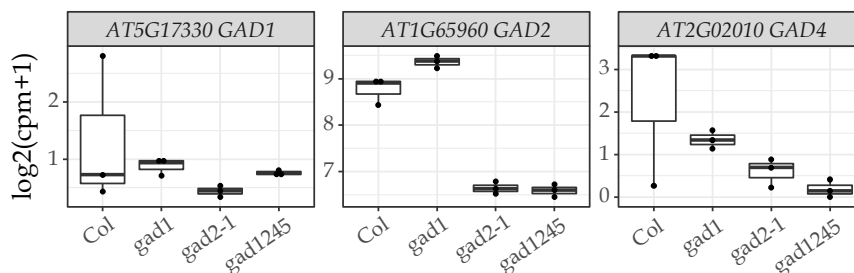


Figure 5.3. The expression level of GADs in Col-0, *gad1* *gad2-1* and *gad1245*. The detected gene expression level presented in log2 counts per million (cpm) with 3 biological replicates. The cpm value had 1 added to all values to avoid any sample equal to zero before log transformation.

whereas GAD2 is the major isoform expressed in shoots (Scholz et al., 2015). Hence, *gad1* was omitted from the comparison. As more mutations were introduced, more down-regulated DE genes were found among each comparison. Among comparisons of *gad2-1* and *gad1245* with Col-0, or each other, 2 DE genes were commonly shared between the 3 comparisons, while 368, 478 and 4 DE genes were uniquely obtained in *gad2-1* compared to Col-0, *gad1245* to Col-0 and *gad1245* to *gad2-1* respectively (Figure 5.4). Large proportions of DE genes were shared between the comparison *gad2-1* to Col-0 and *gad1245* to Col-0 as they had much more similar gene expression profiles compared to Col-0, as shown in Figure 5.1. As can be seen few DE genes were shared between either *gad2-1*-Col-0 or *gad1245*-Col-0 and *gad1245*-*gad2-1*.

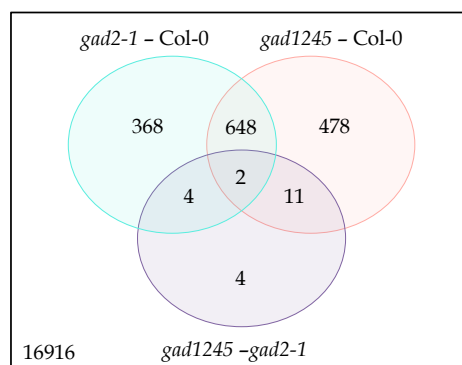
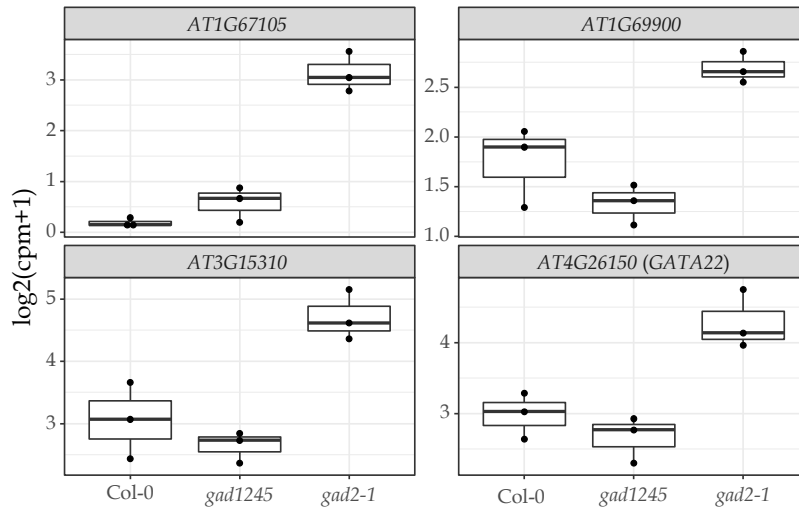


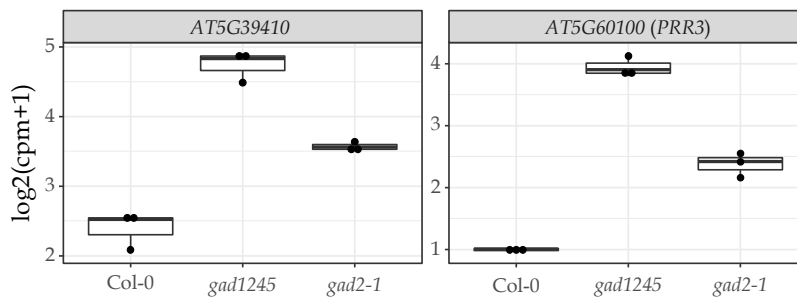
Figure 5.4. Number of shared DE genes with the *gad2-1* and *gad1245* mutations compared to their baseline control. Differentially expressed (DE) genes from the comparison of *gad2-1* to Col-0, *gad1245* to Col-0 and *gad1245* to *gad2-1* were compared to obtain the shared number of DE genes between comparisons.

The DE genes between *gad2-1*, *gad1245* and Col-0 feature several shared genes which are interesting in regard to their expression level (Figure 5.5). There are 4 genes presented as DE genes in the comparison of *gad2-1*-Col-0 and *gad1245*-*gad2-1*, but these are absent in *gad1245*-Col-0 (Figure 5.5(a)). In other words, the expression level

(a) Genes in *gad1245* that are returned to Col-0-like expression



(b) DE genes shared in *gad2-1* and *gad1245* compare to Col-0 or each other



(c) Genes in *gad1245* that are expressed differently to both Col-0 and *gad2-1*

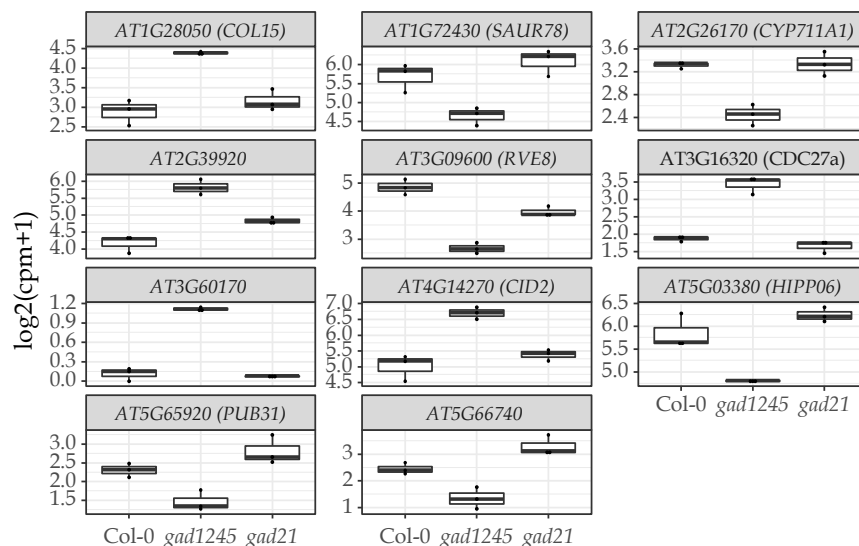


Figure 5.5. The expression level of selected DE genes in Col-0, *gad2-1* and *gad1245*. The expression level presented in log₂ counts per million (cpm) with 3 biological replicates. The cpm value had 1 added to all values to avoid any sample equal to zero before log transformation.

of *AT1G67105*, *AT1G69900*, *AT3G15310* and *AT4G26150* in *gad1245* are similar to that in the Col-0, but are different from that in *gad2-1*. *AT5G39410* and *AT5G60100* presented as DE genes in all three of the comparison and had highest expression level in *gad1245*, which showed a trend that the expression level increases when more *gad* mutations were introduced (Figure 5.5(b)). Another 11 genes are DE genes in the comparison of *gad1245*-Col-0 and *gad1245-gad2-1*, but not in *gad2-1*-Col-0 (Figure 5.5(c)). The expression level of these genes in *gad1245* are different from both Col-0 and *gad2-1*: 5 DE genes are up-regulated while others are down-regulated in *gad1245*.

5.1.3 Gene Ontology (GO) enrichment

To understand which Gene Ontologies (GOs) were significantly changed by an introduced mutation, DE genes from the comparisons between mutants and Col-0 were split into up and down-regulated genes to test the GO over-representation (i.e. enrichment). As more down-regulated DE genes were introduced with more mutations, most of the over-represented GO terms were enriched through down-regulated genes (Figure 5.6). The majority of the enriched GO terms belonged to biological process (BP). *gad1245* had the most GO enrichments compared to *gad1* and *gad2-1*, and the enrichment pattern of *gad1245*-Col-0 is more like *gad2-1* rather than *gad1*. As seen in Table 5.1, stress defence response and amino acid metabolism related GO functions were commonly enriched as more *gad* mutations were introduced. Three GO terms were enriched in both up and down-regulated DE genes in *gad1245*-Col-0: response to abscisic acid (GO:0009737); response to lipid (GO:0033993) and response to alcohol (GO:0097305). Lots of GO terms that enriched by down-regulated DE gene were stress associated: such as a series of jasmonic acid related regulation, response and signalling (GO:0050832, GO:0009753, GO:0009867, GO:2000022), defense response to fungus (GO:0050832) and response to salt stress (GO:0009651).

Interestingly, some GO terms present as enriched by the DE genes that had opposite regulation across mutants. For instance, cold acclimation (GO:0009631) was both enriched in *gad1245*-Col-0 and *gad1*-Col-0 by DE genes in the opposite direction. 7/10 DE genes from *gad1245*-Col-0 that were associated with cold acclimation (GO:0009631) were up-regulated including *AT1G29395* (*COR413IM1*), whereas all 10 of the enriched DE genes were down-regulated in *gad1* (Figure 5.7). *gad2-1* had similar DE genes enriched as *gad1245*, but not enough number of DE genes enriched to make this GO term as an over-representative GO (i.e. a significant enriched GO term).

Table 5.1. Shared GO terms between *gad1*, *gad2-1* and *gad1245* compared to Col-0

GO accession	Description	Ontology*	DE gene ratio**		
			<i>gad1</i>	<i>gad2-1</i>	<i>gad1245</i>
GO:0009737	Response to abscisic acid	BP	53/603	36/603	(21+50)/603
GO:0033993	Response to lipid	BP	74/966	76/966	(29+95)/966
GO:0097305	Response to alcohol	BP	53/610		(21+50)/610
GO:0009631	Cold acclimation	BP	10/54		7/54
GO:0036293	Response to decreased oxygen levels	BP	24/269	13/269	33/269
GO:0036294	Cellular response to decreased oxygen levels	BP	23/241	13/241	33/241
GO:0071453	Cellular response to oxygen levels	BP	23/241	13/241	33/241
GO:0071456	Cellular response to hypoxia	BP	22/239	13/239	33/239
GO:0000162	Tryptophan biosynthetic process	BP		7/27	8/27
GO:0006568	Tryptophan metabolic process	BP		8/37	10/37
GO:0006576	Cellular biogenic amine metabolic process	BP		10/70	13/70
GO:0006586	Indolalkylamine metabolic process	BP		8/37	10/37
GO:0008652	Cellular amino acid biosynthetic process	BP		20/233	26/233
GO:0009072	Aromatic amino acid family metabolic process	BP		11/84	18/84
GO:0009309	Amine biosynthetic process	BP		9/50	10/50
GO:0009627	Systemic acquired resistance	BP		12/84	14/84
GO:0009651	Response to salt stress	BP	36/470	35/470	42/470
GO:0009753	Response to jasmonic acid	BP	21/196	42/196	48/196
GO:0009867	Jasmonic acid mediated signaling pathway	BP		14/98	17/98
GO:0016054	Organic acid catabolic process	BP	14/167	17/167	18/167
GO:0019752	Carboxylic acid metabolic process	BP		65/1049	75/1049
GO:0042401	Cellular biogenic amine biosynthetic process	BP		9/50	10/50
GO:0042430	Indole-containing compound metabolic process	BP		13/79	17/79
GO:0042435	Indole-containing compound biosynthetic process	BP		10/55	14/55
GO:0042542	Response to hydrogen peroxide	BP	10/69	11/69	
GO:0043436	Oxoacid metabolic process	BP		74/1179	86/1179
GO:0044106	Cellular amine metabolic process	BP		11/81	14/81
GO:0046219	Indolalkylamine biosynthetic process	BP		7/27	8/27
GO:0050832	Defense response to fungus	BP	30/562	36/562	47/562
GO:0070542	Response to fatty acid	BP	21/200	42/200	48/200
GO:0071395	Cellular response to jasmonic acid stimulus	BP		14/103	18/103
GO:0071398	Cellular response to fatty acid	BP		14/107	18/107
GO:1901605	Alpha-amino acid metabolic process	BP		27/298	35/298
GO:1901607	Alpha-amino acid biosynthetic process	BP		18/191	24/191
GO:1901701	Cellular response to oxygen-containing compound	BP	35/741	44/741	54/741
GO:2000022	Regulation of jasmonic acid mediated signaling pathway	BP		10/41	13/41
GO:0099503	Secretory vesicle	CC		20/173	24/173
GO:0016844	Strictosidine synthase activity	MF	5/15	6/15	

Note: * GO classifications are in the category of biological process (BP), cellular component (CC) and molecular function (MF). ** DE gene ratio is presented by number of DE genes present in a GO term divided by the total number of genes present within the GO term. The colour indicates whether the DE gene enriched GO term is up-regulated (red) or down-regulated (blue).

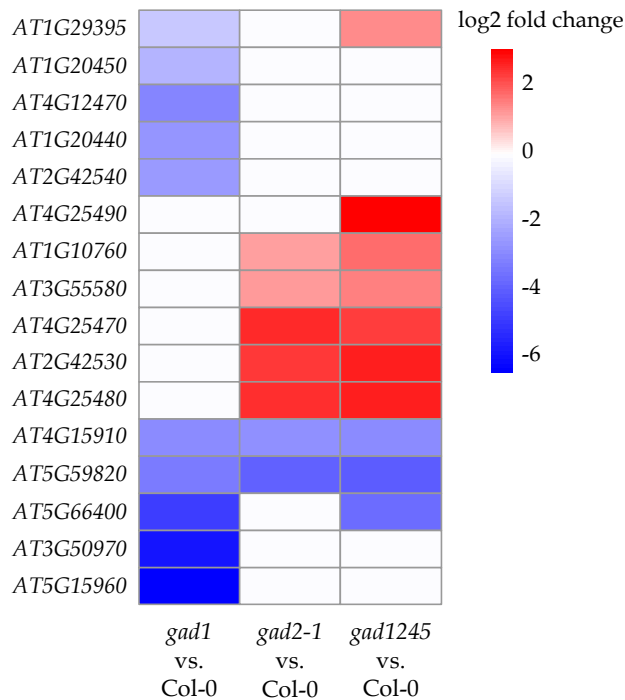


Figure 5.7. The log₂ fold change of mutation induced DE gene enriched for the GO cold acclimation (GO:0009631). Heatmap visualized the log₂ fold charge (log₂FC) of cold acclimation enriched DE genes compare to Col-0. Up and down-regulated genes were colored in red and blue. Darker colours depict higher level of expression changes according to log₂FC.

Similarly, four GO terms were enriched by DE genes from *gad1245*-Col-0 in the opposite direction compared to *gad2-1*: response to decreased oxygen levels (GO:0036293); cellular response to hypoxia (GO:0071456); cellular response to decreased oxygen levels (GO:0036294) and cellular response to oxygen levels (GO:0071453). Four GO terms were linked in a hierarchical relationship which means the gene set belongs to lower level GO (child GO) of this hierarchy, it is also a part of the higher level GO (parent GO). Here, 13 of up-regulated genes of *gad2-1*-Col-0 that are directly related to cellular response to hypoxia (GO:0071456) include 3 of parent GO terms (GO:0036294, GO:0071453 and GO:0036293) with same DE genes enriched (Figure 5.8(a)). Although these GO terms were presented as significantly enriched GO terms by the DE genes in a opposite direction, it is not necessarily that they are enriched by same set of genes. As illustrated in Figure 5.8(b), except 4 for the up-regulated genes that are both presented in *gad2-1* and *gad1245*, the rest of the up-regulated genes are uniquely shown as DE genes in *gad2-1*-Col-0.

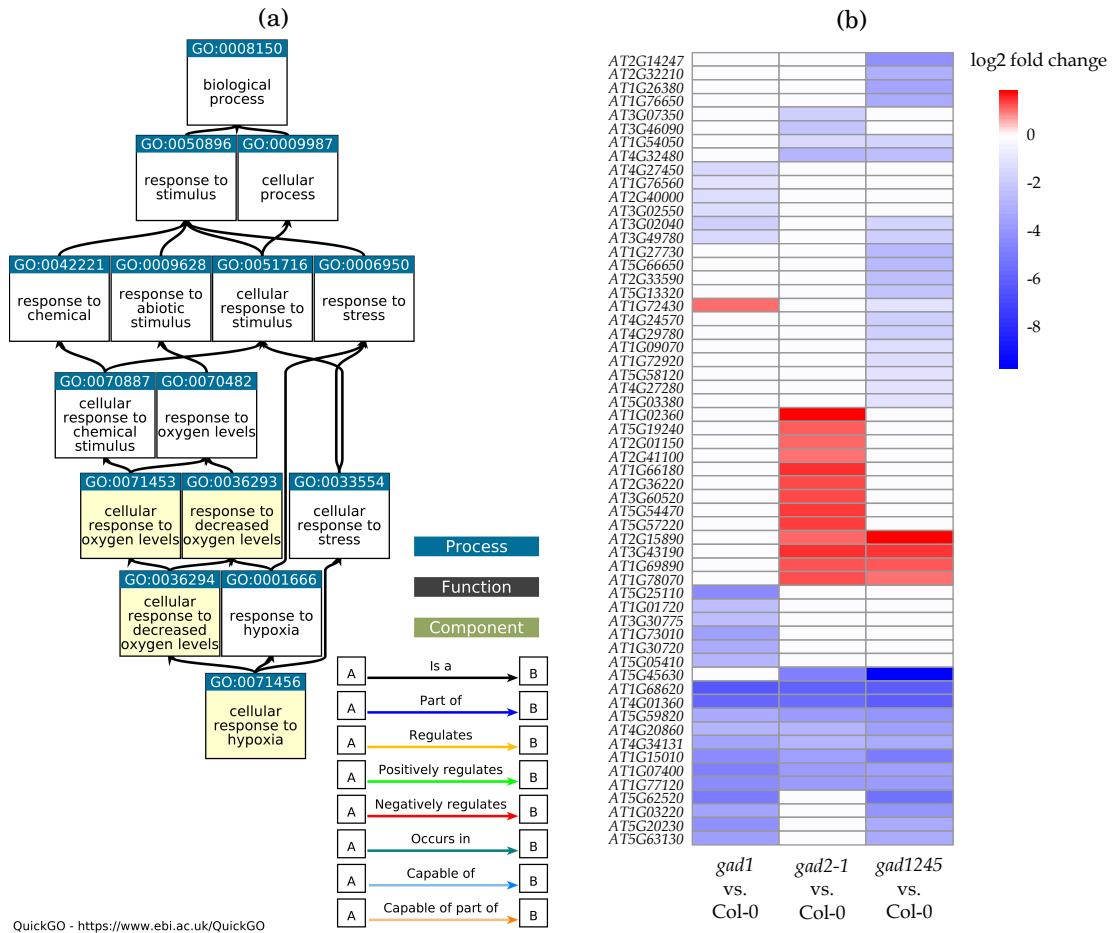


Figure 5.8. The hierarchical relationship of GO terms associated with hypoxia (a) and log₂ fold change of DE genes enriched (b). (a) Four of highlighted GO terms are shown as significantly enriched by DE genes in the functional analysis (GO:0071456, GO:0036294, GO:0071453 and GO:0036293) that are shown as enriched in the opposite direction for DE genes in *gad2-1*-Col-0 compared to *gad1* and *gad1245*. The sub-figure was generated from <https://www.ebi.ac.uk/QuickGO>. (b) The heatmap visualized the log₂ fold change (log₂FC) of hypoxia related GO enriched DE genes compared to Col-0. DE genes are colour coded according to their log₂FC in each comparison.

In the comparison of *gad1245*-Col-0, 30 GO terms were uniquely enriched and summarised in Table 5.2. The GO terms enriched by up-regulated genes are all associated with starch degradation in hierarchical relationships (Figure 5.9). In total, 21 DE genes from *gad1245* were involved in the GO enrichment: *AT1G69830*, *AT2G36390*, *AT3G46970*, *AT4G09020* and *AT5G64860* belong to the KEGG pathway – starch and sucrose metabolism (ath00500); *AT3G09540* and *AT4G33220* are in pentose and glucuronate interconversions (ath00040); *AT5G09730* is in amino sugar and nucleotide sugar metabolism (ath00520); and *AT1G68050* belong to circadian rhythm – plant (ath04712). The rest of DE genes are not matched to the current KEGG database, and this might be due to an incomplete pathway map.

Table 5.2. GO terms uniquely enriched in comparison *gad1245*-Col-0

GO accession*	Description	DE gene ratio**	Ontology***
GO:0006073	Cellular glucan metabolic process	16/249	BP
GO:0005983	Starch catabolic process	6/18	BP
GO:0044042	Glucan metabolic process	16/255	BP
GO:0044247	Cellular polysaccharide catabolic process	8/48	BP
GO:0044264	Cellular polysaccharide metabolic process	17/325	BP
GO:0005976	Polysaccharide metabolic process	21/494	BP
GO:0009251	Glucan catabolic process	8/56	BP
GO:0044275	Cellular carbohydrate catabolic process	8/74	BP
GO:0005982	Starch metabolic process	8/76	BP
GO:0000272	Polysaccharide catabolic process	11/189	BP
GO:0031347	Regulation of defense response	28/273	BP
GO:0046394	Carboxylic acid biosynthetic process	42/542	BP
GO:0009813	Flavonoid biosynthetic process	14/81	BP
GO:0010243	Response to organonitrogen compound	26/261	BP
GO:0071396	Cellular response to lipid	41/540	BP
GO:0016053	Organic acid biosynthetic process	43/577	BP
GO:0010200	Response to chitin	18/138	BP
GO:0000257	Nitrilase activity	4/4	MF
GO:0016815	Hydrolase activity, acting on carbon-nitrogen (but not peptide) bonds, in nitriles	4/4	MF
GO:0018822	Nitrile hydratase activity	4/4	MF
GO:0047427	Cyanoalanine nitrilase activity	4/4	MF
GO:0080061	Indole-3-acetonitrile nitrilase activity	4/4	MF
GO:0009073	Aromatic amino acid family biosynthetic process	11/57	BP
GO:0042742	Defense response to bacterium	34/457	BP
GO:1901606	Alpha-amino acid catabolic process	11/68	BP
GO:1901136	Carbohydrate derivative catabolic process	13/96	BP
GO:0006749	Glutathione metabolic process	12/85	BP
GO:0016616	Oxidoreductase activity, acting on the CH-OH group of donors, NAD or NADP as acceptor	18/180	MF
GO:0009684	Indoleacetic acid biosynthetic process	5/12	BP
GO:0010168	ER body	5/12	CC

Note: * The colour indicates the up-regulated (red) or down-regulated (blue) DE gene enriched GO term. ** DE gene ratio equals the number of DE genes present in a GO term divided by the total number of genes present within the GO term. *** GO classifications are in the category of biological process (BP), cellular component (CC) and molecular function (MF).

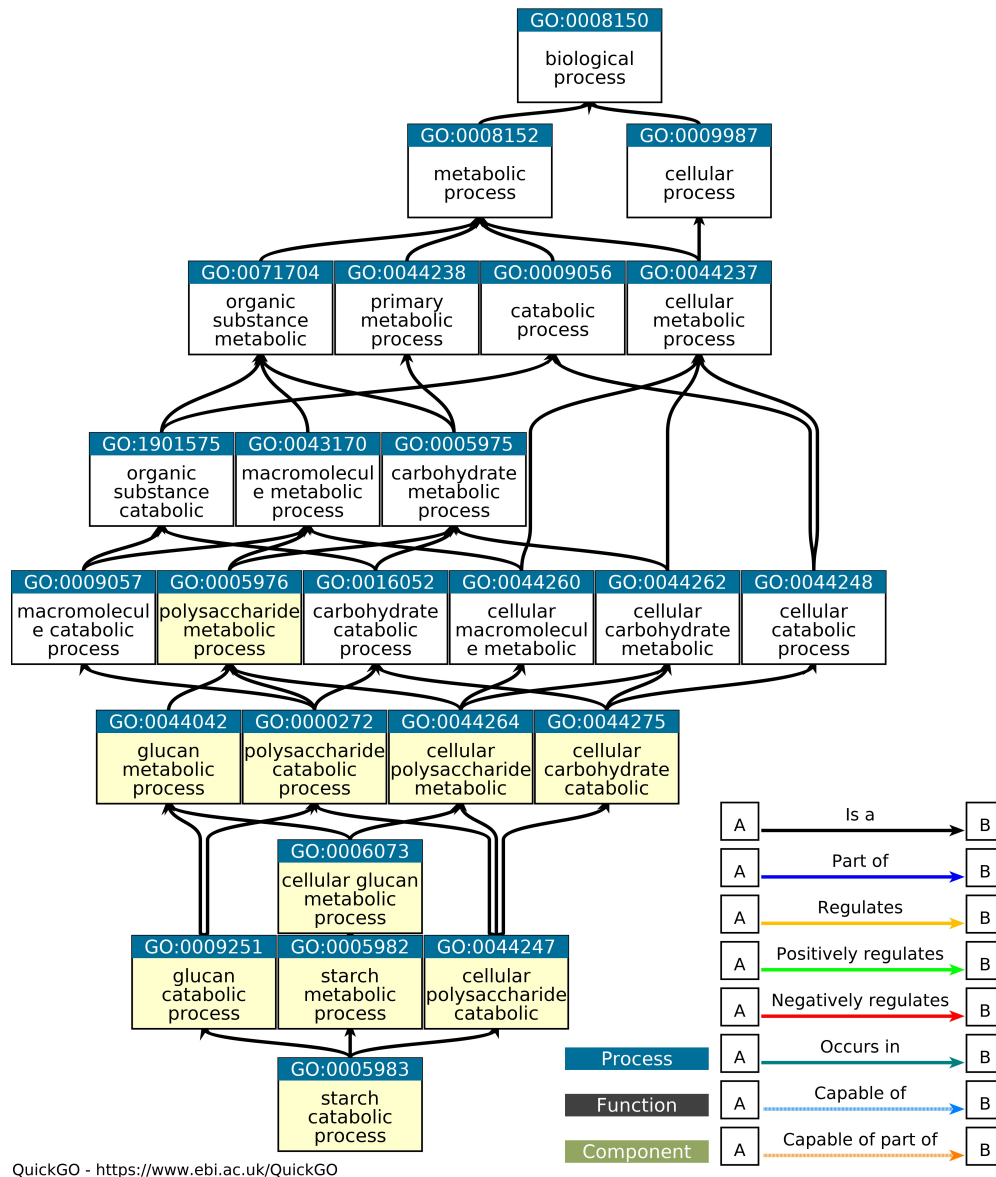


Figure 5.9. The hierarchical relationship of GO terms associated with starch degradation in *gad1245*. The highlighted GO terms are shown as significantly enriched according to functional analysis of DE genes in *gad1245*, but not *gad1* and *gad2-1*. Figure was generated from <https://www.ebi.ac.uk/QuickGO>.

The comparison *gad2-1*-Col-0 shared the majority of enriched GO terms with *gad1245*, except 4 GO terms that were uniquely enriched, while the comparison *gad1*-Col-0 had 8 uniquely enriched GO terms (details are summarised in Table 5.3). In the comparison of *gad1*-Col-0, the three GO terms were related to similar aspects – nutrition. Due to its hierarchical relationship as a parent term, the cellular response to starvation (GO:0009267) is the main contributor to cellular response to nutrient levels (GO:0009267) and response to nutrient levels (GO:0031667); the summary of enrichment is shown in Table 5.3. Figure 5.10 highlights the relationship of these three nutrient associated GO terms and 19 DE genes as enriched among these GO terms. Except for *AT5G49450*, which is directly related to cellular response to starvation, 13/19 DE genes were found directly associated with the starvation of 5 different nutrients (shown in the lowest level of highlighted GO terms in Figure 5.10; details in direct related GO terms of the DE genes are in Appendix Section D.2).

Table 5.3. Uniquely enriched GO terms found when comparing *gad1* or *gad2-1* with Col-0

GO accession*	Description	DE gene ratio**	Ontology***	Comparison
GO:0009505	Plant-type cell wall	6/237	CC	
GO:0043565	Sequence-specific DNA binding	53/1301	MF	
GO:0016151	Nickel cation binding	5/12	MF	
GO:0009267	Cellular response to starvation	15/164	BP	<i>gad1</i>
GO:1900057	Positive regulation of leaf senescence	6/18	BP	vs.
GO:0031667	Response to nutrient levels	19/232	BP	Col-0
GO:0031669	Cellular response to nutrient levels	17/179	BP	
GO:0010150	Leaf senescence	16/143	BP	
GO:0016843	Amine-lyase activity	6/20	MF	<i>gad2-1</i>
GO:0002213	Defense response to insect	7/29	BP	vs.
GO:0000302	Response to reactive oxygen species	16/159	BP	Col-0
GO:0030515	snoRNA binding	8/25	MF	.

Note: * The colour indicates the up-regulated (red) or down-regulated (blue) DE gene enriched GO term. ** DE gene ratio equals the number of DE genes present in a GO term divided by the total number of genes present within the GO term. *** GO classifications are in the category of biological process (BP), cellular component (CC) and molecular function (MF).

Due to the limited number of DE genes found in *gad1245-gad2-1*, direct associated GO terms from Ensembl database (<https://plants.ensembl.org>) could not be assessed through an automated GO enrichment test. Gene functional annotations are broader when a given GO is positioned closer to top of a root ontology category (i.e. biological process (BP), cellular component (CC) and molecular function (MF)); 15 out of 21 genes were found as GO terms that were at least 4 levels away from root ontology categories. Details of DE genes to associated GO are listed in Appendix Section D.3.

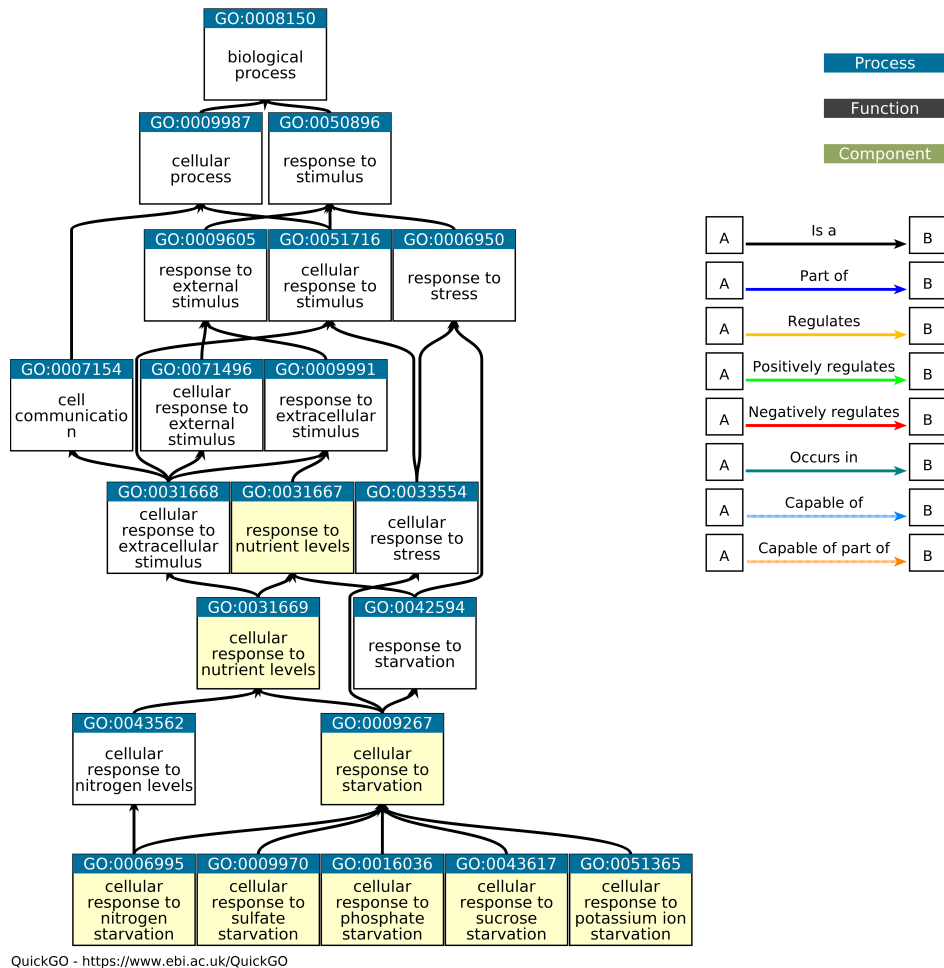


Figure 5.10. The hierarchical relationship of GO terms associated with nutrient starvation. The upper 3 highlighted GO terms are shown as significantly enriched by DE genes in the functional analysis (GO:0031667, GO:0009267 and GO:0009267) following comparison of *gad1*-Col-0. Five GO terms highlighted in the lowest level are the GO terms that have direct associations from matched DE genes according to Ensembl database (<https://plants.ensembl.org>). Figure was generated from <https://www.ebi.ac.uk/QuickGO>.

5.1.4 KEGG pathway enrichment

To understand which pathways were significantly changed by the introduced mutations, lists of DE genes from each comparison between a mutant and Col-0 were used to determine the over-representation (i.e. enrichment) of pre-defined pathways from the Kyoto Encyclopedia of Genes and Genomes (KEGG) database. The enrichment pattern of KEGG pathways that were induced by mutations show some unique enrichment (Figure 5.11). The commonly changed pathways following *gad* mutations were involved in amino acid metabolism. Others are pathways in metabolism of carbohydrates, lipid, terpenoids and polyketides; biosynthesis of secondary metabolites; MAPK signaling pathway and circadian rhythms (summarised in Table 5.4).

Many pathways were also uniquely enriched among these comparisons. The amino acid related metabolism pathway such as cysteine, methionine, arginine, proline, tyrosine and glutathione, were present only in the comparison of *gad1245*-Col-0. Other unique pathways in the comparison of *gad1245*-Col-0 were linoleic acid metabolism and biosynthesis of flavonoid, flavone, flavonol, glucosinolate, ubiquinone and other terpenoid-quinone. Ribosome biogenesis in eukaryotes and metabolic pathways like ni-

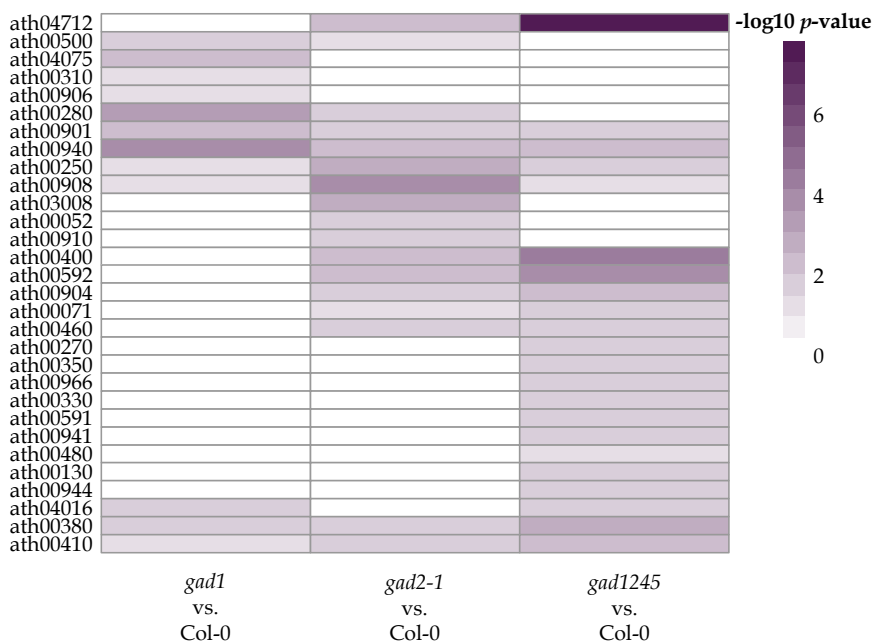


Figure 5.11. KEGG pathways enriched following DE gene analysis of *gad* mutants and Col-0. Enrichment pattern of significantly enriched KEGG pathways using DE genes from the comparison of *gad1* to Col-0, *gad2-1* to Col-0 and *gad1245* to Col-0 displayed with $-\log_{10} p$ -value. Darker colour indicates more significantly enriched KEGG pathways.

trogen and galactose metabolism were uniquely present in *gad2-1*-Col-0 while pathway lysine degradation, carotenoid biosynthesis and plant hormone signal transduction are enriched in *gad1*-Col-0 (summarised in Table 5.5).

Table 5.4. Shared KEGG pathways between *gad1*, *gad2-1* and *gad1245* compared to Col-0

Class	KEGG pathway	Pathway accession	DE gene ratio*		
			<i>gad1</i>	<i>gad2-1</i>	<i>gad1245</i>
Signal transduction	MAPK signaling pathway – plant	ath04016	9/139		16/139
Amino acid metabolism	Alanine, aspartate and glutamate metabolism	ath00250	4/51	9/51	8/51
	Valine, leucine and isoleucine degradation	ath00280	7/52	7/52	
	Tryptophan metabolism	ath00380	5/64	8/64	11/64
	Phenylalanine, tyrosine and tryptophan biosynthesis	ath00400		8/56	12/56
Carbohydrate metabolism	Starch and sucrose metabolism	ath00500	10/171	15/171	
Lipid metabolism	Fatty acid degradation	ath00071		6/47	7/47
	Alpha-Linolenic acid metabolism	ath00592		7/43	10/43
Metabolism of other amino acids	Beta-Alanine metabolism	ath00410	4/47	7/47	8/47
	Cyanoamino acid metabolism	ath00460		8/70	9/70
Biosynthesis of other secondary metabolites	Indole alkaloid biosynthesis	ath00901	2/4	2/4	2/4
	Phenylpropanoid biosynthesis	ath00940	14/176	18/176	19/176
Metabolism of terpenoids and polyketides	Diterpenoid biosynthesis	ath00904		4/21	5/21
	Zeatin biosynthesis	ath00908	3/32	5/32	8/32
Environmental adaptation	Circadian rhythm – plant	ath04712		7/39	14/39

Note: * DE gene ratio is presented by number of DE genes present in a KEGG pathway divided by the total number of genes present within the KEGG pathway.

Table 5.5. Uniquely enriched KEGG pathway in *gad1*, *gad2-1* and *gad1245* compared to Col-0

Class	KEGG pathway	Pathway accession	DE gene ratio*		
			<i>gad1</i>	<i>gad2-1</i>	<i>gad1245</i>
Amino acid metabolism	Lysine degradation	ath00310	3/31		
	Cysteine and methionine metabolism	ath00270			14/120
	Arginine and proline metabolism	ath00330			8/54
	Tyrosine metabolism	ath00350			7/41
Metabolism of other amino acids	Glutathione metabolism	ath00480			11/103
Lipid metabolism	Linoleic acid metabolism	ath00591			3/9
Energy metabolism	Nitrogen metabolism	ath00910		6/43	
Carbohydrate metabolism	Galactose metabolism	ath00052		7/57	
Biosynthesis of other secondary metabolites	Flavonoid biosynthesis	ath00941			5/25
	Flavone and flavonol biosynthesis	ath00944			2/4
	Glucosinolate biosynthesis	ath00966			5/26
Metabolism of terpenoids and polyketides	Carotenoid biosynthesis	ath00906	3/29		
Metabolism of cofactors and vitamins	Ubiquinone and other terpenoid-quinone biosynthesis	ath00130			6/39
Translation	Ribosome biogenesis in eukaryotes	ath03008		13/101	
Signal transduction	Plant hormone signal transduction	ath04075	16/289		

Note: * DE gene ratio is presented by number of DE genes present in a KEGG pathway divided by the total number of genes present within the KEGG pathway.

For the comparison of *gad1245-gad2-1*, the numbers of DE genes were not sufficient to perform the enrichment analysis, so the DE genes belonging to a KEGG pathway were matched instead. In total, 5 out of 21 genes were found matched to a pathway and were listed in Table 5.6.

Table 5.6. *gad1245-gad2-1* DE genes direct matched KEGG pathways

Gene ID	KEGG pathway accession	KEGG pathway	Class
<i>AT3G16320</i>	ath04120	Ubiquitin mediated proteolysis	Folding, sorting and degradation
<i>AT3G27540</i>	ath00510	N-Glycan biosynthesis	Glycan biosynthesis and metabolism
<i>AT4G03400</i>	ath04075	Plant hormone signal transduction	Signal transduction
<i>AT5G37770</i>	ath04626	Plant-pathogen interaction	Environmental adaptation
<i>AT5G60100</i>	ath04712	Circadian rhythm – plant	

5.2 Discussion

The initial data projection on the MDS plot suggested the sample differences were mainly driven by the introduced mutations within the *Arabidopsis* genome (Figure 5.1). With obtained DE genes from each comparison, GO and KEGG pathway changes were detected when impairing *GAD* homologues in the first step of the GABA shunt pathways with indicated mutation specific changes.

5.2.1 Stress sensitivity increased with GABA deficiency

In general, a series of stress defence response related GO terms were commonly shown across all mutants compared to wildtype (Table 5.1). For instance, the response to salt stress (GO:0009651) and defence response to fungus (GO:0050832) with a list of jasmonic acid response and jasmonic acid mediated pathway related GO terms (GO:0050832, GO:0009753, GO:0009867, GO:2000022) that are well known as a signaling responses against pathogen were all down-regulated, which means that mutations may have less capability for abiotic and biotic stress defence (Antico et al., 2012). In addition to this, the MAPK signaling pathway, which is suggested to be a convergence point for the defense-signaling network was also indicated as a significantly changed pathway according to KEGG, and was enriched by several down-regulated genes in each mutant compared to wildtype controls (Figure 5.12; Zhang and Klessig, 2001). Down-regulation of genes from the MAPK signaling pathway clearly gives a similar indication compared to the GO results, that *gad* mutants are potentially more sensitive to abiotic and biotic stress. Physiologically, a lack of GABA synthesis was reported to increase the sensitivity of mutants to stresses such as salinity and pathogenesis (Deng et al., 2020; Mekonnen et al., 2016; Su et al., 2019). Therefore, *gad* knockout muta-

tions are likely to increase stress sensitivity as both transcriptional and physiological indicators appear to agree. Whilst there are these shared transcriptional signatures between the mutants, each individual mutant seems to have unique altered pathways in response to the lack of GABA production.

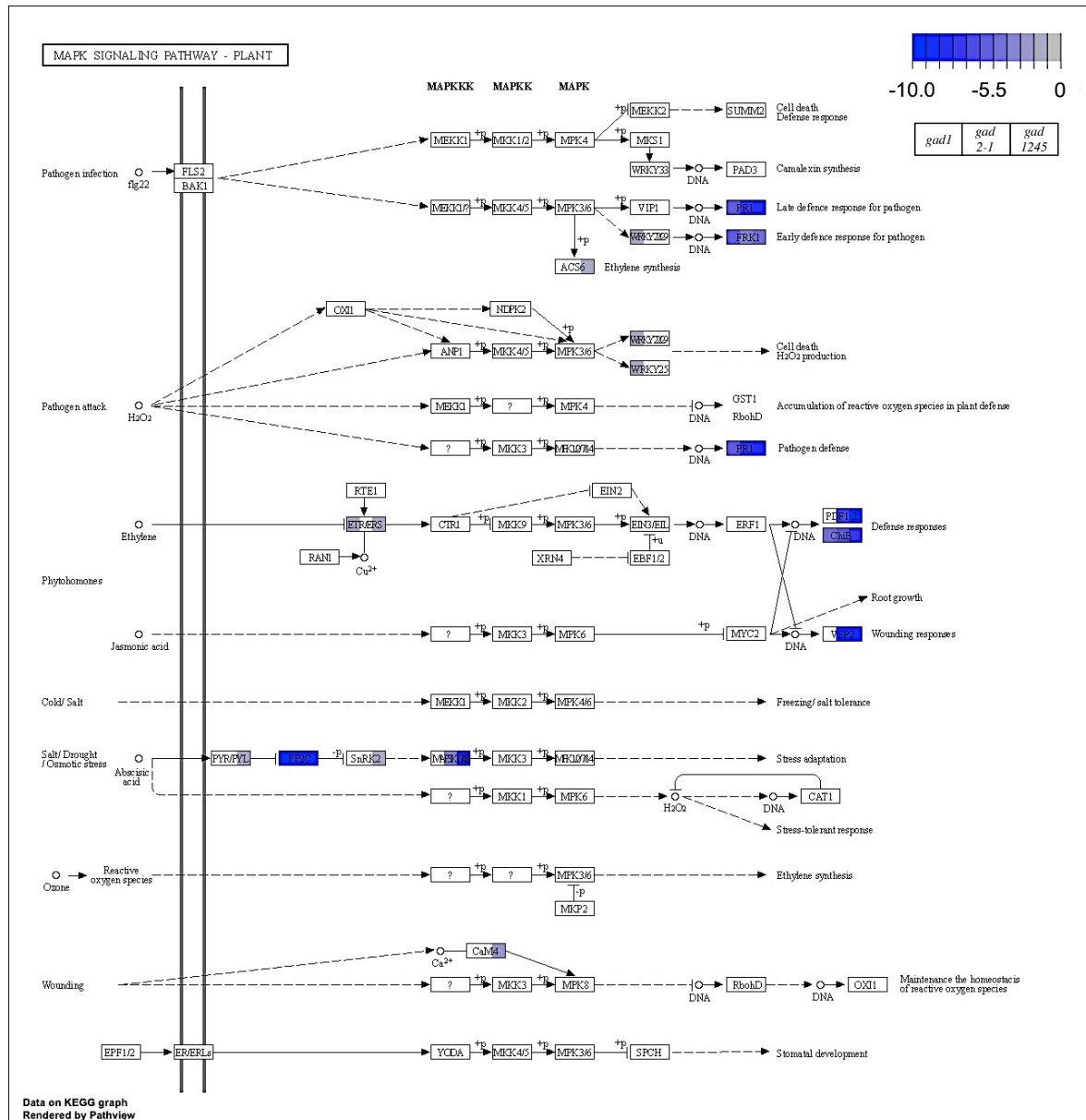


Figure 5.12. KEGG pathway visualisation of DE genes matched on the plant MAPK signaling pathway. Each rectangle represents a protein coding gene and split into three parts for colour coding corresponding to log₂ fold changes (log₂FC) in the order of *gad1*, *gad2-1* and *gad1245* compared to Col-0. Detailed KEGG pathway map notation is available at https://www.genome.jp/kegg/document/help_pathway.

5.2.2 *gad1* mutant and leaf senescence

gad1 has less induced changes in both GO and KEGG enrichment results as occurred for *gad2-1* and *gad1245*. It is possible that the tissue preferential expression of *GAD1* within roots, resulted in fewer induced changes in pathways in leaves (Bouché et al., 2004). However, following the *gad1* mutation being introduced, the functional analysis indicated leaf senescence related GO terms (GO:0010150 and GO:1900057) were enriched by down-regulated genes. As leaf senescence is a developmental event, nutrients are recycled from old leaves and transferred to younger tissues and this leads to nutrient starvation in old leaves (Diaz et al., 2005; Stoddart and Thomas, 1982). In another words, leaf senescence and nutrient starvation are highly linked. In our data, *gad1* also shows nutrients starvation related GO terms (GO:0031667, GO:0031669 and GO:0009267; Table 5.3). Here, leaf senescence and nutrient starvation were both present in the GO functional analysis; however, how *GAD1*, a root-predominately expressed gene, influences processes related to leaf senescence is uncertain. Increased concentrations of GABA have previously been observed in leaf senescence experiments Diaz et al. (2005), but further exploration is required to reveal the relationship between *GAD1* and the process of leaf senescence.

5.2.3 *gad2-1* maybe pre-prepared for hypoxia

In *gad2-1* compared to Col-0, the first distinct difference presents in 4 hypoxia and oxygen levels related GO terms (GO:0071456, GO:0036294, GO:0071453 and GO:0036293) that are enriched with up-regulated genes while in *gad1* and *gad1245* were enriched through down-regulated DE genes (Table 5.1). From the gene expression heatmap of the hypoxia related genes (Figure 5.8(b)), it is possible that *gad2-1* is primed at a transcriptional level to respond to hypoxia, but no indications of this yet exist in the literature whether *gad2* performs better during hypoxia than other *gad* mutants. Still, the genes in these lists are worth paying attention to in further analysis of how these gene changes compare before and after hypoxia.

In addition, *gad2-1* presents another defence response GO function that is enriched through down-regulated genes: defence response to insect (GO:0002213), along with response to reactive oxygen species (GO:0000302) shown in Table 5.3. Reactive oxygen species (ROS) are a well known plants stress signal that is the essential for inter-pathway crosstalk in order to respond environmental changes (Baxter et al., 2013; Kerchev et al., 2012). As discussed in Chapter 4, ROS production could be induced by GABA either through SnRK2.4 maintained homeostasis of ROS (Szymańska et al., 2019) or enhanced of photosynthetic activity (Vijayakumari and Puthur, 2015). Since

GAD2 is the major producer of GABA in plants, a greater stress sensitivity of *gad2-1* could be expected as ROS is a key signal involved in abiotic and biotic stress (Baxter et al., 2013).

5.2.4 *gad1245* could have altered cold/freezing tolerance and has relationship to starch degradation

In the comparison of *gad1245* to Col-0, the GO term cold acclimation (GO:0009631), presented three different outcomes of enrichment: the GO term was enriched by down-regulated DE genes from *gad1*, while in *gad1245* this was by up-regulated genes, and did not present as a significantly enriched GO in *gad2-1* (Table 5.1). DE genes in *gad1245* that enriched within the term cold acclimation were mostly different from *gad1*. *AT1G29395* is shared between *gad1*-Col-0 and *gad1245*-Col-0 on the opposite regulation direction. (Figure 5.7). *AT1G29395*, known as *COR413IM* or *COR413-TM1*, is a freezing tolerance related gene that is regulated by water stress, light and abscisic acid (Breton et al., 2003; Okawa et al., 2008) In this data, down-regulation of cold response was expected with GABA deficiency, because a range of genes in MAPK signalling pathways were more or less down-regulated in all *gad* mutants. However, *gad1245* presents a different set of DE genes and mainly up-regulated genes compared to Col-0, while all DE genes enriched in this GO from *gad1* are down-regulated (Figure 5.7). The result suggests that *gad1245* could have better cold/freezing tolerance than *gad1*, but this is a primary hypothesis based on transcriptional changes following the *gad* mutations. Further physiological experiments are needed to be followed to test this hypothesis, for instance through cold treatment followed by analysis of electrolyte leakage (Okawa et al., 2008).

In Table 5.2, a series of GO enrichments for starch degradation through up-regulated genes occur in *gad1245* compared to Col-0, but not in *gad1* and *gad2-1*. As mentioned in the results, 21 DE genes from *gad1245* that are involved in the GO enrichment are presented in the KEGG pathway – starch and sucrose metabolism (ath00500), pentose and glucuronate interconversions (ath00040), amino sugar and nucleotide sugar metabolism (ath00520) and circadian rhythm – plant (ath04712). These results gives a clue that starch degradation is correlated with circadian rhythm. In guard cells, starch synthesis starts 1 hour after light and continue to the middle of the night, then starch degradation is initiated and processes slowly. About half of the starch in guard cells has been degraded by dawn; and then starch is rapidly degraded within 1 hour of light exposure and the cycle starts over again (Daloso et al., 2017; Santelia and Lawson, 2016). This cycle of starch synthesis/degradation cycle could provide sugars and organic acids that

are required for increasing guard cell turgor pressure and promoting stomatal opening (Horrer et al., 2016). The transcripts of genes that are associated to starch degradation are also regulated in diurnal patterns which are driven by the circadian clock (Streb and Zeeman, 2012). In our data, the α -amylase3 (*AMY3*; *AT1G69830*) and β -amylase1 (*BAM1*; *AT3G23920*) were presented as DE genes uniquely in *gad1245*-Col-0 and they are highly and preferentially expressed in guard cells, and are responsible for starch degradation (Horrer et al., 2016). *bam1/amy3* double mutants showed excessive starch accumulation in guard cell after light exposure and fail to open stomata (Horrer et al., 2016). This information linked diurnal cycle, stomatal movement to starch degradation and further examination of starch content difference could possibly reveal the stomatal phenotype difference between *gad2-1* and *gad1245*.

5.2.5 Potential candidate genes in *gad1245* that may restore a wildtype-like stomatal phenotype

5.2.5.1 Genes in *gad1245* restore the Col-0-like expression

In Figure 5.5(a), 4 of genes from *gad1245* showed similar expression levels to Col-0 whereas *gad2* had significantly higher expression levels of these genes. This means the *gad2* contribution on these four genes in *gad1245* was cancelled with the other mutations present. Obulareddy et al. (2013) detected all 4 of these genes as expressed in guard cells via RNA sequencing with high quality guard cell RNA. Specifically, *AT4G26150*, known as *GATA22* or *CGA1*, is a transcription factor which is regulated by light, nitrogen and cytokinin (Hudson et al., 2011; Naito et al., 2007). It has been found that *CGA1* modifies *glutamate synthase* (*GLU1/Fd-GOGAT*) expression; the key gene localized in chloroplasts that is involved in nitrogen assimilation (Hudson et al., 2011). Chloroplast nitrogen assimilation is essential for chlorophyll biosynthesis, specifically by building up the glutamate pool (Potel et al., 2009), the precursor of GABA. In addition, chloroplast number and starch content in leaf was altered in *cga1* (Hudson et al., 2011). As discussed in last section that synthesis/degradation cycle is involving stomata opening and the chloroplast has been considered as a primary location of starch biosynthesis (Eckhardt et al., 2004), having wildtype-like expression level of *CGA1* might contribute to the wildtype-like stomatal aperture phenotype.

5.2.5.2 Genes with the additive effect of *gad* mutations

AT5G39410 and *AT5G60100* were up-regulated in both *gad2-1* and *gad1245* compared to Col-0, but were more highly expressed in *gad1245* when compared to *gad2-1* (Figure 5.5(b)). The *AT5G39410* protein is localized to the mitochondrial outer membrane and

reported to be a saccharopine dehydrogenase involved in lysine catabolism (Duncan et al., 2011; Ramel et al., 2013). *AT5G60100* (*PSEUDO-RESPONSE REGULATOR 3*, *PRR3*) participates in the circadian clock progression as a pseudo-response regulator and is co-expressed with *TIMING OF CAB EXPRESSION 1* (*TOC1*) and regulates *TOC1* protein stability (Para et al., 2007). *PRR3* deficiency could lead to a shortens circadian period and significant lower biomass accumulation and water use, whereas over-expression alters flowering time (Choudhary et al., 2015; Simon et al., 2020).

TOC1 is a repressor of *CIRCADIAN CLOCK-ASSOCIATED 1* (*CCA1*)/*LATE ELONGATED HYPOCOTYL* (*LHY*) expression in the circadian rhythm feedback loop (Gendron et al., 2012). In our data, the regulation pattern of identified DE genes in the circadian rhythm feedback loop from *gad1245-col-0* matched with the pattern described in the literature above (Figure 5.13). However, DE genes from *gad2-1* did not include *TOC1* to suppress *CCA1/LHY*, even through *PRR3* the co-expressed regulator of *TOC1*

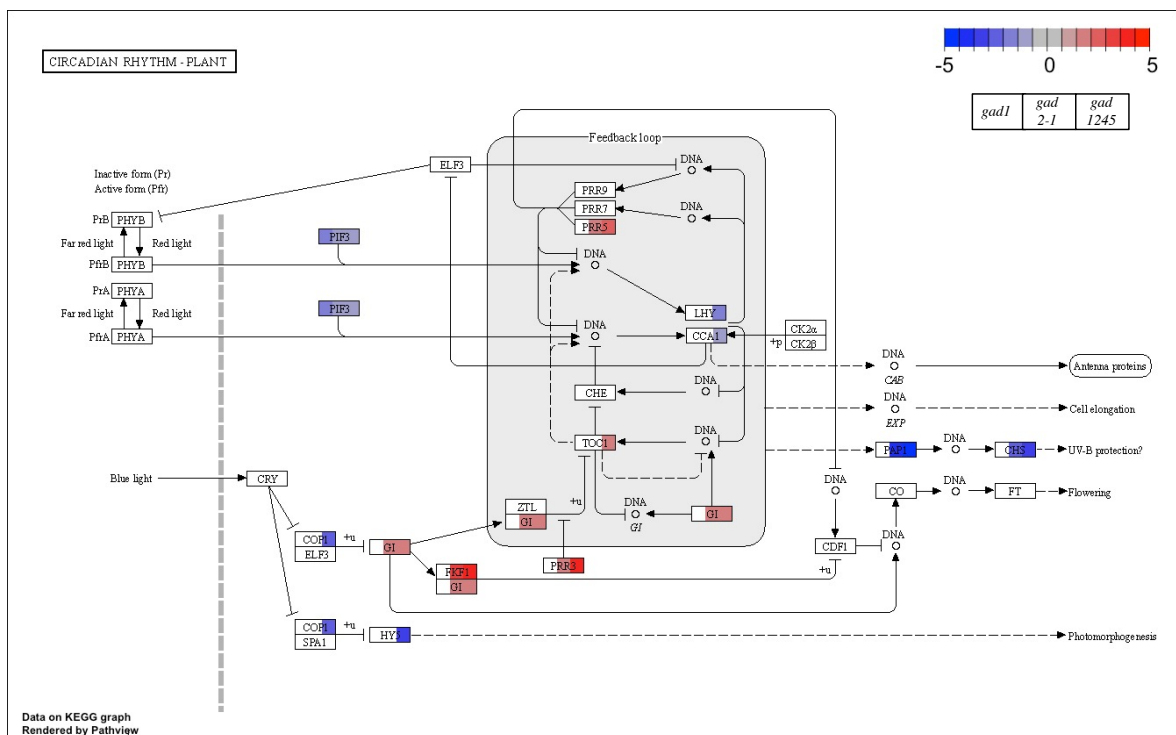


Figure 5.13. KEGG pathway visualisation of DE genes mapped on circadian rhythms -plant. Each rectangle represents a protein coding gene and is split into three parts for colour coding corresponding to a log₂ fold change (log₂FC) in the order of *gad1*, *gad2-1* and *gad1245* compared to Col-0. Detailed explanation of KEGG pathway map notation is available at https://www.genome.jp/kegg/document/help_pathway.

was up-regulated. This might imply a similar relationship to another gene that regulates *TOC1 – AT5G37770* (also known as *CML24*). Ruiz et al. (2018) proposed that *CML24* regulates *TOC1* through a post-transcriptional approach with a cytosolic Ca^{2+} -dependent manner, but the mechanism is not clear. It is known that stomatal movement is tightly linked to Ca^{2+} signals (Laanemets et al., 2013) and *CML24* was shown as a DE gene in the comparison of *gad1245-gad2-1* (Table 5.6) with lower expression levels in *gad1245* compared to *gad2-1*, which indicates the level of cytosolic Ca^{2+} signal in *gad2-1* and *gad1245* could also be different. Overall, our data indicated that the circadian rhythm feedback loop was more disrupted in *gad1245* than *gad2* regarding the number of DE genes presented in this pathway (Table 5.4).

5.2.5.3 Genes in *gad1245* behave uniquely to Col-0 and *gad2-1*

In *gad1245*, 11 DE genes had an expression level significantly different from both Col-0 and *gad2-1*, while *gad2-1* had Col-0-like level of expression of these genes (Figure 5.4, 5.5(c)). This means these genes are behaving differently to both wildtype and *gad2-1*, and *gad2-1* is not contributing to these expression changes. Among these genes, *AT1G72430* (*SAUR78*) and *AT5G03380* (*HIPP06*) are directly related to the GO function – cellular response to hypoxia (GO:0071456) as displayed in Figure 5.8. There is a number of down-regulated hypoxia response DE genes shown only in *gad1245* in addition to those commonly down-regulated DE genes across *gad1*, *gad2-1* and *gad1245*, which suggests that *gad1245* might be more hypoxia sensitive than *gad1* and *gad2-1*. *AT5G65920* (*PUB31*) is a plant U-box type E3 ubiquitin ligase. Zhang et al. (2017) found that the T-DNA insertion mutant *pub31* is sensitive to salinity stress at the germination stage. In our data, the expression level of *PUB31* is down-regulated in *gad1245* compared to both Col-0 and *gad2-1*. As discussed above, lack of GABA synthesis may lead to an increase in the sensitivity to salinity (Su et al., 2019); the expression changes of *PUB31* in *gad1245* could be contributing to this phenotype.

In summary, the selected potential candidate genes identified through their expression level differences suggest some unique changes occur in *gad1245* in several different aspects including gene regulation or stress responses. The majority of the listed DE gene above have not been directly implicated in stomatal control as of yet, so it is not clear how they may be involved in altering *gad1245* stomata to bestow wildtype-like stomatal behavior, except the possibility that cytosolic Ca^{2+} may be different which is highly related to stomata regulation (Huang et al., 2019; Laanemets et al., 2013), and that there are alterations in circadian clock pathways, which can impact WUE, stomatal behaviour and photosynthesis (Dodd et al., 2006; Joo et al., 2017; Simon et al.,

2020). These identified differences provide a framework from which the relationships or interactions can be explored in terms of how they may influence stomatal behaviour.

5.3 Material and Methods

5.3.1 Plant material and RNA-Seq data

Arabidopsis wildtype (Columbia-0, Col-0) and GABA mutant seeds were sown in a mixture of vermiculite, perlite, and soil (1:1:3 by volume). All *Arabidopsis* plants were grown in climate-controlled chambers at 22 °C with 65% relative humidity and 14/10 hour day/night cycles with a 120 m⁻²s⁻¹ photo flux density using Philips Master T Green Power LEDs (400w).

Arabidopsis leaf number 5-10 were sampled when plants had grown to about 4.5 weeks old and total RNA was isolated using the Spectrum™ plant total RNA kit (Sigma-Aldrich) according to the manufacturer's instructions. DNA was removed via on-column DNase digestion using the RNase-Free DNase kit (Sigma). The RNA was eluted in molecular grade DNase- and RNase-free water (Sigma) and integrity validated on agarose gels. The sequencing library was constructed with a TruSeq Stranded mRNA Library Prep Kit according to the manufacturer's instructions (Illumina) and sequenced on a NextSeq 500 (Illumina) resulting in 76 bp single-end reads. Plant material growth and RNA extraction were done by Ying Meng from the University of Adelaide, and RNA-Seq library were prepared and sequenced in the Whelan lab at La Trobe University.

The whole experiment included Col-0 with 4 GABA deficient mutant lines (*GAD1* knockdown and knockout, *gad2-1* and *gad1245*) and 2 GABA accumulation mutants (*GAD2* over-express and *pop2*) in both control and water submergence condition with 3 replicates. In this chapter, the main focus is to compare the transcriptional difference in an optimal condition between Col-0 and the GABA deficient mutant lines. Therefore, the bioinformatics analysis performed in this chapter only considers GABA deficient mutant lines: *GAD1* knockout (written as *gad1* in this chapter), *gad2-1* and *gad1245* with Col-0 under control conditions.

5.3.2 Bioinformatics workflow

To process raw sequencing data to gene counts, multiple tools were used for the read quality checking and trimming, mapping and counting. Raw sequencing reads were

quality-checked with *FastQC* (version 0.11.8; <http://www.bioinformatics.babraham.ac.uk/projects/fastqc>) and adapters trimmed with *Trimmomatic* (version 0.39; Bolger et al., 2014). The trimmed FASTQ reads were aligned to the TAIR10 reference genome (Swarbreck et al., 2007) using *STAR* (version 2.7.3a; Dobin et al., 2012). Aligned reads of each gene were counted based on the Araport11 genome annotation (Cheng et al., 2017) by *featureCounts* in *Subread* (version 1.6.4; Liao et al., 2013). The above described steps were managed in *Snakemake* (Köster and Rahmann, 2012) and processed on the University of Adelaide’s High Performance Compute (HPC) Service – “Phoenix”.

The following analysis of differential gene expression, functional and pathway analysis were conducted in R (version 4.1.0). Low expressed genes were excluded with the filtering function *filterByExpr()* in *edgeR*, and differential gene expression analysis was performed between genotypes using *edgeR* (Robinson et al., 2009). Gene Ontology analysis (with *biomaRt*, *GO.db* and *annotate*) and Kyoto Encyclopedia of Genes and Genomes (KEGG) pathway analysis (with *KEGGREST*) was then performed to determine the genotype specific functional and pathway enrichment among GABA deficient mutants (Carlson, 2021; Durinck et al., 2009; Gentleman, 2021; Tenenbaum and Maintainer, 2021). Detailed parameter settings are contained within the Snake-make workflow and R code available on GitHub (<https://github.com/CharlotteSai/ArabidopsisSubmergence>) and the R session information is presented in appendix D, section D.1.

References

- C. J. Antico, C. Colon, T. Banks, and K. M. Ramonell. Insights into the role of jasmonic acid-mediated defenses against necrotrophic and biotrophic fungal pathogens. *Frontiers in Biology*, 7(1):48–56, 2012.
- A. Baxter, R. Mittler, and N. Suzuki. ROS as key players in plant stress signalling. *Journal of Experimental Botany*, 65(5):1229–1240, 2013.
- A. M. Bolger, M. Lohse, and B. Usadel. Trimmomatic: a flexible trimmer for Illumina sequence data. *Bioinformatics*, 30(15):2114–2120, 2014.
- N. Bouché, A. Fait, M. Zik, and H. Fromm. The root-specific glutamate decarboxylase (GAD1) is essential for sustaining GABA levels in Arabidopsis. *Plant Molecular Biology*, 55(3):315–325, 2004.
- G. Breton, J. Danyluk, J.-B. F. Charron, and F. Sarhan. Expression profiling and bioinformatic analyses of a novel stress-regulated multispinning transmembrane protein family from cereals and arabidopsis. *Plant Physiology*, 132(1):64–74, 2003.
- M. Carlson. *GO.db: A set of annotation maps describing the entire Gene Ontology*, 2021.
- C. Y. Cheng, V. Krishnakumar, A. P. Chan, F. Thibaud-Nissen, S. Schobel, and C. D. Town. Araport11: a complete reannotation of the *Arabidopsis thaliana* reference genome. *The Plant Journal*, 89(4):789–804, 2017.
- M. K. Choudhary, Y. Nomura, L. Wang, H. Nakagami, and D. E. Somers. Quantitative circadian phosphoproteomic analysis of Arabidopsis reveals extensive clock control of key components in physiological, metabolic, and signaling pathways. *Molecular & Cellular Proteomics*, 14(8):2243–2260, 2015.
- D. M. Daloso, D. B. Medeiros, L. Anjos, T. Yoshida, W. L. Araújo, and A. R. Fernie. Metabolism within the specialized guard cells of plants. *New Phytologist*, 216(4):1018–1033, 2017.
- X. Deng, X. Xu, Y. Liu, Y. Zhang, L. Yang, S. Zhang, and J. Xu. Induction of γ -aminobutyric acid plays a positive role to Arabidopsis resistance against *Pseudomonas syringae*. *Journal of Integrative Plant Biology*, 62(11):1797–1812, 2020.
- C. Diaz, S. Purdy, A. Christ, J.-F. Morot-Gaudry, A. Wingler, and C. Masclaux-Daubresse. Characterization of markers to determine the extent and variability of leaf senescence in Arabidopsis. a metabolic profiling approach. *Plant Physiology*, 138(2):898–908, 2005.

- A. Dobin, C. A. Davis, F. Schlesinger, J. Drenkow, C. Zaleski, S. Jha, P. Batut, M. Chaisson, and T. R. Gingeras. STAR: ultrafast universal RNA-seq aligner. *Bioinformatics*, 29(1):15–21, 2012.
- A. N. Dodd, M. K. Jakobsen, A. J. Baker, A. Telzerow, S. W. Hou, L. Laplaze, L. Barrot, R. Scott Poethig, J. Haseloff, and A. A. R. Webb. Time of day modulates low-temperature Ca^{2+} signals in Arabidopsis. *The Plant Journal*, 48(6):962–973, 2006.
- O. Duncan, N. L. Taylor, C. Carrie, H. Eubel, S. Kubiszewski-Jakubiak, B. Zhang, R. Narsai, A. H. Millar, and J. Whelan. Multiple lines of evidence localize signaling, morphology, and lipid biosynthesis machinery to the mitochondrial outer membrane of Arabidopsis. *Plant Physiology*, 157(3):1093–1113, 2011.
- S. Durinck, P. T. Spellman, E. Birney, and W. Huber. Mapping identifiers for the integration of genomic datasets with the R/Bioconductor package biomart. *Nature protocols*, 4(8):1184, 2009.
- U. Eckhardt, B. Grimm, and S. Hörtensteiner. Recent advances in chlorophyll biosynthesis and breakdown in higher plants. *Plant Molecular Biology*, 56(1):1–14, 2004.
- X. Feng. *GABA regulation of stomatal function in Arabidopsis thaliana*. PhD thesis, University of Adelaide, 2021.
- J. Gendron, J. Pruneda-Paz, C. Doherty, A. Gross, S. Kang, and S. Kay. Arabidopsis circadian clock protein, TOC1, is a DNA-binding transcription factor. *Proceedings of the National Academy of Sciences*, 109(8):3167–3172, 2012.
- R. Gentleman. *annotate: Annotation for microarrays*, 2021.
- D. Horrer, S. Flütsch, D. Pazmino, J. S. Matthews, M. Thalmann, A. Nigro, N. Leonhardt, T. Lawson, and D. Santelia. Blue light induces a distinct starch degradation pathway in guard cells for stomatal opening. *Current Biology*, 26(3):362–370, 2016.
- S. Huang, R. Waadt, M. Nuhkat, H. Kollist, R. Hedrich, and M. R. G. Roelfsema. Calcium signals in guard cells enhance the efficiency by which abscisic acid triggers stomatal closure. *New Phytologist*, 224(1):177–187, 2019.
- D. Hudson, D. Guevara, M. W. Yaish, C. Hannam, N. Long, J. D. Clarke, Y. M. Bi, and S. J. Rothstein. GNC and CGA1 modulate chlorophyll biosynthesis and glutamate synthase (GLU1/Fd-GOGAT) expression in Arabidopsis. *PLoS ONE*, 6(11):e26765, 2011.

- Y. Joo, V. Fragoso, F. Yon, I. T. Baldwin, and S. G. Kim. Circadian clock component, LHY, tells a plant when to respond photosynthetically to light in nature. *Journal of Integrative Plant Biology*, 59(8):572–587, 2017.
- P. I. Kerchev, B. Fenton, C. H. Foyer, and R. D. Hancock. Plant responses to insect herbivory: interactions between photosynthesis, reactive oxygen species and hormonal signalling pathways. *Plant, Cell & Environment*, 35(2):441–453, 2012.
- J. Köster and S. Rahmann. Snakemake – a scalable bioinformatics workflow engine. *Bioinformatics*, 28(19):2520–2522, 2012.
- K. Laanemets, B. Brandt, J. Li, E. Merilo, Y. F. Wang, M. M. Keshwani, S. S. Taylor, H. Kollist, and J. I. Schroeder. Calcium-dependent and -independent stomatal signaling network and compensatory feedback control of stomatal opening via Ca²⁺ sensitivity priming. *Plant Physiology*, 163(2):504–513, 2013.
- Y. Liao, G. K. Smyth, and W. Shi. featureCounts: an efficient general purpose program for assigning sequence reads to genomic features. *Bioinformatics*, 30(7):923–930, 2013.
- D. W. Mekonnen, U. I. Flügge, and F. Ludewig. Gamma-aminobutyric acid depletion affects stomata closure and drought tolerance of *Arabidopsis thaliana*. *Plant Science*, 245:25–34, 2016.
- Y. Miyashita and A. G. Good. Contribution of the GABA shunt to hypoxia-induced alanine accumulation in roots of *Arabidopsis thaliana*. *Plant and Cell Physiology*, 49(1):92–102, 2008.
- T. Naito, T. Kiba, N. Koizumi, T. Yamashino, and T. Mizuno. Characterization of a unique GATA family gene that responds to both light and cytokinin in *Arabidopsis thaliana*. *Bioscience, Biotechnology, and Biochemistry*, 71:1557–1560, 2007.
- N. Obulareddy, S. Panchal, and M. Melotto. Guard cell purification and RNA isolation suitable for high-throughput transcriptional analysis of cell-type responses to biotic stresses. *Molecular Plant-Microbe Interactions*, 26(8):844–849, 2013.
- K. Okawa, K. Nakayama, T. Kakizaki, T. Yamashita, and T. Inaba. Identification and characterization of Cor413im proteins as novel components of the chloroplast inner envelope. *Plant, Cell & Environment*, 31(10):1470–1483, 2008.
- A. Para, E. M. Farré, T. Imaizumi, J. L. Pruneda-Paz, F. G. Harmon, and S. A. Kay. PRR3 is a vascular regulator of TOC1 stability in the *Arabidopsis* circadian clock. *The Plant Cell*, 19(11):3462–3473, 2007.

- F. Potel, M.-H. Valadier, S. Ferrario-Méry, O. Grandjean, H. Morin, L. Gaufichon, S. Boutet-Mercey, J. Lothier, S. J. Rothstein, N. Hirose, et al. Assimilation of excess ammonium into amino acids and nitrogen translocation in *Arabidopsis thaliana* – roles of glutamate synthases and carbamoylphosphate synthetase in leaves. *The FEBS journal*, 276(15):4061–4076, 2009.
- F. Ramel, C. Sulmon, G. Gouesbet, and I. Couée. Regulatory effects of atrazine differentially override sucrose repression of amino acid catabolism. *Acta Physiologiae Plantarum*, 35(7):2329–2337, 2013.
- M. D. Robinson, D. J. McCarthy, and G. K. Smyth. edgeR: a Bioconductor package for differential expression analysis of digital gene expression data. *Bioinformatics*, 26(1):139–140, 2009.
- M. C. M. Ruiz, K. E. Hubbard, M. J. Gardner, H. J. Jung, S. Aubry, C. T. Hotta, N. I. Mohd-Noh, F. C. Robertson, T. J. Hearn, Y. C. Tsai, A. N. Dodd, M. Hannah, I. A. Carré, J. M. Davies, J. Braam, and A. A. R. Webb. Circadian oscillations of cytosolic free calcium regulate the arabidopsis circadian clock. *Nature Plants*, 4(9):690–698, 2018.
- D. Santelia and T. Lawson. Rethinking guard cell metabolism. *Plant Physiology*, 172(3):1371–1392, 2016.
- S. S. Scholz, M. Reichelt, D. W. Mekonnen, F. Ludewig, and A. Mithöfer. Insect herbivory-elicited GABA accumulation in plants is a wound-induced, direct, systemic, and jasmonate-independent defense response. *Frontiers in Plant Science*, 6:1128, 2015.
- N. M. L. Simon, C. A. Graham, N. E. Comben, A. M. Hetherington, and A. N. Dodd. The circadian clock influences the long-term water use efficiency of arabidopsis. *Plant Physiology*, 183(1):317–330, 2020.
- J. L. Stoddart and H. Thomas. Leaf senescence. In *Nucleic Acids and Proteins in Plants I*, pages 592–636. Springer Berlin Heidelberg, 1982.
- S. Streb and S. C. Zeeman. Starch metabolism in arabidopsis. *The Arabidopsis Book*, 10, 2012.
- N. Su, Q. Wu, J. Chen, L. Shabala, A. Mithöfer, H. Wang, M. Qu, M. Yu, J. Cui, and S. Shabala. GABA operates upstream of H⁺-ATPase and improves salinity tolerance in Arabidopsis by enabling cytosolic K⁺ retention and Na⁺ exclusion. *Journal of Experimental Botany*, 70(21):6349–6361, 2019.

- D. Swarbreck, C. Wilks, P. Lamesch, T. Z. Berardini, M. Garcia-Hernandez, H. Foerster, D. Li, T. Meyer, R. Muller, L. Ploetz, A. Radenbaugh, S. Singh, V. Swing, C. Tissier, P. Zhang, and E. Huala. The arabidopsis information resource (TAIR): gene structure and function annotation. *Nucleic Acids Research*, 36(suppl_1):D1009–D1014, 2007.
- K. P. Szymańska, L. Polkowska-Kowalczyk, M. Lichočka, J. Maszkowska, and G. Dobrowolska. SNF1-related protein kinases SnRK2.4 and SnRK2.10 modulate ROS homeostasis in plant response to salt stress. *International Journal of Molecular Sciences*, 20(1):143, 2019.
- D. Tenenbaum and B. P. Maintainer. *KEGGREST: Client-side REST access to the Kyoto Encyclopedia of Genes and Genomes (KEGG)*, 2021.
- F. J. Turano and T. K. Fang. Characterization of two glutamate decarboxylase cDNA clones from arabidopsis. *Plant Physiology*, 117(4):1411–1421, 1998.
- K. Vijayakumari and J. T. Puthur. γ -aminobutyric acid (GABA) priming enhances the osmotic stress tolerance in *Piper nigrum* linn. plants subjected to PEG-induced stress. *Plant Growth Regulation*, 78(1):57–67, 2015.
- B. Xu, Y. Long, X. Feng, X. Zhu, N. Sai, L. Chirkova, A. Betts, J. Herrmann, E. J. Edwards, M. Okamoto, R. Hedrich, and M. Gilliam. GABA signalling modulates stomatal opening to enhance plant water use efficiency and drought resilience. *Nature Communications*, 12(1):1–15, 2021.
- M. Zhang, J. Zhao, L. Li, Y. Gao, L. Zhao, S. B. Patil, J. Fang, W. Zhang, Y. Yang, M. Li, and X. Li. The Arabidopsis U-box E3 ubiquitin ligase PUB30 negatively regulates salt tolerance by facilitating BRI1 kinase inhibitor 1 (BKI1) degradation. *Plant, Cell & Environment*, 40(11):2831–2843, 2017.
- S. Zhang and D. F. Klessig. MAPK cascades in plant defense signaling. *Trends in Plant Science*, 6(11):520–527, 2001.
- M. Zik, T. Arazi, W. A. Snedden, and H. Fromm. Two isoforms of glutamate decarboxylase in Arabidopsis are regulated by calcium/calmodulin and differ in organ distribution. *Plant Molecular Biology*, 37(6):967–975, 1998.

SAI: FAST AUTOMATED QUANTIFICATION OF STOMATAL PARAMETERS FROM MICROSCOPE IMAGES

A plant physiologist slaves away into late hours of the evening; analysing small details within the biopsy slides she captured through microscopy earlier that same day. She endeavours in the face of sleep deprivation to understand how and why our green counterparts survive and thrive in our farms, yards and forests. Her ultimate goal is to bestow physiological armour to our crops, tress and flowers. A noble cause by any measure – after all we may very well need them more than they need us. A stark reality plagues these pure motivations; her experimental controls are ensured through a pain staking process of measurement, measurement and more measurement. At first an exciting addition to her professional repertoire – now as routine as brushing their teeth; consumes hours, days and months of valuable time. *"But this is what science demands of me, ensuring the validity and reproducibility of my work"* She tells herself *"There's no way around it – it has to be done, but does it have to be done by me?"* Short of attracting a new graduate student to assign under the guise of *learning*, another option presented itself; the great automator – silicon. *"If computers can take everyone else's jobs I am sure it can take one of mine."*

By
Model Trainer of SAI
James Paul Bockman

Statement of Authorship

Title of Paper	SAI: Fast automated quantification of stomatal parameters from microscope iamges.
Publication Status	<input type="checkbox"/> Published <input type="checkbox"/> Accepted for Publication <input checked="" type="checkbox"/> Submitted for Publication <input type="checkbox"/> Unpublished and Unsubmitted work written in manuscript style
Publication Details	Na Sai, James Paul Bockman, Hao Chen, Nathan Watson-Haigh, Bo Xu, Xueying Feng, Adriane Piechatzek, Chunhua Shen, and Matthew Gilliam. "SAI: Fast automated quantification of stomatal parameters on microscope images."

Principal Author

Name of Principal Author (Candidate)	Na Sai				
Contribution to the Paper	Producing barley training data images. Development and labelling all model training data annotation. Development in post-processing procedures to improve measurement quality and remove outliers. Runtime benchmarking analysis of the tool on various hardware. Providing advice on development of a web demo showcasing and a user-friendly web application that is accessible to those without a computer science background. Development and conducting experiment for Average-Human/Machine Test (Figure 6.2, Appendix E1). Conducting experiment for section "SAI in practice" (Figure 6.3, Appendix E2). Writing and editing of final submission.				
Overall percentage (%)	25%				
Certification:	This paper reports on original research I conducted during the period of my Higher Degree by Research candidature and is not subject to any obligations or contractual agreements with a third party that would constrain its inclusion in this thesis. I am the primary author of this paper.				
Signature	<table border="1" style="width: 100%;"> <tr> <td style="width: 80%;"></td> <td style="width: 20%;">Date</td> </tr> <tr> <td></td> <td>13/12/2021</td> </tr> </table>		Date		13/12/2021
	Date				
	13/12/2021				

Co-Author Contributions

By signing the Statement of Authorship, each author certifies that:

- i. the candidate's stated contribution to the publication is accurate (as detailed above);
- ii. permission is granted for the candidate to include the publication in the thesis; and
- iii. the sum of all co-author contributions is equal to 100% less the candidate's stated contribution.

Name of Co-Author	James Paul Bockman				
Contribution to the Paper	Literature summary comparing machine vision techniques used in the field so far. Translating the measurement problem into a set of machine vision tasks. Converting human annotations on Arabidopsis data to machine learning compatible format. Deep learning experiments to determine feasibility, model type and hyperparameters for both plant species examined (Appendix E3-E9). Development and testing of post-processing procedures to improve measurement quality and remove outliers. Production of matched human-machine dataset used to statistically verify the quality of measurements produced. Writing, editing and proofing of final submission. Development and deployment of a web demo showcasing examples of the technique's measurements. Adaptation and development of the method to a user-friendly web application that is accessible to those without a computer science background. Runtime benchmarking analysis of the tool on various hardware.				
Signature	<table border="1" style="width: 100%;"> <tr> <td style="width: 80%;"></td> <td style="width: 20%;">Date</td> </tr> <tr> <td></td> <td>15 DEC 21</td> </tr> </table>		Date		15 DEC 21
	Date				
	15 DEC 21				

CHAPTER 6. SAI: FAST AUTOMATED QUANTIFICATION OF STOMATAL PARAMETERS FROM MICROSCOPE IMAGES

Name of Co-Author	Hao Chen		
Contribution to the Paper	Translating the measurement problem into a set of machine vision tasks. Setting up the experimental framework for Mask-RCNN. Translating human annotations for barley stomata into a machine learning compatible format.		
Signature		Date	13/12/2021

Name of Co-Author	Nathan Watson-Haigh		
Contribution to the Paper	Guidance in development of Average-Human/Machine Test. Proof reading and editing final submission.		
Signature		Date	14/12/2021

Name of Co-Author	Bo Xu		
Contribution to the Paper	Providing Arabidopsis test images and corresponding human processed measurements. Providing human processed measurements for Average-Human/Machine Test. Proof reading and editing final submission.		
Signature		Date	17/12/2021

Name of Co-Author	Xueying Feng		
Contribution to the Paper	Providing Arabidopsis images for model training. Providing human processed measurements for Average-Human/Machine Test.		
Signature		Date	17/12/2021

Name of Co-Author	Adriane Piechatzek		
Contribution to the Paper	Providing human processed measurements for Average-Human/Machine Test.		
Signature		Date	17/12/2021

Name of Co-Author	Chunhua Shen		
Contribution to the Paper	Guidance on competing literature, techniques and methods already published. Translating the measurement problem into a set of machine vision tasks. Providing advice and grounding to machine learning approaches explored as potential candidates. Proof reading and editing final submission. Management of timelines and key milestones.		
Signature		Date	13/12/2021

Name of Co-Author	Matthew Gilliam		
Contribution to the Paper	Providing advice on data interpretation of test data with biological experimental design. Proof reading and editing final submission. Management of timelines and key milestones.		
Signature		Date	17/12/2021

Using microscopy to investigate stomatal behaviour is a common in plant physiology research. Manual inspection and measurement of stomatal features is a low throughput process in terms of time and human effort, which relies on expert knowledge to identify and measure stomata accurately. This process represents a significant bottleneck in research pipelines, adding significant researcher time to any project that requires it. To alleviate this, we introduce StomaAI (SAI): a reliable and user-friendly tool that measures stomata of the model plant *Arabidopsis* (dicot) and the crop plant barley (monocot grass) via the application of deep computer vision. We evaluated the reliability of predicted measurements: SAI is capable of producing measurements consistent with human experts and reproduced conclusions of published datasets in a fraction of the time taken manually. Hence, SAI boosts the number of images that biologists could evaluate at one time to obtain more accurate measurements.

Introduction

Stomata, derived from the Greek word *mouth*, are small pores penetrating the epidermal surface of plant aerial organs. In monocot grasses, such as barley or maize, the stomatal apparatus includes a pair of subsidiary cells flanking the dumbbell-shaped guard cells surrounding the stomatal pore^{1,2}. Dicot plants, instead, have a pair of kidney-shape guard cells surrounding each stomatal pore. Stomatal pores play a critical role in plant physiology. By limiting the diffusion of carbon dioxide (CO₂) into leaves, stomata control the rate of photosynthesis. Photosynthesis produces the carbohydrates, adenosine triphosphate (ATP), and nicotinamide adenosine phosphate (NADPH) required for plant metabolic functions, growth and development; releasing oxygen as a by-product. At the same time, water vapour released via stomatal pores enables water transport through plants^{3,4}. Some plants survive during excessive heat by keeping stomata open, cooling leaves through the evaporation of water. Conversely, stomata are closed during droughts to prevent water loss⁴. Stomata also respond to diel cycles, such as light and dark, and a multitude of other signals to optimise CO₂ gain and water loss^{5,6}. As a consequence, stomatal aperture regulation during daily light and dark cycles, or in response to environmental stresses, directly impacts plant growth, development and survival⁶⁻⁸.

Due to the important role that stomata play, investigating stomatal regulation has become a common task for biologists studying plant signalling pathways and stress perception^{6,9,10}. To study stomata traits (i.e. size or density) researchers commonly use microscopy¹¹⁻¹³. This method of examining stomatal behaviour, although commonplace, is not straightforward. Morphological differences in stomata of different species (Figure

6.1) and variable image quality make accurate stomatal measurement a task that requires experience and training. Traditionally, stomatal measurement requires manual inspection of each image to identify and measure relevant features (i.e. stomatal pore area and aperture). Hundreds of images need to be analyzed this way to gain sufficient statistical power to support a biological conclusion; a time consuming and laborious process. Although manual measurement can be aided by image processing software such as Fiji-ImageJ¹⁴, manually tuned parameters are required to produce acceptable performance¹⁵. An automated stomatal measurement system is thus highly desirable and will accelerate plant physiology research.

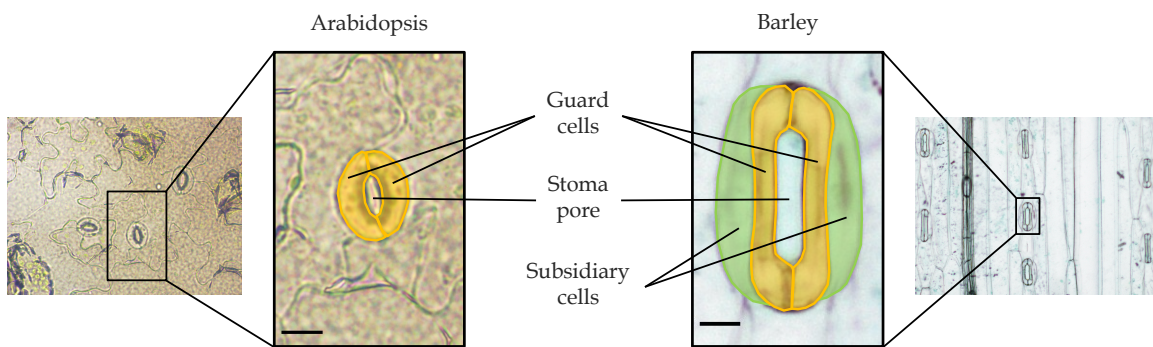


Figure 6.1. The stomata of *Arabidopsis thaliana* and barley (*Hordeum vulgare*). Components of Arabidopsis and barley stoma are highlighted and labelled; the scale bar equates to 10 μm for both Arabidopsis and barley.

Microscopy imaging presents a uniquely controlled environment for the application of modern computer vision techniques. Images can be captured in high-resolution via calibrated optics, reducing systematic noise, and plant anatomy enforces regularity in pattern, appearance and orientation (in monocot grasses). These factors remove several of the common *Achilles' Heels* of applied vision systems. Previous attempts have been made to quantify stomatal attributes using traditional computer vision techniques to predict stomatal density, width and area^{16–21}. Although these methods demonstrate efficacy on their respective tasks, they rely on handcrafted and/or multi-stage processes. The use of Convolutional Neural Networks (CNNs) to detect stomatal attributes has recently increased in popularity^{22–29}. CNNs enable a series of pertinent operations to be learnt from examples – acting as a data driven approximation of a sequence of computer vision operations.

More recently, Mask Regions with Convolutional Neural Network features (Mask

R-CNN) has been used to perform identification and localisation of stomata. This involves the entire stomatal complex being detected, encircled by a polygon with its orientation and stomatal complex area captured, inferring axis length³⁰ or stomata density³¹. The algorithms were successfully used across different species with varying image quality³⁰. Of the techniques surveyed, many studies only estimate stomatal counts for use in density calculations^{17,19,21,25,26,29,31} with Fetter et al. (2019)²⁶ providing a user friendly online application named "Stomata Counter". Fewer studies are focused on stomatal pore measurements, with methods that are semi-automated requiring handcrafted feature extractors or manual post-processing following model inference^{18,22,24,27,28}. Ellipse fitting is the common solution used among these studies for estimating the pore area, width and length through calculating the fitted ellipse's area, minor-axis and major-axis^{22,24,27,28,32}. However, the fitting method is restricted to stomata with an ovular-shaped pore (e.g. Arabidopsis stomata), and other shapes of the stomatal pore (e.g. barley) cannot be represented correctly with an ellipse and result in under or over estimation of pore features (Figure 6.1). Besides, none of the above studies offers a usable automated stomatal pore measurement tool available for use.

Here, we present StomaAI (SAI) as an accessible automated tool that allows stomatal pore measurement of microscope images. The precise stomatal pore feature measurement is the core novelty of StomaAI (SAI), measuring pore area, length, width (i.e. aperture), and width/length ratio. We demonstrate that measurements obtained using SAI are comparable to those taken by human experts, providing assurance of prediction reliability. This key comparison is not provided by contemporary studies that use traditional computer vision evaluation criteria such as F1 score or average precision (AP) to evaluate machine performance. Due to differences in stomata morphology, SAI includes two class-specific models: a dicot model trained with Arabidopsis data and a monocot cereal model trained with barley data. We demonstrate that with approximately 150 annotated images containing about 1700 stomata, SAI can be trained to measure pores of two different plant species. The online demonstrator software where model inference can be viewed is hosted at <https://sai.aimgl.team>. To use SAI to measure user acquired samples, we provide a local version that can be accessed via <https://github.com/xdynamics/sai-app>.

Results

Model performance. Stomatal measurement was carried out on two plant species: Arabidopsis and barley. Validation samples of barley stoma were kept at their native

resolution of 2880×2048 when used to evaluate model measurements. Our model obtained a mAP of $84.91\% \pm 0.59$ for bounding boxes, $70.44\% \pm 0.12$ for segmentation masks and $84.28\% \pm 0.17$, $67.09\% \pm 10.60$ for keypoint detections on open and closed samples respectively. Arabidopsis measurements were evaluated on validation images at their native resolution of 2592×1944 . Models trained to measure Arabidopsis stomatal pores obtained a mean average precision (mAP) of $73.81\% \pm 1.14$ for bounding boxes, $44.18\% \pm 0.23$ for segmentation masks and $53.11\% \pm 1.53$, $32.21\% \pm 4.5$ for keypoint detections on open and closed samples respectively. Mean and sample standard deviation estimates were obtained by training five models with different random initializations.

SAI achieves human-level performance. Beyond assessing performance using traditional metrics, we show that SAI produces measurements that are equivalent to *human-level* performance. To compare independent human operators (multiple plant physiology researchers) with SAI we applied an Average-Human/Machine Test. To reduce rater’s bias, the average measurements taken by 4 human experts were used to provide a *human-level* reference. The concordance correlation coefficient (CCC; ranging from -1 to 1) was used to evaluate the agreement between different human’s measurements, the *human-level* reference and SAI³³. Stomatal width, length, area and width/length ratio were measured by SAI (Figure 6.2, Appendix Figure E.1) and human experts (Appendix Figure E.2). Width measurements obtained from SAI, when plotted against reference measurements, generally align with $y = x$; indicating that width measurements are consistent with the reference (Figure 6.2). Incorrectly classified samples (i.e. where the predicted opening status disagree with the reference) can be identified as those points along the x or y axes. SAI achieves a CCC of 0.891 and 0.984 for Arabidopsis and barley respectively. Considering that any Arabidopsis open stomata have its stomatal width less than $1 \mu\text{m}$ have a minimal impact on transpiration, the Arabidopsis stomatal width achieves a CCC at 0.916 with the human-level reference, when excluding stomata that have a width of less than $1 \mu\text{m}$. Human experts show an average CCCs of 0.9449 on Arabidopsis samples and 0.9853 when measuring barley (Appendix Figure E.2). Measurements performed on barley samples exhibited improved correspondence with the reference in all cases.

Relative errors (RE) in measurements from SAI are distributed in a similar pattern to those from human measurements (Appendix Figure E.2). Judging aperture extent in stomata that are almost closed is more difficult than when they are open. This creates a skew in the RE histogram where errors are more frequently observed in small measurements. Estimation of stomatal length were not affected by stomatal opening status, so REs were evenly spread between under and over estimation. The mean

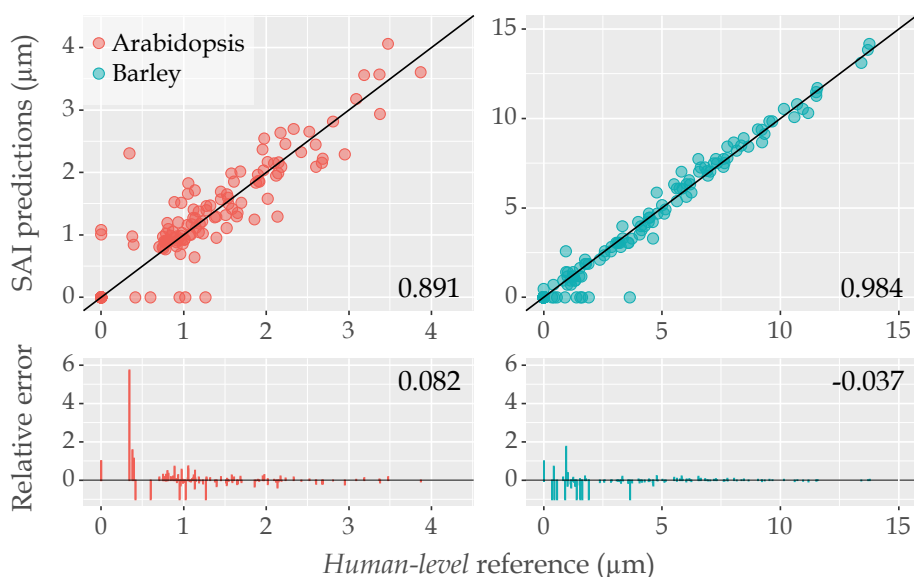


Figure 6.2. SAI prediction vs average *human-level* reference set in Arabidopsis and barley stomatal width (μm). Stomata morphology measurements from 4 human experts were collected and an average width of each stoma were calculated as the *human-level* reference. In upper panel, SAI predictions were compared against the reference and the concordance correlation coefficient (CCC, ranging from -1 to 1) was displayed as the determination of the accuracy performance. The black diagonal line is the $y = x$ line and CCC is a measure of dispersion for the points from that line. The corresponding relative error (RE) to *human-level* reference was presented at lower panel with mean RE presented. Data points are color coded by plant species. (Arabidopsis: $N > 120$, barley: $N > 160$)

stomatal width, length, area and width/length ratio were calculated for each source of measurements and compared using one-way ANOVA with Tukey HSD (Appendix Table E.1). This comparison aims to test whether measurement sources exhibit a statistically significant difference. No such significance was found in measured stomatal features across both Arabidopsis and barley samples when SAI was compared to the *human-level* reference measurements (Appendix Figure E.3). Additionally, SAI exhibits no significant difference from individual human expert measurements, except in the case of expert 2's length measurements for Arabidopsis. Interestingly, human expert 2's Arabidopsis measurements were significantly smaller in area, length and width to both human expert 1 and 3. In all cases, expert 2 tends to measure stomata more conservatively compared to others.

SAI produces consistent replication of human processed datasets. SAI was used to measure two sets of published physiological experiments. The original images

from Xu et al.¹¹ Supplementary Figure 3b & 5g were processed with SAI. Traditionally, researcher's will exercise their discretion by consciously measuring only stomata they deem as mature. SAI measures indiscriminately. However, we were able to emulate elimination of immature stomata via filtering of detections based on their estimated length. To exclude immature stomata, we eliminate detections of Arabidopsis stomata with lengths shorter than 2 μm and barley stomata shorter than 16 μm in length. SAI and the original manual measurements were compared using ANOVA with Tukey HSD, as in Xu et al. (2021)¹¹ (Figure 6.3). Scientific conclusions drawn from the statistical tests were consistent with those of Xu et al. (2021)¹¹. Arabidopsis stomata were closed in response to 25 μM ABA in the presence and absence of 2 mM GABA, and light induced barley stomatal opening was inhibited by the presence of 1 mM GABA.

The mean and distribution of stomatal width in each treatment group obtained using SAI were compared to the original manual measurements. SAI detected 66.37%

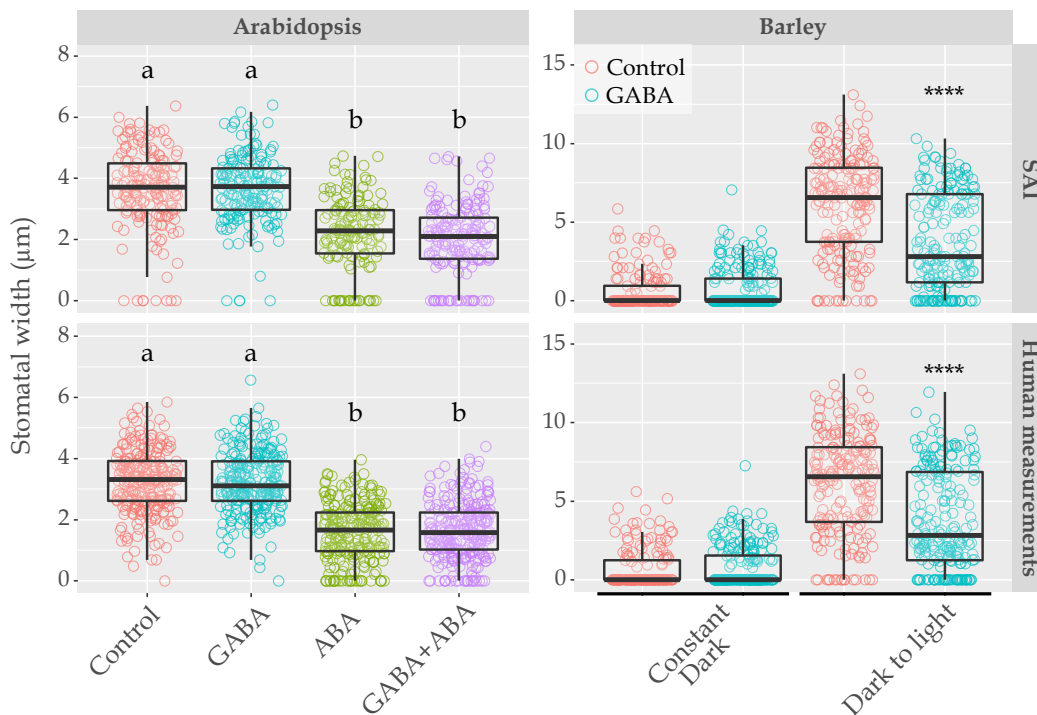


Figure 6.3. SAI predicted measurements are consistent with outcomes obtained by human researchers. Stomatal width in SAI predictions and human measurements collected with treatment under 25 μM ABA with 2 mM GABA (Arabidopsis) or 1 mM GABA (barley) during a dark-to-light transition¹¹. All data was tested using one-way ANOVA followed by Tukey HSD ($N > 140/\text{group}$ in Arabidopsis, $N > 150/\text{group}$ in barley. a and b represent groups with no difference, $p \leq 0.0001$ between groups, **** $p \leq 0.0001$).

and 91.39% of manually measured data in Arabidopsis and barley, respectively. This indicates SAI performs better when detecting barley stomata than Arabidopsis. Measurement distributions of stomatal width produced by SAI are similar in shape to those produced via manual inspection (Appendix Figure E.4). Human expert 2, who was identified as the most conservative measurer, performed the human measurement of Arabidopsis stomata (Figure 6.3, Appendix Figure E.3). Thus, the lower mean value for stomatal width obtained from human measurements was expected. When SAI measures barley samples, the distribution of measurements is almost identical to that of human measurements. This observation is likely due to the more uniform structure and higher image quality present in barley images.

SAI significantly reduces human effort. Model inference time is predominantly limited by image resolution and computation speed. Due to this, barley data (2880×2048 in resolution) generally took a longer time to process than Arabidopsis data (2592×1944 in resolution) when using the same processor. Figure 6.4 shows the average time required to process a microscope image on a range of commonly available hardware.

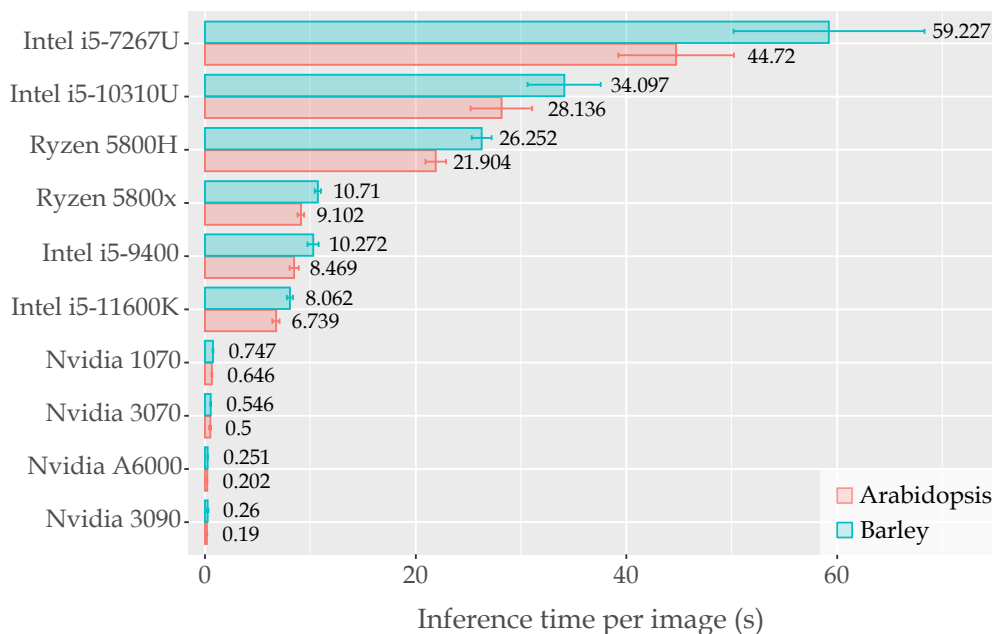


Figure 6.4. Wall clock time measured when processing a single microscope image using SAI. All processors are tested on the same image set of Arabidopsis and barley at the respective species native resolution. For all tests the confidence threshold is set to 0.5. Mean of inference time per sample is displayed with estimated sample standard deviation. All processors were on desktop, except Intel i5-10310U, Intel i5-7267U (MacBook Pro 2017), Ryzen 5800H and Nvidia 3070 were on a laptop.

Discussion

SAI provides a new way to analyse stomata, one of the most studied plant cell types. Our tool allows a series of stomatal features to be extracted. Specifically, opening status, complex location, width, length, and area of stomatal pores. Throughout testing, SAI generally produces better predictions on barley than Arabidopsis. This is observed for both the number of true detections made and measurement quality reflected by CCC. This might be due to image quality and leaf epidermis morphological structure. Although stomata have a relatively uniform structure, the random distribution and orientation of Arabidopsis stomata make the measurement task more challenging than for barley, which has stomata that are aligned in parallel rows with fixed orientations (Figure 6.1). Using the criteria outlined in Jayakody et al. (2021)³⁰ to assess image quality, we found that Arabidopsis samples are rated as medium quality – due to the presence of mesophyll cell debris in the images, whereas barley samples are considered high quality. The observed disparity in measurement quality supports the claim made in Jayakody et al. (2021)³⁰ that image quality has a major impact on model performance.

The common technique used in automated stomatal pore measurement systems is to use ellipse fitting to estimate pore area, width and length from the fitted ellipse's area, minor-axis and major-axis^{22,24,27,28,32}. Ellipse fitting is limited to stomatal pores that have oval shapes, such as those delineated by kidney-shaped guard cells (Figure 6.1). Plants like barley, which have stomatal pores delineated by dumbbell-shaped guard cells, do not have elliptical pores (Figure 6.1). Their stomatal pores resemble a coin slot, which cannot be represented accurately with an ellipse, leading to under or over estimation in derived measurements. In contrast, SAI uses direct mask segmentation of the stomata pores, which is flexible to represent any pore shape and obtain pore area by calculating masked pixel area. Moreover, the efficacy of ellipse fitting is positively correlated with the extent of stomatal pore opening²⁸. Therefore ellipse fitting cannot be used effectively for stomatal assays under experimental conditions that require measurement of stomata that are partially open or completely closed, e.g., stomata exposed to ABA, high CO₂, H₂O₂ and darkness to induce stomatal closure^{11,13}. SAI classified stomata before performing the measuring task and recorded the closed stomata with width and area as zero. This process includes closed stomata in the dataset and allows SAI to deal with the real-world experimental design in plant research.

From our analysis we have determined that SAI achieves *human-level* performance and when used leads to conclusions consistent with human researchers. However,

SAI has many advantages compared to manual measurement. SAI produce stable and reproducible measurements. We observed that manual measurements contains rater's bias in Average-Human/Machine Test, therefore, measurements produced by two different experts will vary (Appendix Figure E.2). In contrast, SAI's predictions are consistent, regardless of the researcher using it. This guarantees that measurements are reproducible from the same set of samples. Of particular importance to the future of plant physiology, SAI enables researchers to verify other's conclusions without weeks of human effort. Provided that the samples from which a biologist draws their conclusions are available, SAI can produce a set of measurements within minutes. These measurements can then be used to verify claims through the application of statistical analysis.

In our experiments, SAI detects less stomata than experts. Human experts are able to use their experience to extract measurements from some stomata that are blurry, occluded or unresolved. When SAI views such samples, it will ascribe a low level of confidence to its associated measurements. To prevent false positives, where SAI predicts there is a stoma present incorrectly, we discard measurements corresponding to detections below a minimum value of confidence. Confidence is an arbitrary scale from 0 to 1 that indicates how strongly the model responded to the region. In our experience, a confidence threshold of 0.5 allows the majority of false positives to be removed while retaining valid detections. Due to this process, stomata capable of being salvaged by experts are often discarded by SAI. It is important to note that the extraction of measurements from every single stoma from an image becomes less important due to SAI's high throughput and ability to quickly measure orders of magnitude more stomata.

Compared to manual measurement, SAI is exceptionally efficient. Depending on the confidence threshold, SAI can produce measurements from a high-resolution image in 6-12 seconds, while running on a mid-range desktop computer's central processing unit (CPU) (Figure 6.4). For a human, the equivalent process takes between 2 and 5 minutes depending on image quality, the number of stomata per image, measurements required and stomatal opening status. When using a graphics processing unit (GPU), SAI further increases this disparity. On an NVIDIA GTX 1070, SAI is able to process an image every 600 milliseconds. This means that with an entry-level GPU, SAI can process hundreds of images within a minute – the equivalent of 7-9 human hours. Automatically processing hundreds of images by SAI, makes it trivial to achieve minimum measurement numbers required per treatment group for statistical testing. In fact, SAI enables researchers to increase the statistical power of their conclusions. Here, SAI decouples human effort from the number of measurements per treatment group, making measuring additional pores an attractive prospect. This enables researchers to

measure previously unthinkable quantities of stomata per treatment group, allowing the law of large numbers to provide more accurate summary statistics of stomatal response.

SAI makes it possible to produce more accurate population measurements by processing a greater number of stomata in a shorter time period. This hassle-free, high resolution, time-efficient data acquisition assistant has the potential to accelerate research that has a major impact on plant physiology. Moreover, SAI's ability to learn how to measure stoma on both barley and *Arabidopsis* gives us confidence in its ability to do so in other species. Towards this, we provide an additional model with SAI which has been trained on a combined species data set. As pores share some common visual features, this model can be used as a starting point for researchers wishing to use SAI on a new type of plant. To do this, a set of measured examples that conform to our annotation format could be used to *fine tune* the provided combined species model. In this study, we only consider SAI's use in measuring pore features. However, given sufficient labelled data, extension to measurement of other relevant cell structures would be possible. More generally, SAI could be used to measure other structures captured via microscopy.

SAI is a reliable, fast and simple solution to automate stomatal measuring for plant biologists via a user friendly web app (online demo is available at <https://sai.ai.ml.team>, full version is available at <https://github.com/XDynamics/SAI-app>). SAI is a new tool that can free researchers from labour intensive low-throughput measuring tasks; accelerating the speed of physiology-based research, regardless of the shape of the stomatal pore.

Method

Data annotation and Modeling. *Arabidopsis thaliana* ecotype Col-0 and barley (*Hordeum vulgare*, Barke) were prepared as plant material¹¹. *Arabidopsis* images were captured using Axiophot Pol Photomicroscope (Carl Zeiss). A Nikon DS-Fi3 digital camera with a Nikon diaphot 200 inverted microscope was used to capture barley images. All images were annotated using RectLabel (version 3.03.8, <https://rectlabel.com>). Creation of pore feature annotations followed the procedure of manual measurement carried out in Fiji-ImageJ. In a given annotation, two labels were ascribed to each stoma (Figure 6.5). A bounding box which contains a single stoma with associated opening status (open or closed). Measurements of the stomatal pore were also taken.

These were recorded as a polygon or a line for open and closed stomata respectively. All information was organised for compatibility with Microsoft Common Objects in Context (MS-COCO); which is a widely used computer vision benchmark³⁴. Summary statistics of the created database of microscopy images are presented in Table 6.1.

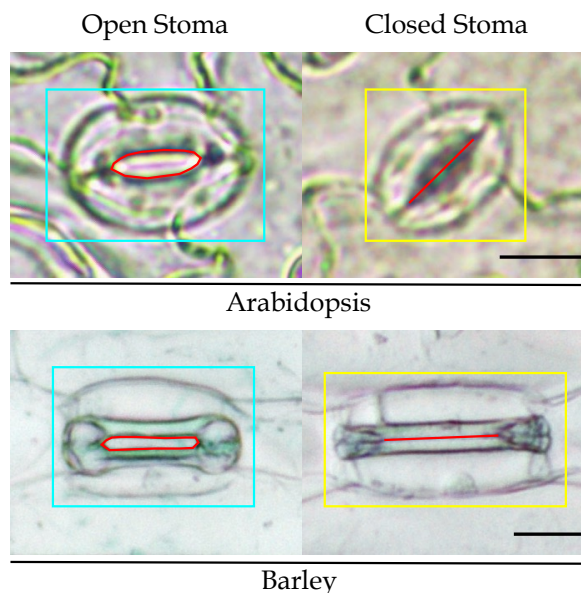


Figure 6.5. Annotation examples of Arabidopsis and barley stomata. Bounding boxes contain a single Arabidopsis or barley stoma (i.e. a pair of guard cells and a pair of subsidiary cells if from a relevant plant) and its opening status is determined in different label (open stoma in cyan, closed stoma in yellow). The red polygon and line present defined stomatal pore in each annotation. Scale bar represents 10 μm in Arabidopsis and 20 μm in barley.

Table 6.1. Summary metrics for stomatal pore dataset used in model training and evaluation.

	Slide Images		Stoma Instances	
	Train	Validation	Train	Validation
Arabidopsis	200	42	Open: 974 Closed: 293	Open: 235 Closed: 55
Barley	150	33	Open: 1000 Closed: 692	Open: 268 Closed: 89

Traditionally, researchers inspect each captured microscope image and measure relevant structures of a stoma. The measurement procedure will depend on the pore opening status. The area of an open stoma is measured by drawing a polygon that encloses its *mouth*. To determine the pore’s width and length, researchers either directly

measure or apply fitting methods to the aforementioned polygon. Closed pore lengths are acquired by selecting points which mark the beginning and end of their tightly shut *mouth*. For a computer model to emulate a researcher performing the measurement it must: localise target structures within a sample; comment on their state and gather relevant measurements. To enable this, we have reformulated each one of these tasks into a computer vision task. A researcher's initial identification of stomata and their opening status is re-framed as object detection. Object detection consists of drawing boxes around salient objects and predicting the enclosed object's semantics. Drawing polygons indicating stomatal openings maps to segmentation, which highlights regions of interest within images. Selecting end points for a stomatal pore is analogous to keypoint detection, which reduces visual features of interest to a defining pixel. Each of these tasks has a library of possible models capable of solving them individually. By requiring an all-inclusive solution, candidates are significantly reduced. Mask R-CNN represents an incremental change atop of an already established series of deep-learning architectures^{35–38}. This iteration comes armed with requisite predictive powers for our physiological needs. Through the use of specialised predictive *heads*, Mask-RCNN is capable of learning object detection, segmentation and keypoint detection in tandem.

Deep-learning models were built using Detectron 2; an open-source framework sitting on top of Pytorch. Both of these packages were created by Facebook's Artificial Intelligence Research division (FAIR)^{39,40}. Adaptions were made to FAIR's Mask R-CNN model to better suit stomatal measurement. Specifically, increasing the resolution of prediction heads responsible for segmentation and keypoint detection. Mean average precision (*mAP*), as defined in the MS-COCO challenge, was used to evaluate and compare models on all tasks³⁴. Justification and verification of model design choices and training regimes are presented in Appendices E.3-E.9. Pseudo-code for the tool's core measurement and processing loop is provided in Appendix E.10. Code used to train models and associated model weights can be found at <https://github.com/xdynamics/sai-training>.

Average-Human/Machine Test. To determine whether SAI predictions were consistent with human measurement, an Average-Human/Machine Test was designed. In total, 35 microscopy images, 15 of barley and 20 of Arabidopsis, were collated as a test dataset (summarised in Table 6.2). Four plant stomata morphology experts participated by manually measuring the 35 random selected images. The mean measurements of 4 human experts on each stoma were used as a *human-level* reference. This reference was used to quantify the extent to which a single researcher may vary within their own judgement and assess SAI. Participants used the same annotation schema

Table 6.2. Summary of Average-Human/Machine Test dataset.

	Images	Stomata	
		Open	Closed
Arabidopsis	20	129	20
Barley	15	109	66

outlined above data preparation. To understand how measurements retrieved from images change with respect to their measurers, all measurements were matched to a *human-level* reference at the single stoma level. Differences between measurement sources against the *human-level* reference were visualised with scatter plots and quantified by relative error. To evaluate the agreement between SAI/human experts and *human-level* reference, the concordance correlation coefficient (CCC; ranging from -1 to 1) was applied³³. Furthermore, the means of each measurement, for each measurer, was compared using one-way ANOVA with Tukey HSD.

SAI in practice. To support our claim that SAI is a replacement for traditional measurement methods, we demonstrate that scientific conclusions drawn from measurements produced by SAI align with those of expert physiologists. Manually measured image datasets of both Arabidopsis and barley were obtained from Xu et al. (2021)¹¹. Two different experimental designs were selected to evaluate SAI’s real-world performance: the 25 μM ABA with presence and absent of 2 mM GABA for Arabidopsis and dark-to-light transition with or without 1 mM GABA for barley (see Table 6.3). Reference measurements for the two datasets were made by different researchers. Arabidopsis measurements were taken by human expert 2. Barley samples were measured by human expert 4. Measurements produced by SAI were subjected to the same statistical tests used in Xu et al. (2021)¹¹ to examine whether SAI enables consistent

Table 6.3. Summary of the experimental design¹¹.

Species	Experimental design	Treatment group	
Arabidopsis	25 μM ABA 2 mM GABA	Control	
		ABA	
		GABA	
		GABA+ABA	
Barley	Dark to light transition with present or absent of 1 mM GABA	Constant dark	Control GABA
		Dark-to-light transition	Control GABA

conclusions as those reached by expert measurements.

Inference time assay. The efficiency of SAI compared to manual labelling was tested on a range of commonly available computer hardware. We do this using the same set of sample images used in the Average-Human/Machine Test (Table 6.2). Time to process each image was recorded and used to estimate the average inference time and sample standard deviation for each processor. These measures were then used to compare their throughput.

Acknowledgement

This research was supported by GRDC/ARC CoE Plant Energy Biology Scholarship (UWA1708-010RTX) to NS and Australian Government Research Training Program (RTP) Scholarship to JPB. MG was supported by CE14010008. High performance compute resources used in this work were funded by the Australian Research Council via LE190100080. Lockheed Martin Australia supported this research via a research scholarship awarded to JPB.

Author Contribution

NS produced barley images; developed and labelled all model training data annotation and developed and conducted experiment for Average-Human/Machine Test (Figure 6.2, Appendix E.1) and conducted experiment for section “SAI in practice” (Figure 6.3, Appendix E.2); provided advice on development of SAI online demo and offline application and drafted all figures. JPB translated the measurement problem into a set of machine vision tasks; converted human annotations to machine learning compatible format for Arabidopsis; conducted deep learning experiments to determine feasibility, model type and hyperparameters (Appendix E.3-E.10); developed and deployed SAI online demo showcasing and offline application. NS and JPB developed the post-processing procedures for improvement of measurement quality and immature stomata filtration; and conducted run time benchmarking analysis of SAI on various hardware (Figure 6.4). HC set up the experimental framework for Mask-RCNN and translated human annotations for barley into a machine learning compatible format. NW-H, CS, NS and JPB developed evaluation system for Average-Human/Machine Test. BX and XF provided Arabidopsis images. BX, XF, AP and NS provided human processed measurements for Average-Human/Machine Test. MG, CS and NS conceived the research. NS and JPB

drafted the original manuscript, NS, JPB, MG, CS, NW-H, BX and HC provided edits and revision to the final manuscript.

References

- [1] Gray, A., Liu, L. & Facette, M. Flanking support: How subsidiary cells contribute to stomatal form and function. *Frontiers in Plant Science* **11**, 881 (2020).
- [2] Cai, S., Papanatsiou, M., Blatt, M. R. & Chen, Z.-H. Speedy grass stomata: Emerging molecular and evolutionary features. *Molecular Plant* **10**, 912–914 (2017).
- [3] Sinha, R. K. *Modern plant physiology* (CRC Press, 2004).
- [4] Rizhsky, L. *et al.* When defense pathways collide. The response of arabidopsis to a combination of drought and heat stress. *Plant Physiology* **134**, 1683–1696 (2004).
- [5] Roelfsema, M. R. G. & Hedrich, R. In the light of stomatal opening: new insights into ‘the watergate’. *New Phytologist* **167**, 665–691 (2005).
- [6] Shimazaki, K. I., Doi, M., Assmann, S. M. & Kinoshita, T. Light regulation of stomatal movement. *Annu. Rev. Plant Biol.* **58**, 219–247 (2007).
- [7] McLachlan, D. H., Kopischke, M. & Robatzek, S. Gate control: guard cell regulation by microbial stress. *New Phytologist* **203**, 1049–1063 (2014).
- [8] Hetherington, A. M. & Woodward, F. I. The role of stomata in sensing and driving environmental change. *Nature* **424**, 901–908 (2003).
- [9] Kim, T. H., Böhmer, M., Hu, H., Nishimura, N. & Schroeder, J. I. Guard cell signal transduction network: Advances in understanding abscisic acid, CO₂, and Ca²⁺ signaling. *Annual Review of Plant Biology* **61**, 561–591 (2010).
- [10] Ye, W. & Murata, Y. Microbe associated molecular pattern signaling in guard cells. *Frontiers in Plant Science* **7**, 583 (2016).
- [11] Xu, B. *et al.* GABA signalling modulates stomatal opening to enhance plant water use efficiency and drought resilience. *Nature Communications* **12**, 1952 (2021).
- [12] Eisele, J. F., Fäßler, F., Bürgel, P. F. & Chaban, C. A rapid and simple method for microscopy-based stomata analyses. *PLoS One* **11**, e0164576 (2016).
- [13] Chater, C. *et al.* Elevated CO₂-induced responses in stomata require ABA and ABA signaling. *Current Biology* **25**, 2709–2716 (2015).

- [14] Schindelin, J. *et al.* Fiji: an open-source platform for biological-image analysis. *Nature Methods* **9**, 676–682 (2012).
- [15] Cheng, Y. *et al.* Analyses of plant leaf cell size, density and number, as well as trichome number using cell counter plugin. *Bio-protocol* **4**, e1165 (2014).
- [16] Omasa, K. & Onoe, M. Measurement of stomatal aperture by digital image processing. *Plant and Cell Physiology* **25**, 1379–1388 (1984).
- [17] Violet-Chabrand, S. & Brendel, O. Automatic measurement of stomatal density from microphotographs. *Trees* **28**, 1859–1865 (2014).
- [18] Laga, H., Shahinnia, F. & Fleury, D. Image-based plant stomata phenotyping. In *13th International Conference on Control Automation Robotics & Vision (ICARCV)*, 217–222 (IEEE, 2014).
- [19] Duarte, K. T. N., Carvalho, M. A. G. & Martins, P. S. Segmenting high-quality digital images of stomata using the wavelet spot detection and the watershed transform. In *the 12th International Joint Conference on Computer Vision, Imaging and Computer Graphics Theory and Applications - Volume 4: VISAPP, (VISIGRAPP 2017)*, 540–547. INSTICC (SciTePress, 2017).
- [20] Bourdais, G. *et al.* The use of quantitative imaging to investigate regulators of membrane trafficking in arabidopsis stomatal closure. *Traffic* **20**, 168–180 (2019).
- [21] Sakoda, K. *et al.* Genetic diversity in stomatal density among soybeans elucidated using high-throughput technique based on an algorithm for object detection. *Scientific Reports* **9**, 7610 (2019).
- [22] Jayakody, H., Liu, S., Whitty, M. & Petrie, P. Microscope image based fully automated stomata detection and pore measurement method for grapevines. *Plant Methods* **13**, 94 (2017).
- [23] Saponaro, P. *et al.* Deepxscope: Segmenting microscopy images with a deep neural network. In *the IEEE Conference on Computer Vision and Pattern Recognition (CVPR) Workshops*, 843–850 (2017).
- [24] Bhugra, S. *et al.* Automatic quantification of stomata for high-throughput plant phenotyping. In *2018 24th International Conference on Pattern Recognition (ICPR)*, 3904–3910 (IEEE, 2018).
- [25] Meeus, S., Van den Bulcke, J. & wyffels, F. From leaf to label: A robust automated workflow for stomata detection. *Ecology and Evolution* **10**, 9178–9191 (2020).

- [26] Fetter, K. C., Eberhardt, S., Barclay, R. S., Wing, S. & Keller, S. R. Stomata-Counter: a neural network for automatic stomata identification and counting. *New Phytologist* **223**, 1671–1681 (2019).
- [27] Bhugra, S. *et al.* Deep convolutional neural networks based framework for estimation of stomata density and structure from microscopic images. In *the European Conference on Computer Vision (ECCV) Workshops* (2018).
- [28] Li, K. *et al.* Automatic segmentation and measurement methods of living stomata of plants based on the cv model. *Plant Methods* **15**, 67 (2019).
- [29] Falk, T. *et al.* U-net – deep learning for cell counting, detection, and morphometry. *Nature Methods* **16**, 67–70 (2019).
- [30] Jayakody, H., Petrie, P., de Boer, H. J. & Whitty, M. A generalised approach for high-throughput instance segmentation of stomata in microscope images. *Plant Methods* **17**, 1–13 (2021).
- [31] Bheemanahalli, R. *et al.* Classical phenotyping and deep learning concur on genetic control of stomatal density and area in sorghum. *Plant Physiology* **186**, 1562–1579 (2021).
- [32] Liang, X. *et al.* StomataScorer: A portable and high-throughput leaf stomata trait scorer combined with deep learning and an improved cv model. *Plant Biotechnology Journal* 1–15 (2021).
- [33] Lin, L. I. A concordance correlation coefficient to evaluate reproducibility. *Biometrics* **45**, 255–268 (1989).
- [34] Lin, T. Y. *et al.* Microsoft COCO: Common objects in context. In *the European Conference on Computer Vision (ECCV)*, 740–755 (Springer, 2014).
- [35] He, K., Gkioxari, G., Dollár, P. & Girshick, R. Mask R-CNN. In *the IEEE International Conference on Computer Vision (ICCV)*, 2961–2969 (2017).
- [36] Girshick, R., Donahue, J., Darrell, T. & Malik, J. Rich feature hierarchies for accurate object detection and semantic segmentation. In *Proceedings of the IEEE conference on computer vision and pattern recognition*, 580–587 (2014).
- [37] Girshick, R. Fast R-CNN. In *Proceedings of the IEEE international conference on computer vision*, 1440–1448 (2015).

- [38] Ren, S., He, K., Girshick, R. & Sun, J. Faster R-CNN: Towards real-time object detection with region proposal networks. *IEEE Transactions on Pattern Analysis and Machine Intelligence* **39**, 1137–1149 (2017).
- [39] Wu, Y., Kirillov, A., Massa, F., Lo, W. Y. & Girshick, R. Detectron2 (2019).
- [40] Paszke, A. *et al.* Pytorch: An imperative style, high-performance deep learning library. In Wallach, H. *et al.* (eds.) *Advances in Neural Information Processing Systems*, vol. 32, 8026–8037 (Curran Associates, Inc., 2019).

GENERAL DISCUSSION

The non-proteinogenic amino acid – GABA, is first shown here to act as a regulator of stomatal pore movement in barley. This has been examined physiologically using stomatal assays and gas exchange with a combination of stimuli such as light, darkness and ABA (Chapter 3), and as transcriptional modulator via external GABA application (Chapter 4). Additionally, transcriptome profiling of GABA deficient Arabidopsis mutants was analysed to explore the changes raised by absence of GABA and the potential relationship between GABA and guard-cell regulation in Arabidopsis (Chapter 5). Throughout all the experiments conducted, stomatal assay took the longest time to complete with large amount of repetitive measurements and repeated experiments to ensure accuracy in defining the biology. StomaAI (SAI) was then developed as an accurate, high-throughput and high-efficiency methods to speed up the experiment process (Chapter 6). The following discussions mainly focus on research gaps and future directions.

7.1 GABA act as a signal in stomata regulation

In epidermal strip assays, 1 mM GABA did not elicit stomatal movement itself under steady state conditions, but reduced stomatal movement stimulated by opening or closing signals (Section 3.1.1.1). Two millimolar GABA, however, closed stomata in epidermal strips. Using intact leaves, the stomatal opening process triggered by light was reduced by GABA feeding (Figure 3.3); however, such feeding did result in less closed stomata in the dark, in fact stomata if anything were more closed with GABA treatment (Figure 3.2). Furthermore, up to 8 mM GABA did not close stomata in intact leaves under steady state conditions. In Section 3.1.2.1, the sensitivity of ABA was shifted for barley epidermal peels by GABA supplement. Low-doses of GABA (1 mM in stomata assay) itself does not elicit stomatal pore change and reduces stomatal sensitivity to ABA ($EC_{50} = 5.533 \mu\text{M}$ vs. $17.95 \mu\text{M}$); whereas at high-doses (2 mM GABA) stomata had the same sensitivity as non-GABA treated, as well as inducing stomatal closure by ~25% (Figure 3.6). Such inconsistencies in stomatal sensitivity to GABA between epidermal strips and intact leaves has also been observed in Arabidopsis where GABA only inhibits stomatal opening in both leaves and epidermal strips (Figure 3.1(b); Xu et al., 2021). Clearly more work is required to unravel these complexities, and are necessary to unravel the role of GABA in barley leaves.

The inconsistent observation between intact leaf and epidermal peels might be due to the removal of mesophyll cells from epidermal peels. Indeed, mesophyll cells do contribute to guard-cell signalling and stomatal regulation, such as malate, sucrose and GABA (Lawson et al., 2014, Lima et al., 2018, Xu et al., 2021). For instance, previous research from Arabidopsis indicated that the guard-cell specific complementation of native *GAD2* only restored *gad2* mutant performance under water-deficit stress; whilst GABA metabolism in mesophyll cells might contribute to stomatal performance under non-stressed conditions (Xu et al., 2021). Over expression of GAD in the stomata of barley, and in whole leaves would be interesting and help to further define what impact GABA has on stomatal control in barley.

The mechanism by which GABA acts in barley is undefined. Is it, like in Arabidopsis through inhibition of a vacuolar ALMT, or a distinct mechanism? Hints to alternative mechanisms occur in the transcriptional data and are discussed below. Furthermore, as discussed in Chapter 3, treatment with 10 mM GABA stimulates K^+ efflux in Arabidopsis root epidermis likely via the GORK channel, therefore our barley results raise new questions: (1) Does GABA have similar effect on K^+ efflux on barley roots; (2) Does GABA act on guard-cell GORK in barley?; (3) Does GABA acts on barley GORK

via a similar mechanism as ALMTs which contains a putative GABA binding motif? Or indirectly through its role in controlling membrane potential via altering ALMT activity. (4) Does 2 mM GABA (stomatal assay)/8 mM GABA (gas exchange) activate K⁺ efflux from barley guard cells? It is known that GABA accumulated in the apoplastic space through the transpiration stream in gas exchange experiment. An alternative question is: does the presence of higher GABA accumulation change the water potential (Ψ_w), like sucrose (Kang et al., 2007, Lu et al., 1997); and/or the apoplastic pH (Hedrich et al., 2001), and impact stomatal pore movement via these indirect effects. All these questions require additional and varied assays such as ion flux analysis, pH and osmotic potential measurement, heterologous expression and characterization of target proteins, and genetic manipulation of barley.

7.2 Interactions of GABA and plant signals at the transcriptional level

Through physiological experiments, GABA appears to act as a signal by interacting with other signals, such as light, darkness and ABA. Here, the interactions at the transcriptome level were assessed by externally applying GABA as a treatment (on barley) and GABA deficient mutants (on Arabidopsis). By manipulating the GABA content, several key changes were found:

1. MAPK signalling pathway is affected by GABA accumulation, regardless of GABA supplement or deficiency.
2. GABA effects are distinct from those of ABA, but GABA may interact with ABA through impacting ROS signaling.
3. Mutation of *GAD* may disrupt the circadian clock and potentially lead to changes of water use and stomatal regulation.

7.2.1 GABA and the MAPK signalling pathway

The reduction of GABA content in Arabidopsis leads to a series of GO and KEGG changes involving signalling molecules such as jasmonic acid (JA), abscisic acid (ABA) and reactive oxygen species (ROS) by down-regulate associated genes that reflected on our enriched GO terms (Table 5.1 and 5.3). Moreover, many genes from MAPK signalling pathways, the convergence point of the defense-signalling network, were down-regulated due to the GABA deficiency (Figure 5.12). By externally applying GABA, enrichment projection of GO terms and KEGG pathway are quite distinct compared to

enrichment results following ABA external application (Figure 4.4 and 4.5) with few shared terms and pathways. Here, the MAPK signalling pathway was significantly changed under both GABA and ABA application. This pathway is consistently enriched whether plants were under GABA deficiency or external application suggesting GABA should play a key regulatory role via interacting with the broad defence-signalling network. Further exploration should focus on the co-expressed gene groups in relation to ABA and GABA, and find potential hub genes from a constricted gene network (Li et al., 2016).

7.2.2 GABA and ROS production

In chapter 4, we aim to reveal the gene functions and pathways that are involved in GABA signalling and how it could interact with ABA signalling transcriptionally. Our data indicated that both GABA and ABA may interact with ROS production. ROS involvement in the regulation of stomatal movement is known and documented (Song et al., 2014), especially Yao et al. (2013) illustrated that H₂O₂ mediated stomatal closure involves the accumulation of H₂O₂ in maize subsidiary cells. In ABA-induced ROS production, we know that SnRK2s is required for phosphorylation of RbohF (Sirichandra et al., 2009). However, with GABA, we observe the gene expression changes induced by GABA but the interaction with guard cell RbohD and/or RbohF with or without SnRK2.4 is not clear, not mention high-doses GABA also inducing stomatal closure. Further exploration starting from examine ROS contents (e.g. H₂O₂) in guard cells and subsidiary cells with series concentration of GABA. Furthermore, there were differences in ROS responsive genes in *gad2* and *gad1245* in Arabidopsis. It would be worth examining the differences in ROS contents of these genotypes.

7.2.3 GABA deficiency leads to disruption of the circadian clock

With Arabidopsis deficient in GABA, the extent to which disruption of circadian regulated genes is aligned with the number of GAD mutations introduced (Figure 5.13). In plants, the circadian oscillator contributes to many important physiology aspects, including stomatal movement, photosynthesis and key time point of developmental processes (e.g. flowering time; Choudhary et al., 2015, Dodd et al., 2005, Hassidim et al., 2017, Simon et al., 2020). Transpiration and carbon assimilation are tightly controlled through stomata. Simon et al. (2020) examined 32 circadian oscillator misexpression mutants in their relative WUE and biomass production. They found +80% to -70% changes to WUE, with 44% of mutant lines significantly different from wildtype; however, this was not confined to a specific part of the circadian oscillator. Specifically,

over-expression of *CCA1* and *TOC1* (two DE genes found in *gad1245*) had a significantly lower WUE. [Dodd et al. \(2005\)](#) illustrated that Arabidopsis with matched circadian clock period with environment could perform better i.e. contains more chlorophyll, fix more carbon and grow faster, than those that have a different period from the environment. All above literature indicates that correct expression of circadian related genes gain advantages in plant growth and development.

Additionally, a list of starch degradation GO terms over-represented in the GO functional analysis from *gad1245*-Col-0. As discussed in Chapter 5, the cycle of starch synthesis/degradation diurnal pattern in the key component of stomatal movement regulation ([Daloso et al., 2017](#), [Horrer et al., 2016](#), [Santelia and Lawson, 2016](#)) and expression of genes associated with starch degradation is aligned by the circadian clock ([Streb and Zeeman, 2012](#)). Mutants that lack the clock component LHY and CCA1 exhausted starch as the shorter circadian clock anticipated dawn earlier than actual dawn ([Graf et al., 2010](#)). Therefore, circadian rhythms are related to stomatal regulation and WUE, but the mechanism of the interactions between GABA and circadian rhythms remain unknown and further investigation of stomatal movement, gas exchange and guard cell starch content are needed with mutant combinations of disrupting circadian oscillator expression and GABA production.

7.3 SAI is a reliable and time-saving solution for stomata measuring

StomaAI (SAI), a user-friendly web application, was developed with advanced deep learning methods for the aim of accelerating plant physiology research. Unlike the other contemporary studies that use conventional evaluation criteria of computer vision like F1 scores and average precision ([Fetter et al., 2019](#), [Jayakody et al., 2021](#)), or square of the correlation coefficient (R^2 ; [Bheemanahalli et al., 2021](#), [Liang et al., 2021](#)), the Average-Human/Machine Test is the critical method introduced here to determine whether SAI predictions reach *human-level* performance. Concordance correlation coefficient (CCC) is core to this test, to evaluate the reproducibility of SAI compared to humans ([Lin, 1989](#)). Considering rater's bias as shown in Appendix E, one human cannot represent general *human-level* performance. Therefore, the actual *human-level* reference defined in our test was generated with measurements from 4 human exports to minimise the personal bias in measurements. With all the preparation, the Average-Human/Machine Test ensured SAI produces comparable measurements to human researchers with CCC score and scattered data points as indicators.

We found that SAI performed with *human-level* accuracy on Arabidopsis and barley stomatal area, width (aperture), length and width/length ratio. Although the performance varies across plant species due to the stomatal distribution and orientation (Figure 6.1), SAI gives stable and reproducible measurements regardless of computer device and operator. SAI also decouples the human effort from the number of measurements acquired per experimental condition by its high efficiency of data processing with a mid-range desktop CPU (Figure 6.4). The high efficiency boosts the number of stomata measurements per experiment group that can be acquired in one attempt, and therefore, enhances the statistical power of stomatal analysis. In addition, SAI is made for the real-world physiology experiments which in some scenarios involve closed stomata (i.e. ABA or darkness induced stomatal closure) that previous studies ignore (Chater et al., 2015, Li et al., 2019, Xu et al., 2021). SAI performs measurement corresponding to the stomata opening status: length, width and area are measured for open stomata while closed stomata only measure length and 0 assigned to width and area. The length filtration excluded the immature stomata that are directly ignored during human measuring process. Such design help SAI behaving like a human on decision making with stomata selection and measurement. Together, SAI provide a high-throughput, reliable and stable solution to plant physiology researchers.

This solution is not limiting to the Arabidopsis and barley, or stomatal pore. In further development, more features such as estimation of stomatal density or dynamic stomatal pore measurement from video recording; and guard cell/subsidiary cell feature measurements (for monocots) could be explored and providing diverse measurement solution for microscope images or videos. Benefit from relatively conserved anatomy of stomata, SAI could be trained towards any preferred type of plant species or cell structure in the future with sufficient annotation provided. This will expand the potential flexibility of SAI to cover more physiological measurements from difference plant species and may further speed up plant physiology research.

7.4 Conclusion

This thesis as a whole explored the relationship of GABA and barley stomatal regulation at both physiological and transcriptional levels; followed by the development of automated measurement of stomata parameters from high resolution microscope images – SAI. The theory of GABA regulation on stomata was first illustrated in Arabidopsis (Xu et al., 2021), and here, consistent observations of barley stomatal response in physiological experiments indicate GABA works similarly in barley. Especially, the

WUE was improved with GABA feeding application (Figure 3.5), which is meaningful to the development of drought stress resilience. However, the effect of high-GABA concentrations (2 mM on barley epidermal peels; Figure 3.6) that behave opposite to low-doses is not yet fully explained and needs to be further explored. Throughout the transcriptome data, the MAPK signaling pathway were invoked in both GABA deficient conditions or following external application. It is possible that GABA act as a signal through utilising the MAPK pathway to crosstalk to other stress signals. Besides, the possible mechanism of interactions in GABA–ROS signalling and GABA–circadian clock are key points will further reveal the role of GABA in stomata regulation. SAI was developed for automating the stomatal measuring procedure to reduces the time that researchers spend on the repetitive work and increase the number of stomata measured per treatment group. Hence, it increases the amount of images captured per group and enhances the statistical power for stomatal assays. This fast, high-throughput *human-level* accurate method frees researcher from having to retrieve stomatal measurements on microscope images manually, and potentially can accelerate plant physiological research by generating statistical results faster.

References

- R. Bheemanahalli, C. Wang, E. Bashir, A. Chiluwal, M. Pokharel, R. Perumal, N. Moghimi, T. Ostmeier, D. Caragea, and S. V. K. Jagadish. Classical phenotyping and deep learning concur on genetic control of stomatal density and area in sorghum. *Plant Physiology*, 186:1562–1579, 2021.
- C. Chater, K. Peng, M. Movahedi, J. A. Dunn, H. J. Walker, Y.-K. Liang, D. H. McLachlan, S. Casson, J. C. Isner, I. Wilson, S. J. Neill, R. Hedrich, J. E. Gray, and A. M. Hetherington. Elevated CO₂-induced responses in stomata require ABA and ABA signaling. *Current Biology*, 25(20):2709–2716, 2015.
- M. K. Choudhary, Y. Nomura, L. Wang, H. Nakagami, and D. E. Somers. Quantitative circadian phosphoproteomic analysis of Arabidopsis reveals extensive clock control of key components in physiological, metabolic, and signaling pathways. *Molecular & Cellular Proteomics*, 14(8):2243–2260, 2015.
- D. M. Daloso, D. B. Medeiros, L. Anjos, T. Yoshida, W. L. Araújo, and A. R. Fernie. Metabolism within the specialized guard cells of plants. *New Phytologist*, 216(4):1018–1033, 2017.
- A. N. Dodd, N. Salathia, A. Hall, E. Kévei, R. Tóth, F. Nagy, J. M. Hibberd, A. J. Millar, and A. A. R. Webb. Plant circadian clocks increase photosynthesis, growth, survival, and competitive advantage. *Science*, 309(5734):630–633, 2005.
- K. C. Fetter, S. Eberhardt, R. S. Barclay, S. Wing, and S. R. Keller. StomataCounter: a neural network for automatic stomata identification and counting. *New Phytologist*, 223(3):1671–1681, 2019.
- A. Graf, A. Schlereth, M. Stitt, and A. Smith. Circadian control of carbohydrate availability for growth in arabidopsis plants at night. *Proceedings of the National Academy of Sciences*, 107(20):9458–9463, 2010.
- M. Hassidim, Y. Dakhiya, A. Turjeman, D. Hussien, E. Shor, A. Anidjar, K. Goldberg, and R. M. Green. CIRCADIAN CLOCK ASSOCIATED1 (CCA1) and the circadian control of stomatal aperture. *Plant Physiology*, 175(4):1864–1877, 2017.
- R. Hedrich, S. Neimanis, G. Savchenko, H. H. Felle, W. M. Kaiser, and U. Heber. Changes in apoplastic pH and membrane potential in leaves in relation to stomatal responses to CO₂, malate, abscisic acid or interruption of water supply. *Planta*, 213(4):594–601, 2001.

- D. Horrer, S. Flütsch, D. Pazmino, J. S. Matthews, M. Thalmann, A. Nigro, N. Leonhardt, T. Lawson, and D. Santelia. Blue light induces a distinct starch degradation pathway in guard cells for stomatal opening. *Current Biology*, 26(3):362–370, 2016.
- H. Jayakody, P. Petrie, H. J. de Boer, and M. Whitty. A generalised approach for high-throughput instance segmentation of stomata in microscope images. *Plant Methods*, 17(1):1–13, 2021.
- Y. Kang, W. H. Outlaw Jr, P. C. Andersen, and G. B. Fiore. Guard-cell apoplastic sucrose concentration – a link between leaf photosynthesis and stomatal aperture size in the apoplastic phloem loader *Vicia faba L.* *Plant, Cell & Environment*, 30(5):551–558, 2007.
- T. Lawson, A. J. Simkin, G. Kelly, and D. Granot. Mesophyll photosynthesis and guard cell metabolism impacts on stomatal behaviour. *New Phytologist*, 203(4):1064–1081, 2014.
- D. Li, J. B. Brown, L. Orsini, Z. Pan, G. Hu, and S. He. MODA: Module differential analysis for weighted gene co-expression network. *arXiv*, 2016.
- K. Li, J. Huang, W. Song, J. Wang, S. Lv, and X. Wang. Automatic segmentation and measurement methods of living stomata of plants based on the cv model. *Plant Methods*, 15(1):67, 2019.
- X. Liang, X. Xu, Z. Wang, L. He, K. Zhang, B. Liang, J. Ye, J. Shi, X. Wu, M. Dai, and W. Yang. StomataScorer: A portable and high-throughput leaf stomata trait scorer combined with deep learning and an improved cv model. *Plant Biotechnology Journal*, 20(3):577–591, 2021.
- V. F. Lima, D. B. Medeiros, L. D. Anjos, J. Gago, A. R. Fernie, and D. M. Daloso. Toward multifaceted roles of sucrose in the regulation of stomatal movement. *Plant Signaling & Behavior*, 13(8):1–8, 2018.
- L. I. Lin. A concordance correlation coefficient to evaluate reproducibility. *Biometrics*, 45(1):255–268, 1989.
- P. Lu, W. H. Outlaw Jr, B. G. Smith, and G. A. Freed. A new mechanism for the regulation of stomatal aperture size in intact leaves (accumulation of mesophyll-derived sucrose in the guard-cell wall of *Vicia faba*). *Plant Physiology*, 114(1):109–118, 1997.
- D. Santelia and T. Lawson. Rethinking guard cell metabolism. *Plant Physiology*, 172(3):1371–1392, 2016.

- N. M. L. Simon, C. A. Graham, N. E. Comben, A. M. Hetherington, and A. N. Dodd. The circadian clock influences the long-term water use efficiency of arabidopsis. *Plant Physiology*, 183(1):317–330, 2020.
- C. Sirichandra, D. Gu, H. C. Hu, M. Davanture, S. Lee, M. Djaoui, B. Valot, M. Zivy, J. Leung, S. Merlot, and J. M. Kwak. Phosphorylation of the Arabidopsis AtrbohF NADPH oxidase by OST1 protein kinase. *FEBS Letters*, 583(18):2982–2986, 2009.
- Y. Song, Y. Miao, and C.-P. Song. Behind the scenes: the roles of reactive oxygen species in guard cells. *New Phytologist*, 201(4):1121–1140, 2014.
- S. Streb and S. C. Zeeman. Starch metabolism in arabidopsis. *The Arabidopsis Book*, 10, 2012.
- B. Xu, Y. Long, X. Feng, X. Zhu, N. Sai, L. Chirkova, A. Betts, J. Herrmann, E. J. Edwards, M. Okamoto, R. Hedrich, and M. Gilliam. GABA signalling modulates stomatal opening to enhance plant water use efficiency and drought resilience. *Nature Communications*, 12(1):1–15, 2021.
- Y. Yao, X. Liu, Z. Li, X. Ma, H. Rennenberg, X. Wang, and H. Li. Drought-induced H₂O₂ accumulation in subsidiary cells is involved in regulatory signaling of stomatal closure in maize leaves. *Planta*, 238(1):217–227, 2013.

APPENDIX



PUBLISHED ARTICLES

PUBLICATION I

**The emerging role of GABA as a transport
regulator and physiological signal**

Statement of Authorship

Title of Paper	The emerging role of GABA as a transport regulator and physiological signal
Publication Status	<input checked="" type="checkbox"/> Published <input type="checkbox"/> Accepted for Publication <input type="checkbox"/> Submitted for Publication <input type="checkbox"/> Unpublished and Unsubmitted work written in manuscript style
Publication Details	Xu, B., Sai, N. and Gilliam, M., 2021. The emerging role of GABA as a transport regulator and physiological signal. Plant Physiology, 187(4), pp.2005-2016.

Principal Author

Name of Principal Author (Candidate)	Na Sai
Contribution to the Paper	I conducted the gas exchange experiment that measured stomatal conductance and iWUE of barley in dark-to-light transition with presence and absent of GABA (Fig 1B and 1C) and edited manuscript.
Overall percentage (%)	20%
Certification:	This paper reports on original research I conducted during the period of my Higher Degree by Research candidature and is not subject to any obligations or contractual agreements with a third party that would constrain its inclusion in this thesis.
Signature	_____ Date 13/12/2021

Co-Author Contributions

By signing the Statement of Authorship, each author certifies that:

- i. the candidate's stated contribution to the publication is accurate (as detailed above);
- ii. permission is granted for the candidate to include the publication in the thesis; and
- iii. the sum of all co-author contributions is equal to 100% less the candidate's stated contribution.

Name of Co-Author	Bo Xu
Contribution to the Paper	Developed and wrote the paper.
Signature	_____ Date 17/12/2021




Name of Co-Author	Matthew Gilliam
Contribution to the Paper	Developed and wrote the paper.
Signature	_____ Date 17/12/2021

doi:10.1093/plphys/kiab347

PLANT PHYSIOLOGY 2021; 187: 2005–2016

Plant Physiology[®]

The emerging role of GABA as a transport regulator and physiological signal

Bo Xu ^{1,2,*}, Na Sai ^{1,2}, and Matthew Gilliam ^{1,2}

- 1 Plant Transport and Signalling Lab, ARC Centre of Excellence in Plant Energy Biology, Waite Research Institute, Glen Osmond, South Australia 5064, Australia
- 2 School of Agriculture, Food and Wine, University of Adelaide, Glen Osmond, South Australia 5064, Australia

*Author for communication: b.xu@adelaide.edu.au

[†]Senior author.

B.X. and M.G. developed and wrote the paper, and N.S. conducted the experiments in Figure 1. All the authors provided edits.

The author responsible for distribution of materials integral to the findings presented in this article in accordance with the policy described in the Instructions for Authors (<https://academic.oup.com/plphys/pages/general-instructions>) is Bo Xu (b.xu@adelaide.edu.au).

Update

Abstract

While the proposal that γ -aminobutyric acid (GABA) acts a signal in plants is decades old, a signaling mode of action for plant GABA has been unveiled only relatively recently. Here, we review the recent research that demonstrates how GABA regulates anion transport through aluminum-activated malate transporters (ALMTs) and speculation that GABA also targets other proteins. The ALMT family of anion channels modulates multiple physiological processes in plants, with many members still to be characterized, opening up the possibility that GABA has broad regulatory roles in plants. We focus on the role of GABA in regulating pollen tube growth and stomatal pore aperture, and we speculate on its role in long-distance signaling and how it might be involved in cross talk with hormonal signals. We show that in barley (*Hordeum vulgare*), guard cell opening is regulated by GABA, as it is in *Arabidopsis thaliana*, to regulate water use efficiency, which impacts drought tolerance. We also discuss the links between glutamate and GABA in generating signals in plants, particularly related to pollen tube growth, wounding, and long-distance electrical signaling, and explore potential interactions of GABA signals with hormones, such as abscisic acid, jasmonic acid, and ethylene. We conclude by postulating that GABA encodes a signal that links plant primary metabolism to physiological status to fine tune plant responses to the environment.

Introduction

The nonproteinogenic amino acid γ -aminobutyric acid (GABA) has been proposed to be an agent of cellular communication that emerged very early in evolution, being conserved across modern animals and plants (Shelp et al., 2006; Ben-Ari et al., 2007; Žárský, 2015; Ramesh et al., 2017). Cellular GABA metabolism (synthesis and catabolism) predominantly occurs via the GABA shunt pathway and is enacted by orthologous key enzymes in both kingdoms (Bouché et al., 2003; Bown and Shelp, 2016). GABA is primarily synthesized from glutamate by glutamate

decarboxylase (GAD) in the cytosol, and is degraded by GABA transaminase (GABA-T) into succinic semialdehyde (SSA) in mitochondria, bypassing two stress-inhibited reactions of the mitochondrial-based tricarboxylic acid (TCA) cycle (Bouché et al., 2003; Bown and Shelp, 2016). Polyamine-derived GABA synthesis can also have a significant impact on plant function under certain scenarios (Zarei et al., 2016). GABA synthesis in plants is stimulated by stress, and its known or proposed roles—as a metabolite in plants—were traditionally thought to be confined to processes such as pH regulation, redox status, and carbon-

Received March 09, 2021. Accepted July 10, 2021. Advance access publication August 30, 2021

© American Society of Plant Biologists 2021. All rights reserved. For permissions, please email: journals.permissions@oup.com

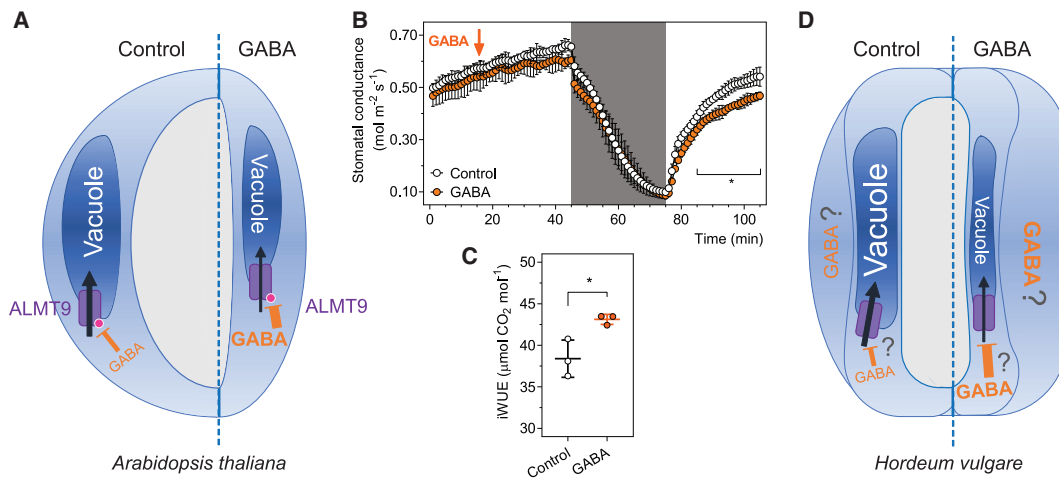


Figure 1 Proposed model of GABA-improved WUE in plants. A, A proposed model of GABA supplementation reducing stomatal opening in dicots *A. thaliana*, adapted from (Xu et al., 2021). Increases in cellular GABA have an inhibitory effect on anion uptake through tonoplast ALMT9 into guard-cell vacuoles, reducing stomatal opening and water loss through stomatal pores (A). B and C, GABA supplementation reduces stomatal opening (B) and increases transient iWUE (C) of detached barley leaves. B, Leaves detached from 2- to 3-week-old *H. vulgare* L. Barke seedlings were fed through the xylem sap, and gas exchange was recorded using a LI-COR LI-6400XT Portable Photosynthesis System following protocols as described in Xu et al. (2021); GABA was applied into xylem sap solution to a final concentration of 8 mM as indicated by an arrow, allowing for a 30 min pretreatment for uptake of GABA through leaf petiole, followed by 30 min dark (shaded region) to close stomata and 30 min light (white region, $1,000 \mu\text{mol m}^{-2} \text{s}^{-1}$) to reopen stomata. C, iWUE of detached leaves was calculated as the ratio of photosynthetic rate (Supplemental Figure S1) versus stomatal conductance within a range that showed significant difference between control and GABA treatments (Leakey et al., 2019). Data represent means \pm SD, $n = 3$; statistical analysis was determined by two-sided Student's *t* test, $^*P < 0.05$ (B and C). D, A proposed model of GABA-enhanced WUE in monocot *H. vulgare*. Similar to Arabidopsis (Xu et al., 2021), GABA supplement did not affect stomatal closing, but reduced the extent of opening of barley leaves; GABA's proposed mode of action in barley guard cells based on observation from (B) and GABA's function in Arabidopsis guard cells from (A); GABA may be associated with negative regulation of anion uptake through unidentified anion channels, perhaps, for example, tonoplast-localized HvALMT(s) in guard cells to reduce opening extent of stomatal pores; however, it is unknown whether GABA acts in subsidiary cells in this regulation, as stomatal opening of barley plants is modulated by ionic influx into guard cells and efflux from subsidiary cells (Chen et al., 2017).

nitrogen balance (Shelp et al., 1999; Batushansky et al., 2014; Bor and Turkan, 2019).

In mammals, GABA acts as a signal via receptor-mediated membrane hyperpolarization of neuronal cells (Owens and Kriegstein, 2002; Žárský, 2015). In plants, alongside its established roles as a metabolic bypass to sustain cellular energy production, GABA was proposed to fulfil a signaling role decades ago when it was found that GABA modulated the growth of pollen tubes, and disruption of GABA catabolism impacted fertilization (Palanivelu et al., 2003). Subsequent studies have shown that modulating GABA metabolism, or applying GABA as a supplement, impacts plant physiological response, for example, water use, drought tolerance, salt and osmotic responses (Krishnan et al., 2013; Li et al., 2016b, 2016c; Farooq et al., 2017; Cheng et al., 2018; Abdel Razik et al., 2020). Nevertheless, experimental evidence providing a mode of action for GABA, including the existence of a plant GABA receptor or elements in a GABA signaling pathway had not been obtained (Palanivelu et al., 2003; Bouche and Fromm, 2004; Michaeli and Fromm, 2015).

In 2015, the discovery that anion flux through plant-specific aluminum-activated malate transporters (ALMTs) was negatively regulated by GABA, altering plasma membrane

potential and resulting in a downstream physiological response, represented a plausible mechanism by which GABA may act as a signal in plants (Ramesh et al., 2015; Gilliam and Tyerman, 2016). Moreover, it was subsequently shown that: GABA is likely to act directly upon ALMTs (Domingos et al., 2019; Long et al., 2019); ALMTs also facilitate the transport of GABA (Ramesh et al., 2018; Kamran et al., 2020); and, GABA responses of ALMTs are dependent upon the presence of specific amino acid residues within ALMTs (ALMTs share no homology to mammalian Cys-loop [GABA] receptors except a region of 12 amino acid residues predicted to bind GABA in GABA_A receptors; Ramesh et al., 2015, 2017, 2018; Long et al., 2019; Xu et al., 2021). Furthermore, revealing a mechanism by which GABA acts via ALMTs in guard cells—to regulate drought tolerance—(Xu et al., 2021), and that ALMTs are involved in GABA responses in pollen (Domingos et al., 2019), is the strongest evidence yet that GABA is an endogenous plant signal that links primary metabolism to physiological responses (Gilliam and Tyerman, 2016). Additional GABA targets have also been nominated in plants, including 14-3-3 proteins, H⁺-ATPases, and potassium channels (Lancien and Roberts, 2006; Ramesh et al., 2017; Su et al., 2019; Adem et al., 2020), which have the potential to form

part of the GABA signaling network. Here, we elaborate upon the work cited above, and further recent outputs, to outline the case for GABA being a credible signaling molecule in plants, and the ways in which it may interact with other known signals to modulate plant physiology.

GABA as a stomatal guard cell signal regulating plant water loss

Stomatal guard cells delineate the stomatal pores on plant aerial surfaces and respond to environmental signals by regulating the stomatal pore aperture to modulate plant water loss and carbon assimilation (Hetherington and Woodward, 2003; Kim et al., 2010; Murata et al., 2015; Xu et al., 2021). It has been shown numerous times that water loss was minimized from a variety of plants when GABA was applied as a treatment (Krishnan et al., 2013; Li et al., 2016a; Farooq et al., 2017; Abdel Razik et al., 2020). GAD1 and GAD2 are the major GAD isoforms in roots and leaves of *Arabidopsis thaliana*, respectively, and their knockout leads to negligible GABA concentrations in tissues (Mekonnen et al., 2016); further, it was proposed that depletion of GABA concentration in *gad1/gad2* leaves led to plants that were more drought prone (Mekonnen et al., 2016).

The greater stomatal conductance and drought sensitivity of *gad1/gad2* mutants were initially attributed to their more open stomatal phenotype and greater stomatal density (Mekonnen et al., 2016). The minor developmental phenotype of *gad1/gad2* is likely due to the smaller leaves of the line tested compared to the wild-type, as other GAD mutants do not share this feature (Xu et al., 2021), so it is unlikely that GABA plays a significant role in stomatal development. The greater stomatal aperture of *gad1/gad2* was proposed to be due to H⁺-ATPases mediating a greater proton (H⁺) efflux across the plasma membrane leading to greater pore opening and inhibition of stomatal closure; this was inferred after it was observed that *gad1/gad2* roots had a greater acidification capacity of the surrounding media (Mekonnen et al., 2016). Interestingly, when direct microelectrode-based measurements of *gad1/gad2* roots were made, their H⁺ efflux capacity was diminished compared to wild-type plants but was increased in GABA overaccumulating mutants, and that the membrane potential was relatively depolarized in *gad1/gad2* roots when exposed to 100-mM NaCl (Su et al., 2019). It was suggested that GABA inhibited NaCl stimulated K⁺-efflux from roots and that this was associated to a greater ability to quench reactive oxygen species (ROS), whereas *gad1/gad2* had greater K⁺-efflux, which was proposed to occur via guard cell outwardly rectifying K⁺ channel (GORK; Su et al., 2019). GABA has previously been implicated in activating transcription of 14-3-3 proteins, which are known activators of H⁺-ATPases and GORK (Alsterford et al., 2004; Lancien and Roberts, 2006; Van Kleeff et al., 2018). Furthermore, GORK has been shown to be activated by ROS (Demidchik et al., 2010; Wang et al., 2017), and GABA has been implicated in ROS detoxification through an unidentified mechanism (Wu et al., 2021). In a further study, 10-mM GABA was shown to activate K⁺-efflux

from roots in a GORK-dependent manner, and it was argued that GORK shared the same putative GABA-sensitive motif found in ALMTs (Adem et al., 2020; Wu et al., 2021). These seemingly contradictory observations raise several questions including: Is there a dose dependent effect of GABA on H⁺-efflux and K⁺-efflux from roots?; Is the impact of GABA on ion fluxes different in roots and guard cells?; How does GABA regulate H⁺-ATPases?; Is GORK directly regulated by GABA or indirectly via GABA's impact on ROS, or another route?; and, Are there alternative explanations for the stomatal and root phenotypes of GABA-depleted mutants?

In Ramesh et al. (2015), it was proposed that negative regulation of anion efflux via ALMT would indirectly reduce the activity of the plasma membrane H⁺-ATPase. ALMT activity is a prime candidate for contributing to the short circuit (equal and opposite charge exchange) that maintains H⁺-ATPase activity by preventing it stalling at extremely hyperpolarized membrane potentials. This hypothesis is compatible with the above observations of altered membrane potential, and is a possible explanation for the inconsistencies observed for K⁺ and H⁺-fluxes between studies if the H⁺-ATPase and K⁺ channels are not direct targets of GABA. The hypothesis that GABA regulation of ALMT constituted a physiological signal was furthered in Xu et al. (2021) using the stomatal guard cell as an experimental system.

Similar to *gad1/gad2* mutants, *gad2* mutants exhibited high stomatal conductance and drought sensitivity; however, *gad2* mutants do not share the developmental differences of *gad1/gad2* when compared to wild-type plants, for example, smaller rosettes or higher stomatal densities (Mekonnen et al., 2016; Xu et al., 2021). Furthermore, the high stomatal conductance and drought sensitivity of *gad2* plants were complemented by the additional loss of *ALMT9* (Xu et al., 2021). *ALMT9* is a tonoplast localized anion transporter that catalyzes malate and chloride (Cl⁻) uptake across the vacuolar membrane of the guard-cell to contribute to the osmotic increase that is required for stomatal opening (Kovermann et al., 2007; De Angeli et al., 2013). The loss of *ALMT9* impairs light-induced stomatal opening and led to *almt9* mutants being more drought tolerant (De Angeli et al., 2013); ablation of *ALMT9* also abolished the ability of GABA to inhibit stomatal opening, which was restored by native *ALMT9* complementation (Xu et al., 2021). This signifies that GABA inhibits stomatal opening via acting on *ALMT9* (Figure 1A). Attempted complementation of *almt9* plants with *ALMT9*^{F243C/Y245C} (containing mutations within the putative GABA interacting motif first characterized in the wheat [*Triticum aestivum*] TaALMT1; Ramesh et al., 2015, 2017; Long et al., 2019) failed to restore the sensitivity of stomatal opening to GABA, but instead phenocopied the higher stomatal conductance of the *gad2* mutant (Xu et al., 2021). These data are consistent with *ALMT9* being the predominant "GABA receptor" in guard cells, and when GABA synthesis is inhibited, *ALMT9* is deregulated resulting in increased opening and pore aperture, and an increase in

drought sensitivity of the plant (Figure 1A; Xu et al., 2021). An assay is now required to demonstrate whether GABA has a direct effect on ALMT9, as has been demonstrated for TaALMT1 via electrophysiology (Long et al., 2019), or whether GABA acts on ALMT9 via a distinct mechanism. What is not in doubt though is that ALMT9 (and the putative GABA binding domain) is required for the response to GABA, even if other signaling elements are involved. It is noted that a range of candidates for interaction with GABA were nominated by Ramesh et al. (2017) based on the presence of a putative GABA binding site within a number of plant proteins, with none of these other candidates yet being examined in planta.

There were a number of other significant observations in regard to the nature of GABA as a signal stemming from Xu et al. (2021). First, overproduction of GABA in wild-type plants improved water use efficiency (WUE) and led to an improvement in drought resilience (Xu et al., 2021). This suggests that GABA metabolism can be manipulated to improve stress tolerance in plants over and above wild-type levels. Second, Xu et al. (2021) showed supplementation to epidermal peels of GABA or muscimol (a GABA analog) suppressed stomatal movement in response to multiple opening (e.g. light and coronatine; Melotto et al., 2006; Shimazaki et al., 2007; Sussmilch et al., 2019) or closing signals (e.g. dark, low-dose abscisic acid [ABA], and H₂O₂; Shimazaki et al., 2007; Sussmilch et al., 2019). This differentiates it from many of the more well-defined guard-cell signals, such as ABA, hydrogen peroxide (H₂O₂), and calcium (Ca²⁺; Kim et al., 2010; Murata et al., 2015), as GABA itself does not stimulate stomatal movement when its treatment falls within the physiological range (Xu et al., 2021; i.e. under nonstressed and stressed conditions, e.g. ~1 μmol g⁻¹ fresh weight [FW] and ~2 μmol g⁻¹ FW, equivalent to 1–2 mM respectively; Ramesh et al., 2015, 2018; Deng et al., 2020; Xu et al., 2021). When GABA was fed to leaves through the petiole to corroborate the findings in epidermal peels it was found that GABA only impacted stomatal opening, not closure (Xu et al., 2021), indicating the loss of the mesophyll in epidermal peels impairs the ability to reproduce the standard physiological response of intact plants (Lee and Bowling, 1992; Lawson et al., 2008, 2014). This finding also suggests that under the conditions tested GABA neither regulate stomatal closure, nor activate GORK. The physiological conditions where GABA impacts closure in planta are yet to be determined. However, it was found that GABA was unable to inhibit, in epidermal peels, closure of knockout mutants of ALMT12 (otherwise known as QUAC1—Quick-activating Anion Channel 1; Xu et al., 2021) and so this is likely to represent a mechanism by which GABA could inhibit guard cell closure.

The high stomatal conductance, low WUE and drought sensitivity of the *gad2* mutant could be complemented to wild-type levels by guard cell specific expression of GAD2Δ (a constantly active form of GAD2 with truncation of a Ca²⁺/Calmodulin [Ca²⁺/CaM] binding domain), but not by

mesophyll-cell complementation of GAD2Δ (Turano and Fang, 1998; Zik et al., 1998; Akama and Takaiwa, 2007; Xu et al., 2021). This suggests, on first examination, that the generation of GABA within the guard cell cytosol is sufficient to constitute a signal, and that mesophyll GABA accumulation does not overtly contribute to stomatal regulation. However, full-length GAD2 complementation driven by a constitutive 35S promoter recovered the higher stomatal conductance of *gad2* to wild-type levels under normal conditions, whereas gain of GAD2 in guard cells only complemented *gad2* under water-deficit stress (Xu et al., 2021). This indicates the importance of posttranslational control in shaping GABA signals, and that different cell types are likely to contribute to the nature of the signal under different conditions.

GABA synthesis is stimulated by acidification of the cytosolic pH and Ca²⁺/CaM-dependent activation of GAD (Carroll et al., 1994; Crawford et al., 1994; Turano and Fang, 1998; Zik et al., 1998). GABA breakdown is catalyzed by GABA-T in mitochondria (Clark et al., 2009). Both synthesis and degradation elements (GADs and GABA-T, respectively) have distinct expression patterns in plants (Clark et al., 2009; Renault et al., 2010; Scholz et al., 2015). It is possible, therefore, that GABA metabolomic levels may be differentially controlled in different cell types. Intracellular pH and Ca²⁺ signals, the key regulators of GAD-catalyzed GABA synthesis (Zik et al., 1998) are known to be spatially and temporally regulated in response to the environment (Behera et al., 2018; Li et al., 2021). It can therefore be expected that cellular GABA signals are dynamically shaped in plant tissue, and this will need to be investigated with the application of technologies such as intensity-based GABA sensing fluorescence reporters (e.g. iGABASnFR) in planta (Marvin et al., 2019; Fromm, 2020).

GABA's impact on stomatal pore movement occurs across a range of crop plants and relatives, including broad bean (*Vicia faba*), soybean (*Glycine max*), *Nicotiana benthamiana*, and barley (*Hordeum vulgare*; Xu et al., 2021). Here, we show GABA supplementation of detached, but intact, barley leaves reduces stomatal opening and does not affect stomatal closure (Figure 1B). The mechanism behind this is unknown. The only well-characterized barley ALMT, HvALMT1, is localized at plasma membrane and is expressed in roots and guard cells (Gruber et al., 2010). While its anion transport capacity was inhibited by GABA (Ramesh et al., 2015), its overexpression resulted in greater closure with no opening phenotype (Gruber et al., 2010), and RNAi knockdown resulted in diminished closure in the dark and greater water loss (Xu et al., 2015)—opposite to that observed for *almt9* (Xu et al., 2021) and for GABA treated barley (Figure 1B). Here, we show that GABA improves intrinsic WUE (iWUE) of barley (Figure 1C). Therefore, it is not likely that HvALMT1 is the target that leads to GABA reducing stomatal opening (Gruber et al., 2010; Ramesh et al., 2015; Xu et al., 2015). As the barley gas exchange response to GABA parallels the phenotype of Arabidopsis, it is entirely possible

that GABA's effects are actioned through inhibition of barley tonoplast ALMTs that have a role in opening pores. While a simple bioinformatic search can reveal the barley ALMTs, without functional characterization it would not be possible to identify the correct target or indeed those present on the tonoplast (David et al., 2019). Additional questions are relevant here, as barley—a cereal monocot crop—has a different stomatal morphology. In barley, the stomatal complex is formed by dumbbell-shaped guard cells flanked by subsidiary cells; it is possible then that GABA signals may regulate ionic flux across both barley guard- and/or subsidiary cell membranes (Figure 1D; Merilo et al., 2014; Chen et al., 2017), and this would need to be tested. Nevertheless, it appears that the cell-type manipulation of GABA metabolism has potential to improve the drought tolerance of crop plants, considering the responsiveness to GABA in crops, and that overproduction of GABA leads to improved WUE in Arabidopsis (Xu et al., 2021).

GABA regulation of pollen tube growth

Pollen–pistil interactions guide pollen tube apical growth during sexual production in flowering plants (Higashiyama and Takeuchi, 2015), which involves the regulation of complex signaling and ionic flux networks as extensively reviewed previously (Lampert et al., 2018; Johnson et al., 2019). GABA has been proposed to form a gradient within pistil to accelerate the pollen tube growth toward the ovule as part of growth guidance (Palanivelu et al., 2003; Yu et al., 2014). Palanivelu et al. (2003) gave an initial indication that GABA may have a signaling role in plants. However, conclusive genetic proof that GABA signaling modulates plant fertility, and by which mechanism, is yet to be revealed despite recent evidence that implicate ALMTs have a role in the responses of pollen tubes to GABA (Domingos et al., 2019). Further, the existence of the pistil GABA gradient would benefit from confirmation, or otherwise, via other techniques, as well as further investigation into the molecular mechanism of its establishment and the response of pollen to GABA. Here, we concentrate on the evidence for GABA having a role in regulating pollen tube growth and fertility (Figure 2).

In vitro assays have shown that micromolar GABA stimulates pollen tube elongation of Arabidopsis and tobacco (*Nicotiana tabacum*), while >10 mM suppresses pollen tube growth (Palanivelu et al., 2003; Yu et al., 2014). The supplementation of low concentrations of muscimol (the potent GABA analogue) mimic the high dose effects of GABA, that is, it produces an inhibitory effect on pollen tube growth of Arabidopsis and grapevine (*Vitis vinifera*), which can be attenuated by bicuculline, a competitive GABA receptor antagonist (Ramesh et al., 2015, 2017). Domingos et al. (2019) determined that both GABA and muscimol significantly reduce anionic currents from Arabidopsis pollen protoplasts by up to 90% when supplied from the cytoplasmic side, but not the extracellular face, and that this effect of muscimol was abolished in *almt12* mutants (Domingos et al., 2019).

The inhibitory effect of externally supplied muscimol on the growth of pollen tubes was also abolished in *almt12*; further, the length of *almt12* pollen tubes was similar to the length of those from wild-type plants supplied with muscimol (Domingos et al., 2019). Interestingly, anion efflux at the tip of *almt12* mutants was not decreased, and ALMT12 has not yet been localized to the plasma membrane (Gutermuth et al., 2018; Domingos et al., 2019). However, GABA also inhibits ALMT13- and 14-mediated malate efflux from *Xenopus laevis* oocytes (Ramesh et al., 2015), as was shown for ALMT12 induced currents from COS-7 cells (Domingos et al., 2019), and ALMT13 and 14 have been localized to the pollen tube plasma membrane (Gutermuth et al., 2018). ALMT12-14 catalyze anionic (Cl⁻ and malate) efflux from pollen protoplasts, which play an important role in establishing anionic gradients formed within pollen tubes, which are proposed to have a role in navigating their growth (Gutermuth et al., 2018). Other factors reported to regulate ALMT12 and ALMT14 anion transport capacity in pollen are cytosolic Ca²⁺ and the Ca²⁺-dependent kinase CPK6 (and other CPK; Gutermuth et al., 2018). Oscillations in tip cytosolic Ca²⁺ concentration, anion efflux and growth are synchronous (Gutermuth et al., 2018). GAD activity is also stimulated by cytosolic Ca²⁺ concentration. Thus, the opposing effects of Ca²⁺ and GABA on ALMT12-14 activity may contribute to the oscillations in pollen tube tip anion efflux and growth modulation (Figure 2; Ramesh et al., 2015; Domingos et al., 2019). This said, the reproductive phenotypes of either *almt12/almt13* or *almt12/almt14* are minor in terms of seed set and pollen tube growth regulation in the conditions tested (Gutermuth et al., 2018; Domingos et al., 2019). This is similar to the impact of ALMT12 on stomatal pore control by GABA—impacts were detected in vitro but these did not extrapolate to intact plant phenotypes. When GABA breakdown is impaired in the Arabidopsis *gaba-t/pop2* mutant, aberrant pollen tube growth to ovules and lower seed set than the wild-type was recorded. Collectively, this suggests that GABA metabolism could impact reproductive processes through other proteins in addition to ALMTs. One possibility is GABA modulation of the plasma membrane proton (H⁺) ATPases (i.e. AHA6/8/9), which are essential for pollen tube elongation and reproductive production (Figure 2; Su et al., 2019; Hoffmann et al., 2020). In root tissue, GABA accumulation has been positively correlated with the magnitude of H⁺ efflux under salt by contrasting the Arabidopsis (GABA-overaccumulation) *gaba-t/pop2* mutant that exhibits net H⁺ release and the (GABA-deficiency) *gad1/2* mutant, which exhibits net H⁺ uptake (Su et al., 2019). As such, GABA may also modulate H⁺-ATPase catalyzed H⁺ flux either directly (or through GABA activated 14-3-3 proteins; Alsterfjord et al., 2004; Lancien and Roberts, 2006), or indirectly through regulation of ALMT (Ramesh et al., 2015, 2018), which will impact the pollen tube growth (Figure 2). To our knowledge, the impact of GABA on H⁺ fluxes of pollen tubes has not been examined.

We propose that GABA fluxes across pollen tubes may also be an important regulatory factor in their growth. This

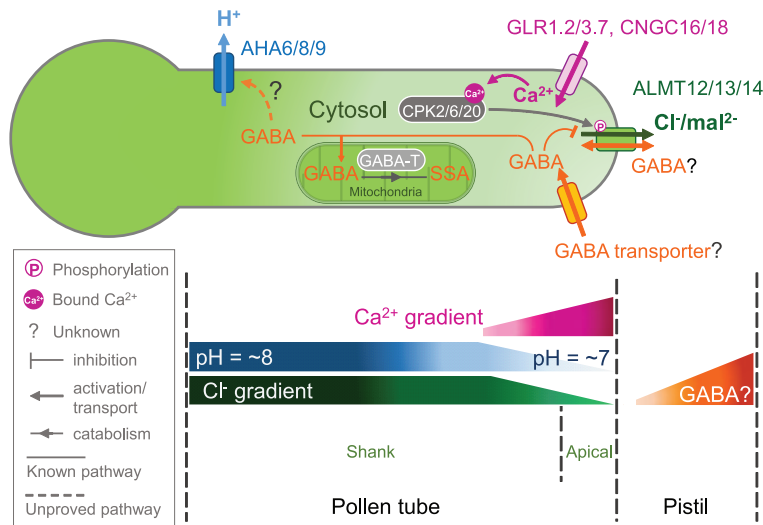


Figure 2 Proposed model of GABA action on pollen tube growth. Ca^{2+} , H^{+} , and Cl^{-} form gradients within the pollen tubes to facilitate its growth to ovules. Glutamate-dependent Ca^{2+} channels (GLR1.2/3.7) and cyclic nucleotide gated channels (CNGC16/18) conduct apical Ca^{2+} influx and form a Ca^{2+} gradient; this triggers calcium-dependent protein kinases (CPK2/6/20)-dependent activation of anion efflux (Cl^{-} and malate [mal^{2-}]) via ALMT12-14 (Gutermuth et al., 2018); and H^{+} -ATPases (AHA6/8/9) to establish a pH gradient across the pollen tube plasma membrane (Chen et al., 2020; Hoffmann et al., 2020). We propose that cytosolic GABA (together with Ca^{2+} /CPKs) fine tune apical anion efflux via ALMT12-14 and may be associated with H^{+} gradient and membrane potential regulation within pollen tubes via its actions on the H^{+} -ATPase. Such cytosolic GABA homeostasis may be shaped via uptake by unidentified GABA transporter(s) (and/or ALMT) from the apoplast (pistil; Ramesh et al., 2018) and via degradation by GABA-T into SSA in mitochondria (Palanivelu et al., 2003). All these elements work together to facilitate pollen tube growth to ovules during sexual production. Adapted from Domingos et al. (2019) combined with information from Gutermuth et al. (2018); Ramesh et al. (2018); Domingos et al. (2019); Hoffmann et al. (2020).

stems from the observation that crossing *pop2* mutant pollen onto wild-type pistils, or wild-type pollen onto *pop2* mutant pistils, obtained wild-type-like self-crossed fertilization levels of seed set (Palanivelu et al., 2003), and the following: (1) GABA signals are likely to act from the cytosolic side (Long et al., 2019; Xu et al., 2021); (2) TaALMT1 can facilitate GABA transport across the plasma membrane (Ramesh et al., 2018); (3) extracellular (i.e. pistil) GABA fine tunes pollen tube growth (Palanivelu et al., 2003; Yu et al., 2014; Ramesh et al., 2015); and (4) GABA-T-catalyzed GABA breakdown is essential for plant fertility (Palanivelu et al., 2003). A competent GABA flux could compensate for the lack of GABA breakdown ability in either pollen or pistil tissue to maintain cytosolic GABA within pollen tubes, unless GABA over-accumulates on both sides (e.g. ♂ *pop2* × ♀ *pop2*; Palanivelu et al., 2003). Therefore, the combined impact of GABA catabolism via GABA-T and transport via GABA transporters (i.e. ALMTs and/or unidentified proteins) could contribute to fine-tuning pollen tube elongation within pistil to ovules, as summarized in Figure 2. This could be tested by simultaneously knocking out GABA-T and GABA transporter genes expressed in pollen, together with in vivo intensity-based GABA fluorescence imaging using iGABASnFR in planta.

This is an intriguing combination of evidence and restrained speculation that indicates GABA could be a signal important for regulating pollen tube growth in coordination with other well-defined signals and transport networks as

defined below. In summary, we propose that GABA has the potential to act as a signal that regulates pollen tube growth via its impact on anion efflux and potentially pH, and that this may occur through a Ca^{2+} mediated pathway (Figure 2).

Communication between glutamate and GABA signals in plants

GABA and glutamate are intimately linked through the synthesis of GABA via GAD. Not only is glutamate the substrate for GABA synthesis but also glutamate may stimulate Ca^{2+} entry into cells to activate GAD. Both glutamate and GABA have been implicated in playing a role in plant responses to wounding; thereby, we will discuss the potential relationship between GABA and glutamate in the context of wound signaling.

In response to wounding, plants generate long-distance electrical signaling, such as systemic surface potential changes and action potentials (APs; Hedrich et al., 2016; Farmer et al., 2020). Glutamate-dependent Ca^{2+} channels (i.e. GLR3.3 and 3.6) mediate wound-induced transient long-distance Ca^{2+} signal transduction and surface electrical changes via plasmodesmata that later stimulate distal jasmonate biosynthesis and systemic ROS propagation; this has been recently reviewed (Johns et al., 2021).

Wounding caused by the robotic caterpillar MecWorm on Arabidopsis (on leaf 8, the typical leaf for testing signal

transduction to younger leaves) is also known to provoke systemic GABA accumulation in distal leaves (i.e. leaves 5, 11, and 13; Farmer et al., 2013; Scholz et al., 2015, 2017). It is unclear whether such systemic GABA accumulation is linked to glutamate-dependent Ca^{2+} activation of GAD(s), but the role of tonoplast-localized two pore calcium channel protein 1 in increasing cytosolic Ca^{2+} was ruled out (Scholz et al., 2017; Toyota et al., 2018). Cellular GABA metabolic status has been observed to affect stress (i.e. NaCl and hypoxia) triggered H^+ flux, membrane potential changes and ROS signaling, where greater GABA accumulation is associated with faster restoration from stress-depolarized membrane potential and less ROS production (Su et al., 2019; Wu et al., 2021). Therefore, the question arises of whether GABA can facilitate the recovery of local cell membrane potential and/or mitigation of ROS damage if both are primed by glutamate-activated (GLR-mediated) Ca^{2+} influx during wound responses (Lew et al., 2020; Fichman et al., 2021).

Similar to surface potential changes, wound-stimulated APs involves long-distance transmission (Felle and Zimmermann, 2007; Zimmermann et al., 2009; Hedrich et al., 2016). APs can be propagated in barley by the application of many substances, such as NaCl, KCl, CaCl_2 , glutamate, and GABA (Felle and Zimmermann, 2007). Amongst these, glutamate and GABA were proposed to act on putative “receptors” to prime Ca^{2+} influx, Ca^{2+} -dependent Cl^- efflux, and initiate APs together with transient apoplastic pH regulation (Felle and Zimmermann, 2007). Later, Hedrich et al. (2016) proposed that AP are excited by membrane depolarization via anion efflux through R-type anion channels (e.g. ALMT12/QUAC1), followed by depolarization-activated K^+ release through GORK and/or shaker-like outwardly-rectifying K^+ channel (SKOR) to rehyperpolarize membrane potential. Indeed, the Arabidopsis GORK knock-out mutant (*gork*) had impaired APs in magnitude and duration when generated by electrical stimulation (Cuin et al., 2018), and GABA-stimulated K^+ efflux was abolished in the root epidermis of *gork1* mutants (Adem et al., 2020).

Although it has been noted that both glutamate and GABA may facilitate long-distance electrical signal transmission through plants, such as APs (Felle and Zimmermann, 2007), it is unclear whether they interact to shape such signals. On one hand, intracellular Ca^{2+} signal modulated by glutamate-dependent GLR may shape GAD activity and GABA signals (Zik et al., 1998; Toyota et al., 2018; Shao et al., 2020; Xu et al., 2021); on the other hand, GABA may be associated with apoplastic pH balance and cellular H^+ flux via ALMTs and/or H^+ -ATPases that work together with glutamate to regulate the activity of GLR-mediated Ca^{2+} influx, membrane potential changes and ROS propagations (Ramesh et al., 2018; Kamran et al., 2020; Shao et al., 2020; Wu et al., 2021).

The following questions regarding the potential interaction of GABA and glutamate with APs would be important to examine: (1) Does GABA regulation of ALMT12 play a

role? (Domingos et al., 2019; Xu et al., 2021); (2) Does ALMT-facilitated GABA efflux affect apoplastic pH? (Ramesh et al., 2018; Kamran et al., 2020); (3) What is the impact of cellular GABA metabolism on H^+ and K^+ (via GORK) flux regulation, and does this impact GLR activated Ca^{2+} waves and surface potential changes? (Su et al., 2019; Adem et al., 2020; Wu et al., 2021); and (4) Does GLR based activation of Ca^{2+} influx activate GABA synthesis and does this impact AP regulation?

Cross talk between GABA and plant hormones

Emerging evidence suggests that GABA as a signaling molecule interacts with other signals to coordinate particular physiological processes. In terms of guard cell signaling, ABA closes stomata via activation of Open Stomata 1/Snf1-Related protein Kinase 2.6- and/or CPK(s)-dependent phosphorylation on Slow Anion Channel-associated 1 (SLAC1)/SLAC1-homolog protein 3 (SLAH3) and ALMT12 to release anions (Mori et al., 2006; Geiger et al., 2011; Brandt et al., 2012, 2015; Imes et al., 2013; Gutermuth et al., 2018). ABA also phosphorylates tonoplast-localized ALMT4 to activate anion release from guard cell vacuoles to facilitate stomatal closure (Eisenach et al., 2017). GABA can attenuate ABA-induced stomatal closure at low doses (2.5 μM), presumably acting via the inhibition of ALMT12, since the loss of ALMT12 function in the *almt12* mutant reduced stomatal sensitivity to both signals (Meyer et al., 2010; Imes et al., 2013; Xu et al., 2021). However, it is unknown whether GABA attenuates ABA's effect also via reducing ALMT4-mediated anion release from vacuoles in this process. This could play out in a physiological scenario when cellular GABA increases to reduce the sensitivity of the guard cell to low ABA concentrations. However, GABA has no impact on the effect of high concentrations of ABA (25 μM) on stomatal closure implicating that reduced anion efflux via ALMT12 by GABA may not reverse guard-cell membrane depolarization and anion efflux through SLAC1/SLAH3 in such circumstances (Geiger et al., 2011; Brandt et al., 2012, 2015; Kollist et al., 2014; Xu et al., 2021). Collectively, this suggests that GABA homeostasis may fine adjust tissue sensitivity to cellular signals when the stimulus is of low intensity, but not antagonize the plant response when these signals are of sufficient magnitude. Intriguingly, a high dose of ABA (25 μM) does not fully close stomata on epidermal peels of *gad2* mutants (Xu et al., 2021). The open stomata phenotype here was proposed to be due to deregulation of ALMT9 in *gad2* mutants as discussed in section above; as such ALMT9 appears not to be a target of ABA. This suggests that some GABA-mediated processes may be not overwritten by amplifying other signals, and therefore provides an opportunity to engineer GABA responses in plants for altered outcomes to environmental stress.

Wound or herbivory attack on leaves stimulates systemic jasmonate (JA) and GABA biosynthesis in plants, as discussed above. JA accumulation promotes biosynthesis of

secondary metabolites (e.g. glucosinolates) and proteinase inhibitors to repel herbivory attack, such as the Arabidopsis herbivore—*Arion lusitanicus* and rice (*Oryza sativa*) root-feeding insects—*Diabrotica balteata* and *Lissorhoptrus oryzophilus* (Falk et al., 2014; Lu et al., 2015; Wang et al., 2019). GABA production reduces insect growth and survival (e.g. *Spodoptera littoralis* larvae), probably due to its effects on invertebrate (insect) ionotropic GABA receptors at neuromuscular junctions (Bown et al., 2006; Scholz et al., 2015, 2017; Tarkowski et al., 2020). GABA depletion (in *gad1/gad2*) or overaccumulation (in *pop2-5*) does not alter JA biosynthesis stimulated by *S. littoralis* and MecWorm feeding (Scholz et al., 2015, 2017), and this implicates that endogenous GABA metabolism does not regulate of JA synthesis. But mutation in *JAmonate Resistant 1 (JAR1)*, in *jar1*, did cause greater GABA accumulation when attacked by *S. littoralis* (Scholz et al., 2015), and *JAR1* encodes a jasmonate-amido synthetase that catalyzes the formation of JA-Ile that structurally is an amino acid (Ile) conjugated JA and directly facilitates the JA-signaling core target interaction (i.e. SCF^{COI1}-JAZ1; Staswick et al., 2002; Katsir et al., 2008). The loss of the key JA-Ile receptor (in *coi1*) and lowering JA-Ile stimulation (in *cml37*) both resulted in greater susceptibility to *S. littoralis* (Scholz et al., 2014). Taken together, JA signaling may affect the levels of wound-stimulated GABA production in plants or render the plant more susceptible to insect attack, damage and consequently stimulate more production of GABA.

Exogenous application of 10-mM GABA stimulates ethylene biosynthesis in sunflower (*Helianthus annuus* L.) and the Caryophyllaceae *Stellaria longipes* via up-regulation of ethylene signaling genes—1-Aminocyclopropane-1-carboxylic acid (ACC) synthase (ACS) and ACC oxidase (ACO) (Kathiresan et al., 1997, 1998; Booker and DeLong, 2015). Salt stress increased ethylene biosynthesis at 24 h and GABA production at 48 h in *Caragana intermedia* roots (Shi et al., 2010). Interestingly, 10-mM GABA supplement suppressed this early 24-h ethylene accumulation, whilst promoting ethylene production and further enhancing endogenous GABA accumulation 48 h post treatment (Shi et al., 2010). Similarly, GABA treatment has also been found to affect ethylene production in poplar (*Populus tomentosa* Carr) with a low dose of GABA (0.25 mM) enhancing ethylene synthesis, again through up regulation of ACS and ACOs (Ji et al., 2018). Together, this suggests that the GABA metabolism appears to affect ethylene synthesis response to salt stress in plants, and different plant species may vary in sensitivity to endogenous GABA in order to stimulate ethylene synthesis.

In plants, ethylene is a key hormone that controls (climacteric) fruit ripening and malate impacts fruit flavour (Alexander and Grierson, 2002; Liu et al., 2015; Hu et al., 2019; Wege, 2020). The downregulation of ethylene biosynthesis via silencing ACS and ACO genes is associated with low ethylene production in apple (*Malus domestica*) fruits (Dandekar et al., 2004; Defilippi et al., 2004). The malate

content in apple fruit is expected to be significantly reduced at 2 weeks postharvest; however, it remains unchanged in low-ethylene transgenic apple fruits that can be reversed by exogenous ethylene application (Dandekar et al., 2004; Defilippi et al., 2004). Exogenous GABA treatment (10 mM) increases GABA and malate contents, but lowers ethylene synthesis in apple fruit during storage up to 70 d (Han et al., 2018). Malate storage in apple and tomato (*Solanum lycopersicum*) fruit is respectively linked with *MdALMT9/MdMa1* and *SlALMT9* (Ye et al., 2017; Li et al., 2020). *MdALMT9/MdMa1*, an ortholog of *ALMT9* from Arabidopsis, encodes a tonoplast-localized channel catalyzing malate uptake into the vacuoles and facilitating malate accumulation in apple fruit (Li et al., 2020). Moreover, *MdALMT9/MdMa1* contains identical amino-acid residues (FIYPIWAGEDLH) of the GABA regulation motif within Arabidopsis *ALMT9*, in which the mutation of two aromatic residues (F243 and Y245) abolished its GABA sensitivity in planta (Ramesh et al., 2017; Li et al., 2020; Xu et al., 2021), implicating that *MdALMT9* might have GABA sensitivity as well. Intriguingly, both ethylene and GABA have been demonstrated to negatively regulate malate efflux through *TaALMT1* at wheat root apices (Tian et al., 2014; Ramesh et al., 2015). Accordingly, the equilibrium between ethylene and GABA signaling may regulate fruit taste via the modulation of tonoplast-localized *ALMT*-mediated malate storage within fruit during ripening and postharvest storage. This provides a mechanistic link between GABA and ethylene that goes beyond the proposed association of GABA and ethylene production with malate metabolism (Defilippi et al., 2004; Han et al., 2018). Experiments would have to be performed to explore the explicit link between *ALMT* and GABA in apple and the other species mentioned in this section to determine whether this anion channel family provides the mechanism of cross talk between GABA and other signals.

Conclusion

Recent research has shown that GABA can fulfill a signaling role in plants that ultimately may regulate key growth, development and stress tolerance processes. As GABA synthesis increases during stress, to sustain energy production via the TCA cycle (Bown and Shelp, 2016; Gilliham and Tyerman, 2016), GABA has the potential to modulate other signals; cross talk of GABA therefore has the potential to fine tune plant physiology rather than initiating a physiological response per se. This appears to be the case with the interaction with known signals such as ethylene and ABA, and in the regulation of guard cell movement, while GABA has the potential to fulfill a more overt role in signaling for pollen tube growth and fertilization and wound signaling—but this remains to be demonstrated. Many questions remain, such as: Are there additional GABA responsive elements beyond *ALMTs* (e.g. *GORK* and H^+ -ATPases)?; How does GABA flux through *ALMTs* relate to GABA signaling, and does this

occur through two states of the same protein as suggested by Long et al. (2019), or through alternative transporters?; and how does GABA flux regulate GABA distribution in tissues? Future research will no doubt explore these, and additional questions related to GABA's physiological role in plants.

ADVANCES

- GABA regulation of ALMT-mediated anion flux represents a class of physiological signal in plants that links primary metabolism to environmental responses.
- GABA mode of action in guard cells demonstrates that GABA modulates physiological responses rather than stimulates a response per se.
- Glutamate and GABA are intimately linked, with glutamate being a GABA precursor, and both modulate ion transport, indicating the concentrations of these metabolites may represent part of a homeostatic mechanism of membrane potential control and signaling.
- As a signal, GABA likely interacts with other hormonal signals to shape physiological processes.

OUTSTANDING QUESTIONS

- Does cytosolic GABA directly interact with ALMT9 and 12 in stomatal regulation?
- How does cellular GABA equilibrium fine tune the ionic flux and gradient during pollen tube growth?
- Do Arabidopsis ALMT9 or 12-14 facilitate GABA transport in stomatal and pollen tubes, as shown for TaALMT1?
- Does the GABA inhibitory effect on stomatal closing signals (e.g. dark, ABA, and H₂O₂) have a physiological role?
- How does GABA activate GORK-mediated K⁺ efflux?
- Are there other protein targets for GABA in plants beyond ALMTs?

Supplemental data

The following materials are available in the online version of this article.

Supplemental Figure S1. GABA supplementation does not affect the photosynthetic rate of detached barley leaves.

Acknowledgments

We apologize to those researchers whose work was not cited in this review due to length limitations.

Funding

This work was supported by ARC Discovery (grant no. DP210102828), ARC Centre of Excellence (grant no. CE140100008), and Grains Research and Development Corporation funding (grant no. UWA00173) to M.G.

Conflict of interest statement. None declared.

References

- Abdel Razik ES, Alharbi BM, Pirzadah TB, Alnusairi GS, Soliman MH, Hakeem KR (2020) γ -Aminobutyric acid (GABA) mitigates drought and heat stress in sunflower (*Helianthus annuus* L.) by regulating its physiological, biochemical and molecular pathways. *Physiol Plant* **172**: 505–527
- Adem GD, Chen G, Shabala L, Chen Z-H, Shabala S (2020) GORK channel: a master switch of plant metabolism? *Trends Plant Sci* **25**: 434–445
- Akama K, Takaiwa F (2007) C-terminal extension of rice glutamate decarboxylase (OsGAD2) functions as an autoinhibitory domain and overexpression of a truncated mutant results in the accumulation of extremely high levels of GABA in plant cells. *J Exp Bot* **58**: 2699–2707
- Alexander L, Grierson D (2002) Ethylene biosynthesis and action in tomato: a model for climacteric fruit ripening. *J Exp Bot* **53**: 2039–2055
- Alsterfjord M, Sehnke PC, Arkell A, Larsson H, Svnenlid F, Rosenquist M, Ferl RJ, Sommarin M, Larsson C (2004) Plasma membrane H⁺-ATPase and 14-3-3 isoforms of Arabidopsis leaves: evidence for isoform specificity in the 14-3-3/H⁺-ATPase interaction. *Plant Cell Physiol* **45**: 1202–1210
- Batushansky A, Kirma M, Grillich N, Toubiana D, Pham PA, Balbo I, Fromm H, Galili G, Fernie AR, Fait A (2014) Combined transcriptomics and metabolomics of *Arabidopsis thaliana* seedlings exposed to exogenous GABA suggest its role in plants is predominantly metabolic. *Mol Plant* **7**: 1065–1068
- Behera S, Xu Z, Luoni L, Bonza MC, Doccula FG, De Michelis MI, Morris RJ, Schwarzländer M, Costa A (2018) Cellular Ca²⁺ signals generate defined pH signatures in plants. *Plant Cell* **30**: 2704–2719
- Ben-Ari Y, Gaiarsa J-L, Tyzio R, Khazipov R (2007) GABA: a pioneer transmitter that excites immature neurons and generates primitive oscillations. *Physiol Rev* **87**: 1215–1284
- Booker MA, DeLong A (2015) Producing the ethylene signal: regulation and diversification of ethylene biosynthetic enzymes. *Plant Physiol* **169**: 42–50
- Bor M, Turkan I (2019) Is there a room for GABA in ROS and RNS signalling? *Environ Exp Bot* **161**: 67–73
- Bouche N, Fromm H (2004) GABA in plants: just a metabolite? *Trends Plant Sci* **9**: 110–115
- Bouché N, Lacombe B, Fromm H (2003) GABA signaling: a conserved and ubiquitous mechanism. *Trends Cell Biol* **13**: 607–610
- Bown AW, MacGregor KB, Shelp BJ (2006) Gamma-aminobutyrate: defense against invertebrate pests? *Trends Plant Sci* **11**: 424–427
- Bown AW, Shelp BJ (2016) Plant GABA: not just a metabolite. *Trends Plant Sci* **21**: 811–813
- Brandt B, Brodsky DE, Xue S, Negi J, Iba K, Kangasjärvi J, Ghassemian M, Stephan AB, Hu H, Schroeder JI (2012) Reconstitution of abscisic acid activation of SLAC1 anion channel by CPK6 and OST1 kinases and branched AB11 PP2C phosphatase action. *Proc Natl Acad Sci USA* **109**: 10593–10598

- Brandt B, Munemasa S, Wang C, Nguyen D, Yong T, Yang PG, Poretsky E, Belknap TF, Waadt R, Alemán F** (2015) Calcium specificity signaling mechanisms in abscisic acid signal transduction in *Arabidopsis* guard cells. *eLife* **4**: e03599
- Carroll AD, Fox GG, Laurie S, Phillips R, Ratcliffe RG, Stewart GR** (1994) Ammonium assimilation and the role of γ -aminobutyric acid in pH homeostasis in carrot cell suspensions. *Plant Physiol* **106**: 513–520
- Chen W, Jia PF, Yang WC, Li HJ** (2020) Plasma membrane H^+ -ATPases-mediated cytosolic proton gradient regulates pollen tube growth. *J Integr Plant Biol* **62**: 1817–1822
- Chen Z-H, Chen G, Dai F, Wang Y, Hills A, Ruan Y-L, Zhang G, Franks PJ, Nevo E, Blatt MR** (2017) Molecular evolution of grass stomata. *Trends Plant Sci* **22**: 124–139
- Cheng B, Li Z, Liang L, Cao Y, Zeng W, Zhang X, Ma X, Huang L, Nie G, Liu W** (2018) The γ -aminobutyric acid (GABA) alleviates salt stress damage during seeds germination of white clover associated with Na^+/K^+ transportation, dehydrins accumulation, and stress-related genes expression in white clover. *Int J Mol Sci* **19**: 2520
- Clark SM, Di Leo R, Dhanoa PK, Van Cauwenberghe OR, Mullen RT, Shelp BJ** (2009) Biochemical characterization, mitochondrial localization, expression, and potential functions for an *Arabidopsis* γ -aminobutyrate transaminase that utilizes both pyruvate and glyoxylate. *J Exp Bot* **60**: 1743–1757
- Crawford LA, Bown AW, Breikreuz KE, Guinel FC** (1994) The synthesis of γ -aminobutyric acid in response to treatments reducing cytosolic pH. *Plant Physiol* **104**: 865–871
- Cuin TA, Dreyer I, Michard E** (2018) The role of potassium channels in *Arabidopsis thaliana* long distance electrical signalling: AKT2 modulates tissue excitability while GORK shapes action potentials. *Int J Mol Sci* **19**: 926
- Dandekar AM, Teo G, Defilippi BG, Uratsu SL, Passey AJ, Kader AA, Stow JR, Colgan RJ, James DJ** (2004) Effect of down-regulation of ethylene biosynthesis on fruit flavor complex in apple fruit. *Transgenic Res* **13**: 373–384
- David R, Byrt CS, Tyerman SD, Gilliam M, Wege S** (2019) Roles of membrane transporters: connecting the dots from sequence to phenotype. *Ann Bot* **124**: 201–208
- De Angeli A, Zhang J, Meyer S, Martinoia E** (2013) AtALMT9 is a malate-activated vacuolar chloride channel required for stomatal opening in *Arabidopsis*. *Nat Commun* **4**: 1804
- Defilippi BG, Dandekar AM, Kader AA** (2004) Impact of suppression of ethylene action or biosynthesis on flavor metabolites in apple (*Malus domestica* Borkh) fruits. *J Agric Food Chem* **52**: 5694–5701
- Demidchik V, Cuin TA, Svistunenko D, Smith SJ, Miller AJ, Shabala S, Sokolik A, Yurin V** (2010) *Arabidopsis* root K^+ -efflux conductance activated by hydroxyl radicals: single-channel properties, genetic basis and involvement in stress-induced cell death. *J Cell Sci* **123**: 1468–1479
- Deng X, Xu X, Liu Y, Zhang Y, Yang L, Zhang S, Xu J** (2020) Induction of γ -aminobutyric acid plays a positive role to *Arabidopsis* resistance against *Pseudomonas syringae*. *J Integr Plant Biol* **62**: 1797–1812
- Domingos P, Dias PN, Tavares B, Portes MT, Wudick MM, Konrad KR, Gilliam M, Bicho A, Feijó JA** (2019) Molecular and electrophysiological characterization of anion transport in *Arabidopsis thaliana* pollen reveals regulatory roles for pH, Ca^{2+} and GABA. *New Phytol* **223**: 1353–1371
- Eisenach C, Baetz U, Huck NV, Zhang J, De Angeli A, Beckers G, Martinoia E** (2017) ABA-Induced stomatal closure involves ALMT4, a phosphorylation-dependent vacuolar anion channel of *Arabidopsis*. *Plant Cell* **29**: 2552–2569
- Falk KL, Kästner J, Bodenhausen N, Schramm K, Paetz C, Vassão DG, Reichelt M, Von Knorre D, Bergelson J, Erb M** (2014) The role of glucosinolates and the jasmonic acid pathway in resistance of *Arabidopsis thaliana* against molluscan herbivores. *Mol Ecol* **23**: 1188–1203
- Farmer E, Mousavi S, Lenglet A** (2013) Leaf numbering for experiments on long distance signalling in *Arabidopsis*. *Protoc Exch* doi: 10.1038/protex.2013.1071. (Accessed on July 30, 2021)
- Farmer EE, Gao YQ, Lenzone G, Wolfender JL, Wu Q** (2020) Wound-and mechanostimulated electrical signals control hormone responses. *New Phytol* **227**: 1037–1050
- Farooq M, Nawaz A, Chaudhry M, Indrasti R, Rehman A** (2017) Improving resistance against terminal drought in bread wheat by exogenous application of proline and gamma-aminobutyric acid. *J Agron Crop Sci* **203**: 464–472
- Felle HH, Zimmermann MR** (2007) Systemic signalling in barley through action potentials. *Planta* **226**: 203–214
- Fichman Y, Myers RJ, Grant DG, Mittler R** (2021) Plasmodesmata-localized proteins and ROS orchestrate light-induced rapid systemic signaling in *Arabidopsis*. *Sci Signal* **14**: 1–12
- Fromm H** (2020) GABA signaling in plants: targeting the missing pieces of the puzzle. *J Exp Bot* **71**: 6238–6245
- Geiger D, Maierhofer T, Al-Rasheid KA, Scherzer S, Mumm P, Liese A, Ache P, Wellmann C, Marten I, Grill E** (2011) Stomatal closure by fast abscisic acid signaling is mediated by the guard cell anion channel SLAH3 and the receptor RCAR1. *Sci Signal* **4**: 1–12
- Gilliam M, Tyerman SD** (2016) Linking metabolism to membrane signaling: the GABA-malate connection. *Trends Plant Sci* **21**: 295–301
- Gruber BD, Ryan PR, Richardson AE, Tyerman SD, Ramesh S, Hebb DM, Howitt SM, Delhaize E** (2010) HvALMT1 from barley is involved in the transport of organic anions. *J Exp Bot* **61**: 1455–1467
- Gutermuth T, Herbell S, Lassig R, Brosché M, Romeis T, Feijó JA, Hedrich R, Konrad KR** (2018) Tip-localized Ca^{2+} -permeable channels control pollen tube growth via kinase-dependent R- and S-type anion channel regulation. *New Phytol* **218**: 1089–1105
- Han S, Nan Y, Qu W, He Y, Ban Q, Lv Y, Rao J** (2018) Exogenous γ -aminobutyric acid treatment that contributes to regulation of malate metabolism and ethylene synthesis in apple fruit during storage. *J Agric Food Chem* **66**: 13473–13482
- Hedrich R, Salvador-Recatalà V, Dreyer I** (2016) Electrical wiring and long-distance plant communication. *Trends Plant Sci* **21**: 376–387
- Hetherington AM, Woodward FI** (2003) The role of stomata in sensing and driving environmental change. *Nature* **424**: 901–908
- Higashiyama T, Takeuchi H** (2015) The mechanism and key molecules involved in pollen tube guidance. *Annu Rev Plant Biol* **66**: 393–413
- Hoffmann RD, Portes MT, Olsen LI, Damineli DSC, Hayashi M, Nunes CO, Pedersen JT, Lima PT, Campos C, Feijó JA** (2020) Plasma membrane H^+ -ATPases sustain pollen tube growth and fertilization. *Nat Commun* **11**: 1–15
- Hu B, Sun D-W, Pu H, Wei Q** (2019) Recent advances in detecting and regulating ethylene concentrations for shelf-life extension and maturity control of fruit: a review. *Trends Plant Sci* **91**: 66–82
- Imes D, Mumm P, Böhm J, Al-Rasheid KA, Marten I, Geiger D, Hedrich R** (2013) Open stomata 1 (OST1) kinase controls R-type anion channel QUAC1 in *Arabidopsis* guard cells. *Plant J* **74**: 372–382
- Ji J, Yue J, Xie T, Chen W, Du C, Chang E, Chen L, Jiang Z, Shi S** (2018) Roles of γ -aminobutyric acid on salinity-responsive genes at transcriptomic level in poplar: involving in abscisic acid and ethylene-signalling pathways. *Planta* **248**: 675–690
- Johns S, Hagihara T, Toyota M, Gilroy S** (2021) The fast and the furious: rapid long-range signaling in plants. *Plant Physiol* **185**: 694–706
- Johnson MA, Harper JF, Palanivelu R** (2019) A fruitful journey: pollen tube navigation from germination to fertilization. *Annu Rev Plant Biol* **70**: 809–837
- Kamran M, Ramesh SA, Gilliam M, Tyerman SD, Bose J** (2020) Role of TaALMT1 malate-GABA transporter in alkaline pH tolerance of wheat. *Plant Cell Environ* **43**: 2443–2459

- Kathiresan A, Miranda J, Chinnappa C, Reid D** (1998) γ -aminobutyric acid promotes stem elongation in *Stellaria longipes*: the role of ethylene. *Plant Growth Regul* **26**: 131–137
- Kathiresan A, Tung P, Chinnappa C, Reid DM** (1997) [gamma]-Aminobutyric acid stimulates ethylene biosynthesis in sunflower. *Plant Physiol* **115**: 129–135
- Katsir L, Chung HS, Koo AJ, Howe GA** (2008) Jasmonate signaling: a conserved mechanism of hormone sensing. *Curr Opin Plant Biol* **11**: 428–435
- Kim T-H, Böhmer M, Hu H, Nishimura N, Schroeder JI** (2010) Guard cell signal transduction network: advances in understanding abscisic acid, CO₂, and Ca²⁺ signaling. *Annu Rev Plant Biol* **61**: 561–591
- Kollist H, Nuhkat M, Roelfsema MRG** (2014) Closing gaps: linking elements that control stomatal movement. *New Phytol* **203**: 44–62
- Kovermann P, Meyer S, Hörtensteiner S, Picco C, Scholz-Starke J, Ravera S, Lee Y, Martinoia E** (2007) The Arabidopsis vacuolar malate channel is a member of the ALMT family. *Plant J* **52**: 1169–1180
- Krishnan S, Laskowski K, Shukla V, Merewitz EB** (2013) Mitigation of drought stress damage by exogenous application of a non-protein amino acid γ -aminobutyric acid on perennial ryegrass. *J Am Soc Hortic Sci* **138**: 358–366
- Lampert DT, Tan L, Held MA, Kieliszewski MJ** (2018) Pollen tube growth and guidance: Occam's razor sharpened on a molecular arabinogalactan glycoprotein Rosetta Stone. *New Phytol* **217**: 491–500
- Lancien M, Roberts MR** (2006) Regulation of Arabidopsis thaliana 14-3-3 gene expression by γ -aminobutyric acid. *Plant Cell Environ* **29**: 1430–1436
- Lawson T, Lefebvre S, Baker NR, Morison JI, Raines CA** (2008) Reductions in mesophyll and guard cell photosynthesis impact on the control of stomatal responses to light and CO₂. *J Exp Bot* **59**: 3609–3619
- Lawson T, Simkin AJ, Kelly G, Granot D** (2014) Mesophyll photosynthesis and guard cell metabolism impacts on stomatal behaviour. *New Phytol* **203**: 1064–1081
- Leakey AD, Ferguson JN, Pignon CP, Wu A, Jin Z, Hammer GL, Lobell DB** (2019) Water use efficiency as a constraint and target for improving the resilience and productivity of C₃ and C₄ crops. *Annu Rev Plant Biol* **70**: 781–808
- Lee J, Bowling D** (1992) Effect of the mesophyll on stomatal opening in *Commelina communis*. *J Exp Bot* **43**: 951–957
- Lew TTS, Koman VB, Silmore KS, Seo JS, Gordichuk P, Kwak S-Y, Park M, Ang MC-Y, Khong DT, Lee MA** (2020) Real-time detection of wound-induced H₂O₂ signalling waves in plants with optical nanosensors. *Nat Plants* **6**: 404–415
- Li C, Dougherty L, Coluccio AE, Meng D, El-Sharkawy I, Borejsza-Wysocka E, Liang D, Piñeros MA, Xu K, Cheng L** (2020) Apple ALMT9 requires a conserved C-terminal domain for malate transport underlying fruit acidity. *Plant Physiol* **182**: 992–1006
- Li K, Prada J, Damineli DS, Liese A, Romeis T, Dandekar T, Feijó JA, Hedrich R, Konrad KR** (2021) An optimized genetically encoded dual reporter for simultaneous ratio imaging of Ca²⁺- and H⁺ reveals new insights into ion signaling in plants. *New Phytol* **230**: 2292–2310
- Li Z, Peng Y, Huang B** (2016a) Physiological effects of γ -aminobutyric acid application on improving heat and drought tolerance in creeping bentgrass. *J Am Soc Hortic Sci* **141**: 76–84
- Li Z, Yu J, Peng Y, Huang B** (2016b) Metabolic pathways regulated by γ -aminobutyric acid (GABA) contributing to heat tolerance in creeping bentgrass (*Agrostis stolonifera*). *Sci Rep* **6**: 1–16
- Li M, Guo S, Yang X, Meng Q, Wei X** (2016c) Exogenous gamma-aminobutyric acid increases salt tolerance of wheat by improving photosynthesis and enhancing activities of antioxidant enzymes. *Biol Plant* **60**: 123–131
- Liu M, Pirrello J, Chervin C, Roustan J-P, Bouzayen M** (2015) Ethylene control of fruit ripening: revisiting the complex network of transcriptional regulation. *Plant Physiol* **169**: 2380–2390
- Long Y, Tyerman SD, Gilliam M** (2019) Cytosolic GABA inhibits anion transport by wheat ALMT1. *New Phytol* **225**: 671–678
- Lu J, Robert CAM, Riemann M, Cosme M, Mène-Saffrané L, Massana J, Stout MJ, Lou Y, Gershenzon J, Erb M** (2015) Induced jasmonate signaling leads to contrasting effects on root damage and herbivore performance. *Plant Physiol* **167**: 1100–1116
- Marvin JS, Shimoda Y, Magloire V, Leite M, Kawashima T, Jensen TP, Kolb I, Knott EL, Novak O, Podgorski K** (2019) A genetically encoded fluorescent sensor for in vivo imaging of GABA. *Nat Methods* **16**: 763–770
- Mekonnen DW, Flügge U-I, Ludewig F** (2016) Gamma-aminobutyric acid depletion affects stomata closure and drought tolerance of *Arabidopsis thaliana*. *Plant Sci* **245**: 25–34
- Melotto M, Underwood W, Koczan J, Nomura K, He SY** (2006) Plant stomata function in innate immunity against bacterial invasion. *Cell* **126**: 969–980
- Merilo E, Jöesaar I, Brosché M, Kollist H** (2014) To open or to close: species-specific stomatal responses to simultaneously applied opposing environmental factors. *New Phytol* **202**: 499–508
- Meyer S, Mumm P, Imes D, Endler A, Weder B, Al-Rasheid KA, Geiger D, Marten I, Martinoia E, Hedrich R** (2010) AtALMT12 represents an R-type anion channel required for stomatal movement in Arabidopsis guard cells. *Plant J* **63**: 1054–1062
- Michaeli S, Fromm H** (2015) Closing the loop on the GABA shunt in plants: are GABA metabolism and signaling entwined? *Front. Plant Sci* **6**: 1–7
- Mori IC, Murata Y, Yang Y, Munemasa S, Wang Y-F, Andreoli S, Tiriaco H, Alonso JM, Harper JF, Ecker JR** (2006) CDPKs CPK6 and CPK3 function in ABA regulation of guard cell S-type anion- and Ca²⁺-permeable channels and stomatal closure. *PLoS Bio* **4**: 1749–1762
- Murata Y, Mori IC, Munemasa S** (2015) Diverse stomatal signaling and the signal integration mechanism. *Annu Rev Plant Biol* **66**: 369–392
- Owens DF, Kriegstein AR** (2002) Is there more to GABA than synaptic inhibition? *Nature Rev Neurosci* **3**: 715–727
- Palanivelu R, Brass L, Edlund AF, Preuss D** (2003) Pollen tube growth and guidance is regulated by POP2, an Arabidopsis gene that controls GABA levels. *Cell* **114**: 47–59
- Ramesh SA, Kamran M, Sullivan W, Chirkova L, Okamoto M, Degryse F, McLaughlin M, Gilliam M, Tyerman SD** (2018) Aluminium-activated malate transporters can facilitate GABA transport. *Plant Cell* **30**: 1147–1164
- Ramesh SA, Tyerman SD, Gilliam M, Xu B** (2017) γ -Aminobutyric acid (GABA) signalling in plants. *Cell Mol Life Sci* **74**: 1577–1603
- Ramesh SA, Tyerman SD, Xu B, Bose J, Kaur S, Conn V, Domingos P, Ullah S, Wege S, Shabala S, et al.** (2015) GABA signalling modulates plant growth by directly regulating the activity of plant-specific anion transporters. *Nat Commun* **6**: 1–9
- Renault H, Roussel V, El Amrani A, Arzel M, Renault D, Bouchereau A, Deleu C** (2010) The Arabidopsis *pop2-1* mutant reveals the involvement of GABA transaminase in salt stress tolerance. *BMC Plant Biol* **10**: 1–16
- Scholz SS, Malabarba J, Reichelt M, Heyer M, Ludewig F, Mithöfer A** (2017) Evidence for GABA-induced systemic GABA accumulation in Arabidopsis upon wounding. *Front Plant Sci* **8**: 1–9
- Scholz SS, Reichelt M, Mekonnen DW, Ludewig F, Mithöfer A** (2015) Insect herbivory-elicited GABA accumulation in plants is a wound-induced, direct, systemic, and jasmonate-independent defense response. *Front Plant Sci* **6**: 1–11
- Scholz SS, Vadassery J, Heyer M, Reichelt M, Bender KW, Snedden WA, Boland W, Mithöfer A** (2014) Mutation of the Arabidopsis calmodulin-like protein CML37 deregulates the jasmonate pathway and enhances susceptibility to herbivory. *Mol Plant* **7**: 1712–1726

- Shao Q, Gao Q, Lhamo D, Zhang H, Luan S (2020) Two glutamate- and pH-regulated Ca^{2+} channels are required for systemic wound signaling in *Arabidopsis*. *Sci Signal* **13**: 1–13
- Shelp BJ, Bown AW, Faure D (2006) Extracellular γ -aminobutyrate mediates communication between plants and other organisms. *Plant Physiol* **142**: 1350–1352
- Shelp BJ, Bown AW, McLean MD (1999) Metabolism and functions of gamma-aminobutyric acid. *Trends Plant Sci* **4**: 446–452
- Shi SQ, Shi Z, Jiang ZP, Qi LW, Sun XM, Li CX, Liu JF, Xiao WF, Zhang SG (2010) Effects of exogenous GABA on gene expression of *Caragana intermedia* roots under NaCl stress: regulatory roles for H_2O_2 and ethylene production. *Plant Cell Environ* **33**: 149–162
- Shimazaki K-i, Doi M, Assmann SM, Kinoshita T (2007) Light regulation of stomatal movement. *Annu Rev Plant Biol* **58**: 219–247
- Staswick PE, Tiriyaki I, Rowe ML (2002) Jasmonate response locus JAR1 and several related *Arabidopsis* genes encode enzymes of the firefly luciferase superfamily that show activity on jasmonic, salicylic, and indole-3-acetic acids in an assay for adenylation. *Plant Cell* **14**: 1405–1415
- Su N, Wu Q, Chen J, Shabala L, Mithöfer A, Wang H, Qu M, Yu M, Cui J, Shabala S (2019) GABA operates upstream of H^+ -ATPase and improves salinity tolerance in *Arabidopsis* by enabling cytosolic K^+ retention and Na^+ exclusion. *J Exp Bot* **70**: 6349–6361
- Sussmilch FC, Schultz J, Hedrich R, Roelfsema MRG (2019) Acquiring control: the evolution of stomatal signalling pathways. *Trends Plant Sci* **24**: 342–351
- Tarkowski ŁP, Signorelli S, Höfte M (2020) γ -Aminobutyric acid and related amino acids in plant immune responses: emerging mechanisms of action. *Plant Cell Environ* **43**: 1103–1116
- Tian Q, Zhang X, Ramesh S, Gilliam M, Tyerman SD, Zhang W-H (2014) Ethylene negatively regulates aluminium-induced malate efflux from wheat roots and tobacco cells transformed with TaALMT1. *J Exp Bot* **65**: 2415–2426
- Toyota M, Spencer D, Sawai-Toyota S, Jiaqi W, Zhang T, Koo AJ, Howe GA, Gilroy S (2018) Glutamate triggers long-distance, calcium-based plant defense signaling. *Science* **361**: 1112–1115
- Turano FJ, Fang TK (1998) Characterization of two glutamate decarboxylase cDNA clones from *Arabidopsis*. *Plant Physiol* **117**: 1411–1421
- Van Kleeff P, Gao J, Mol S, Zwart N, Zhang H, Li K, De Boer A (2018) The *Arabidopsis* GORK K^+ -channel is phosphorylated by calcium-dependent protein kinase 21 (CPK21), which in turn is activated by 14-3-3 proteins. *Plant Physiol Biochem* **125**: 219–231
- Wang F, Chen Z-H, Liu X, Colmer TD, Shabala L, Salih A, Zhou M, Shabala S (2017) Revealing the roles of GORK channels and NADPH oxidase in acclimation to hypoxia in *Arabidopsis*. *J Exp Bot* **68**: 3191–3204
- Wang J, Wu D, Wang Y, Xie D (2019) Jasmonate action in plant defense against insects. *J Exp Bot* **70**: 3391–3400
- Wege S (2020) Sweet or Sour? Important link between nitrate signaling and malate accumulation identified in Apple. *Plant Physiol* **183**: 439–440
- Wu Q, Su N, Huang X, Cui J, Shabala L, Zhou M, Yu M, Shabala S (2021) Hypoxia-induced increase in GABA content is essential for restoration of membrane potential and preventing ROS-induced disturbance to ion homeostasis. *Plant Commun* **2**: 1–12
- Xu B, Long Y, Feng X, Zhu X, Sai N, Chirkova L, Betts A, Herrmann J, Edwards JE, Okamoto M, et al. (2021) GABA signaling modulates stomatal opening to enhance plant water use efficiency and drought resilience. *Nat Commun* **12**: 1–13
- Xu M, Gruber BD, Delhaize E, White RG, James RA, You J, Yang Z, Ryan PR (2015) The barley anion channel, HvALMT1, has multiple roles in guard cell physiology and grain metabolism. *Physiol Plant* **153**: 183–193
- Ye J, Wang X, Hu T, Zhang F, Wang B, Li C, Yang T, Li H, Lu Y, Giovannoni JJ (2017) An InDel in the promoter of *AI-ACTIVATED MALATE TRANSPORTER9* selected during tomato domestication determines fruit malate contents and aluminum tolerance. *Plant Cell* **29**: 2249–2268
- Yu G-H, Zou J, Feng J, Peng X-B, Wu J-Y, Wu Y-L, Palanivelu R, Sun M-X (2014) Exogenous γ -aminobutyric acid (GABA) affects pollen tube growth via modulating putative Ca^{2+} -permeable membrane channels and is coupled to negative regulation on glutamate decarboxylase. *J Exp Bot* **65**: 3235–3248
- Zarei A, Trobacher CP, Shelp BJ (2016) *Arabidopsis* aldehyde dehydrogenase 10 family members confer salt tolerance through putrescine-derived 4-aminobutyrate (GABA) production. *Sci Rep* **6**: 1–11
- Žárský V (2015) Signal transduction: GABA receptor found in plants. *Nat Plants* **1**: 1–2
- Zik M, Arazi T, Snedden WA, Fromm H (1998) Two isoforms of glutamate decarboxylase in *Arabidopsis* are regulated by calcium/calmodulin and differ in organ distribution. *Plant Mol Biol* **37**: 967–975
- Zimmermann MR, Maischak H, Mithöfer A, Boland W, Felle HH (2009) System potentials, a novel electrical long-distance apoplastic signal in plants, induced by wounding. *Plant Physiol* **149**: 1593–1600

PUBLICATION II

**GABA signalling modulates stomatal opening to
enhance plant water use efficiency and drought
resilience**

Statement of Authorship

Title of Paper	GABA signalling modulates stomatal opening to enhance plant water use efficiency and drought resilience
Publication Status	<input checked="" type="checkbox"/> Published <input type="checkbox"/> Accepted for Publication <input type="checkbox"/> Submitted for Publication <input type="checkbox"/> Unpublished and Unsubmitted work written in manuscript style
Publication Details	Xu, Bo, Yu Long, Xueying Feng, Xujun Zhu, Na Sai, Larissa Chirkova, Annette Betts, Johannes Herrmann, Everard Edwards, Mamoru Okamoto, Rainer Hedrich, and Matthew Gilliam. "GABA signalling modulates stomatal opening to enhance plant water use efficiency and drought resilience." Nature Communications (2021).

Principal Author

Name of Principal Author (Candidate)	Na Sai
Contribution to the Paper	I conducted experiments of measuring barley stomatal aperture during light/dark transition with present and absent of GABA (Fig 5g and 5h).
Overall percentage (%)	5%
Certification:	This paper reports on original research I conducted during the period of my Higher Degree by Research candidature and is not subject to any obligations or contractual agreements with a third party that would constrain its inclusion in this thesis.
Signature	_____ Date 5/5/2021

Co-Author Contributions

By signing the Statement of Authorship, each author certifies that:

- i. the candidate's stated contribution to the publication is accurate (as detailed above);
- ii. permission is granted for the candidate to include the publication in the thesis; and
- iii. the sum of all co-author contributions is equal to 100% less the candidate's stated contribution.

Name of Co-Author	Bo Xu
Contribution to the Paper	Conceived research and designed experiments. Conducted all experiments not listed above or below. Co-wrote paper.
Signature	_____ Date 6/5/2021

Name of Co-Author	Yu Long
Contribution to the Paper	Constructed almt9/almt12 knockouts, conducted assays on almt12 and almt9/almt12 plants. Repeated experiments with gad2 and WT.
Signature	_____ Date 5/5/2021

APPENDIX A. PUBLISHED ARTICLES

Name of Co-Author	Xueying Feng		
Contribution to the Paper	Constructed and screened homozygous lines of <i>alm19</i> mutants. Conducted experiments for Fig 8a, Fig 9, and Supp Fig 16a,b. Repeated experiments of the WT and <i>gad2</i> , <i>alm19</i> drought assays and stomatal response assays (replicate data for figure 1, 3; Supp Fig 6, 7).		
Signature		Date	6/5/2021

Name of Co-Author	Xujun Xu		
Contribution to the Paper	Conducted Supp Fig 5a,f.		
Signature		Date	5/5/2021

Name of Co-Author	Larissa Chirkova		
Contribution to the Paper	Performed UPLC interpreted data. Edited manuscript.		
Signature		Date	5/5/2021

Name of Co-Author	Annette Betts		
Contribution to the Paper	Performed LC interpreted data. Edited manuscript.		
Signature		Date	7/5/2021

Name of Co-Author	Johannes Hermann		
Contribution to the Paper	Performed Fig 1. Commented on manuscript.		
Signature		Date	6/5/2021

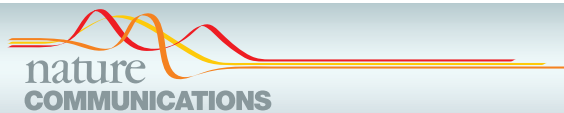
Name of Co-Author	Everard Edwards		
Contribution to the Paper	Supervised LC, interpreted data. Edited manuscript.		
Signature		Date	6/5/2021

Name of Co-Author	Mamouru Okamoto		
Contribution to the Paper	Supervised UPLC, interpreted data. Edited manuscript.		
Signature		Date	5/5/2021

APPENDIX A. PUBLISHED ARTICLES

Name of Co-Author	Rainer Hedrich		
Contribution to the Paper	Designed experiments, interpreted data and edited manuscript.		
Signature		Date	5/5/2021

Name of Co-Author	Matthew Gilliam		
Contribution to the Paper	Conceived research, designed experiments, interpreted data and co-wrote manuscript.		
Signature		Date	10/5/2021











ARTICLE

<https://doi.org/10.1038/s41467-021-21694-3>

OPEN

GABA signalling modulates stomatal opening to enhance plant water use efficiency and drought resilience

Bo Xu ^{1,2}, Yu Long^{1,2}, Xueying Feng ^{1,2}, Xujun Zhu ^{1,3}, Na Sai ^{1,2}, Larissa Chirkova^{2,4}, Annette Betts⁵, Johannes Herrmann⁶, Everard J. Edwards ⁵, Mamoru Okamoto ^{2,4}, Rainer Hedrich ⁶ & Matthew Gilliham ^{1,2}✉

The non-protein amino acid γ -aminobutyric acid (GABA) has been proposed to be an ancient messenger for cellular communication conserved across biological kingdoms. GABA has well-defined signalling roles in animals; however, whilst GABA accumulates in plants under stress it has not been determined if, how, where and when GABA acts as an endogenous plant signalling molecule. Here, we establish endogenous GABA as a bona fide plant signal, acting via a mechanism not found in animals. Using *Arabidopsis thaliana*, we show guard cell GABA production is necessary and sufficient to reduce stomatal opening and transpirational water loss, which improves water use efficiency and drought tolerance, via negative regulation of a stomatal guard cell tonoplast-localised anion transporter. We find GABA modulation of stomata occurs in multiple plants, including dicot and monocot crops. This study highlights a role for GABA metabolism in fine tuning physiology and opens alternative avenues for improving plant stress resilience.

¹Plant Transport and Signalling Lab, ARC Centre of Excellence in Plant Energy Biology, Waite Research Institute, Glen Osmond, SA, Australia. ²School of Agriculture, Food and Wine, Waite Research Precinct, University of Adelaide, Glen Osmond, SA, Australia. ³College of Horticulture, Nanjing Agricultural University, Nanjing, China. ⁴ARC Industrial Transformation Research Hub for Wheat in a Hot and Dry Climate, Waite Research Institute, University of Adelaide, Glen Osmond, SA, Australia. ⁵CSIRO Agriculture & Food, Glen Osmond, SA, Australia. ⁶Institute for Molecular Plant Physiology and Biophysics, University of Würzburg, Würzburg, Germany. ✉email: matthew.gilliham@adelaide.edu.au

The regulation of stomatal pore aperture is a key determinant of plant productivity and drought resilience, and profoundly impacts climate due to its influence on global carbon and water cycling^{1–3}. The stomatal pore is delineated by a guard cell pair. Fine control of ion and water movement across guard cell membranes, via transport proteins, determines cell volume and pore aperture following opening and closing signals such as light and dark^{2,4,5} (Fig. 1). Due to their critical roles and their ability to respond to and integrate multiple stimuli, stomatal guard cells have become a preeminent model system for investigating plant cell signalling⁶ resulting in the elucidation of many critical pathways involved in plant biotic and abiotic stress tolerance^{7–9}.

GABA signalling in mammals relies upon receptor-mediated polarization of neuronal cell membranes^{10,11}. Speculation that GABA could be a signal in plants is decades old¹², but a definitive demonstration of its mode of action remains elusive. GABA production in plants is upregulated by stress^{13,14}. It is synthesised in the cytosol via the GABA shunt pathway, bypassing two stress-inhibited reactions of the mitochondrial-based tricarboxylic acid (TCA) cycle^{15,16}. GABA is therefore well known as a stress-induced plant metabolite that is fed back into the mitochondrial TCA cycle to sustain cellular energy production^{12,17}. The discovery that the activity of aluminium-activated malate transporters (ALMTs) can be regulated by GABA¹⁸ represents a plausible mechanism by which GABA signals could be transduced in plants, providing a putative—but unproven—novel signalling link between primary metabolism and physiology¹⁹. Stomatal guard cells contain a number of ALMTs that impact stomatal movement and transpirational water loss^{20–22}. Therefore, stomatal guard cells represent an ideal system to test whether GABA signalling occurs in plants.

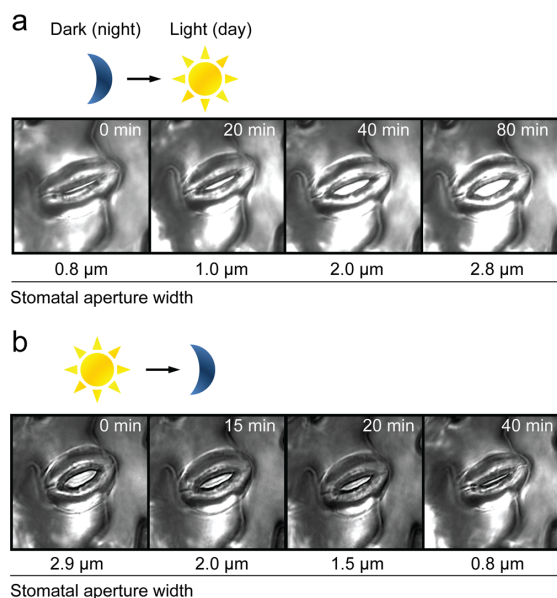


Fig. 1 Guard cells respond to light signals. **a**, **b** Time course of light-induced stomatal opening (**a**) and dark-induced stomatal closure (**b**) with actual stomatal aperture width indicated below; dark-to-light transition mimics night-to-day transition which opens stomatal pores (**a**) and light-to-dark transition mimics day-to-night transition which closes stomatal pores (**b**), light intensity 150 μmol m⁻² s⁻¹.

Significantly, here, we show that GABA does not initiate changes in stomatal pore aperture, rather it antagonises changes in pore size, which differentiates it from many of the signals known to regulate stomatal aperture^{3–8}. Specifically, we find that GABA concentration increases under a water deficit and this reduces stomatal opening in an ALMT9-dependant manner. The anion channel ALMT9 is a major pathway for mediating anion uptake into the vacuole during stomatal opening²¹; GABA signal transduction via ALMT9 leads to reduced transpirational water loss, increased water use efficiency (WUE) and improved drought resilience. As such, even though guard cell signalling is relatively well defined^{6,23}, this study has been able to uncover another pathway regulating plant water loss. Furthermore, by revealing a mechanism by which GABA acts in stomatal guard cells, we demonstrate that GABA is a legitimate plant signalling molecule¹⁶.

Results

GABA antagonises both stomatal pore opening and closure in epidermal peels, but only opening in leaf feeding experiments.

To validate whether GABA is a physiological signal that modulates stomatal pore aperture, our initial experiments used excised *Arabidopsis thaliana* epidermal peels where stomatal guard cells are directly accessible to a chemical stimuli^{8,24–26}. When exogenous GABA or its analogue muscimol¹⁴ were applied under constant light or dark conditions, neither elicited a change in stomatal aperture (Fig. 2a, b; Supplementary Fig. 1a, b). Interestingly though, we found that both compounds suppressed light-induced stomatal opening and dark-induced stomatal closure (Fig. 2a, b; Supplementary Fig. 1a, b). We then fed intact leaves with an artificial sap solution through the detached petiole with or without the addition of GABA or muscimol and examined whether this affected gas exchange rates. We found, in the GABA and muscimol fed leaves, that the increase in water loss (transpiration) stimulated by a dark-to-light transition was dampened compared to leaves fed just the artificial sap solution due to reduced stomatal conductance (Fig. 2c; Supplementary Figs. 1c, d and 2a). This is consistent with the reduced extent of stomatal opening that we observed in epidermal peels in the presence of GABA or muscimol upon a dark-to-light transition (Fig. 2b; Supplementary Fig. 1a). The gas exchange values of fed leaves were used to calculate instantaneous intrinsic WUE (iWUE) and WUE (ratios of carbon gained through photosynthesis per unit of water lost), which are key traits underpinning drought tolerance in plants²⁷, and both values were greater (i.e. improved) in GABA fed leaves (Fig. 2d; Supplementary Fig. 2a–c).

GABA is a universal stomatal behaviour modifier. To examine whether GABA or muscimol can modulate stomatal aperture beyond the response to light and dark, we examined their impact on a range of opening and closing signals using epidermal peels of *Arabidopsis*. We found both GABA and muscimol inhibited abscisic acid- (ABA, 2.5 μM) or H₂O₂-stimulated stomatal closure and coronatine-induced opening (Supplementary Fig. 3a, c, e, f)^{8,28}. However, stomatal pores were fully closed in response to high concentrations of ABA (25 μM) (Supplementary Fig. 3b, d) or exogenous calcium in the presence of GABA or muscimol (Supplementary Fig. 3g), which indicated stomatal closure could occur in epidermal peels in the presence of GABA when the closing signal was of sufficient magnitude.

We tested whether our results could be explained by GABA or muscimol treatment permanently locking guard cells in a closed (or open) state and preventing further change in stomatal pore aperture, which would argue against GABA being a physiological signal. We did this by incubating epidermal peels in GABA or

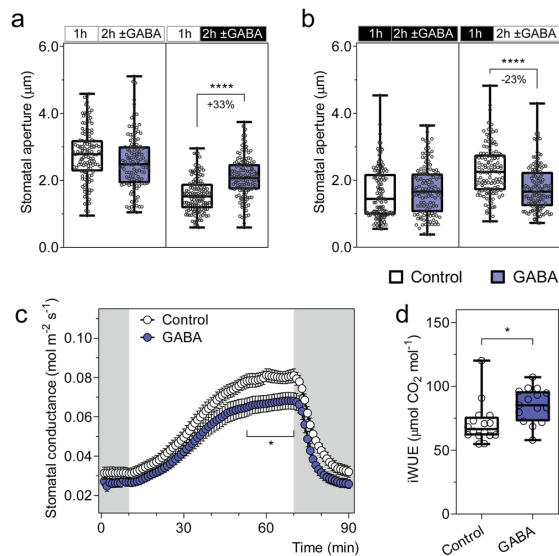


Fig. 2 Exogenous GABA antagonises changes in stomatal pore aperture and increases intrinsic water use efficiency. **a, b** Stomatal aperture of wild-type *A. thaliana* leaves in response to light or dark. Epidermal strips were pre-incubated in stomatal pore measurement buffer for 1 h under light (**a**) or dark (**b**), followed by a 2 h incubation under constant light (**a**), dark (**b**), light-to-dark transition (**a**) or dark-to-light transition (**b**) as indicated in the above graphs by the black (dark) or white (light) bars, together with the application of 2 mM GABA; $n = 129$ for control (constant light), $n = 121$ for GABA (constant light), $n = 137$ for control (light-to-dark transition) and $n = 135$ for GABA (light-to-dark transition) (**a**); $n = 122$ for control (constant dark), $n = 124$ for GABA (constant dark), $n = 123$ for control (dark-to-light transition) and $n = 130$ for GABA (dark-to-light transition) (**b**); all experiments were repeated twice in steady-state conditions (for both light or dark) or four times for dark-to-light or light-to-dark transitions in different batches of plants using blind treatments with similar results (**a, b**). GABA feeding of excised leaves reduces stomatal conductance (**c**) and increases intrinsic water use efficiency (iWUE) (**d**). **c** Stomatal conductance of detached leaves from 5- to 6-week-old *A. thaliana* wild-type plants was recorded using a LI-COR LI-6400XT in response to dark (shaded region) and 200 $\mu\text{mol m}^{-2} \text{s}^{-1}$ light (white region), fed with artificial xylem sap solutions ± 4 mM GABA. **d** iWUE efficiency of detached leaves was calculated as the ratio of photosynthetic rate (Supplementary Fig. 2b) versus stomatal conductance (**c**); $n = 16$ independent leaves for control and $n = 15$ independent leaves for GABA, data collected from three different batches of plants (**c, d**). All data are plotted with box and whiskers plots: whiskers plot represents minimum and maximum values, and box plot represents second quartile, median and third quartile (**a, b, d**), or data are represented as mean \pm s.e.m (**c**); statistical difference was determined by two-way ANOVA (**a, b**), or two-sided Student's *t* test (**c, d**), * $P < 0.05$ and **** $P < 0.0001$.

muscimol, then removing this treatment and performing a light or dark transition. As would be expected from viable cells, after removal of the GABA or muscimol treatment, we found that stomatal guard cells responded to a light treatment by opening the pores (Supplementary Fig. 4a, b) or to a dark treatment by closing pores (Supplementary Fig. 4c, d). Collectively, these data again indicate that GABA signals would likely act to modulate stomatal aperture in the face of a stimulus rather than stimulating a transition itself.

To test whether GABA is a universal modulator of stomatal control, we explored whether GABA or muscimol treatment of

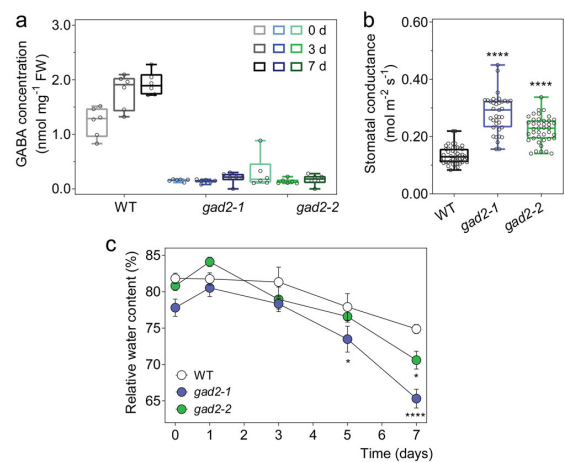


Fig. 3 Leaf GABA concentration regulates transpiration. **a** Leaf GABA concentration of 5–6-week-old *A. thaliana* wild-type (WT), *gad2-1* and *gad2-2* plants following drought treatment for 0, 3 and 7 days, $n = 6$. **b** Stomatal conductance of *Arabidopsis* WT, *gad2-1* and *gad2-2* plants determined using an AP4 porometer; $n = 48$ for WT, $n = 37$ for *gad2-1* and $n = 41$ for *gad2-2*, data collected from three independent batches of plants. **c** Relative leaf water content of WT, *gad2-1* and *gad2-2* plants following drought treatment for 0, 1, 3, 5 and 7 days, $n = 6$. All data are plotted with box and whiskers plots: whiskers plot represents minimum and maximum values, and box plot represents second quartile, median and third quartile (**a, b**), or data are represented as mean \pm s.e.m (**c**); statistical difference was determined using two-way ANOVA (**a, c**) or one-way ANOVA (**b**); * $P < 0.05$ and **** $P < 0.0001$.

epidermal strips attenuated stomatal responses of other plant species to light or dark transitions, including the dicot crops *Vicia faba* (broad bean), *Glycine max* (soybean) and *Nicotiana benthamiana* (tobacco-relative) and the monocot *Hordeum vulgare* (barley) (Supplementary Fig. 5). The widespread inhibition of stomatal pore aperture changes suggests that GABA has the potential to be a universal 'brake' on stomatal movement in plants, including valuable crops.

GABA accumulation in guard cells contributes to the regulation of transpiration and drought performance. Stomatal control is explicitly linked with the regulation of plant water loss, which impacts the survival of plants under drought⁷; the wider the stomatal aperture, the greater the water loss of plants, the poorer the survival of plants under a limited water supply, as excessive water use by the plant diminishes the availability of stored soil water. The observation that the stress-induced metabolite GABA¹³ reduces plant water loss and improves WUE (Fig. 2d; Supplementary Fig. 2c)—key factors underpinning drought tolerance²⁷—implicates GABA as novel signal regulating plant drought resilience. Therefore, to examine the hypothesis that endogenous GABA concentration increases under a water deficit and acts as a signal, we first determined whether we could replicate the previously reported increases in GABA accumulation under drought^{13,14,29} (Fig. 3; Supplementary Fig. 6). In wild-type plants, a drought treatment was applied by withholding watering, which resulted in the gradual depletion of soil gravimetric water and a reduction in leaf relative water content (RWC) (Supplementary Fig. 6a, b). We found that GABA accumulation in drought stressed leaves increased by 35% compared to that of well-watered leaves (water versus drought at

7 days: 1.07 ± 0.08 versus 1.44 ± 0.11 nmol mg⁻¹ FW) (Supplementary Fig. 6c).

To investigate whether GABA has a role during drought, we obtained *Arabidopsis* T-DNA insertional mutants for the major leaf GABA synthesis gene, *Glutamate Decarboxylase 2 (GAD2)*²⁹. Both *gad2-1* and *gad2-2* had >75% less GABA accumulation in leaves than in wild-type plants, whilst GABA concentrations in roots were unchanged (Fig. 3a; Supplementary Fig. 6d–f). Furthermore, leaves of *gad2* plants did not accumulate additional GABA under drought conditions unlike wild-type controls where GABA increased by 45% after 3 days, and was maintained at this elevated level after 7 days of drought (Fig. 3a). Under standard conditions, both *gad2* mutant lines exhibited greater stomatal conductance and wider stomatal pores than wild-type plants (Fig. 3b; Supplementary Fig. 6g), whereas stomatal density was identical to wild type (Supplementary Fig. 6h). The application of exogenous GABA to *gad2* leaves inhibited stomatal pore aperture changes in response to light treatments (Supplementary Fig. 6i, j), indicating that *gad2* stomata would be competent in a GABA response if sufficient GABA was present. Furthermore, the aperture of GABA pre-treated *gad2* stomata after a dark-to-light transition were statistically insignificant from non-GABA treated wild-type stomata (Supplementary Fig. 6j), which is consistent with GABA playing a role in modulating opening of wild-type stomata under non-stressed conditions. It has been shown previously that both *GAD2* transcription and GABA accumulation exhibit diurnal regulation; GABA usually peaks at the end of the dark cycle prior to stomatal opening and reaches a minimum when stomatal conductance is at its maximum near subjective mid-day³⁰. However, during stress, both *GAD2* transcript abundance and GABA accumulation remain high³⁰. This suggests GABA may further minimise stomatal opening under stress and contribute to drought tolerance.

Under drought, the leaf RWC of *gad2* plants lowered more quickly than in wild type (Fig. 3c). Transcriptional profiles of key ABA-marker gene (*RD22*) and GABA-related genes (other than *GAD2*) were similar in wild type and *gad2* lines, although *RD29A* was significantly higher in *gad2-1* than wild type and *gad2-2* on day 0 and day 7 of the drought treatment (Supplementary Fig. 7), which is consistent with the lower RWC of *gad2-1* after 7 days (Fig. 3c). These results confirm that *GAD2* is critical for leaf GABA production under stress, and suggests that GABA itself may regulate plant water loss and drought tolerance²⁹.

Histochemical staining corroborated that *GAD2* is highly expressed in leaves, particularly in guard cells²⁹ (Supplementary Fig. 8a, b). *GAD2* is a cytosolic enzyme³¹; to examine if cytosolic GABA biosynthesis within the guard cell was sufficient to modulate transpiration we expressed—specifically in the guard cell³²—a constitutively active form of *GAD2 (GAD2Δ)* that has a C-terminal autoinhibitory domain removed^{31,33} (Fig. 4a). This led to a large increase in leaf GABA accumulation (Fig. 4b) and to complementation of the steady-state stomatal conductance and aperture phenotypes of *gad2* plants to wild-type levels (Fig. 4c; Supplementary Fig. 8c, d). At the same time, no change in stomatal density or leaf ABA accumulation was detected under standard conditions (Supplementary Fig. 8e, f), suggesting the complementation of the *gad2* phenotype was due to the restoration of GABA synthesis in the guard cell. Other phenotypes restored to wild-type levels by guard cell-specific expression of *GAD2Δ* included the exaggerated stomatal opening and closure kinetics and decreased instantaneous iWUE/WUE of *gad2-1* (Fig. 4d–f; Supplementary Fig. 8g–i). The drought sensitivity of *gad2*, compared to wild type, was also abolished by guard cell-specific expression of *GAD2Δ* (Fig. 4g, h). This demonstrates GABA synthesis in guard cells was sufficient to modulate stomatal movement, regulate water loss and improve drought resilience.

To examine whether GABA metabolism can be modulated to improve drought resilience beyond wild-type levels, *GAD2Δ* was expressed specifically in the guard cells of wild-type *Arabidopsis* plants (Fig. 5a), this resulted in leaf GABA concentrations being increased to beyond wild-type levels (Fig. 5b). The steady-state stomatal conductance of the GABA overproducing transgenic plants in standard and drought conditions was lowered compared to wild-type plants (Fig. 5c). Consistent with this, the plants overexpressing *GAD2Δ* in the wild-type background maintained higher leaf RWC than wild-type plants after 10 days of drought treatment (Fig. 5d, e). Furthermore, a greater percentage of plants overexpressing *GAD2Δ* in the wild-type background survived following re-watering after a 12-day drought treatment (Supplementary Fig. 9). As such, we show here that GABA overproduction can reduce water loss and improve drought resilience.

Guard cell cytosolic GABA modulates stomatal movement and drought resilience. Our data show that although guard cell synthesised GABA can rescue the *gad2* phenotype, it is clear that exogenously applied GABA can also modulate stomatal movement (e.g. Fig. 2 for wild type or Supplementary Fig. 6i, j for *gad2*). It is known that GABA can pass the membrane through a variety of transporters^{34–36}, so it is unclear whether the site of guard cell GABA action is from the apoplast or cytoplasm. We expressed *GAD2Δ* specifically in the spongy mesophyll³⁷, adjacent to the abaxial stomatal layer, to test whether it could complement *gad2* (Supplementary Fig. 10a, b). This resulted in a significant increase in leaf GABA, but no change in stomatal conductance (Supplementary Fig. 10c, d). As such, unlike guard cell-specific expression, *GAD2Δ* in the spongy mesophyll was insufficient to complement the *gad2-1* phenotype.

To further probe the role of guard cell synthesised GABA, we expressed full-length *GAD2* under the guard cell-specific promoter (*gad2-1/GC1::GAD2*) (Supplementary Fig. 11a). This form of *GAD2* requires activation by Ca²⁺/calmodulin or low pH to synthesise GABA¹⁴. Interestingly, guard cell-specific expression of full-length *GAD2* failed to complement the high stomatal conductance of the *gad2-1* line to wild-type levels under standard conditions, whereas its constitutive expression (driven by pro35S-CAMV) did (Supplementary Fig. 11b, f, g). Under drought, the *gad2-1/GC1::GAD2* lines increased GABA production, reduced their stomatal conductance significantly more than that of *gad2-1* plants and had a comparable leaf RWC to wild-type plants following 5 days of drought (Supplementary Fig. 11c–e). This suggests that activation of full-length *GAD2* via its regulatory domain³¹ is important in stimulating GABA production under drought in guard cells.

We extended our investigation of GABA's site of action through an epidermal peel experiment. We compared the effects of exogenously applied muscimol or muscimol-BODIPY, a muscimol molecule conjugated with a BODIPY fluorophore, which is active against GABA targets in plants and animals, but lacks cell-membrane permeability^{38,39}. We found that unlike muscimol, membrane impermeable muscimol-BODIPY was unable to inhibit stomatal opening or closure (Supplementary Fig. 12). This result—alongside the differential effects of *gad2* complementation by full-length *GAD2* when expressed constitutively or solely in the guard cell (Supplementary Fig. 11a–e)—provides further evidence that GABA is likely to pass the plasma membrane and that it acts from the cytosol, consistent with our feeding assays (e.g. Fig. 2c). Collectively, the data in this section demonstrate that guard cell-specific cytosolic GABA accumulation is sufficient and necessary for controlling stomatal aperture and transpiration under drought, but suggests a role for other cell types in fine-tuning GABA signals under standard conditions.

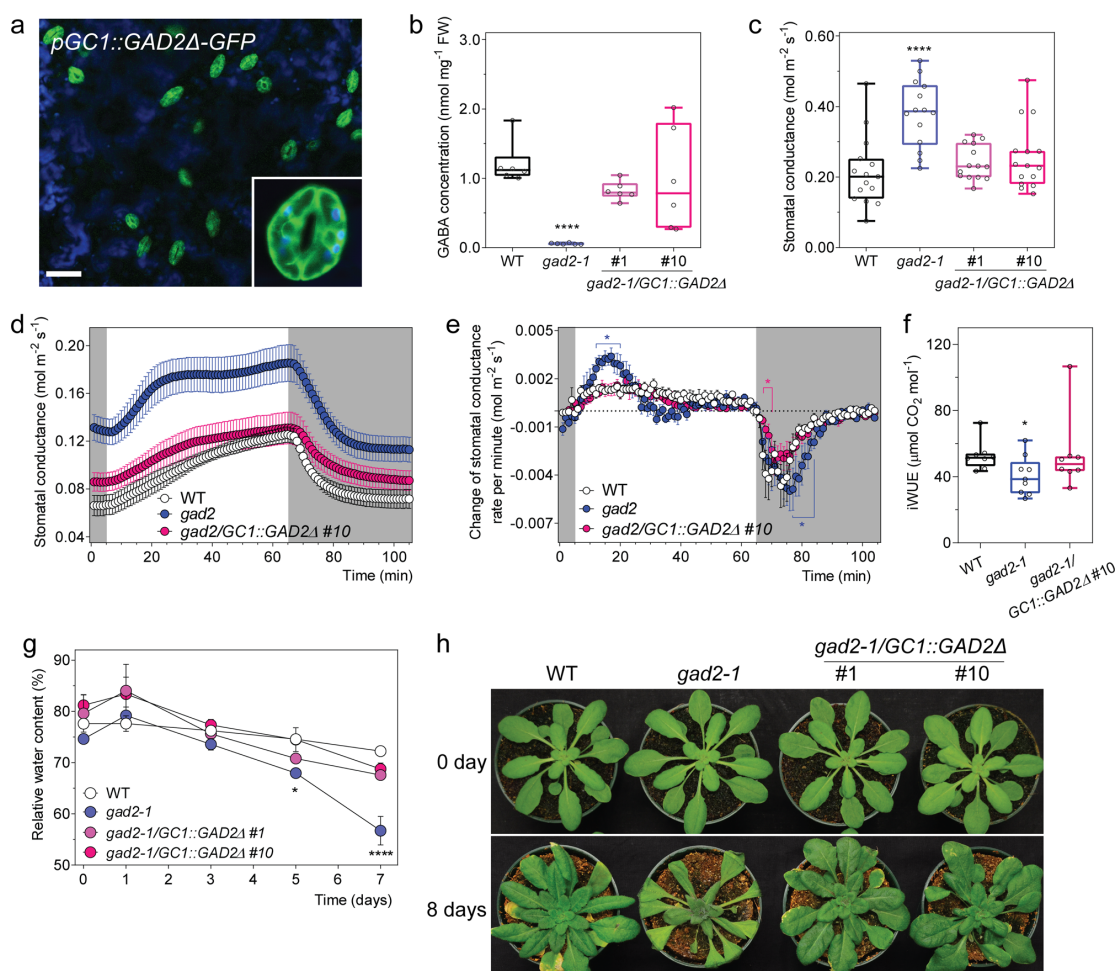


Fig. 4 Guard cell GABA regulates water loss and drought tolerance. **a** Representative confocal images of *gad2-1* plants expressing *G1::GAD2Δ-GFP* (*gad2-1/GC1::GAD2Δ-GFP*); GFP fluorescence and chlorophyll autofluorescence (blue) of the leaf abaxial side of 3–4-week-old *gad2-1/GC1::GAD2Δ-GFP* plant indicates that the *G1* promoter drives *GAD2Δ* expression specifically in guard cells, similar pattern images are obtained from multiple *gad2-1/GC1::GAD2Δ-GFP* plants, scale bars = 50 μm . **b** Leaf GABA accumulation of 5–6-week-old *A. thaliana* WT, *gad2-1*, *gad2-1/GC1::GAD2Δ* #1 and #10 plants grown under control conditions, $n = 6$. **c** Stomatal conductance of WT ($n = 15$), *gad2-1* ($n = 14$), *gad2-1/GC1::GAD2Δ* #1 ($n = 14$) and #10 ($n = 15$) plants under control conditions determined using an AP4 porometer, data collected from two independent batches of plants. **d** Stomatal conductance of WT, *gad2-1* and *gad2-1/GC1::GAD2Δ* #10 plants in response to dark (shaded region) and 150 $\mu\text{mol m}^{-2} \text{s}^{-1}$ light (white region), measured using a LI-COR LI-6400XT. **e** Change in stomatal conductance each minute calculated using $d\text{Conductance}/dt$ (min) of the data represented in **d**. **f** iWUE of WT, *gad2-1* and *gad2-1/GC1::GAD2Δ* plants was calculated based on the ratio of photosynthetic rate (Supplementary Fig. 8h) versus stomatal conductance represented in **d**; $n = 8$ individual plants for WT, $n = 9$ for *gad2-1* and $n = 8$ for *gad2-1/GC1::GAD2Δ* #10, data collected from two independent batches of plants (**d–f**). **g** Relative leaf water content of WT, *gad2-1*, *gad2-1/GC1::GAD2Δ* #1 and #10 plants following drought treatment for 0, 1, 3, 5 and 7 days; $n = 4$ for 0, 1, 3 and 5 days samples and $n = 5$ for 7 days samples, except that $n = 3$ for 0-day *gad2-1* and 1-day *gad2-1/GC1::GAD2Δ* #1. **h** Representative images of WT, *gad2-1*, *gad2-1/GC1::GAD2Δ* #1 and #10 plants (shown in **i**) before (0 day) and after (8 days) drought treatment as indicated. All data are plotted with box and whiskers plots: whiskers plot represents minimum and maximum values, and box plot represents second quartile, median and third quartile (**b, c, f**), or data are represented as mean \pm s.e.m (**d, e, g**); statistical difference was determined using by two-sided Student's *t* test (**f**), one-way ANOVA (**b, c**) or two-way ANOVA (**e, g**); * $P < 0.05$ and **** $P < 0.0001$.

GABA signalling regulating WUE and drought resilience is ALMT9 dependent. ALMTs are plant-specific anion channels that share no homology to Cys-loop receptors except a region of 12 amino acid residues predicted to bind GABA in GABA_A receptors^{14,18}. In animals, ionotropic GABA receptors are stimulated by GABA; in contrast, anion currents through ALMTs are inhibited by GABA^{10,11}. There are a number of ALMTs expressed in guard cells that contain the putative GABA binding

motif and have the potential to transduce the GABA signal, with most having been shown to have a role in regulating stomatal movement^{20–22,40}. For instance, ALMT12 (also called QUAC1, quickly-activation anion conductance 1) is a plasma membrane localised anion channel, which moves anions out of the guard cell during guard cell closure²⁰.

Under the conditions tested here, the impact of GABA on stomatal closure appears to be limited to epidermal peels, it is not

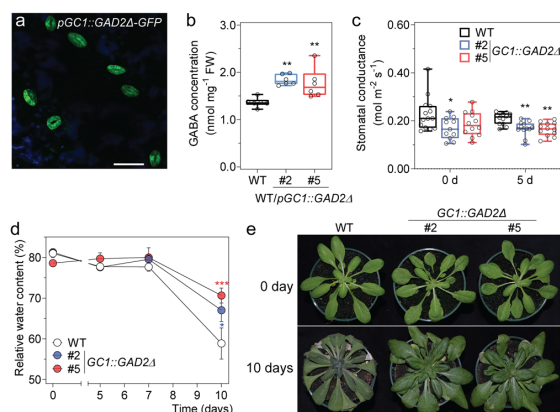


Fig. 5 Guard cell overexpression of *GAD2Δ* decreases plant water loss and increases drought survival. **a** Representative confocal images of *A. thaliana* wild-type plants expressing *GCI::GAD2Δ-GFP*; GFP fluorescence and chlorophyll autofluorescence (blue) of the leaf abaxial side of 3–4-week-old plants, similar pattern images are obtained from multiple wild-type plants expressing *GCI::GAD2Δ-GFP* plants, scale bars = 50 μm. **b** GABA accumulation in the leaves of 5–6-week-old *Arabidopsis* wild type, *GCI::GAD2Δ* #2 and #5 plants; *n* = 6. **c** Stomatal conductance of WT, wild-type *Arabidopsis* expressing *GAD2Δ* in the guard cells using the *GCI* promoter—*GCI::GAD2Δ* #2 and #5 plants before (0 day) and after (5 days) drought treatment determined using an AP4 porometer; *n* = 14 for WT, *n* = 11 for *GCI::GAD2Δ* #2 and *n* = 15 for *GCI::GAD2Δ* #2 at 0 day and *n* = 12 for WT, *GCI::GAD2Δ* #2 and #5 at 5 days. **d** Relative leaf water content of WT, *GCI::GAD2Δ* #2 and #5 plants following drought treatment for 0, 5, 7 and 10 days; *n* = 6 for 0 and 5 days all samples, except *n* = 18 for WT at 10 days, *n* = 12 for *GCI::GAD2Δ* #2 at 10 days and *n* = 13 for *GCI::GAD2Δ* #5 at 10 days. **e** Representative images of WT, *GCI::GAD2Δ* #2 and #5 plants before (0 day) and after (10 days) drought treatment as indicated. Pot size 2.5 inch diameter × 2.25 inch height (LI-COR). All data are plotted with box and whiskers plots: whiskers plot represents minimum and maximum values, and box plot represents second quartile, median and third quartile (**b**, **c**), or data are represented as mean ± s.e.m (**d**); statistical difference was determined using one-way ANOVA (**b**, **c**) or two-way ANOVA (**d**); **P* < 0.05, ***P* < 0.01 and ****P* < 0.001.

seen in intact leaves. However, epidermal peels still represent an assay system that can be used to test whether ALMT might transduce the inhibitory effect of GABA on closure. We observed that, unlike wild-type plants, stomatal closure in *almt12* knock-outs was insensitive to GABA or muscimol when transitioning from light-to-dark (Supplementary Fig. 13a). In contrast, stomatal opening of *almt12* lines showed wild-type-like sensitivity to GABA or muscimol when transitioning from dark to light (Supplementary Fig. 13b). These data indicate that ALMT12 is a plasma membrane GABA target that affects stomatal closure in response to dark—in epidermal peels at least.

However, if GABA inhibition of ALMT12/QUAC1 played a significant role during drought, then the resulting inhibition of closure would translate into an increase in water loss compared to wild-type plants during closure. As we found no evidence that GABA had an effect on closure in intact leaves, under a light-to-dark transition as measured by stomatal conductance or transpiration (Fig. 2c; Supplementary Fig. 2a), and the fact that GABA accumulation led to a net decrease in water loss and improvement in drought resilience, ALMT12 is unlikely to be a major target contributing to this outcome. We therefore focused on tonoplast-localised ALMTs that are involved in stomatal pore

opening²¹, as this is the process where GABA has its predominant affect in intact leaves.

ALMT9 is the major tonoplast-localised channel involved in anion uptake into guard cell vacuoles during stomatal opening, but has no documented role in closure²¹. We hypothesised that GABA might target and inhibit ALMT9 activity to reduce the rate or extent of stomatal opening. We initially attempted in vitro electrophysiological studies to examine the impact of GABA on ALMT9-induced currents, but were unable to consistently detect stable currents following heterologous expression in either *Xenopus laevis* oocytes or tobacco mesophyll cells^{21,41}. Therefore, we examined the potential regulation of ALMT9 by GABA by focusing solely on in planta studies as it is difficult to faithfully replicate regulatory pathways from guard cells in heterologous systems, e.g.^{42–47}. In the first instance, we independently crossed two *almt9* alleles (*almt9-1* and *almt9-2*) with *gad2-1*. We found that, similar to *gad2*, both double mutants (*gad2-1/almt9-1* and *gad2-1/almt9-2*) maintained low GABA accumulation in their leaves (Fig. 6a, b; Supplementary Fig. 14a, e). However, both *gad2-1/almt9-1* and *gad2-1/almt9-2* had wild-type-like stomatal conductance and aperture unlike *gad2-1* where both these parameters are high (Fig. 6c, d; Supplementary Fig. 14d, f). Furthermore, guard cell-specific complementation of *gad2-1/almt9-1* by *GAD2Δ* did not alter stomatal conductance (Supplementary Fig. 14a–d). Collectively, these data are consistent with ALMT9 being required for GABA to regulate gas exchange via stomatal control. An interesting additional observation was that the loss of ALMT9 in *gad2-1* also resulted in ABA inducing stomatal pore closure to wild-type levels (Supplementary Fig. 14g–j), indicating that, although ALMT9 is a channel that regulates stomatal opening, it can influence the extent to which stomatal pores close under certain conditions (in epidermal peels at least). The incomplete stomatal closure of *gad2* coupled to its greater stomatal opening may further contribute to its drought sensitivity. These findings are consistent with the regulation of stomatal aperture being a dynamic equilibrium between the pathways that regulate stomatal opening and closure, with stomatal aperture being weighted towards a particular state dependent upon the dominant stimuli^{48,49}.

To further test whether ALMT9 transduces GABA signalling, we examined the effect of GABA on regulating stomatal opening in *almt9* mutant plants. In wild-type plants, we previously showed that light-induced stomatal opening was inhibited by exogenous GABA (Fig. 2a) or muscimol (Supplementary Fig. 1a). In *almt9* lines, exogenous GABA or muscimol did not antagonise stomatal opening (Fig. 7a, b; Supplementary Fig. 15a, b), whereas dark-induced stomatal closure in *almt9* retained its GABA sensitivity (Fig. 7c, d; Supplementary Fig. 15c, d). These results are consistent with GABA reducing stomatal opening via negative regulation ALMT9-mediated Cl⁻ uptake into guard cell vacuoles. Furthermore, it strongly indicates the corollary of this finding, that the higher stomatal conductance phenotype of *gad2* is the result of greater ALMT9 activity due to its lack of inhibition by GABA.

We tested this hypothesis by attempting to complement *almt9* plants with either the native channel or a site-directed ALMT9 mutant (ALMT9^{F243C/Y245C}). The mutations within ALMT9^{F243C/Y245C} are in the 12 amino acid residue motif that shares homology with a GABA binding region in mammalian GABA_A receptors^{14,18}. Mutations in the aromatic amino acid residues in this motif have been shown for other ALMTs to result in active channels that are not inhibited by GABA when tested in heterologous systems^{36,39} (Fig. 8; Fig. 9). However, no in planta tests have been conducted to date—for any ALMT—to determine whether mutations in this region result in a transport competent protein that lacks GABA sensitivity. Here, we observed that ALMT9 and ALMT9^{F243C/Y245C} had similar

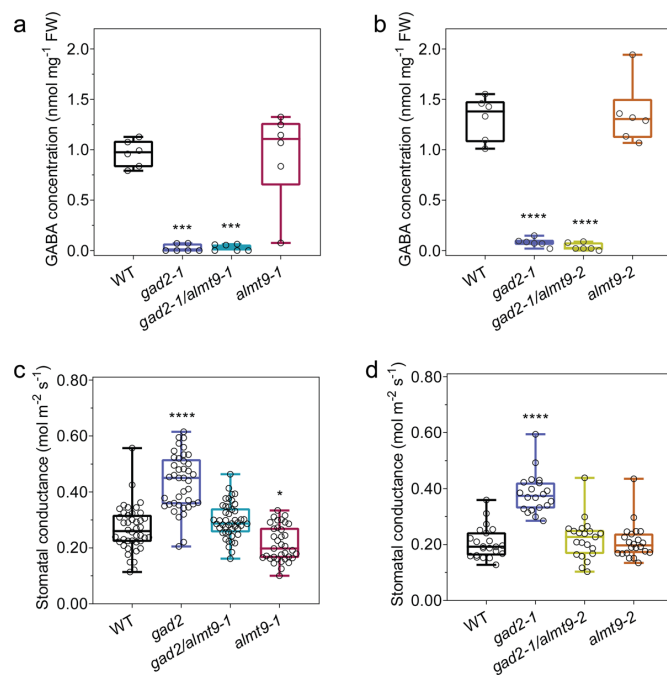


Fig. 6 The loss of ALMT9 suppresses the *gad2* mutant stomatal phenotype. **a–d** Leaf GABA concentration (**a, b**) and stomatal conductance (**c, d**) of 5–6-week-old *A. thaliana* WT, *gad2-1*, *gad2-1/almt9-1*, *almt9-1*, *gad2-1/almt9-2* and *almt9-2* plants; $n = 6$ plants (**a, b**); $n = 42$ for WT, $n = 40$ for *gad2-1*, $n = 45$ for *gad2-1/almt9-1* and $n = 35$ for *almt9-1*, data collected from four independent batches of plants (**c**); $n = 22$ for WT, $n = 20$ for *gad2-1*, $n = 21$ for *gad2-1/almt9-2* and $n = 22$ for *almt9-2*, data collected from two independent batches of plants (**d**); data (**a, c**) were extracted respectively from Supplementary Fig. 13b, c. All data are plotted with box and whiskers plots: whiskers plot represents minimum and maximum values, and box plot represents second quartile, median and third quartile; statistical difference was determined by one-way ANOVA, * $P < 0.05$, *** $P < 0.001$ and **** $P < 0.0001$.

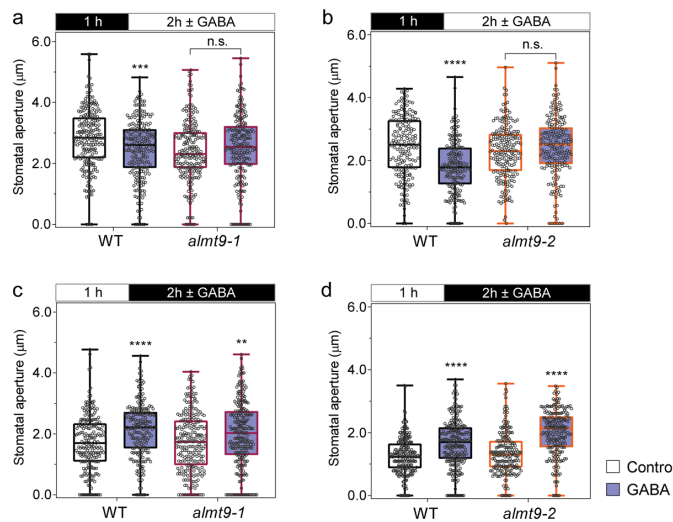


Fig. 7 The loss of ALMT9 abolishes GABA inhibition of stomatal opening but does not affect closure. **a–d** *Arabidopsis* WT and *almt9* knockout plant stomatal aperture in response to light or dark. Epidermal strips were pre-incubated in stomatal measurement buffer for 1 h under dark (**a, b**) or light (**c, d**), followed by 2 h in light (**a, b**) or dark (**c, d**) as indicated by black (dark) or white (light) bars above graphs with ± 2 mM GABA; $n = 236$ for WT and $n = 221$ for *almt9-1* with control treatment, $n = 229$ for WT and $n = 215$ for *almt9-1* with GABA treatment (**a**); $n = 223$ for WT and $n = 242$ for *almt9-1* with control treatment, $n = 215$ for WT and $n = 256$ for *almt9-1* with GABA treatment (**b**); $n = 183$ for WT and $n = 189$ for *almt9-2* with control treatment, $n = 210$ for WT and $n = 197$ for *almt9-2* with GABA treatment (**c**); $n = 236$ for WT and $n = 243$ for *almt9-2* with control treatment, $n = 202$ for WT and $n = 220$ for *almt9-2* with GABA treatment (**d**). All data are plotted with box and whiskers plots: whiskers plot represents minimum and maximum values, and box plot represents second quartile, median and third quartile; statistical difference was determined by two-way ANOVA, ** $P < 0.01$, *** $P < 0.001$ and **** $P < 0.0001$.

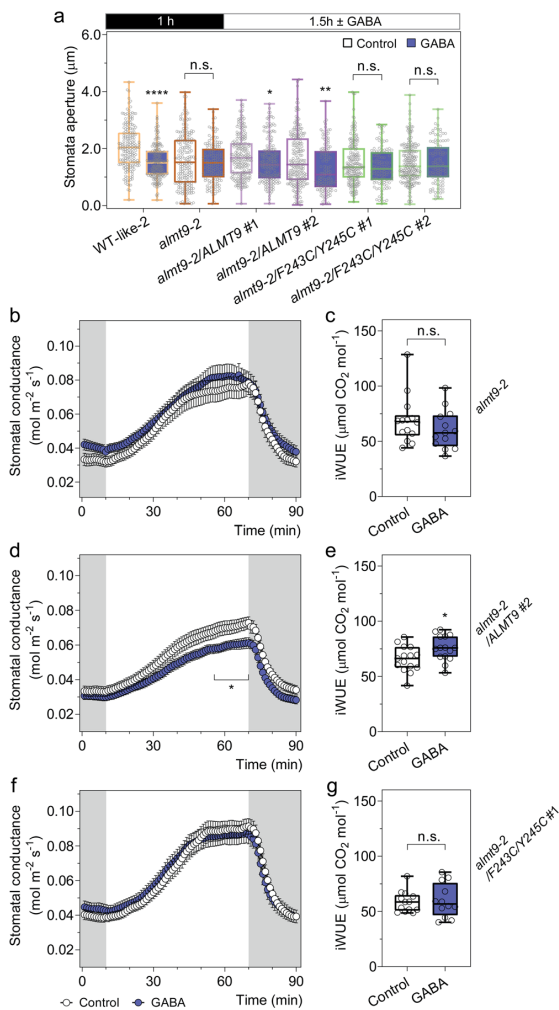


Fig. 8 ALMT9 but not ALMT9^{F243C/Y245C} restores the GABA sensitivity of *almt9-2*. **a** Stomatal aperture measurement of *A. thaliana* WT, *almt9-2* and complementation lines. Epidermal strips were pre-incubated in stomatal measurement buffer for 1 h under dark, followed by a 1.5 h dark-to-light transition, as indicated above graphs by black (dark) or white (light) bars, ±2 mM GABA; $n = 189$ (control) and $n = 195$ (GABA) for WT-like 2 (segregated from *almt9-2*)²¹, $n = 197$ (control) and $n = 153$ (GABA) for *almt9-2*, $n = 213$ (control) and $n = 178$ (GABA) for *almt9-2* complement with 35S::ALMT9 #1 (*almt9-2*/ALMT9 #1), $n = 219$ (control) and $n = 127$ (GABA) for *almt9-2*/ALMT9 #2, $n = 195$ (control) and $n = 115$ (GABA) for *almt9-2* complemented with 35S::ALMT9 with double mutation F243C/Y245C (ALMT9^{F243C/Y245C}) targeting the putative GABA interaction residues^{18,36,39} (*almt9-2*/F243C/Y245C #1), $n = 221$ (control) and $n = 109$ (GABA) for *almt9-2*/F243C/Y245C #2 with control treatment. **b-g** Leaf feeding assay of *almt9-2* and complementation lines. Stomatal conductance of detached leaves from 5–6-week-old *Arabidopsis almt9-2*, *almt9-2*/ALMT9 #2 and *almt9-2*/F243C/Y245C #1 plants was recorded using a LI-COR LI-6400XT in response to dark (shaded region) and 200 $\mu\text{mol m}^{-2} \text{s}^{-1}$ light (white region), fed with artificial xylem sap solutions ± 4 mM GABA (**b, d, f**). The iWUE of *almt9-2* (**c**), *almt9-2*/ALMT9 #2 (**e**) and *almt9-2*/F243C/Y245C #1 (**g**) detached leaves was calculated based on the ratio of photosynthetic rate (Supplementary Fig. 17b, e, h) versus stomatal conductance (**b, d, f**; $n = 14$ (control) and $n = 13$ (GABA) for *almt9-2* (**b, c**); $n = 15$ (control and GABA) for *almt9-2*/ALMT9 #2 (**d, e**); $n = 13$ (control) and $n = 12$ (GABA) for *almt9-2*/F243C/Y245C #1 (**f, g**). All data are plotted with box and whiskers plots: whiskers plot represents minimum and maximum values, and box plot represents second quartile, median and third quartile (**a, c, e, g**), or data are represented as mean ± s.e.m. (**b, d, f**); statistical difference was determined by two-sided Student's *t* test; * $P < 0.05$, ** $P < 0.01$, **** $P < 0.0001$ (**a-g**).

expression in *almt9-2* complementation lines and the mutations (in ALMT9^{F243C/Y245C}) did not alter the membrane localisation with both versions of the ALMT9 protein being clearly present on the tonoplast (Supplementary Fig. 16). Further, we found that similar to *almt9* lines, *almt9-2* expressing ALMT9^{F243C/Y245C} was insensitive to GABA during a dark-to-light transition assayed on epidermal peels and detached leaves, for stomatal opening and stomatal conductance, respectively; this contrasts the GABA sensitivity of wild-type plants and plants expressing native ALMT9 in the *almt9-2* background (Figs. 2c and 8a, b, d, f; Supplementary Fig. 17a, b, d, e, g, h). Furthermore, instantaneous iWUE/WUE of *almt9-2* was improved by native ALMT9 complementation, but not ALMT9^{F243C/Y245C} (Fig. 8c, e, g; Supplementary Fig. 17c, f, i). Steady-state stomatal conductance and aperture of ALMT9^{F243C/Y245C} lines were also significantly greater than that of wild-type and *almt9* lines and were insignificant from *gad2-1* under standard conditions (Fig. 9; Supplementary Fig. 17j). This result indicates that we successfully complemented *almt9* with an active, but GABA-insensitive form of ALMT9, and that this increased transpirational water loss over wild-

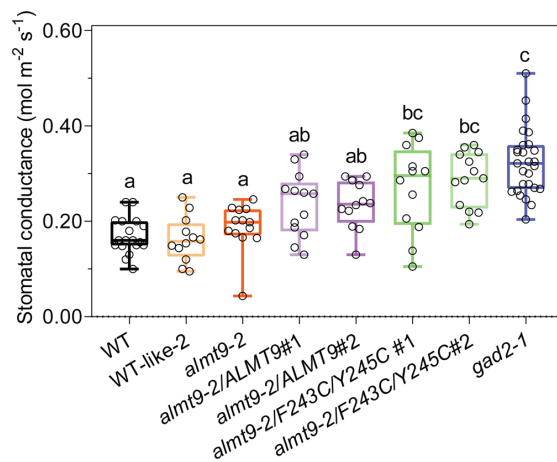


Fig. 9 ALMT9^{F243C/Y245C} increases steady-state stomatal conductance. Stomatal conductance of 5–6-week-old *Arabidopsis* WT, *gad2-1*, *almt9-2* and complementation lines determined using an AP4 Porometer; $n = 18$ for WT, $n = 12$ for WT-like 2, *almt9-2*/ALMT9 #2 and *almt9-2*/F243C/Y245C #1, $n = 13$ for *almt9-2*, *almt9-2*/ALMT9 #1 and *almt9-2*/F243C/Y245C #2, $n = 27$ for *gad2-1*. All data are plotted with box and whiskers plots: whiskers plot represents minimum and maximum values, and box plot represents second quartile, median and third quartile; statistical difference was determined by one-way ANOVA, the letters a, b and c represent data groups that are not statistically different, $P < 0.05$.

type levels. These data are completely consistent with ALMT9 being a GABA target that regulates plant water loss, even under non-stressed conditions, through modulation of ALMT9 activity. The GABA effect is then amplified under a water deficit when GABA concentration increases. We propose that GABA accumulation has a role in promoting drought resilience by reducing the amplitude of stomatal re-opening each morning, which minimises whole plant water loss. As such, the GABA–ALMT pathway is a strong candidate for constituting the ABA-independent stress memory of a decreased soil water status that has been previously proposed without mechanistic attribution^{50,51}.

Discussion

The data in this manuscript have unveiled a GABA signalling pathway in plants, which can be summarised by the simplified models presented in Fig. 10. We propose that cytosolic GABA signals, generated by GAD2, modulate stomatal opening, WUE and drought resilience transduced through negative regulation of ALMT9 activity (Fig. 10).

Collectively our use of leaf feeding, knockouts, complementation and point mutagenesis strongly suggests ALMT9 is an essential and major component transducing GABA signalling in guard cells during well-watered and drought conditions. As has become evident for other guard cell based signalling pathways through their examination over time^{42–47}, we are cognizant of the potential that other GABA response elements, including other ALMT, may be involved in transducing and fine-tuning this signalling pathway. Our finding that GABA does not impact stomatal closure in epidermal peels of *almt12* knockouts infers a potential role for this plasma membrane localised ALMT12 in transducing guard cell GABA signals. The fact that light-induced stomatal opening and dark-induced stomatal closure was completely GABA insensitive in *almt9xalmt12* knockouts (Supplementary Fig. 18) suggests that both channels have the potential to transduce the major effects of GABA in guard cells.

However, it is interesting that GABA inhibition of stomatal opening was consistently seen between epidermal peel assays and leaf feeding, whilst GABA only inhibited stomatal closure during isolated epidermal peel experiments, but not when it was fed to leaves. This suggests that GABA acts through ALMT12 on processes associated with stomatal closure, but in the context of an intact leaf this phenotype is lost, which is likely due to the loss of functional epidermal and/or mesophyll cells. This is consistent with the growing body of evidence that indicates stomatal aperture experiments on isolated epidermal peels require validation via studies on intact leaves to avoid overinterpreting potential artifacts from this reductionist system. However, it also means we cannot fully rule out whether GABA inhibition of stomatal closure does have a role under certain physiological scenarios that are yet to be identified. Therefore, in future studies, it would be pertinent to examine whether ALMT12-dependent GABA inhibition of stomatal closure has a physiological role in transducing GABA signals in conditions not examined here, and, more broadly, whether other ALMTs or additional elements are involved in GABA signal transduction.

ALMT activity appears to be regulated by a suite of factors including anions, (Al^{3+} for ALMT1), pH, ATP, voltage and GABA⁵². As such, it is becoming clear that ALMTs have the potential to act as a key signalling hub in a variety of physiological processes. Following on from this study, leading on from the observed GABA modulation of ABA, H_2O_2 and coronatine effects on stomata, the investigation into cross-talk between GABA and other signals for ALMT9, in particular, and ALMTs, in general, provides the basis for future research areas. Such studies will be able to resolve questions such as ‘whether GABA can act directly on guard cell ALMTs?’, as appears to occur for wheat ALMT1^{18,39}, or ‘whether other signalling intermediates are also involved?’. GABA inhibition of the wheat ALMT1 anion conductance was recently found to occur from the cytosol only, by reducing the open probability of the channel to anions³⁹. However, that study was unable to determine whether this occurred through permeation of uncharged GABA through the ALMT

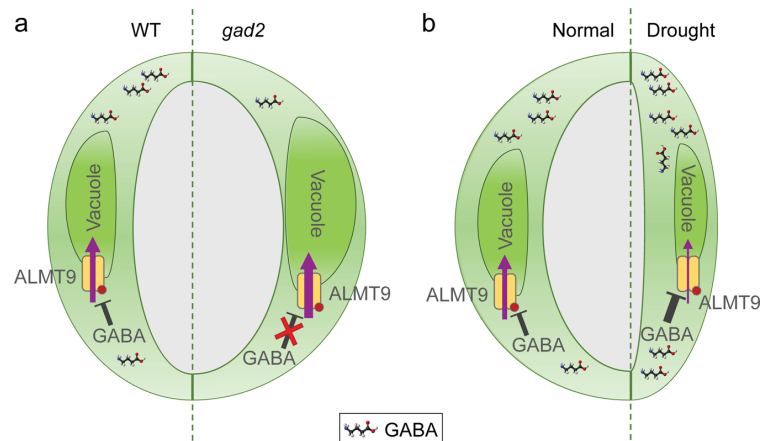


Fig. 10 Proposed model of GABA-mediated signalling for the regulation of water use efficiency. **a** Cytosolic guard cell GABA negatively regulates ALMT9-mediated anion uptake into guard cell vacuoles, which fine tunes stomatal opening (left guard cell of pair). Depletion of GABA accumulation in the leaves of *GAD2* loss-of-function mutant (*gad2*) de-regulates ALMT9, maximizing anion uptake and accumulation in guard cell vacuoles. This leads to a more open stomatal pore, greater water loss and lower WUE of plants (right guard cell of pair). This stomatal phenotype can be replicated by replacing F243/Y245 (red dot) with two cysteines, which abolishes GABA sensitivity of ALMT9. **b** Leaf GABA synthesized and accumulated during water deficit reduces ALMT9-mediated vacuolar anion uptake into guard cells, which requires amino acid residues F243/Y245 (red dot) (right guard cell of pair). This reduces stomatal opening, reducing the pore aperture and enhances plant WUE under drought stress compared to guard cells under standard conditions in the light (left guard cell of pair). Note: We have excluded ALMT12 from this model as we did not find a role for this protein in GABA modulation of water use efficiency in planta, despite its role in GABA modulation of stomatal aperture found within epidermal peels.

pore or through GABA binding modifying channel structure³⁹. Cytosolic GABA inhibition was dependent upon the putative GABA binding residue F213 (equivalent to F243 in ALMT9, which is also predicted to face the cytosol)^{39,53}. Our study therefore highlights the real need to definitively determine whether GABA binds to ALMTs or whether the identified amino acid residues affect GABA sensitivity independent of anion permeability through other means. For instance, future studies should address whether GABA permeability of ALMTs has a role in signal transduction in guard cells and the regulation of other physiological processes³⁶. These later questions would be aided by the determination of GABA concentrations in different cell types and compartments to further understand the co-ordination of GABA signalling across membranes, leaves and other organs, and this could be achieved through the deployment of novel GABA sensors, as recently used in animal tissues^{54,55}.

GABA concentration oscillates over diel cycles and increases in response to multiple abiotic and biotic stresses including drought, heat, cold, anoxia, wounding pathogen infection and salinity¹³. ALMTs have been implicated in modulating multiple developmental and physiological processes in plants^{20–22,56–58} including those underpinning nutrient uptake and fertilization that are affected by GABA^{18,59,60}. Therefore, the discovery that GABA regulates ALMT to form a physiologically relevant signalling mechanism in guard cells is likely to have broad significance beyond stomata, particularly during plant responses to environmental transitions and stress.

GABA's effect on stomata appears to be conserved across a large range of crops from diverse clades including important monocot and dicot crops (Supplementary Fig. 5), indicating that GABA may well be a stomatal signal of economic significance. As we find that the genetic manipulation of cell-type specific GABA metabolism can reduce water loss leading to improved drought performance, our work opens up alternative ways for manipulating crop stress resilience. This statement is tempered in the knowledge that GABA modulated stomatal signalling in the face of another signal and did not stimulate changes in stomatal aperture itself. GABA's role appears to be that of fine-tuning stomatal aperture. Our data suggest that GABA modulated stomatal movement occurs in response to light and dark and low concentrations of signal intermediates, but in the face of a strong stress stimulus its effects may be overridden. As such, GABA may well provide a direct link between the metabolic status of the cell—GABA being produced in the cytosol in times of stress as a bypass of several reactions of the TCA cycle—to regulate and sustain a certain physiological process prior to it being shut down via a more severe stress response pathway. More broadly, this study also provides proof that GABA is a plant signalling molecule and not just a plant metabolite^{12,16}, and in so doing, we conclude that GABA is an endogenous signalling molecule beyond the animal and bacterial kingdoms, enacted through distinct and organism specific mechanisms.

Methods

Plant materials and growth conditions. All experiments were performed on *A. thaliana* were in the Columbia-0 (Col-0) ecotype background, unless stated. *Arabidopsis* wild type, T-DNA insertion mutant and other transgenic plants were germinated and grown on ½ Murashige and Skoog (MS) medium with 0.8% phytagel for 10 days before being transferred to soil for growth in short-day conditions (100–120 $\mu\text{mol m}^{-2} \text{s}^{-1}$, 10 h light/14 h dark) at 22 °C. The T-DNA insertion mutant *gad2-1* (GABI_474_E05) and *gad2-2* (SALK_028819) were obtained from the Arabidopsis Biological Resource Centre (ABRC). *gad2-1* was selected using primer sets:

gad2_LP1 (5'-TATCACGCTAACACCTAACGC-3'), *gad2_RP1* (5'-TTCAAGTTTGTCCGTAATTGG-3') and *GABI_LB* (5'-GGGCTACAC TGAATTGGTAGCTC-3') for removing the second T-DNA insert; *gad2_LP2* (5'-ACGTGATGGATCCAGACAAAG-3'), *gad2_RP2* (5'-TCTTCATTTCCAC ACAAGGC-3') and *GABI_LB* for isolation of the *GAD2* (At1g65960) T-DNA

insertion. *gad2-2* was selected using primer sets: *gad2-2_LP* (5'-AGTTGTATGAA AGTTCATGTGGC-3'), *gad2-2_RP* (5'-TCGACCACGAGATTTAATGG-3') and *SALK_LB* (5'-ATTTGCGGATTTCCGGAAC-3'). *almt9-1* (SALK_055490), *almt9-2* (WiscDsLox499H09), *almt12-1* (SM_3_38592) and *almt12-2* (SM_3_1713) were selected as described previously^{20,21}. The double mutant lines *gad2-1/almt9-1*, *gad2-1/almt9-2*, *almt9-2/12-1* and *almt9-2/12-2* were obtained, respectively, from crossing the respective mutants. The mesophyll enhancer-trap line JR11-2 in the Col-0 background was kindly provided by K. Baerenfaller (ETH Zurich)⁶¹. JR11-2 (Col-0) and *gad2-1/JR11-2* were segregated from crossing *gad2-1* with JR11-2. JR11-2 was selected using primer sets: JR11-2_LP (5'-TTATTTAGGG AAATTACAAGTTGC-3'), JR11-2_RP (5'-AGACACATTTAATAACATTAACAAC AAA-3') and JR11-2_LB (5'-GTTGTCTAAGCGTCAATTTGCTT-3')⁶². All experiments were performed on stable T₃ transgenic plants or confirmed homozygous mutant lines. The other plants *V. faba*, *N. benthamiana* and *G. max* were grown in soil in long-day conditions (400 $\mu\text{mol m}^{-2} \text{s}^{-1}$, 16 h light/8 h dark, 28 °C/25 °C). *H. vulgare* (barley) cv. Barke was grown in a hydroponic system with half-strength Hoagland's solution in long-day conditions (150 $\mu\text{mol m}^{-2} \text{s}^{-1}$, 16 h light/8 h dark, 23 °C)⁶³.

Gene cloning and plasmid construction. For guard cell-specific complementation, the constitutively active form of *GAD2* with a truncation of the calmodulin binding domain (*GAD2Δ*)^{31,33} and the full-length *GAD2* coding sequence (*GAD2*) was driven by a guard cell-specific promoter *GCI* (−1140/+23)³², as designated *GCI::GAD2Δ* and *GCI::GAD2*, respectively. PCR reactions first amplified the truncated *GAD2Δ* with a stop codon and *GCI* promoter (*GCI*) separately using Phusion® High-Fidelity DNA Polymerase (New England Biolabs) with the primer sets: *GAD2_forward* (5'-CACTACTCAAGAAATATGGTTTTCACAAAAACC GC-3') and *GAD2_truncated_reverse* (5'-TTATACATTTTCCGGATCCC-3'); *GCI_forward* (5'-CACCATGGTTGCAACAGAGAGGATG-3') and *GCI_reverse* (5'-ATTTCTTGTAGTAGTATTGGAAG-3'). This was followed by an overlap PCR to fuse the *GCI* promoter to *GAD2Δ* (*GCI::GAD2Δ*) with the *GCI_forward* and *GAD2_truncated_reverse* primer set. The same strategy was used to amplify *GCI::GAD2* without a stop codon (*GCI::GAD2-stop*), *GCI::GAD2* and *GCI::GAD2* without a stop codon (*GCI::GAD2-stop*) with different primer sets: (1) *GCI::GAD2Δ-stop* amplified with *GAD2_forward* and *GAD2_truncated-stop_reverse* (5'-TACATTTTCCGGATCCCCT-3'); (2) *GCI::GAD2* amplified with *GAD2_forward* and *GAD2_reverse* (5'-TTAGCACACACCATTCATCTTCTT-3') and (3) *GCI::GAD2-stop* amplified with *GAD2_forward* and *GAD2-stop_reverse* (5'-CACACCATTCATCTTCTTCC-3'). The fused PCR products were cloned into the pENTR/D-TOPO vector via directional cloning (Invitrogen). pENTR/D-TOPO vectors containing *GCI::GAD2Δ* or *GCI::GAD2* were recombined into a binary vector pMDC99⁶⁴ by an LR reaction using LR Clonase II Enzyme mix (Invitrogen) for guard cell-specific complementation, after an insertion of a NOS Terminator into this vector. A pMDC99 vector was cut by *PacI* (New England Biolabs) and ligated with NOS terminator flanked with *PacI* site using T4 DNA ligase (New England Biolabs). This NOS terminator flanked with *PacI* site was amplified with primer set: *nos_PacI_forward* (5'-TACGTTAATTAAGAAATTCGCCGAT-3') and *nos_PacI_reverse* (5'-GCATTAATTAAGTAACATAGATGACAC-3') and cut by restriction enzyme *PacI* before T4 DNA ligation. *GCI::GAD2Δ-stop* and *GCI::GAD2-stop* were recombined from the pENTR/D-TOPO vector into a pMDC107 vector that contained a GFP tag on the C-terminus (*GCI::GAD2Δ-GFP* and *GCI::GAD2-GFP*)⁶⁴.

To create *GAD2* complementation driven by a constitutive 35S promoter, the full-length *GAD2* was also amplified using primer set *GAD2_forward2* (5'-CACC ATGGTTTTCACAAAAACCGC-3') and *GAD2_reverse* and cloned into pENTR/D-TOPO vector via directional cloning (Invitrogen), followed by an LR reaction recombinant into pMDC32⁶⁴. For mesophyll specific complementation, *GAD2Δ* with a stop codon was amplified with the *GAD2_forward2* and *GAD2_truncated_reverse* primer set, and cloned into the pENTR/D-TOPO vector, followed by an LR reaction recombinant into the pTOOL5 vector (*UAS::GAD2Δ*)⁶⁵.

For *almt9-2* complementation, the pART27 binary vector containing the *ALMT9* coding sequence²¹ was used for native *ALMT9* complementation driven by the 35S promoter, and also used as a template for a site-direct mutagenesis PCR to replace F243 and Y245 of *ALMT9* with two cysteines (*ALMT9^{F243E/Y245C}*) using the primer sets: *ALMT9_DoubleF* (5'-GTTTAGGTGTTAATATGTGTATCTGT CCTATATGGGCTGGAGAGG-3') and *ALMT9_DoubleR* (5'-CCATATAGGACA GATACACATATTAACACCTAACTAACACCAGCACC-3').

For *GAD2* expression analysis, a 1 kb sequence upstream of the *GAD2* start codon was designated as the *GAD2* promoter (*pGAD2*) and amplified using primer set *proGAD2_F* (5'-ATTTTGAATTTGCGGAGAAATCT-3') and *proGAD2_R* (5'-CTTTGTTTCTGTTAGTGAAGAGAA-3'). The *pGAD2* PCR product was cloned into pCR8/GW/TOPO via TA cloning and recombined via an LR reaction into the pMDC162 vector containing the *GUS* reporter gene for histochemical assays⁶⁴. The binary vectors, pMDC32, pMDC99, pMDC107, pMDC162, pTOOL5 and pART27 carrying sequence-verified constructs, were transformed into *Agrobacterium* strain *AGL1* for stable transformation in *Arabidopsis* plants.

Stomatal aperture and density measurement. Soil-grown *Arabidopsis* (5–6-week-old) were used for stomatal aperture and density measurements. Two-to-three-week-old soybean, broad beans and barley and 5–6-week-old tobacco were used for

stomatal aperture assays. Epidermal strips from *Arabidopsis*, soybean, faba bean and tobacco were peeled from abaxial sides of leaves, pre-incubated in stomatal pore measurement buffer containing 10 mM KCl, 5 mM L-malic acid, 10 mM 2-ethanesulfonic acid (MES) with pH 6.0 by 2-amino-2-(hydroxymethyl)-1,3-propanediol (Tris) under light ($200 \mu\text{mol m}^{-2} \text{s}^{-1}$) or darkness and transferred into stomatal pore measurement buffer with blind treatments as stated in the figure legend. For barley epidermal stomatal assays, a modified method was used⁶⁶; the second fully expanded leaf from 2-week-old seedlings was used as experimental material, leaf samples were first detached and bathed in a modified measurement buffer (50 mM KCl, 10 mM MES with pH 6.1 by KOH) under light ($150 \mu\text{mol m}^{-2} \text{s}^{-1}$) for 1.5 h or darkness for 1 h, then pre-treated in the same buffer with or without 1 mM GABA for 0.5 h; after this pre-treatment, samples were incubated in continuous dark, light, light-to-dark or dark-to-light transition for an additional 1 h as indicated in the figure legend before leaf epidermal strips were peeled for imaging. For *Arabidopsis* stomatal density measurement, epidermal strips were peeled from abaxial sides of young and mature leaves, three leaves per plants, three plants per genotype. Epidermal strips for both aperture and density measurement were imaged using an Axiophot Pol Photomicroscope (Carl Zeiss) apart from the barley epidermal strips imaged using a Nikon Diaphot 200 Inverted Phase Contrast Microscope (Nikon). Stomatal aperture and density were analyzed using particle analysis (<http://rsbweb.nih.gov/ij/>).

Stomatal conductance measurement. All stomatal conductance measurements were performed on 5–6-week-old *Arabidopsis* plants. The stomatal conductance determined by the AP4 Porometer (Delta-T Devices) was calculated based on the mean value from 2–3 leaf recordings per plant (Figs. 3b, 4c, 5c, 6c, d and 9; Supplementary Fig. 10d, 11d, g and 14c). The time-dependent stomatal conductance, transpiration and photosynthetic rate was recorded using LI-6400XT Portable Photosynthesis System (LI-COR Biosciences) equipped with an *Arabidopsis* leaf chamber fluorometer (under $150 \mu\text{mol m}^{-2} \text{s}^{-1}$ light with 10% blue light, 150mmol s^{-1} flow rate, 400 ppm CO_2 mixer, ~50% relative humidity at 22°C) as indicated (Fig. 4d; Supplementary Fig. 8g, h).

ABA measurement. The analysis of *Arabidopsis* leaf ABA concentration followed a method as described previously⁶⁷. Briefly, >50 mg of ground fresh leaf samples were used to determine ABA concentration using an Agilent 6410 Series Triple Quad liquid chromatography (LC)-mass spectrometer (MS)/MS, equipped with Agilent 1200 series HPLC (Agilent Technologies) using a Phenomenex C18 column ($75 \text{mm} \times 4.5 \text{mm} \times 5 \mu\text{m}$) with a column temperature set at 40°C . Solvents were nanopure water and acetonitrile, both with 0.05% acetic acid. Samples were eluted with a linear 15-min gradient from 10 to 90% acetonitrile. Compounds were identified by retention times and mass/charge ratio.

Water-deficit drought assay. Plants were germinated on $\frac{1}{2}$ MS medium with 0.8% phytigel for 10 days in short-day conditions ($100\text{--}120 \mu\text{mol m}^{-2} \text{s}^{-1}$, 10 h light/14 h dark) at 22°C before being transferred to pots (size 2.5 inch diameter \times 2.25 inch height, LI-COR Bioscience) with soil, containing coco peat/Irish peat (1:1 ratio). Prior to 10-day-old seedling transfer, all pots were weighed on an Ohaus ARA520 Adventurer Balance and soil was aliquoted into the pots within ± 0.1 g between all replicates within an experimental run, randomly placed in growth cabinet and moved every other day in the same environmental conditions stated above. The starting weight varied amongst experimental runs dependent upon soil moisture (from 75 to 78 g). The drought assay was performed on 5–6-week-old *Arabidopsis* plants (Figs. 3, 4g, h and 5; Supplementary Figs. 6a–c, 9 and 11c–e). All plants were well-watered (saturated) the night before the drought assay, but not watered again during the assay. During the drought assay, all plants were randomly moved around once a day to avoid any bias of uneven light distribution or air flow within the cabinet that may differentially affect water loss.

At each sampling point, fresh weight of 2–3 leaves per plant was determined on an Ohaus Explorer E02140 balance (in Fig. 3a, Supplementary Figs. 6c and 11c, this occurred immediately after the rest of the leaf rosette was snap frozen in liquid nitrogen for later GABA measurement). Sampled leaves were then rehydrated to full turgid weight in ultrapure water overnight and measured after surface water was dried with paper towel. Dry weight was determined at 65°C for 1 day. Leaf RWC was calculated as (Figs. 3c, 4g and 5d; Supplementary Figs. 6a and 11e)

$$\text{RWC} = \frac{\text{Fresh weight} - \text{Dry weight}}{\text{Turgid weight} - \text{Dry weight}} \times 100\% \quad (1)$$

At each sampling point, fresh soil weight of the whole pot (Mwet) and dry soil weight after drying the soil (Mdry) at 105°C for 3 days was measured using an Ohaus ARA520 Adventurer Balance (Supplementary Fig. 6b). Gravimetric soil water content (θ_g) of the whole soil in the pots was calculated as

$$\theta_g = \frac{\text{Mwet} - \text{Mdry}}{\text{Mdry}} \quad (2)$$

Leaf feeding assay. The stomatal conductance, transpiration and photosynthetic rate of the detached leaf feeding assay was recorded using either a LCpro-SD Portable Photosynthesis System (ADC Bioscientific) with $350 \mu\text{mol m}^{-2} \text{s}^{-1}$ light, $200 \mu\text{mol s}^{-1}$ flow rate and 400 ppm CO_2 at 22°C (Supplementary Fig. 1c, d) or

LI-COR LI-6400XT (LI-COR Biosciences) with $200 \mu\text{mol m}^{-2} \text{s}^{-1}$ light, $150 \mu\text{mol s}^{-1}$ flow rate and 400 ppm CO_2 at 22°C (Figs. 2c and 8b, d, f; Supplementary Figs. 2a, b and 17a, b, d, e, g, h). The detached leaf was fed with artificial xylem sap solution modified as described⁶⁸, containing 1 mM KH_2PO_4 , 1 mM K_2HPO_4 , 1 mM CaCl_2 , 0.1 mM MgSO_4 , 1 mM KNO_3 , 0.1 mM MnSO_4 , 1 mM K-H-malate, pH 6.0 (KOH) with or without GABA or muscimol supplement as indicated, detached leaves were pre-fed under $150 \mu\text{mol m}^{-2} \text{s}^{-1}$ light to allow the uptake of treatments for 45–60 min before recording. iWUE and WUE were calculated based on the equation as described in ref. ²⁷.

GABA measurement. GABA concentration was determined using ultra performance LC (UPLC) as described previously³⁶. Briefly, GABA was extracted from samples using 10 mM sodium acetate and derivatized with the AccQ Tag Ultra Derivatization Kit (Waters). Chromatographic analysis of GABA was performed on an Acquity UPLC System (Waters) with a Cortecs or Phenomenex UPLC C18 column (1.6 μm , $2.1 \times 100 \text{mm}$). The gradient protocol for amino acids analysis was used to measure GABA with mobile solvents AccQ Tag Ultra Eluents A and B (Waters). Standard GABA solution was used for calibration ranging from 0 to 150 μM . The results were analyzed by Empower chromatography software version 3 (Waters).

GUS histochemical staining assays. A GUS histochemical assay was performed using the methods described previously⁶⁹. Three-to-four-week-old transgenic *pGAD2::GUS* plants were stained in buffer containing 50 mM Na phosphate pH = 7.0, 10 mM EDTA, 2 mM potassium ferrocyanide, 2 mM potassium ferricyanide, 0.1% (v/v) Triton X-100 and 0.1% (w/v) X-Gluc (5-bromo-4-chloro-3-indolyl β -D-glucuronide) during a 1.5 h incubation at 37°C in the dark. The stained plants were detected in 70% ethanol. GUS-stained plants were imaged using an Axiophot Pol Photomicroscope (Carl Zeiss).

Fluorescence microscopy. The fluorescence of fluorescent proteins in transgenic *gad2-1/GCI::GAD2Δ-GFP*, *gad2-1/GCI::GAD2-GFP* and *WT/GCI::GAD2Δ-GFP* plants was imaged by confocal laser scanning microscopy using a Zeiss Axioviskop 2 mot plus LSM5 PASCAL and argon laser (Carl Zeiss). Sequential scanning and laser excitation was used to capture fluorescence via the LSM5 PASCAL from GFP (excitation = 488 nm, emission band-pass = 505–530 nm), chlorophyll autofluorescence (excitation = 543 nm, emission long-pass = 560 nm). The fluorescence of fluorescent proteins in the mesophyll protoplasts of transgenic *alm9-2* complementation lines and *N. benthamiana* (Supplementary Fig. 16c, d) was imaged using Nikon A1R Laser Scanning Confocal with DS-R1 CCD camera. Sequential scanning and laser excitation was used to capture fluorescence via the Nikon A1R Laser Scanning Confocal from GFP (excitation = 488 nm, emission = 525–575 nm), chlorophyll autofluorescence (excitation = 561 nm, emission = 595–645 nm).

Reverse transcriptional PCR. Reverse transcriptional PCR was determined by PCR amplification on cDNA synthesized from RNA extracted from plants as indicated. PCR amplified *GAD2*, *Actin2*, *GFP*, *GAD2 mRNA*, *UAS::GAD2Δ* and *ALMT9* using Phire Hot Start II DNA Polymerase (Invitrogen) with primer sets: *GAD2_rt_F* (5'-ACGTGATGGATCCAGACAAAG-3') and *GAD2_rt_R* (5'-TACATTTTCCGGATCCCT-3'); *Actin2_rt_F* (5'-CAAAGGCCAACAGAGAGAAGA-3') and *Actin2_rt_R* (5'-CTGTACTTCTTCCAGTGGTG-3'); *GFP_rt_F* (5'-GGAGTTGTCCCAATCTTGT-3') and *GFP_rt_R* (5'-CGCAATTGGAGTATTTGT-3'); *GAD2mRNA_rt_F* (5'-ACGTGATGGATCCAGACAAAG-3') and *GAD2mRNA_rt_R* (5'-TCTTCATTTCCACACAAAGGC-3'); *UAS_GAD2_rt_F* (5'-TCACCTCAATTTCTCCAAGG-3') and *UAS_GAD2_rt_R* (5'-CGGCAACAGGATTCATCTTAAG-3'); *ALMT9_rt_F* (5'-AATACTCGAGAAACGGGAGAG-3') and *ALMT9_rt_R* (5'-CATCCCAAACACCTACGAAT-3').

Quantitative real-time PCR analysis. Quantitative reverse transcription PCR was performed using KAPA SYBR FAST ABI PRISM kit (Kapa Biosystems) using a QuantStudio™ 12K Flex Real-Time PCR System (Thermo Fisher Scientific) to determine the expression levels of *GAD1*, *GAD2*, *GAD3*, *GAD4*, *GAD5*, *GABA-T*, *ALMT9*, *ALMT12*, *RD29A* and *RD22* genes with primer sets: *GAD1_qF* (5'-TCTCAAAGGACGAGGGAGTG-3') and *GAD1_qR* (5'-AACCACACGAAAGACAGTGATG-3'); *GAD2_qF* (5'-GTCTCAAAGGACCAAGGAGTG-3') and *GAD2_qR* (5'-CATCGGACGAGCATAGTGTA-3'); *GAD3_qF* (5'-CCGTTAGTGGCGTTTCTCT-3') and *GAD3_qR* (5'-TCTCTTTGGCTCTCTCTCG-3'); *GAD4_qF* (5'-GTGTTCCGTTAGTGGCGTT-3') and *GAD4_qR* (5'-GTCTCTCTGGCGTCTTCT-3'); *GAD5_qF* (5'-TCAACCCACITTCACITCTCA-3') and *GAD5_qR* (5'-TTCCTTCTTTCAGCTCTCT-3'); *GABA-T_qF* (5'-AGGCAGCACCTGAGAAAGAA-3') and *GABA-T_qR* (5'-GGAGTGATAAAACGGCAAGG-3');

ALMT9_{qF} (5'-CAGAGAGTGGCGCTAGAAGG-3') and ALMT9_{qR} (5'-GGATTTGAAGGCGTAGATTGG-3'); ALMT12_{qF} (5'-TTGACGGAACTCGCAGATAG-3') and ALMT12_{qR} (5'-CGATGGAGGTTAGAGCCAAAG-3'); RD29A_{qF} (5'-AAACGACGACAAAGGAAGTG-3') and RD29A_{qR} (5'-ACCAAACGACCCAGATGATT-3'); RD22_{qF} (5'-AGGGCTGTTCCACTGAGG-3') and RD22_{qR} (5'-CACCACAGATTTATCGTCAGACA-3'). Expression levels of each gene was normalised to three control genes—*Actin2*, *EF1α* and *GAPDH-A*—that were amplified with primer sets: *Actin2*_{qF} (5'-TGAGCAAAGAAATCACAGCACT-3') and *Actin2*_{qR} (5'-CCTGGACCTGCCTCATCATAC-3'); *EF1α*_{qF} (5'-GACAGCGTCTCTGTTGAAGGAG-3') and *EF1α*_{qR} (5'-GCGGAAAGAGTTTGTATGTTCA-3'); *GAPDH-A*_{qF} (5'-TGGTTGATCTCGTTGTCAGGCTC-3') and *GAPDH-A*_{qR} (5'-GTCAGCCAAGTCAACAACCTCTCTG-3').

Reporting summary. Further information on research design is available in the Nature Research Reporting Summary linked to this article.

Data availability

Sequence data used in this paper can be found in The Arabidopsis Information Resource database (<https://www.arabidopsis.org/>) under the following accessions: *GAD1* (At5g17330), *GAD2* (At1g65960), *GAD3* (At2g02000), *GAD4* (At2g02010), *GAD5* (At3g17760), *GABA-T* (At3g22200), *ALMT9* (At3g18440), *ALMT12* (At4g17970), *RD29A* (At5g52310) and *RD22* (At5g25610). Other data that support the findings of this study are available from the corresponding author upon request. Source Data are provided with this paper.

Received: 19 December 2019; Accepted: 4 February 2021;

Published online: 29 March 2021

References

- Keenan, T. F. et al. Increase in forest water-use efficiency as atmospheric carbon dioxide concentrations rise. *Nature* **499**, 324 (2013).
- Papanatsiou, M. et al. Optogenetic manipulation of stomatal kinetics improves carbon assimilation, water use, and growth. *Science* **363**, 1456–1459 (2019).
- Hetherington, A. M. & Woodward, F. I. The role of stomata in sensing and driving environmental change. *Nature* **424**, 901 (2003).
- Shimazaki, K.-i, Doi, M., Assmann, S. M. & Kinoshita, T. Light regulation of stomatal movement. *Annu. Rev. Plant Biol.* **58**, 219–247 (2007).
- Sussmilch, F. C., Schultz, J., Hedrich, R. & Roelfsema, M. R. G. Acquiring control: the evolution of stomatal signalling pathways. *Trends Plant Sci.* **24**, 342–351 (2019).
- Kim, T.-H., Böhrer, M., Hu, H., Nishimura, N. & Schroeder, J. I. Guard cell signal transduction network: advances in understanding abscisic acid, CO₂, and Ca²⁺ signaling. *Annu. Rev. Plant Biol.* **61**, 561–591 (2010).
- Murata, Y., Mori, I. C. & Munemasa, S. Diverse stomatal signaling and the signal integration mechanism. *Annu. Rev. Plant Biol.* **66**, 369–392 (2015).
- Melotto, M., Underwood, W., Koczan, J., Nomura, K. & He, S. Y. Plant stomata function in innate immunity against bacterial invasion. *Cell* **126**, 969–980 (2006).
- Liu, Y. et al. Anion channel SLAH3 is a regulatory target of chitin receptor-associated kinase PBL27 in microbial stomatal closure. *eLife* **8**, e44474 (2019).
- Žárský, V. Signal transduction: GABA receptor found in plants. *Nat. Plants* **1**, 15115 (2015).
- Owens, D. F. & Kriegstein, A. R. Is there more to GABA than synaptic inhibition? *Nat. Rev. Neurosci.* **3**, 715 (2002).
- Bouche, N. & Fromm, H. GABA in plants: just a metabolite? *Trends Plant Sci.* **9**, 110–115 (2004).
- Kinnersley, A. M. & Turano, F. J. Gamma aminobutyric acid (GABA) and plant responses to stress. *Crit. Rev. Plant Sci.* **19**, 479–509 (2000).
- Ramesh, S. A., Tyerman, S. D., Gilliam, M. & Xu, B. γ-Aminobutyric acid (GABA) signalling in plants. *Cell Mol. Life Sci.* **74**, 1577–1603 (2017).
- Bouché, N., Lacombe, B. & Fromm, H. GABA signaling: a conserved and ubiquitous mechanism. *Trends Cell Biol.* **13**, 607–610 (2003).
- Bown, A. W. & Shelp, B. J. Plant GABA: not just a metabolite. *Trends Plant Sci.* **21**, 811–813 (2016).
- Michaeli, S. & Fromm, H. Closing the loop on the GABA shunt in plants: are GABA metabolism and signaling entwined? *Front. Plant Sci.* **6**, 419 (2015).
- Ramesh, S. A. et al. GABA signalling modulates plant growth by directly regulating the activity of plant-specific anion transporters. *Nat. Commun.* **6**, 7879 (2015).
- Gilliam, M. & Tyerman, S. D. Linking metabolism to membrane signaling: the GABA-malate connection. *Trends Plant Sci.* **21**, 295–301 (2016).
- Meyer, S. et al. AtALMT12 represents an R-type anion channel required for stomatal movement in *Arabidopsis* guard cells. *Plant J.* **63**, 1054–1062 (2010).
- De Angeli, A., Zhang, J., Meyer, S. & Martinoia, E. AtALMT9 is a malate-activated vacuolar chloride channel required for stomatal opening in *Arabidopsis*. *Nat. Commun.* **4**, 1804 (2013).
- Eisenach, C. et al. ABA-Induced stomatal closure involves ALMT4, a phosphorylation-dependent vacuolar anion channel of *Arabidopsis*. *Plant Cell* **29**, 2552–2569 (2017).
- Hauser, F., Li, Z., Waadt, R. & Schroeder, J. I. SnapShot: abscisic acid signaling. *Cell* **171**, 1708–1708 (2017).
- Peiter, E. et al. The vacuolar Ca²⁺-activated channel TPC1 regulates germination and stomatal movement. *Nature* **434**, 404 (2005).
- Meidner, H. Measurements of stomatal aperture and responses to stimuli. in *Stomatal Physiology* (ed. Jarvis, P. D. & Mansfield, T. A.) 25–28 (Cambridge University Press, 1981).
- Mori, I. C. et al. CDPKs CPK6 and CPK3 function in ABA regulation of guard cell S-type anion- and Ca²⁺-permeable channels and stomatal closure. *PLoS Biol.* **4**, 1749–1762 (2006).
- Leakey, A. D. et al. Water use efficiency as a constraint and target for improving the resilience and productivity of C₃ and C₄ crops. *Annu. Rev. Plant Biol.* **70**, 781–808 (2019).
- Desikan, R. et al. Hydrogen peroxide and nitric oxide signalling in stomatal guard cells. *J. Exp. Bot.* **55**, 205–212 (2004).
- Mekonnen, D. W., Flügge, U.-I. & Ludewig, F. Gamma-aminobutyric acid depletion affects stomata closure and drought tolerance of *Arabidopsis thaliana*. *Plant Sci.* **245**, 25–34 (2016).
- Espinoza, C. et al. Interaction with diurnal and circadian regulation results in dynamic metabolic and transcriptional changes during cold acclimation in *Arabidopsis*. *PLoS ONE* **5**, e14101 (2010).
- Zik, M., Arazi, T., Snedden, W. A. & Fromm, H. Two isoforms of glutamate decarboxylase in *Arabidopsis* are regulated by calcium/calmodulin and differ in organ distribution. *Plant Mol. Biol.* **37**, 967–975 (1998).
- Yang, Y., Costa, A., Leonhardt, N., Siegel, R. S. & Schroeder, J. I. Isolation of a strong *Arabidopsis* guard cell promoter and its potential as a research tool. *Plant Methods* **4**, 6 (2008).
- Akama, K. & Takaiwa, F. C-terminal extension of rice glutamate decarboxylase (OSGAD2) functions as an autoinhibitory domain and overexpression of a truncated mutant results in the accumulation of extremely high levels of GABA in plant cells. *J. Exp. Bot.* **58**, 2699–2707 (2007).
- Lehmann, S. et al. In planta function of compatible solute transporters of the AtProT family. *J. Exp. Bot.* **62**, 787–796 (2011).
- Meyer, A., Eskandari, S. & Grallath, S. Rentsch D. AtGAT1, a high affinity transporter for γ-aminobutyric acid in *Arabidopsis thaliana*. *J. Biol. Chem.* **281**, 7197–7204 (2006).
- Ramesh, S. A. et al. Aluminium-activated malate transporters can facilitate GABA transport. *Plant Cell* **30**, 1147–1164 (2018).
- Marti, M. C., Stancombe, M. A. & Webb, A. Cell- and stimulus-type-specific intracellular-free Ca²⁺ signals in *Arabidopsis thaliana*. *Plant Physiol.* **163**, 625–634 (2013).
- Kowada, T., Maeda, H. & Kikuchi, K. BODIPY-based probes for the fluorescence imaging of biomolecules in living cells. *Chem. Soc. Rev.* **44**, 4953–4972 (2015).
- Long, Y., Tyerman, S. D. & Gilliam, M. Cytosolic GABA inhibits anion transport by wheat ALMT1. *New Phytol.* **225**, 671–678 (2019).
- Meyer, S. et al. Malate transport by the vacuolar ATALMT6 channel in guard cells is subject to multiple regulation. *Plant J.* **67**, 247–257 (2011).
- Kovermann, P. et al. The *Arabidopsis* vacuolar malate channel is a member of the ALMT family. *Plant J.* **52**, 1169–1180 (2007).
- Negi, J. et al. CO₂ regulator SLAC1 and its homologues are essential for anion homeostasis in plant cells. *Nature* **452**, 483–486 (2008).
- Vahisalu, T. et al. SLAC1 is required for plant guard cell S-type anion channel function in stomatal signalling. *Nature* **452**, 487–491 (2008).
- Geiger, D. et al. Activity of guard cell anion channel SLAC1 is controlled by drought-stress signaling kinase-phosphatase pair. *Proc. Natl Acad. Sci. USA* **106**, 21425–21430 (2009).
- Geiger, D. et al. Guard cell anion channel SLAC1 is regulated by CDPK protein kinases with distinct Ca²⁺ affinities. *Proc. Natl Acad. Sci. USA* **107**, 8023–8028 (2010).
- Hedrich, R. & Geiger, D. Biology of SLAC1-type anion channels—from nutrient uptake to stomatal closure. *New Phytol.* **216**, 46–61 (2017).
- Takahashi, Y. et al. MAP3K kinase-dependent SnRK2-kinase activation is required for abscisic acid signal transduction and rapid osmotic stress response. *Nat. Commun.* **11**, 1–12 (2020).
- Chen, Z.-H. et al. Systems dynamic modeling of the stomatal guard cell predicts emergent behaviors in transport, signaling, and volume control. *Plant Physiol.* **159**, 1235–1251 (2012).

49. Hills, A., Chen, Z.-H., Amtmann, A., Blatt, M. R. & Lew, V. L. OnGuard, a computational platform for quantitative kinetic modeling of guard cell physiology. *Plant Physiol.* **159**, 1026–1042 (2012).
50. Takahashi, F. et al. A small peptide modulates stomatal control via abscisic acid in long-distance signalling. *Nature* **556**, 235 (2018).
51. Kuromori, T., Seo, M. & Shinozaki, K. ABA transport and plant water stress responses. *Trends Plant Sci.* **23**, 513–522 (2018).
52. Sharma, T., Dreyer, I., Kochian, L. & Piñeros, M. A. The ALMT family of organic acid transporters in plants and their involvement in detoxification and nutrient security. *Front. Plant Sci.* **7**, 1488 (2016).
53. Zhang, J. et al. Identification of a probable pore-forming domain in the multimeric vacuolar anion channel AtALMT9. *Plant Physiol.* **163**, 830–843 (2013).
54. Marvin, J. S. et al. A genetically encoded fluorescent sensor for in vivo imaging of GABA. *Nat. Methods* **16**, 763–770 (2019).
55. Fromm, H. GABA signaling in plants: targeting the missing pieces of the puzzle. *J. Exp. Bot.* **71**, 6238–6245 (2020).
56. Liu, J., Zhou, M., Delhaize, E. & Ryan, P. R. Altered expression of a malate-permeable anion channel, OsALMT4, disrupts mineral nutrition. *Plant Physiol.* **175**, 1745–1759 (2017).
57. Balzergue, C. et al. Low phosphate activates STOP1-ALMT1 to rapidly inhibit root cell elongation. *Nat. Commun.* **8**, 15300 (2017).
58. Jie, Y. et al. An InDel in the promoter of Al-activated malate transporter 9 selected during tomato domestication determines fruit malate contents and aluminum tolerance. *Plant Cell* **29**, 2249–2268 (2017).
59. Palanivelu, R., Brass, L., Edlund, A. F. & Preuss, D. Pollen tube growth and guidance is regulated by POP2, an *Arabidopsis* gene that controls GABA levels. *Cell* **114**, 47–59 (2003).
60. Domingos, P. et al. Molecular and electrophysiological characterization of anion transport in *Arabidopsis thaliana* pollen reveals regulatory roles for pH, Ca²⁺ and GABA. *New Phytol.* **223**, 1353–1371 (2019).
61. Svozil, J., Gruißem, W. & Baerenfaller, K. Proteasome targeting of proteins in *Arabidopsis* leaf mesophyll, epidermal and vascular tissues. *Front. Plant Sci.* **6**, 376 (2015).
62. Prusko, K. *Identifizierung Cis-Regulatorischer Elemente der Transkriptionskontrolle in Photosynthetisch Aktiven Blattzellen von Arabidopsis thaliana*, PhD thesis (Heinrich-Heine-Universität Düsseldorf, 2010).
63. Conn, S. J. et al. Protocol: optimising hydroponic growth systems for nutritional and physiological analysis of *Arabidopsis thaliana* and other plants. *Plant Methods* **9**, 4 (2013).
64. Curtis, M. D. & Grossniklaus, U. A gateway cloning vector set for high-throughput functional analysis of genes in planta. *Plant Physiol.* **133**, 462–469 (2003).
65. Møller, I. S. et al. Shoot Na⁺ exclusion and increased salinity tolerance engineered by cell type-specific alteration of Na⁺ transport in *Arabidopsis*. *Plant Cell* **21**, 2163–2178 (2009).
66. Shen, L. et al. Measuring stress signaling responses of stomata in isolated epidermis of graminaceous species. *Front. Plant Sci.* **6**, 533 (2015).
67. Speirs, J., Binney, A., Collins, M., Edwards, E. & Loveys, B. Expression of ABA synthesis and metabolism genes under different irrigation strategies and atmospheric VPDs is associated with stomatal conductance in grapevine (*Vitis vinifera* L. cv Cabernet Sauvignon). *J. Exp. Bot.* **64**, 1907–1916 (2013).
68. Wilkinson, S. & Davies, W. J. Xylem sap pH increase: a drought signal received at the apoplastic face of the guard cell that involves the suppression of saturable abscisic acid uptake by the epidermal symplast. *Plant Physiol.* **113**, 559–573 (1997).
69. Xu, B. et al. A calmodulin-like protein regulates plasmodesmal closure during bacterial immune responses. *New Phytol.* **215**, 77–84 (2017).

Acknowledgements

The authors would like to thank Dr Katja Bärenfaller from the University of Zurich for providing JR11-2 (Col-0) seeds; Prof. Zhonghua Chen from Western Sydney University for assisting with barley epidermal assays; Dr Cornelia Eisenach from the University of Zurich for providing ALMT9 constructs, *almt12* and *almt9* seeds and Prof. Stephen D Tyerman, Prof. Enrico Martinoia and Dr Alexis De Angeli for valuable discussions. This work was funded by Waite Research Institute, funding to M.G. and B.X., ARC Discovery grants DP170104384 and DP21012828 to M.G. and R.H. and ARC Centre of Excellence (CE14010008) and Grains Research and Development Corporation funding (UWA00173) to M.G. Author X.F. was supported by supported by a Chinese Scholarship Council. X.Z. was supported by a Chinese Scholarship Council Travelling Fellowship.

Author contributions

B.X. constructed all materials and performed all experiments except the following: Y.L. generated *almt9/almt12* mutants and performed experiments on stomatal aperture assays treated with hydrogen peroxide and calcium and of *almt12* and *almt9/12* mutants. X.F. generated *almt9* complementation lines, performance aperture and conductance measurement of complementation plants. X.Z. performed all non-*Arabidopsis* aperture measurements, except for barley performed by N.S. Author L.C. performed GABA measurements supervised by M.O. Author A.B. performed ABA quantification supervised by E.J.E. Author J.H. acquired images used in Fig. 1. M.G., B.X. and R.H. conceived the research. B.X. drafted all figures. M.G. and B.X. drafted the manuscript. All authors provided edits.

Competing interests

The authors declare no competing interests.

Additional information

Supplementary information The online version contains supplementary material available at <https://doi.org/10.1038/s41467-021-21694-3>.

Correspondence and requests for materials should be addressed to M.G.

Peer review information *Nature Communications* thanks the anonymous reviewers for their contribution to the peer review of this work. Peer review reports are available.

Reprints and permission information is available at <http://www.nature.com/reprints>

Publisher's note Springer Nature remains neutral with regard to jurisdictional claims in published maps and institutional affiliations.



Open Access This article is licensed under a Creative Commons Attribution 4.0 International License, which permits use, sharing, adaptation, distribution and reproduction in any medium or format, as long as you give appropriate credit to the original author(s) and the source, provide a link to the Creative Commons license, and indicate if changes were made. The images or other third party material in this article are included in the article's Creative Commons license, unless indicated otherwise in a credit line to the material. If material is not included in the article's Creative Commons license and your intended use is not permitted by statutory regulation or exceeds the permitted use, you will need to obtain permission directly from the copyright holder. To view a copy of this license, visit <http://creativecommons.org/licenses/by/4.0/>.

© The Author(s) 2021

GABA signalling modulates stomatal opening to enhance plant water use efficiency and drought resilience

Bo Xu^{1,2}, Yu Long^{1,2}, Xueying Feng^{1,2}, Xujun Zhu^{1,3}, Na Sai^{1,2}, Larissa Chirkova^{2,4}, Annette Betts⁵, Johannes Herrmann⁶, Everard J Edwards⁵, Mamoru Okamoto^{2,4}, Rainer Hedrich⁶ & Matthew Gilliam^{1,2*}

¹ Plant Transport and Signalling Lab, ARC Centre of Excellence in Plant Energy Biology, Waite Research Institute, Glen Osmond, SA 5064, Australia

² School of Agriculture, Food and Wine, Waite Research Precinct, University of Adelaide, Glen Osmond, SA 5064, Australia

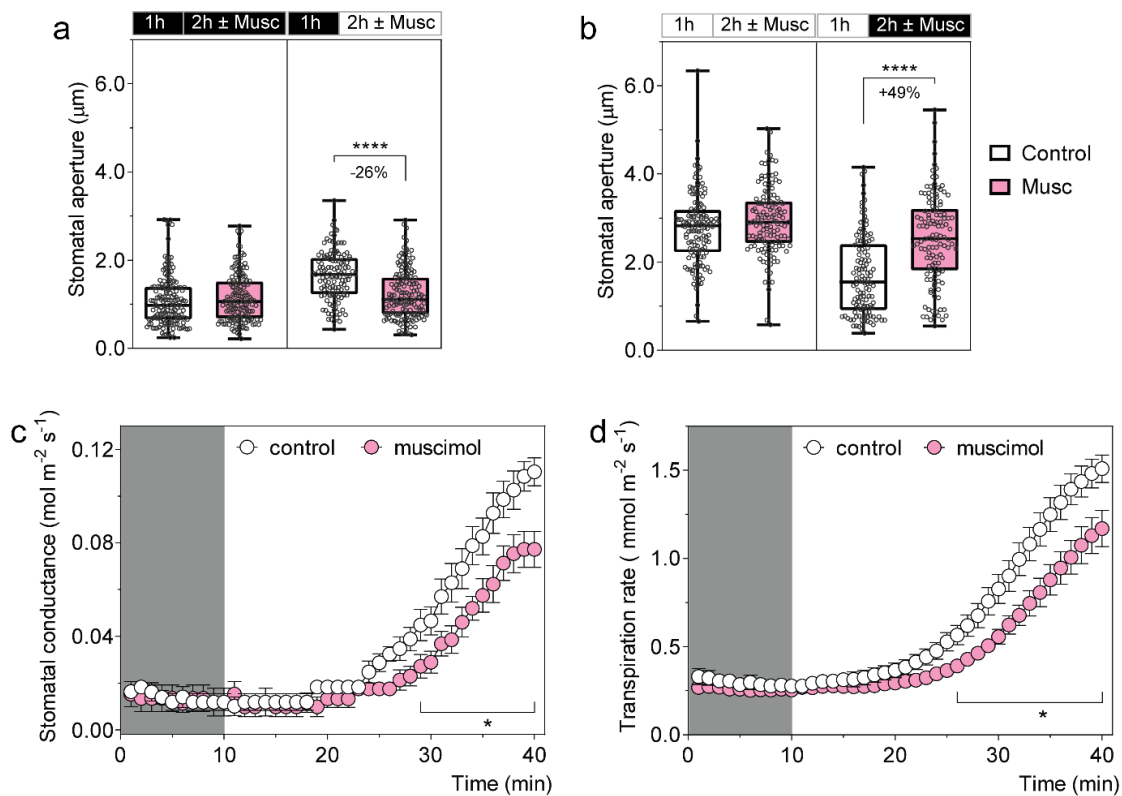
³ College of Horticulture, Nanjing Agricultural University, Nanjing 210095, China

⁴ ARC Industrial Transformation Research Hub for Wheat in a Hot and Dry Climate, Waite Research Institute, University of Adelaide, Glen Osmond, SA 5064, Australia

⁵ CSIRO Agriculture & Food, Locked Bag 2, Glen Osmond, SA, 5064, Australia

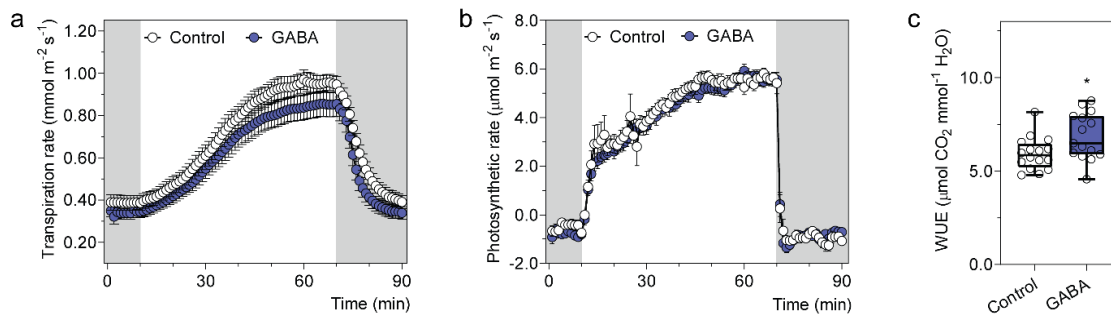
⁶ Institute for Molecular Plant Physiology and Biophysics, University of Würzburg, Würzburg 97070, Germany

SUPPLEMENTARY INFORMATION



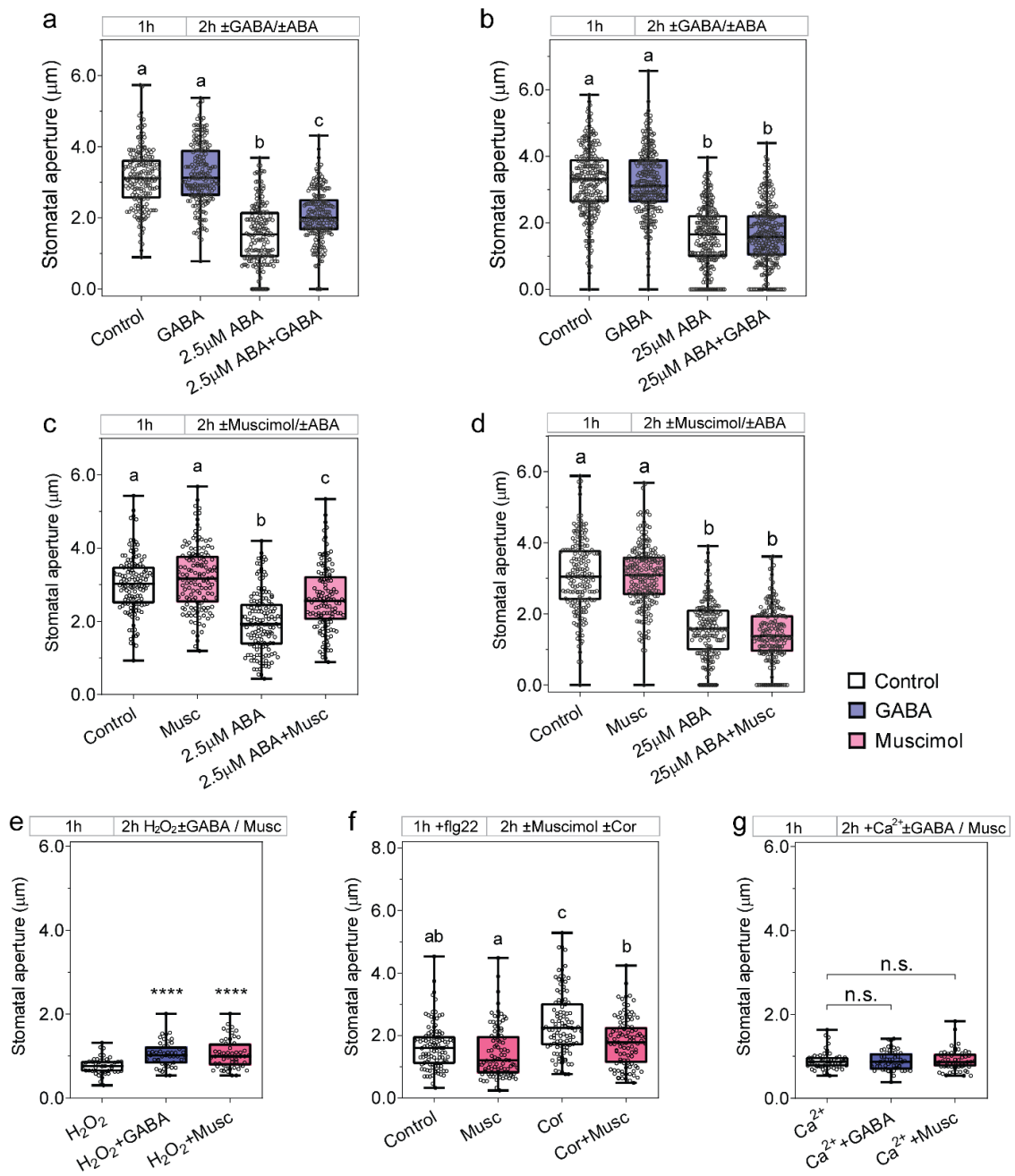
Supplementary Figure 1. Muscimol antagonises stomatal aperture changes initiated by light and dark treatments a-b, Exogenous muscimol application reduces stomatal pore movement in response to light or dark. Epidermal strips were pre-incubated in stomatal pore measurement buffer for 1 h under dark (**a**) or light (**b**), followed by 2 h incubation under constant dark (**a**), light (**b**), dark-to-light transition (**a**) or light-to-dark transition (**b**) as indicated above graphs by black (dark) or white (light) bars, together with the application of 10 μM muscimol (Musc); $n = 156$ for control (constant dark), $n = 151$ for muscimol (constant dark), $n = 127$ for control (dark-to-light transition) and $n = 151$ for muscimol (dark to light transition) (**a**); $n = 134$ for control (constant light), $n = 132$ for muscimol (constant light), $n = 118$ for control (light-to-dark transition) and $n = 120$ for muscimol (light-to-dark transition) (**b**). **c-d**, Muscimol feeding reduces stomatal conductance, transpiration rate of detached leaves. Stomatal conductance (**c**), transpiration rate (**d**) of detached leaves of wildtype *Arabidopsis* plants determined by LCpro-SD Portable Photosynthesis System was fed by artificial

xylem sap solution with or without 10 μ M muscimol supplement; n = 7 for control and n = 8 for muscimol (**c, d**). All data are plotted with box and whiskers plots: whiskers plot represents minimum and maximum values, and box plot represents second quartile, median and third quartile (**a, b**) or data are represented mean \pm s.e.m (**c, d**); statistical difference was determined by Two-way ANOVA (**a, b**), or two-sided Student's *t*-test (**c, d**), * $P < 0.05$ and **** $P < 0.0001$.



Supplementary Figure 2. GABA feeding increases WUE of detached leaves.

GABA feeding reduces transpiration rate and increases water use efficiency (WUE) of detached leaves. Transpiration (**a**) and photosynthetic rate (**b**) of 5-6 week-old leaves of 5-6 week-old *A. thaliana* wildtype plants was recorded using a LiCor LI-6400XT in response to dark (shaded region) and 200 $\mu\text{mol m}^{-2} \text{s}^{-1}$ light (white region), fed with artificial xylem sap solutions \pm 4 mM GABA. **c**, WUE of detached leaves was calculated based on the ratio of photosynthetic rate (**b**) versus transpiration rate (**a**), $n = 16$ independent leaves for control and $n = 15$ for GABA (**a-c**). All data are plotted with box and whiskers plots: whiskers plot represents minimum and maximum values, and box plot represents second quartile, median and third quartile (**c**) or data are represented mean \pm s.e.m (**a, b**), statistical difference was determined by two-sided Student's *t*-test, * $P < 0.05$



Supplementary Figure 3. GABA and muscimol inhibit stomatal aperture

changes triggered by signaling molecules. **a-g**, Exogenous GABA or muscimol

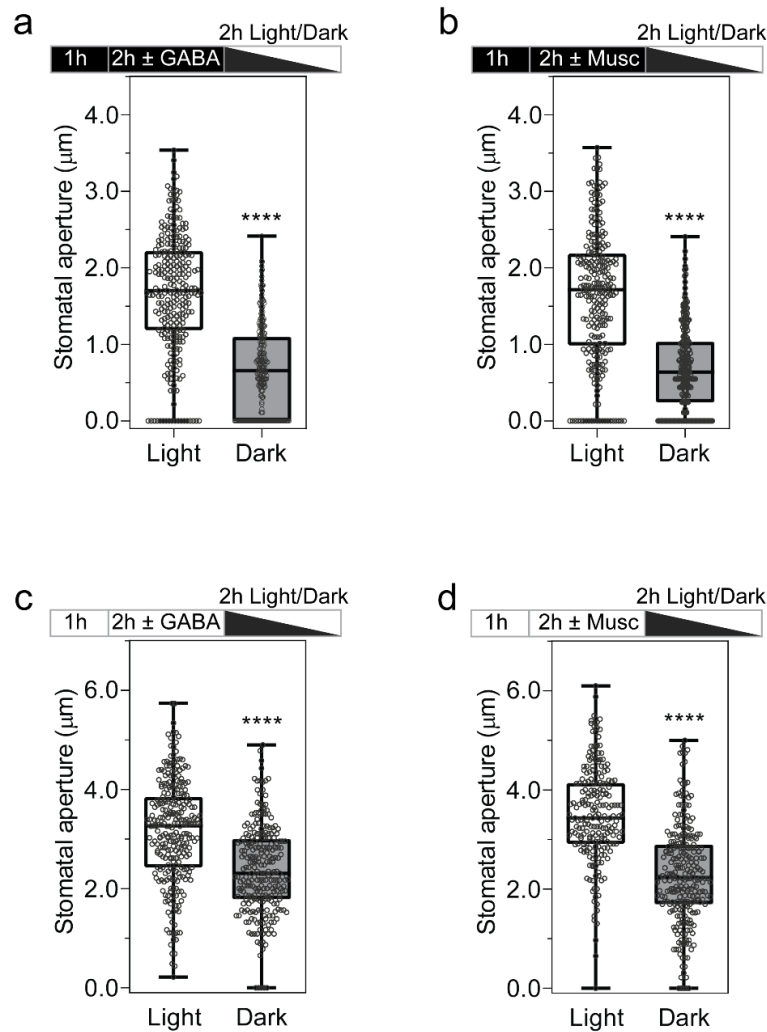
application reduces stomatal closure in response to 2.5 μM ABA (**a, c**), 50 μM H_2O_2 ¹

(**e**) and stomatal opening to 0.5 $\mu\text{g ml}^{-1}$ coronatine² (**f**), but not to 25 μM ABA (**b, d**)

and 2 mM CaCl_2 ¹ (**g**). Epidermal strips were pre-incubated in stomatal pore

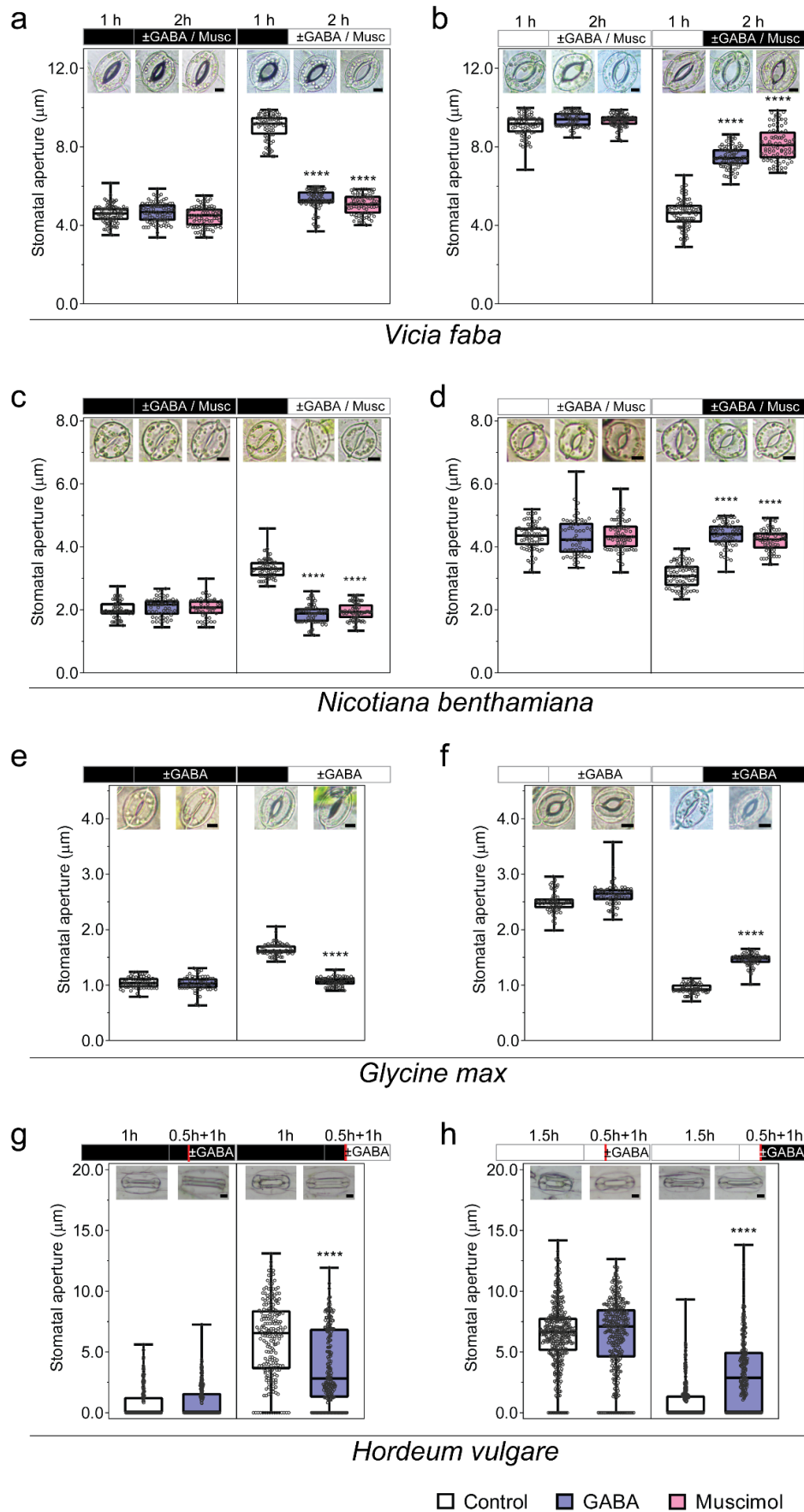
measurement buffer for 1 h under light, followed by 2 h treatment under light with or

without combination of ABA \pm 2 mM GABA (**a, b**) / 10 μ M muscimol (**c, d**), H₂O₂ \pm 2 mM GABA/10 μ M muscimol (Musc) (**e**), coronatine (Cor) \pm 10 μ M muscimol (**f**), and CaCl₂ (Ca²⁺) \pm 2 mM GABA/10 μ M muscimol (**g**) as indicated; n = 183 for control, n = 191 for GABA, n = 171 for ABA and n = 201 for ABA+GABA (**a**); n = 249 for control, n = 249 for GABA, n = 243 for ABA and n = 261 for ABA+GABA (**b**); n = 133 for control, n = 137 for muscimol, n = 142 for ABA and n = 131 for ABA+muscimol (**c**); n = 180 for control, n = 222 for muscimol, n = 176 for ABA and n = 179 for ABA+muscimol (**d**); n = 44 for H₂O₂, n = 47 for H₂O₂+GABA and n = 54 for H₂O₂+Musc (**e**); n = 103 for control, n = 103 for Cor, n = 101 for Cor+muscimol and n = 91 for muscimol (**f**);); n = 52 for Ca²⁺, n = 52 for Ca²⁺+GABA and n = 54 for Ca²⁺+Musc (**g**). All data are plotted with box and whiskers plots: whiskers plot represents minimum and maximum values, and box plot represents second quartile, median and third quartile; statistical difference as determined by One-Way ANOVA (**a-g**), **** $P < 0.0001$, a, b and c represent groups without significant difference, $P < 0.05$ (**a-d, f**).



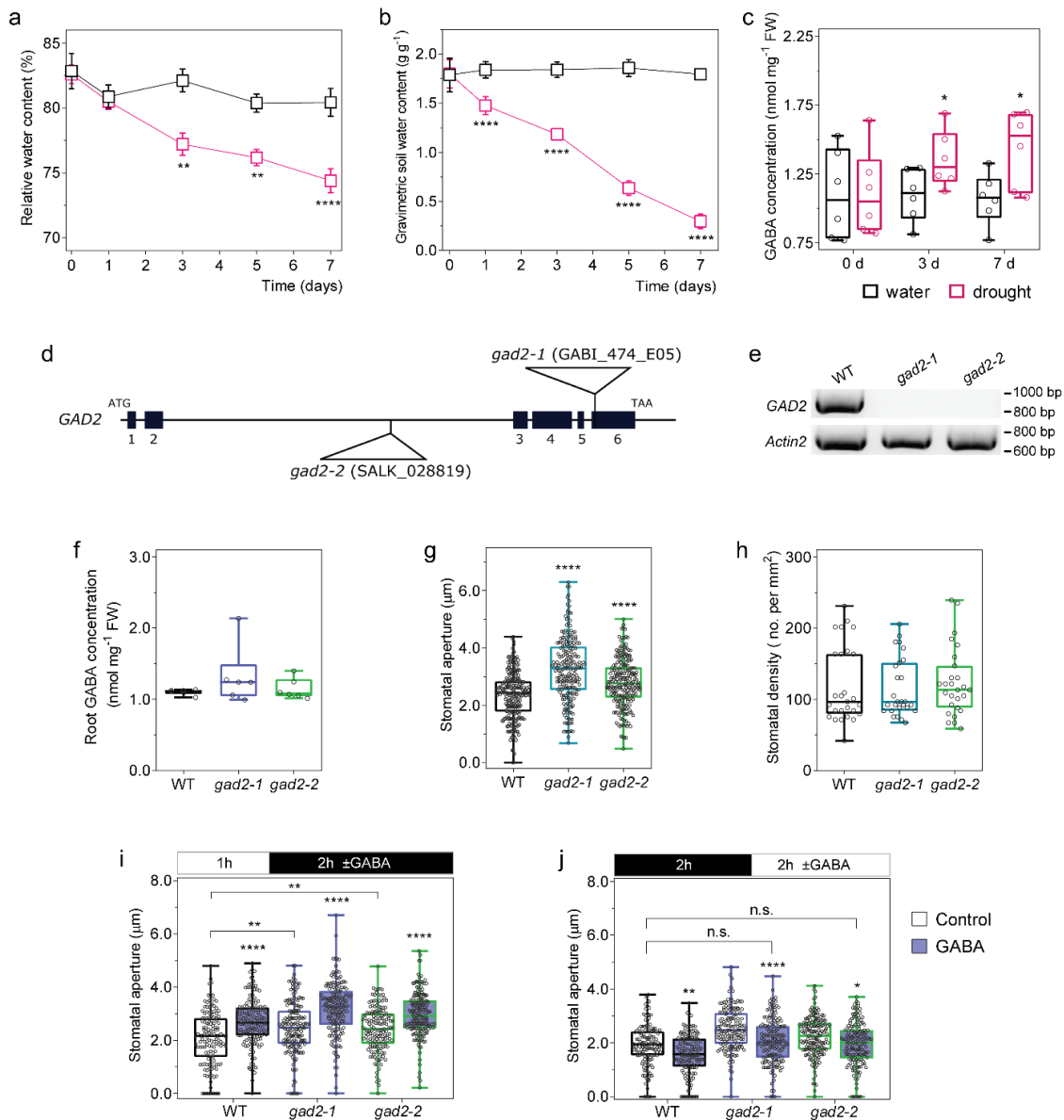
Supplementary Figure 4. Guard cells are viable after treatment with GABA and muscimol. **a-d**, Guard cells were competent in movement after removal of GABA or muscimol treatments, as closed pores opened when exposed to light (**a-b**) or open pores closed when exposed to dark (**c-d**) following removal of GABA or muscimol. Epidermal strips were incubated under dark (**a-b**) or light (**c-d**) for 1 h, followed by 2 h treatment of 2 mM GABA (**a, c**) or 10 µM muscimol (**b, d**), then epidermal strips were transferred into fresh stomatal measurement buffer with 2 h light or dark treatment before measurement; $n = 272$ for light and $n = 247$ for dark (**a**); $n = 251$ for light and $n = 251$ for dark (**b**); $n = 275$ for light and $n = 248$ for dark (**c**); $n = 217$ for light and $n = 261$ for dark (**d**). All data are plotted with box and whiskers plots:

whiskers plot represents minimum and maximum values, and box plot represents second quartile, median and third quartile; statistical difference as determined by two-sided Student's *t*-test (**a-d**), **** $P < 0.0001$.



Supplementary Figure 5. GABA and muscimol inhibit stomatal aperture changes in response to light and dark in *Vicia faba* (broad bean), *Nicotiana benthamiana* (tobacco), *Glycine max* (soybean) and *Hordeum vulgare* (barley). Epidermal strips were pre-incubated in stomatal measurement buffer for 1 h under dark (**a, c, e**) or light (**b, d, f**), followed by 2 h incubation under constant dark (**a, c, e**), light (**b, d, f**) as illustrated by black (dark) or white (light) bars, ± 2 mM GABA or 10 μ M muscimol (Musc) as indicated; barley leaf samples were first detached and bathed in a modified measurement buffer under 2h dark (**g**) or light ($100 \mu\text{mol m}^{-2} \text{s}^{-1}$) (**h**), then pre-treated in the fresh buffer ± 1 mM GABA for 0.5 h as indicated by black or white bars; after this pre-treatment (break by red line), leaf samples were incubated in continuous dark (**g**), light (**h**), dark-to-light (**g**) or light-to-dark (**h**) transition for additional 1 h before the epidermal strips were peeled for imaging. n = 88 for control (constant dark), n = 85 for GABA (constant dark), n = 82 for muscimol (constant dark), n = 78 for control (dark-to-light transition), n = 106 for GABA (dark-to-light transition) and n = 76 for muscimol (dark-to-light transition) (**a**); n = 73 for control (constant light), n = 65 for GABA (constant light), n = 76 for muscimol (constant light), n = 89 for control (light-to-dark transition), n = 85 for GABA (light-to-dark transition) and n = 84 for muscimol (light-to-dark transition) (**b**); n = 50 for control (constant dark), n = 52 for GABA (constant dark), n = 50 for muscimol (constant dark), n = 63 for control (dark-to-light transition), n = 65 for GABA (dark-to-light transition) and n = 64 for muscimol (dark to light transition) (**c**); n = 73 for control (constant light), n = 60 for GABA (constant light), n = 78 for muscimol (constant light), n = 78 for control (light-to-dark transition), n = 67 for GABA (light-to-dark transition) and n = 65 for muscimol (light-to-dark transition) (**d**); n = 61 for control (constant dark), n = 60 for GABA (constant dark), n = 63 for control (dark-to-light transition) and n = 62 for GABA (dark-to-light transition) (**e**); n = 59 for control (constant light), n = 59 for GABA (constant light), n = 60 for control (light-to-dark transition) and

n = 60 (dark-to-light transition) (**f**); n = 177 for control (constant dark), n = 220 for GABA (constant dark), n = 201 for control (dark-to-light transition) and n = 203 for GABA (dark-to-light transition) (**g**); n = 350 for control (constant light), n = 301 for GABA (constant light), n = 289 for control (light-to-dark transition) and n = 228 for GABA (light-to-dark-transition) (**h**). All data are plotted with box and whiskers plots: whiskers plot represents minimum and maximum values, and box plot represents second quartile, median and third quartile; statistical difference was determined by Two-way ANOVA, **** $P < 0.0001$; scale bars = 5 μm (**a-h**).

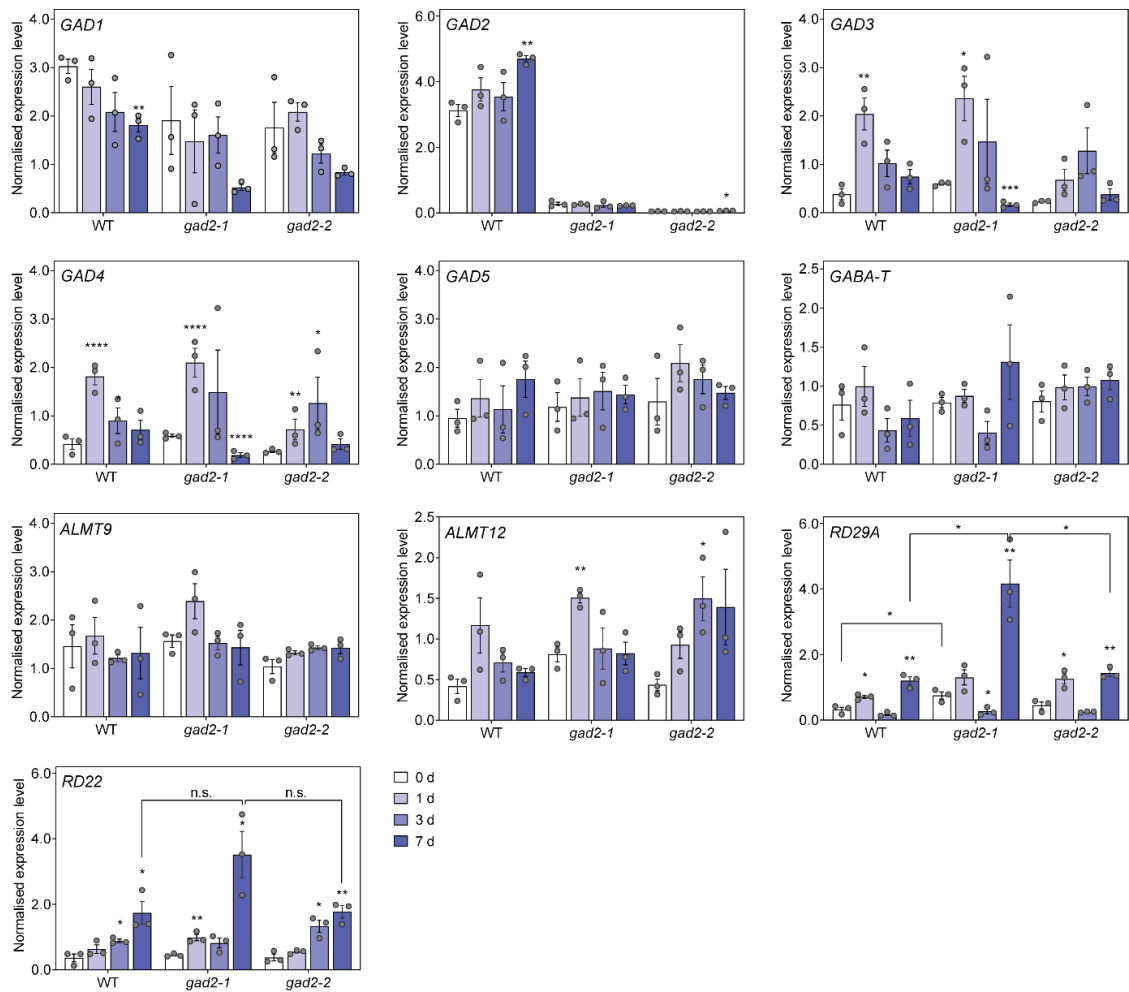


Supplementary Figure 6. GABA accumulates in leaves of Arabidopsis upon drought, and *gad2* knockout plants have greater stomatal apertures but show wildtype (WT)-like responses to exogenous GABA and root GABA accumulation.

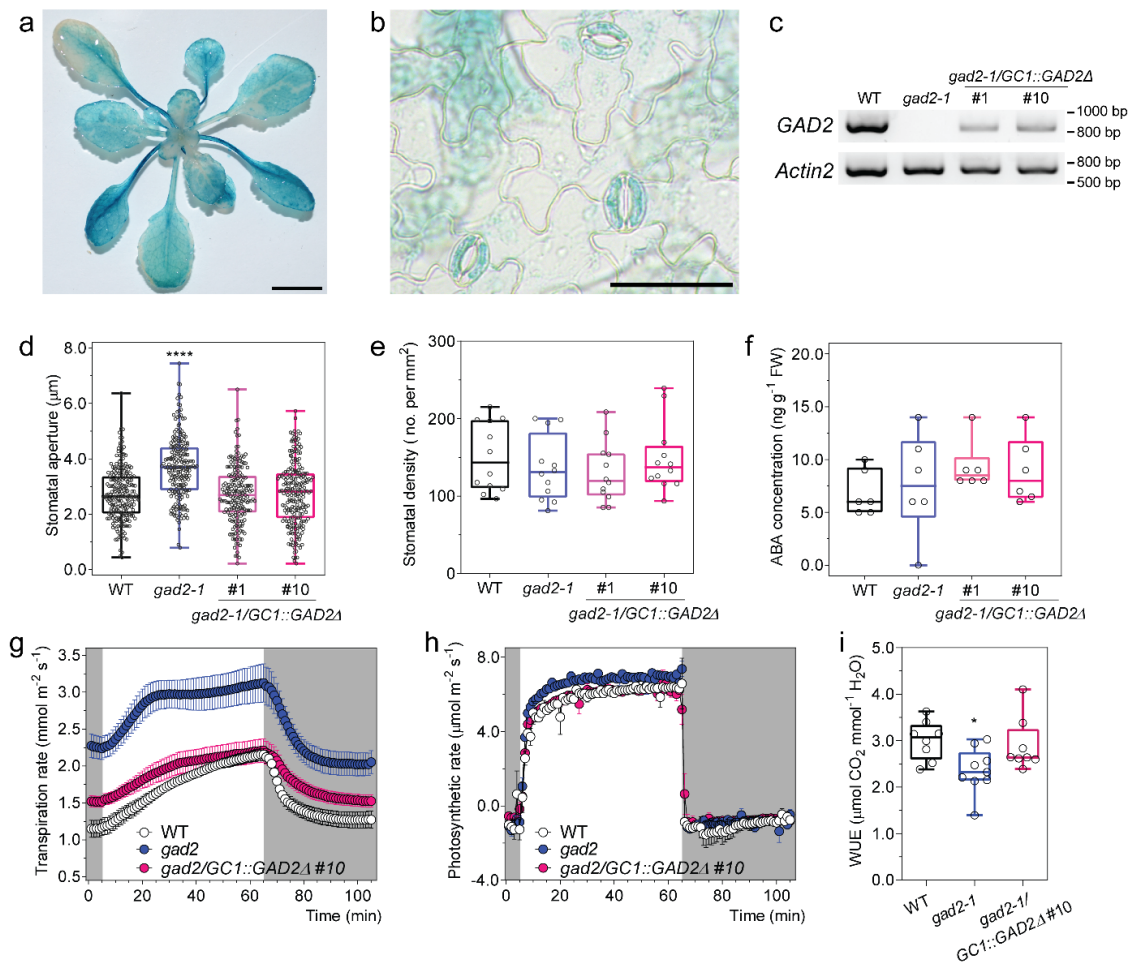
a, Relative water content in wildtype Arabidopsis leaves under well-water (black) or drought (red) treatments as indicated. **b**, Water content in the potted soil corresponding to the plants sampled in **(a)**. **c**, Leaf GABA concentration of wildtype Arabidopsis following well-watered control treatment (black) or drought (red). 2-3 leaves per plant were sampled for relative water content measurement, as shown in

(a); the whole rosette from the sampled plant in (a) was harvested and snap frozen in liquid nitrogen for later GABA measurement, as shown in (c); and the pot soil of corresponding plants harvested in (a, b) was sampled to determine gravimetric soil water content, as shown in (b); n = 6 (a-c). d, A diagram of *GAD2* T-DNA insertional mutant alleles in the Arabidopsis genome. e, Reverse transcriptional PCR semi-quantification of *GAD2* transcripts in Arabidopsis WT and *gad2* knockout plants, *Actin2* used as an internal control, similar results were obtained from three independent biological replicates. f, Root GABA concentration of WT, *gad2-1* and *gad2-2* plants. Roots were harvested from 5-6 week-old plants grown hydroponically in basal nutrient solution (2 mM NH₄NO₃, 3 mM KNO₃, 0.1 mM CaCl₂, 2 mM KCl, 2 mM Ca(NO₃)₂, 2 mM MgSO₄, 0.6 mM KH₂PO₄, 1.5 mM NaCl, 50 μM NaFe(III)EDTA, 50 μM H₃BO₃, 5 μM MnCl₂, 10 μM ZnSO₄, 0.5 μM CuSO₄, 0.1 μM Na₂MoO₃, pH = 5.6 by KOH)³, n = 6 plants. g-j, Stomatal aperture and density on the leaf abaxial side of Arabidopsis WT and *gad2* knockouts; epidermal strips were peeled and incubated in stomatal measurement buffer for 1 h under light before measurement n = 254 for WT, n = 215 for *gad2-1* and n = 226 for *gad2-2* (g); n = 27 sampling areas (0.57 x 0.42 mm) consisting of three areas per leaf, three leaves per plant and three plants per line sampled (h). i-j, Epidermal strips were pre-incubated in stomatal measurement buffer for 1 h under light (i) or 2 h dark (j), followed by 2 h incubation dark (i) or light (j) as indicated by black (dark) or white (light) bars ± blind treatment of 2 mM GABA or control; n = 135, 166 and 157 for WT, *gad2-1* and *gad2-2* with control treatment, n = 146, 162 and 174 for WT, *gad2-1* and *gad2-2* with GABA treatment (i); n = 139, 155 and 160 for WT, *gad2-1* and *gad2-2* with control treatment, n = 136, 155 and 153 for WT, *gad2-1* and *gad2-2* with GABA treatment (j). All data are plotted with box and whiskers plots: whiskers plot represents minimum and maximum values, and box plot represents second quartile, median and third quartile (c, f-j); or data are represented

by mean \pm s.e.m. (**a, b**); statistical difference was determined by two-sided Student's *t*-test (**c**), One-way ANOVA (**f-h**) or Two-way ANOVA (**a, b, i, j**), **P* < 0.05, ***P* < 0.01 and *****P* < 0.0001.



Supplementary Figure 7. *gad2* knockouts have similar transcriptional profiles to wildtype plants of other *GADs*, *GABA-T*, *ALMT9*, *ALMT12* or ABA responsive genes under drought stress. Quantitative real time PCR of *GAD1*, *GAD2*, *GAD3*, *GAD4*, *GAD5*, *GABA-T*, *ALMT9*, *ALMT12* and ABA marker genes –*RD29A* and *RD22*⁴ in the leaves of Arabidopsis wildtype (WT), *gad2-1* and *gad2-2* plants following drought treatment for 0, 1, 3 and 7 days as indicated, expression levels were normalized against three control genes –*Actin2*, *EF1α* and *GAPDH-A*; data are represented by means \pm s.e.m; n = 3, statistical difference as determined via the comparison of genes from drought-treated plants (1, 3 and 7 days) with non-droughted (0 day) plants within the same genotype by two-sided Student's *t*-test, * $P < 0.05$ ** $P < 0.01$, *** $P < 0.001$ and **** $P < 0.0001$.



Supplementary Figure 8. *GAD2* is highly expressed in leaves and guard cells, and guard-cell cell complementation of *GAD2Δ* restores stomatal aperture and WUE without modifying stomatal density. **a-b**, Representative GUS histochemical staining of *pGAD2::GUS* whole rosette; image of 3-4 week-old *pGAD2::GUS* plants after staining in histochemical staining buffer, GUS staining of the guard cells was observed in all plants examined that were expressing *pGAD2::GUS*, scale bar = 5 mm (**a**) and epidermal peels from 3-4 week-old *pGAD2::GUS* leaves (**a**), scale bar = 50 μm (**b**). **c**, Reverse-transcriptional PCR quantification of *GAD2* transcripts in Arabidopsis wildtype (WT), *gad2-1*, *gad2-1/GC1::GAD2Δ* #1 and #10 plants, similar results were obtained from three independent biological replicates. **d-e**, Stomatal aperture (**d**) and density (**e**) on the leaf abaxial side of Arabidopsis WT, *gad2-1*, *gad2-*

1/GC1::GAD2Δ #1 and #10 plants; epidermal strips were peeled and incubated in stomatal measurement buffer for 1 h under light before measurement, n = 223 for WT, n = 212 for *gad2-1*, n = 197 for *gad2-1/GC1::GAD2Δ* #1 and n = 224 for *gad2-1/GC1::GAD2Δ* #10 (**d**); n = 12 leaf areas (0.57 x 0.42 mm); two areas per leaf, two leaves per plant and three plants per line were sampled (**e**). **f**, ABA accumulation in rosette leaves of 5-6 week-old Arabidopsis WT, *gad2-1*, *gad2-1/GC1::GAD2Δ* #1 and #10 plants, n = 6. **g-h**, Transpiration (**g**), photosynthetic rate (**h**) of 5-6 week-old Arabidopsis WT, *gad2-1* and *gad2-1/GC1::GAD2Δ* #10 plants in response to dark (shaded region) and 150 μmol m⁻² s⁻¹ light (white region), measured using a LiCor LI-6400XT, n = 8 for WT, n = 9 for *gad2-1* and n = 8 for *gad2-1/GC1::GAD2Δ* #10 (**g-h**). **i**, WUE of of 5-6 week-old Arabidopsis WT, *gad2-1* and *gad2-1/GC1::GAD2Δ* #10 plants was calculated based on the photosynthetic rate (**h**) against transpiration rate (**g**). All data are plotted with box and whiskers plots: whiskers plot represents minimum and maximum values, and box plot represents second quartile, median and third quartile (**d-f, i**) or data are represented mean ± s.e.m (**g, h**); statistical difference was determined by One-way ANOVA (**d-f, i**), **P* < 0.05 and *****P* < 0.0001.

a

WT
(22.2%)



GC1::GAD2Δ #2
(41.7%)



GC1::GAD2Δ #5
(78.6%)



b

WT
(77.8%)



GC1::GAD2Δ #2
(88.9%)

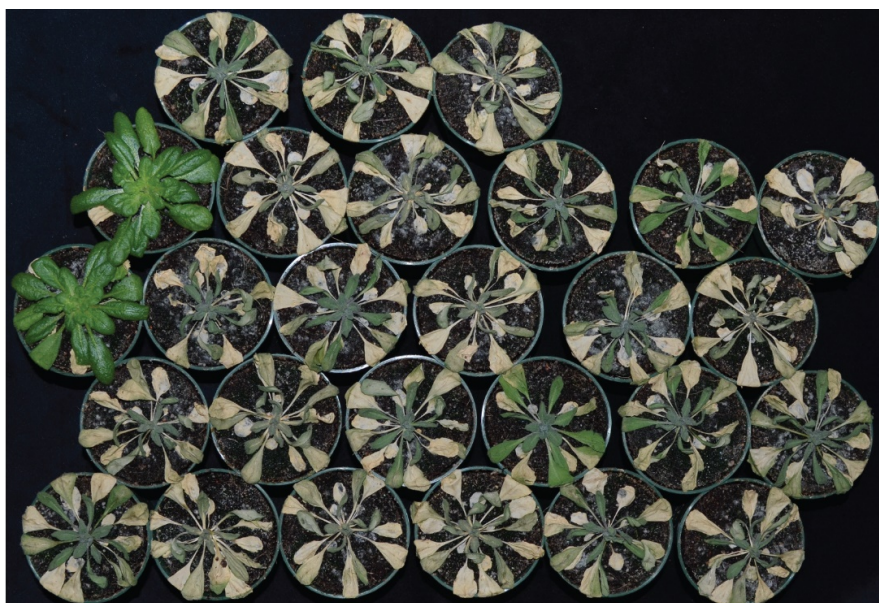


GC1::GAD2Δ #5
(88.9%)



C

WT
(11.1%)



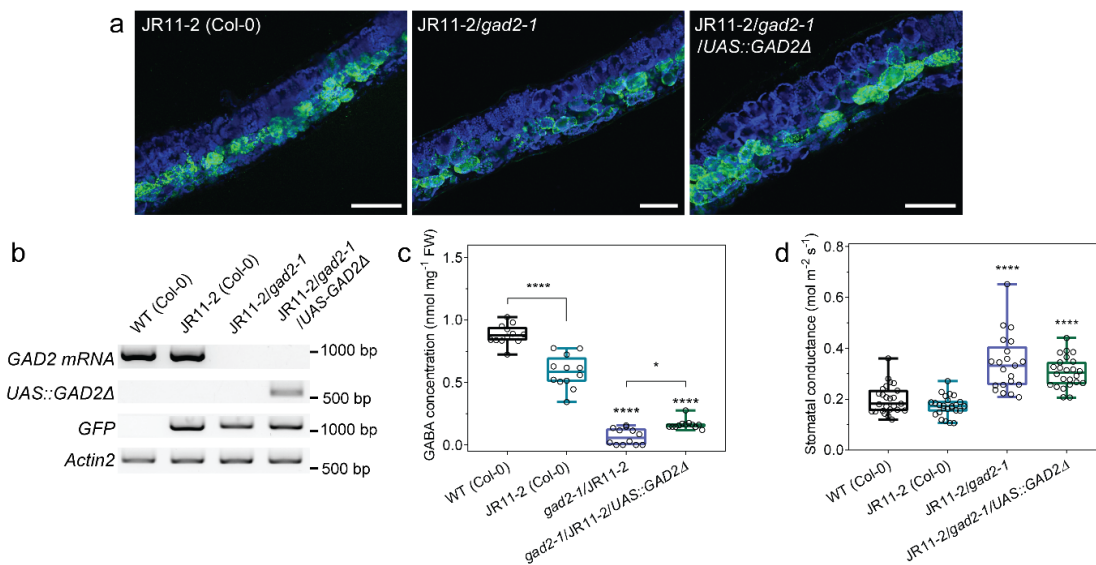
GC1::GAD2Δ #2
(19.0%)



GC1::GAD2Δ #5
(35%)

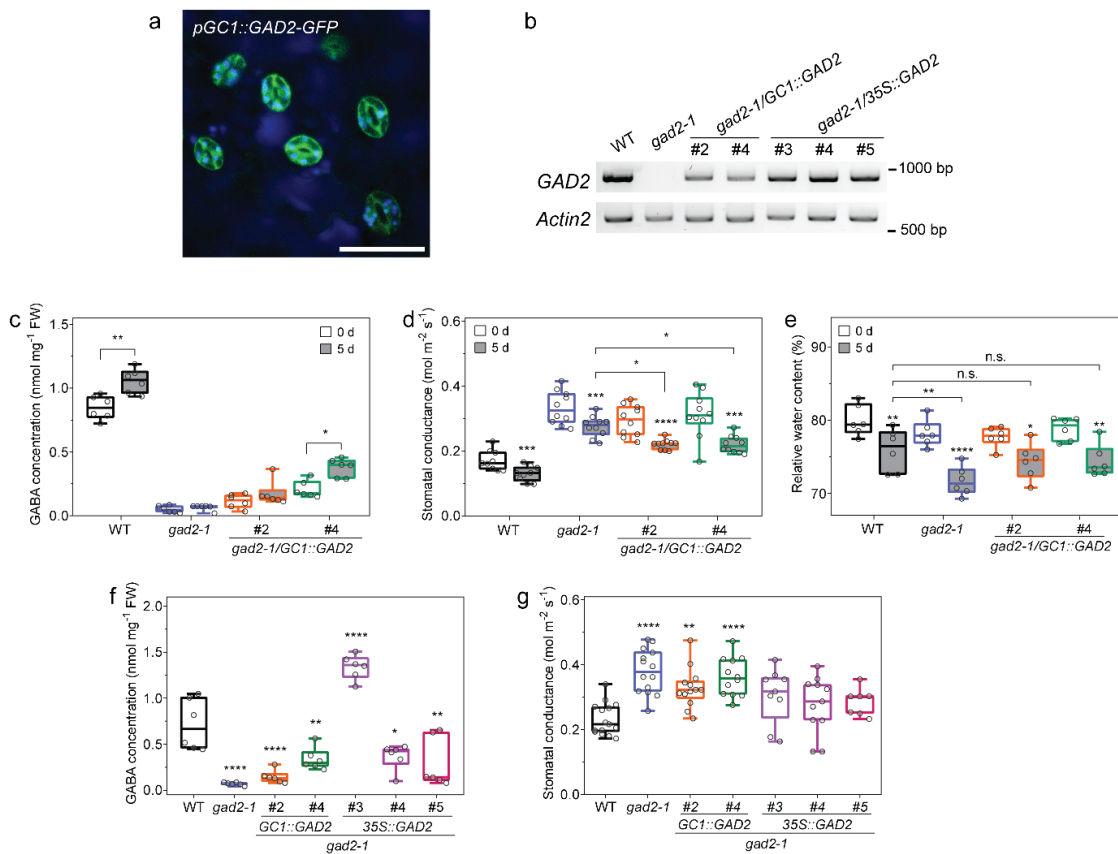


Supplementary Figure 9. Recovery of re-watered Arabidopsis WT, *GC1::GAD2Δ* #2 and #5 from drought treatment. a-c, Re-water recovery of wildtype, *GC1::GAD2Δ* #2 and #5 plants from drought in three different batches of experiments, plants were re-watered at 2 days after all plant wilting by drought. A higher recovery rate of *GC1::GAD2Δ* #2 and #5 plants than WT was observed from re-watering in all three experiments (**a-c**); 4 out of 18 (22%) wildtype, 5 out of 12 (41.7%) *GC1::GAD2Δ* #2 and 11 out of 14 (78.6%) *GC1::GAD2Δ* #5 plants were recovered from re-water in the first trail (**a**); 21 out of 27 (77.8%) wildtype, 24 out of 27 (88.9%) *GC1::GAD2Δ* #2 and 16 out of 18 (88.9%) *GC1::GAD2Δ* #5 plants were recovered from re-water in the second trail (**b**); 3 out of 27 (11.1%) wildtype, 4 out of 21 (19.0%) *GC1::GAD2Δ* #2 and 7 out of 20 (35%) *GC1::GAD2Δ* #5 plants were recovered from re-water in the third trail (**c**).



Supplementary Figure 10. Spongy mesophyll-cell specific expression of *GAD2Δ* in *gad2-1* fails to restore stomatal conductance back to wildtype (WT) levels. a, Representative images of leaf transverse cross-sections (30 μm thickness) of 3-4 week-old segregated mesophyll-specific enhancer-trap line JR11-2⁵ backcrossed into Arabidopsis Col-0 background⁶, JR11-2 in *gad2-1* background (JR11-2/*gad2-1*) and JR11-2/*gad2-1* expressing *UAS::GAD2Δ* (JR11-2/*gad2-1*/*UAS::GAD2Δ*), similar images were obtained from all examined lines, scale bars = 100 μm . GFP fluorescence shown in green indicates cells in which *GAD2* expression will be activated by the yeast transcription factor GAL4, blue indicates chlorophyll autofluorescence. **b,** Reverse-transcriptional PCR quantification of native *GAD2* mRNA (*GAD2*mRNA), *GAD2Δ* driven by *UAS* element (*UAS::GAD2Δ*), *GFP* and *Actin2* transcripts in Arabidopsis WT (Col-0), JR11-2 (Col-0), JR11-2/*gad2-1* and JR11-2/*gad2-1*/*UAS::GAD2Δ* plants, *Actin2* used as an internal control; similar results were obtained from three independent biological replicates. **c-d,** Leaf GABA concentration (**c**) and stomatal conductance (**d**) of 5-6 week-old Arabidopsis WT (Col-0), JR11-2 (Col-0), JR11-2/*gad2-1* and JR11-2/*gad2-1*/*UAS::GAD2Δ* plants, stomatal conductance was measured by AP4 Leaf Porometer (**d**); n = 12 (**c**); n = 25 for WT and JR11-2, n = 21

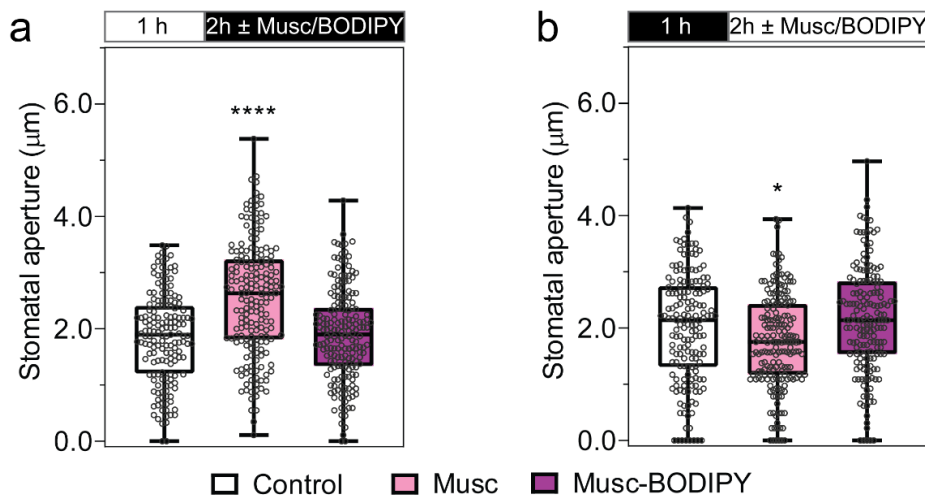
for JR11-2/*gad2-1* and $n = 24$ for JR11-2/*gad2-1/UAS::GAD2Δ*, data collected from two different batches of plants (**d**). All data are plotted with box and whiskers plots: whiskers plot represents minimum and maximum values, and box plot represents second quartile, median and third quartile (**c**, **d**); statistically differences were determined by One-way ANOVA by comparing with JR11-2 (**c**, **d**), * $P < 0.05$ and **** $P < 0.0001$.



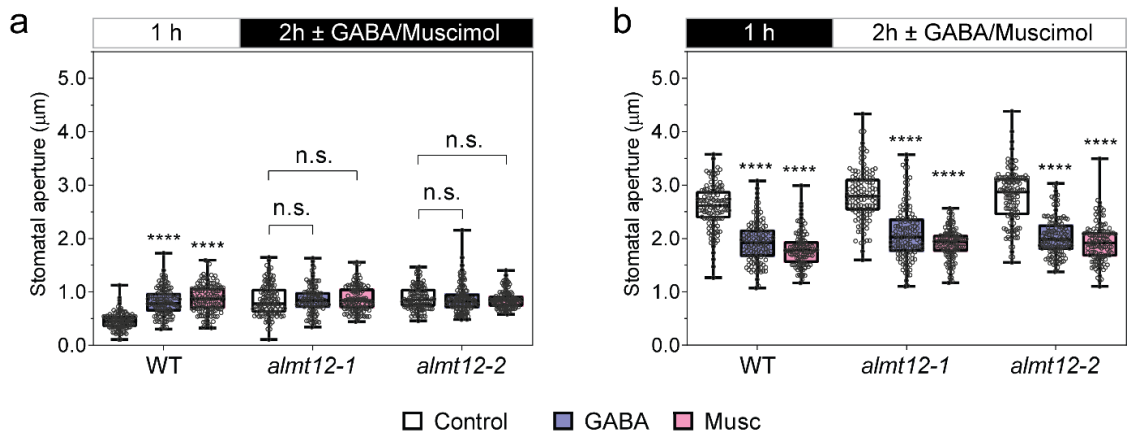
Supplementary Figure 11. Guard-cell specific expression of full-length *GAD2* only reduces the stomatal conductance of *gad2* knockout plants under drought.

a, Representative confocal image of *gad2-1* leaves expressing full-length *GAD2* tagged with *GFP* driven by *GC1* promoter (*GC1::GAD2-GFP*), similar images were obtained from all *gad2-1/ GC1::GAD2-GFP* plants examined, scale bar = 50 μm . **b**, Reverse-transcriptional PCR quantification of *GAD2* transcripts in wildtype (WT), *gad2-1* and *gad2-1* complementation with full-length *GAD2* driven by guard-cell promoter *GC1* (*gad2-1/GC1::GAD2* #2 and #4) or by a pro35S-CAMV constitutive promoter (*gad2-1/35S::GAD2* #3, #4 and #5), *Actin2* used as an internal control; similar results were obtained from three independent biological replicates. **c-e**, Leaf GABA concentration, stomatal conductance and relative water content of Arabidopsis WT, *gad2-1*, *gad2-1/GC1::GAD2* #2 and #4 plants; $n = 6$ plants for GABA measurement before (0 d) and after drought treatment for 5 days (5 d) as indicated

(c); the stomatal conductance of 5-6 week-old plants was determined by AP4 Leaf Porometer at 0 d and 5 d after drought treatment, $n = 9$ for WT and $n = 10$ for *gad2-1*, *gad2-1/GC1::GAD2* #2 and #4 (d); relative leaf water content of corresponding leaf samples at 0 d and 5 d after drought treatment, as shown in (e). f-g, Leaf GABA concentration and stomatal conductance of WT, *gad2-1*, *gad2-1/GC1::GAD2* #2, #4, *gad2-1/35S::GAD2* #3, #4 and #5 plants; $n = 6$ plants (f); the stomatal conductance of WT, *gad2-1*, and *gad2-1* complementation lines; stomatal conductance of 5-6 week-old plants was determined by AP4 Leaf Porometer in normal conditions, $n = 15$ plants for WT, $n = 14$ for *gad2-1*, $n = 13$ for *gad2-1/GC1::GAD2* #2, $n = 12$ for *gad2-1/GC1::GAD2* #4, $n = 9$ for *gad2-1/35S::GAD2* #3, $n = 11$ for *gad2-1/35S::GAD2* #4 and $n = 7$ for *gad2-1/35S::GAD2* #5 (g). All data are plotted with box and whiskers plots: whiskers plot represents minimum and maximum values, and box plot represents second quartile, median and third quartile (c-g); statistically differences were determined by One-way ANOVA by comparing with WT (f, g), or within genotypes or treatment by Two-way ANOVA (c-e), $*P < 0.05$, $**P < 0.01$, $***P < 0.001$ and $****P < 0.0001$.



Supplementary Figure 12. Membrane impermeable muscimol does not antagonises stomatal movement initiated by light and dark treatments a-b, Exogenous muscimol-BODIPY application does not affect stomatal movement. Epidermal strips were pre-incubated in stomatal measurement buffer for 1 h under light (a) or dark (b), followed by 2 h incubation under light-to-dark transition (a) or dark-to-light transition (b) as indicated above graphs by black (dark) or white (light) bars, together with the application of 10 µM muscimol (Musc) or muscimol-BODIPY (Musc-BODIPY); n = 161 for control, n = 185 for muscimol and n = 188 for muscimol-BODIPY (c); n = 168 for control, n = 190 for muscimol and n = 175 for muscimol-BODIPY. All data are plotted with box and whiskers plots: whiskers plot represents minimum and maximum values, and box plot represents second quartile, median and third quartile (a-b); statistical difference was determined by One-way ANOVA, * $P < 0.05$ and **** $P < 0.0001$.



Supplementary Figure 13. Stomatal aperture measurement of WT, *almt12-1* and

***almt12-2* knockout plants in response to dark or light.** Epidermal strips were pre-

incubated in stomatal measurement buffer for 1 h in the light (a) or dark (b), followed by 2 h incubation in the dark (a) or light (b) as indicated by black (dark) or white

(light) bars above the plots ± 2 mM GABA or 10 µM muscimol (Musc); n = 105 for

WT (control), n = 115 for *almt12-1* (control), n = 122 for *almt12-2* (control), n = 122

for WT (GABA), n = 100 for *almt12-1* (GABA), n = 131 for *almt12-2* (GABA), n = 122

for WT (Musc), n = 107 for *almt12-1* (Musc) and n = 118 for *almt12-2* (Musc) (a); n =

116 for WT (control), n = 119 for *almt12-1* (control), n = 120 for *almt12-2* (control), n

= 113 for WT (GABA), n = 123 for *almt12-1* (GABA), n = 124 for *almt12-2* (GABA), n

= 117 for WT (Musc), n = 122 for *almt12-1* (Musc) and n = 116 for *almt12-2* (Musc)

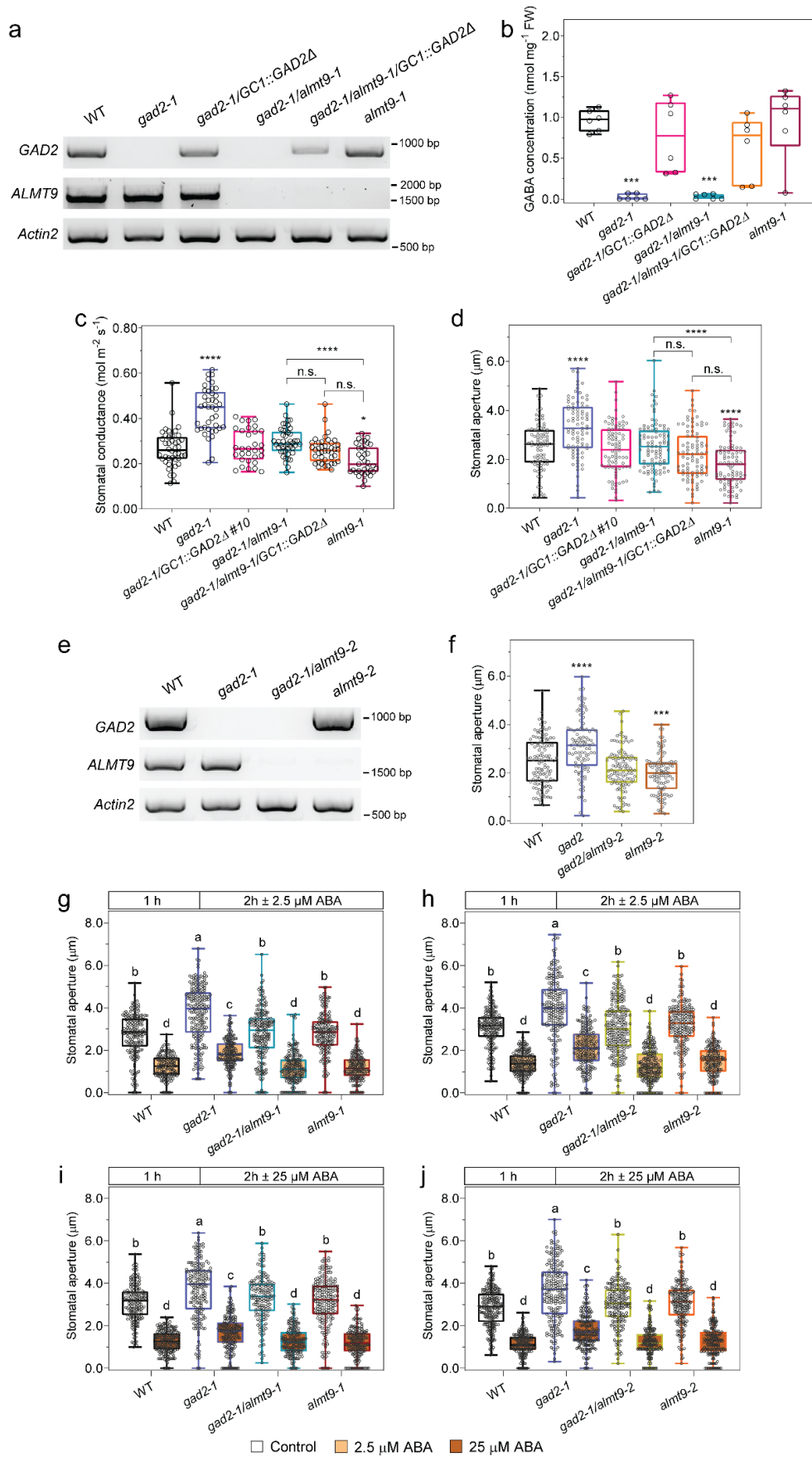
(b). All data are plotted with box and whiskers plots: whiskers plot represents

minimum and maximum values, and box plot represents second quartile, median

and third quartile; statistical difference was determined using Two-way ANOVA,

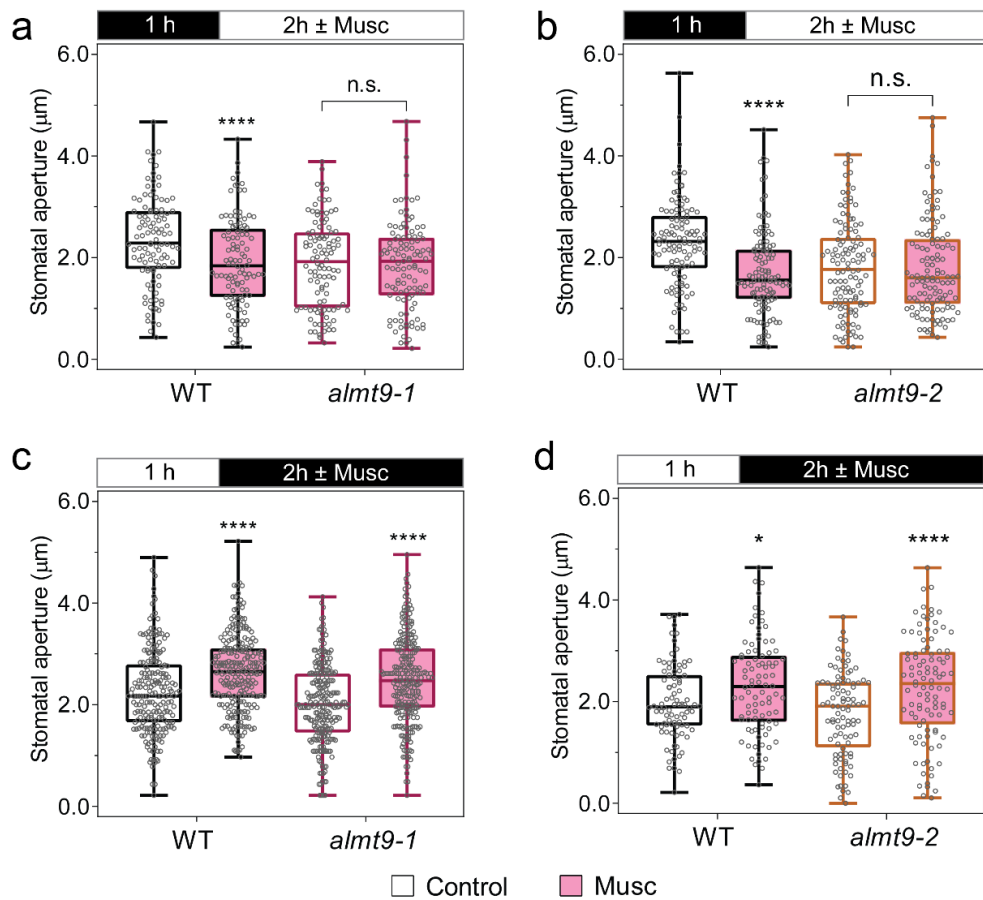
**** $P < 0.0001$; all experiments were repeated at least twice from different batches of

plants with blind treatments.



Supplementary Figure 14. The loss of *ALMT9* rescues the larger stomatal aperture and ABA response of *gad2* knockout plants. **a**, Reverse-transcriptional PCR quantification of *GAD2*, *ALMT9* and *Actin2* transcripts in Arabidopsis wildtype (WT), *gad2-1*, *gad2-1/GC1::GAD2Δ* #10, *gad2-1/alm9-1*, *gad2-1/alm9-1/GC1::GAD2Δ* and *alm9-1* plants, *Actin2* used as an internal control; similar results were obtained from three independent biological replicates. **b-d**, Leaf GABA accumulation, stomatal conductance and aperture of WT, *gad2-1*, *gad2-1/GC1::GAD2Δ* #10, *gad2-1/alm9-1*, *gad2-1/alm9-1/GC1::GAD2Δ* and *alm9-1* plants. The whole rosette leaves of 5-6 week-old plants were harvested for GABA measurement (**b**) and used for stomatal conductance measurement, as determined by AP4 porometer; n = 6 plants (**b**); n = 42 for WT, n = 40 for *gad2-1*, n = 31 for *gad2-1/GC1::GAD2Δ* #10, n = 45 for *gad2-1/alm9-1*, n = 40 for *gad2-1/alm9-1/GC1::GAD2Δ* and n = 35 for *alm9-1*, data collected from four independent batches of plants (**c**). Epidermal strips were peeled and incubated in stomatal measurement buffer for 2 h under light before measurement; n = 86 for WT, *gad2-1*, *gad2-1/GC1::GAD2Δ* #10 and *alm9-1*, n = 95 for *gad2-1/alm9-1* and n = 87 for *gad2-1/alm9-1/GC1::GAD2Δ* (**d**). **e**, Reverse-transcriptional PCR quantification of *GAD2*, *ALMT9* and *Actin2* transcripts in WT, *gad2-1*, *gad2-1/alm9-2* and *alm9-2* plants, *Actin2* used as an internal control; similar results were obtained from three independent biological replicates. **f**, Stomatal aperture of WT (n = 115), *gad2-1* (n = 100), *gad2-1/alm9-2* (n = 106) and *alm9-2* (n = 104) plants; epidermal strips were incubated under light for 2 h before measurement. **g-j**, Stomatal response to ABA of Arabidopsis wildtype (WT), *gad2-1*, *gad2-1/alm9-1*, *alm9-1*, *gad2-1/alm9-2* and *alm9-2* plants. Epidermal strips were pre-incubated in stomatal measurement buffer for 1 h under light, followed by 2 h treatment under light with or without 2.5 μM or 25 μM ABA as indicated; n = 189 (control) and n = 145 (ABA) for WT, n = 208 (control)

and n = 192 (ABA) for *gad2-1*, n = 200 (control) and n = 183 (ABA) for *gad2-1/almt9-1*, n = 182 (control) and n = 181 (ABA) for *almt9-1* (**g**); n = 184 (control) and n = 186 (GABA) for WT, n = 188 (control) and n = 207 (ABA) for *gad2-1*, n = 222 (control) and n = 224 (ABA) for *gad2-1/almt9-2*, n = 197 (control) and n = 182 (ABA) for *almt9-2* (**h**); n = 172 (control) and n = 196 (ABA) for WT, n = 190 (control) and n = 182 (ABA) for *gad2-1*, n = 162 (control) and n = 183 (ABA) for *gad2-1/almt9-1*, n = 192 (control) and n = 181 (ABA) for *almt9-1* (**i**); n = 215 (control) and n = 178 (ABA) for WT, n = 197 (control) and n = 174 (ABA) for *gad2-1*, n = 189 (control) and n = 174 (ABA) for *gad2-1/almt9-2*, n = 195 (control) and n = 180 (ABA) for *almt9-2* (**j**). All data are plotted with box and whiskers plots: whiskers plot represents minimum and maximum values, and box plot represents second quartile, median and third quartile (**b-d, f, g-i**); statistically differences were determined by One-way ANOVA, * $P < 0.05$, *** $P < 0.001$ and **** $P < 0.0001$ (**b-d, f**), or by Two-way ANOVA, a, b, c and d represent data groups that are not statistically different, $P < 0.05$ (**g-i**).



Supplementary Figure 15. *almt9* knockouts abolish muscimol-inhibition of

stomatal opening but not affect closure. a-d, Stomatal aperture of wildtype (WT)

and *almt9* knockout plants in response to dark or light. Epidermal strips were pre-

incubated in stomatal measurement buffer for 1 h under dark (a-b) or light (c-d),

followed by light (a-b) or dark (c-d) for 2 h as indicated by black (dark) or white (light)

bars above graphs, ± 10 µM muscimol (Musc); n = 105 for WT and n = 106 for *almt9*-

1 with control treatment, n = 106 for WT and n = 111 for *almt9*-1 with muscimol

treatment (a); n = 88 for wildtype (WT) (control); n = 108 for WT (control), n = 116 for

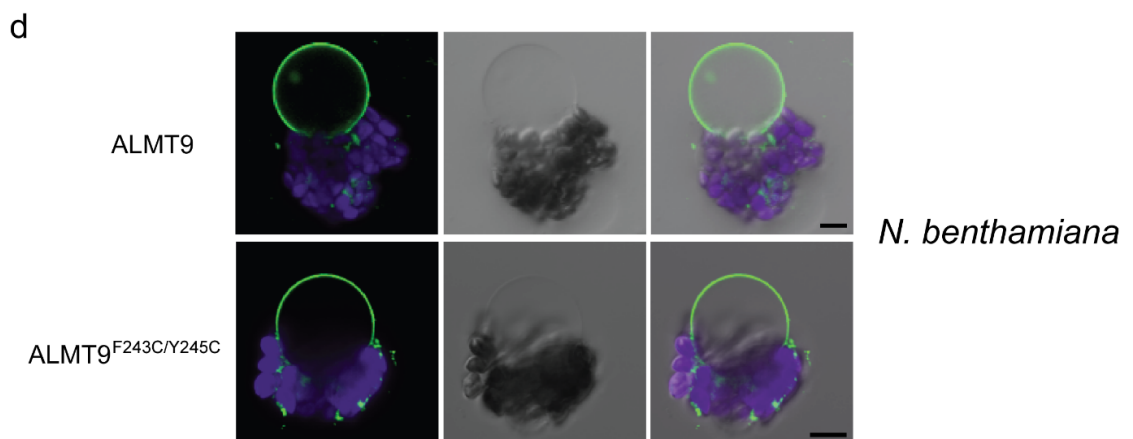
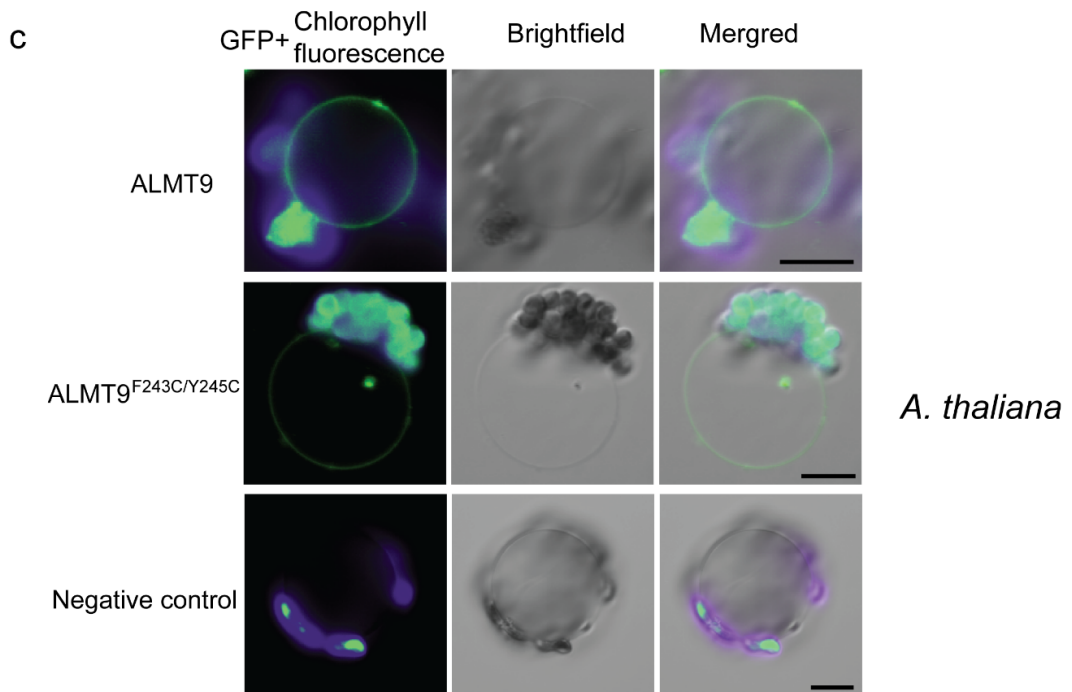
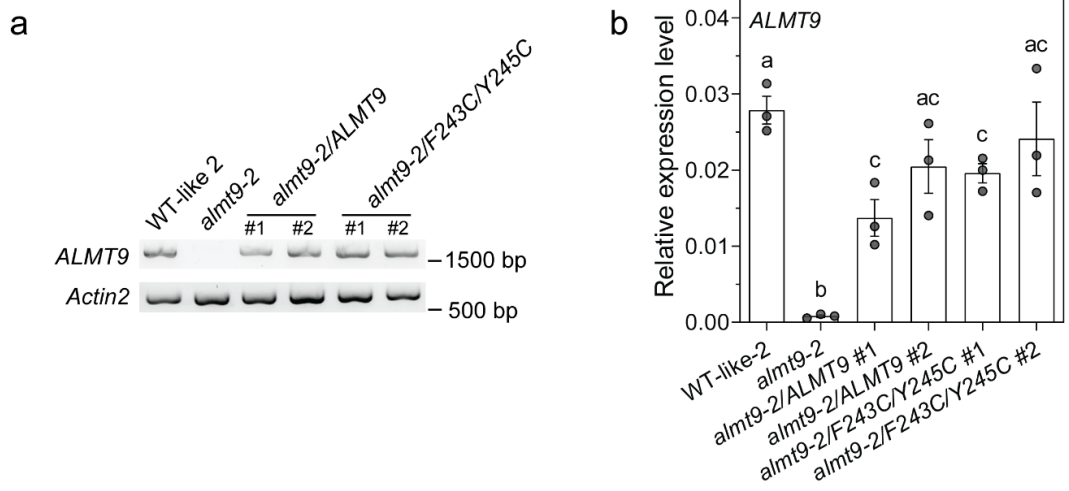
almt9-2 (control), n = 119 for WT (muscimol) and n = 121 for *almt9*-2 (muscimol) (b);

n = 210 for WT and n = 233 for *almt9*-1 with control treatment, n = 240 for WT and n

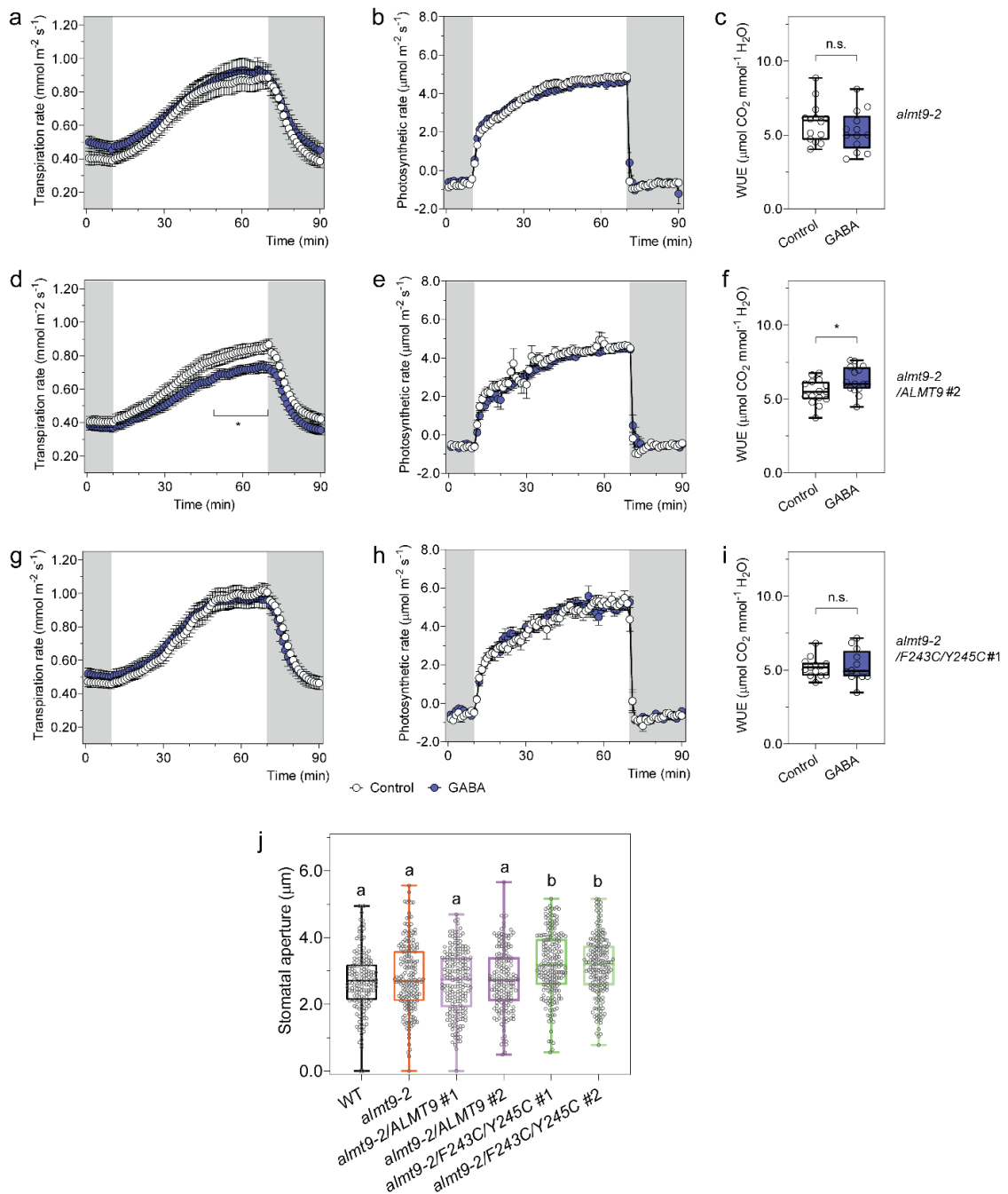
= 245 for *almt9*-1 with muscimol treatment (c); n = 88 for WT (control), n = 96 for *almt9*-

2 (control), n = 90 for WT (muscimol) and n = 100 for *almt9*-2 (muscimol) (d); all

experiments were repeated at least twice from different batches of plants with blind treatments (**a-d**). All data are plotted with box and whiskers plots: whiskers plot represents minimum and maximum values, and box plot represents second quartile, median and third quartile (**a-d**); statistically differences were determined by Two-way ANOVA (**a-d**), * $P < 0.05$ and **** $P < 0.0001$.



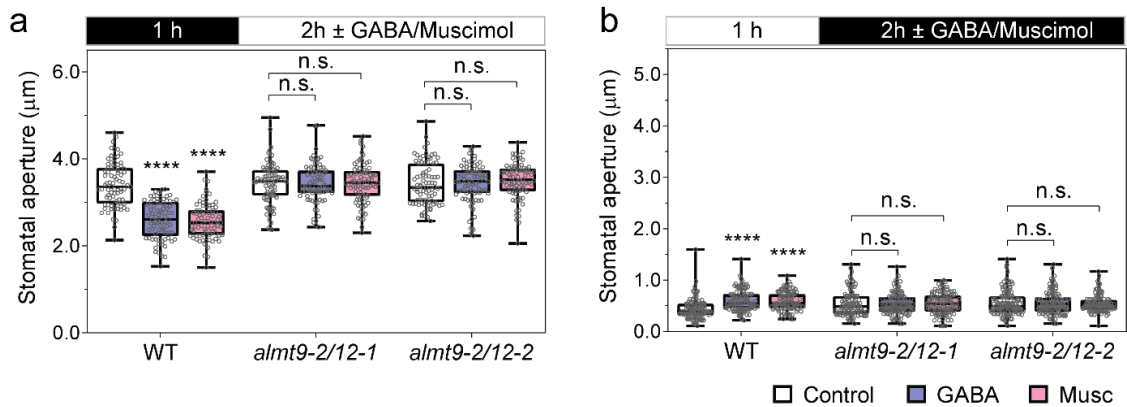
Supplementary Figure 16. *ALMT9* and *ALMT9*^{F243C/Y245C} show similar expression in *almt9-2* complementation lines and both are present on the tonoplast membrane. a-b, Reverse-transcriptional PCR (a) and quantitative real-time PCR (b) of *ALMT9* and *Actin2* transcripts in WT-like 2, *almt9-2*, *almt9-2/ALMT9* and *almt9-2/F243C/Y245C* plants. Similar results were obtained from three independent biological replicates (a); n = 3 plants and data represented by mean ± s.e.m, statistical difference was determined by two-sided Student's *t*-test, a, b and c represent data groups that are not statistically different, *P* < 0.05 (b). **c-d**, Subcellular localisation of *ALMT9* and *ALMT9*^{F243C/Y245C} in *Arabidopsis* (c) and *N. benthamiana* (d). Representative confocal image of *ALMT9* and *ALMT9*^{F243C/Y245C} tagged with GFP in the mesophyll protoplasts of *almt9-2/ALMT9* and *almt9-2/F243C/Y245C* complementation lines, repeated on 3 occasions with consistent results (c), or transiently expressed in *N. benthamiana* by *Agrobacterium* infiltration, repeated on 3 occasions with consistent results (d); the mesophyll protoplasts of wildtype (WT) *Arabidopsis* leaves were imaged as control (c), using the exact same setting to capture the fluorescence of GFP-tagged *ALMT9* and *ALMT9*^{F243C/Y245C}. The mesophyll protoplasts were prepared and lysis as described^{7, 8}, GFP fluorescence (green) and chlorophyll autofluorescence (purple) captured by Nikon A1R Laser Scanning Confocal (c, d).



Supplementary Figure 17. *ALMT9* complementation but not by *ALMT9*^{F234C/245C}.

a-i, Transpiration, photosynthetic rate and WUE of detached leaves from Arabidopsis *almt9-2* (**a-c**), *almt9-2/ALMT9 #2* (**d-f**) and *almt9-2/F243C/Y245C #1* (**g-i**) fed with artificial xylem sap solution ± 4 mM GABA using a LiCor LI-6400XT. The WUE of *almt9-2* (**c**), *almt9-2/ALMT9 #2* (**f**) and *almt9-2/F243C/Y245C #1* (**i**) was calculated the ratio of photosynthetic rate (**b, e, h**) versus transpiration rate (**a, d, g**); n = 14 (control)

and $n = 13$ (GABA) for *almt9-2* (**a-c**); $n = 15$ (control and GABA) for *almt9-2/ALMT9* #2 (**d-f**); $n = 13$ (control) and $n = 12$ (GABA) for *almt9-2/F243C/Y245C* #1 (**g-i**). **j**, Stomatal aperture of WT, *almt9-2* and complementation lines. Epidermal strips were peeled and incubated in stomatal measurement buffer for 2 h under light before measurement; $n = 164$ for WT, $n = 185$ for *almt9-2*, $n = 190$ for *almt9-2/ALMT9* #1, $n = 169$ for *almt9-2/ALMT9* #2, $n = 198$ for *almt9-2/F243C/Y245C* #1 and $n = 186$ for *almt9-2/F243C/Y245C* #2 (**j**). All data are plotted with box and whiskers plots: whiskers plot represents minimum and maximum values, and box plot represents second quartile, median and third quartile (**c, f, i, j**); or data are represented by means \pm s.e.m (**a, b, d, e, g, h**); statistically differences were determined by two-sided Student's *t*-test (**a-i**), $*P < 0.05$; or by One-way ANOVA, a and b represent data groups that are not statistically different, $P < 0.05$ (**j**).



Supplementary Figure 18. The loss of *ALMT9* and *ALMT12* impairs both stomatal opening and closure sensitivity to GABA. Epidermal strips were pre-incubated in stomatal measurement buffer for 1 h in the dark (a) or light (b), followed by 2 h incubation in the light (a) or dark (b) as indicated by black (dark) or white (light) bars above the plots ± 2 mM GABA or 10 μM muscimol (Musc); n = 78 for WT (control), n = 82 for *almt9-2/12-1* (control), n = 83 for *almt9-2/12-2* (control), n = 77 for WT (GABA), n = 77 for *almt9-2/12-1* (GABA), n = 81 for *almt9-2/12-2* (GABA), n = 75 for WT (Musc), n = 81 for *almt9-2/12-1* (Musc) and n = 81 for *almt9-2/12-2* (Musc) (a); n = 114 for WT (control), n = 104 for *almt9-2/12-1* (control), n = 120 for *almt9-2/12-2* (control), n = 113 for WT (GABA), n = 114 for *almt9-2/12-1* (GABA), n = 123 for *almt9-2/12-2* (GABA), n = 107 for WT (Musc), n = 106 for *almt9-2/12-1* (Musc) and n = 127 for *almt9-2/12-2* (Musc) (b). All data are plotted with box and whiskers plots: whiskers plot represents minimum and maximum values, and box plot represents second quartile, median and third quartile; statistical difference was determined using Two-way ANOVA, **** $P < 0.0001$; all experiments were repeated at least twice from different batches of plants with blind treatments.

References

1. Desikan R, Cheung MK, Bright J, Henson D, Hancock JT, Neill SJ. ABA, hydrogen peroxide and nitric oxide signalling in stomatal guard cells. *J Exp Bot* **55**, 205-212 (2004).
2. Melotto M, Underwood W, Koczan J, Nomura K, He SY. Plant stomata function in innate immunity against bacterial invasion. *Cell* **126**, 969-980 (2006).
3. Conn SJ, *et al.* Protocol: optimising hydroponic growth systems for nutritional and physiological analysis of *Arabidopsis thaliana* and other plants. *Plant Methods* **9**, 4 (2013).
4. Sánchez JP, Duque P, Chua NH. ABA activates ADPR cyclase and cADPR induces a subset of ABA-responsive genes in *Arabidopsis*. *Plant J* **38**, 381-395 (2004).
5. Martí MC, Stancombe MA, Webb A. Cell-and stimulus-type-specific intracellular-free Ca²⁺ signals in *Arabidopsis thaliana*. *Plant Physiol*, **163**, 625-634 (2013).
6. Svozil J, Gruissem W, Baerenfaller K. Proteasome targeting of proteins in *Arabidopsis* leaf mesophyll, epidermal and vascular tissues. *Front Plant Sci* **6**, 376 (2015).
7. De Angeli A, Zhang J, Meyer S, Martinoia E. AtALMT9 is a malate-activated vacuolar chloride channel required for stomatal opening in *Arabidopsis*. *Nat Commun* **4**, 1804 (2013).
8. Yoo S-D, Cho Y-H, Sheen J. *Arabidopsis* mesophyll protoplasts: a versatile cell system for transient gene expression analysis. *Nat Protoc* **2**, 1565 (2007).

APPENDIX



**SUPPLEMENTARY DATA OF PHYSIOLOGICAL
EXPERIMENTS**

B.1 Response speed determination of GABA treatment

Table B.1. Summary of slope calculation and analysis of covariance (ANCOVA)

Experiment	N	Measurement	Slope (R square)		Significance of slope difference
			Control	GABA	
Light-to-dark	4	Transportation rate	-0.166 (0.793)	-0.184 (0.804)	No (0.335)
		Stomatal conductance	-0.0253 (0.773)	-0.0262 (0.9)	No (0.702)
Dark-to-light	3	Transportation rate	0.402 (0.935)	0.328 (0.955)	Yes (0.0446)
		Stomatal conductance	0.0498 (0.909)	0.0362 (0.933)	Yes (0.0137)

B.2 Pilot study of GABA leaf feeding

This pilot study was done to explore the concentration of GABA that potentially equivalent to 1 mM of GABA used in stomata assay for later gas exchange assay. The experimental method was same to described in the thesis main chapter 3, section 3.3.3 and used 2 mM, 4 mM and 8 mM GABA as treatment. No water loss difference presented before and after GABA fed form 2 mM up to 8 mM GABA through 2.5 hour recording (Figure B.1).

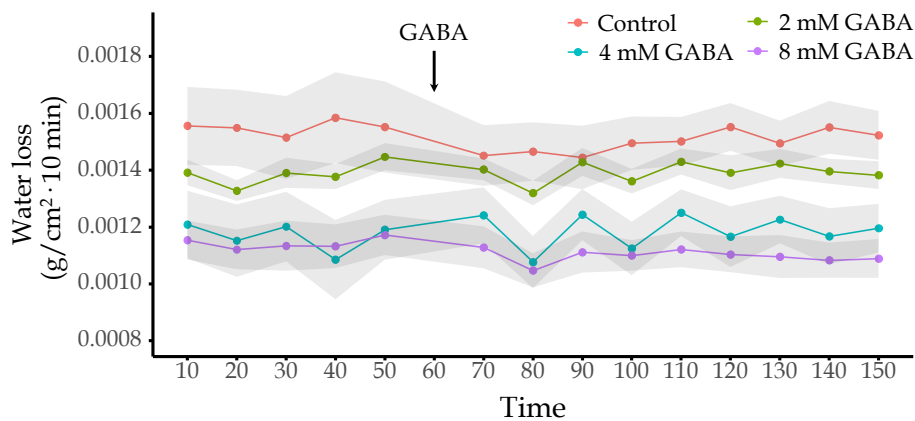


Figure B.1. Water loss assay in response to 2 mM, 4 mM and 8 mM GABA. All leaf samples were weighed sequentially every 10 minutes for an hours to monitor water loss stability, then transferred to its corresponding treatment (indicated by an arrow) and continue weighting for 1.5 hours. Data points present the mean \pm SE (gray ribbon), N = 5 in each group.

B.3 Individual experiments of GABA/ABA stomata assay

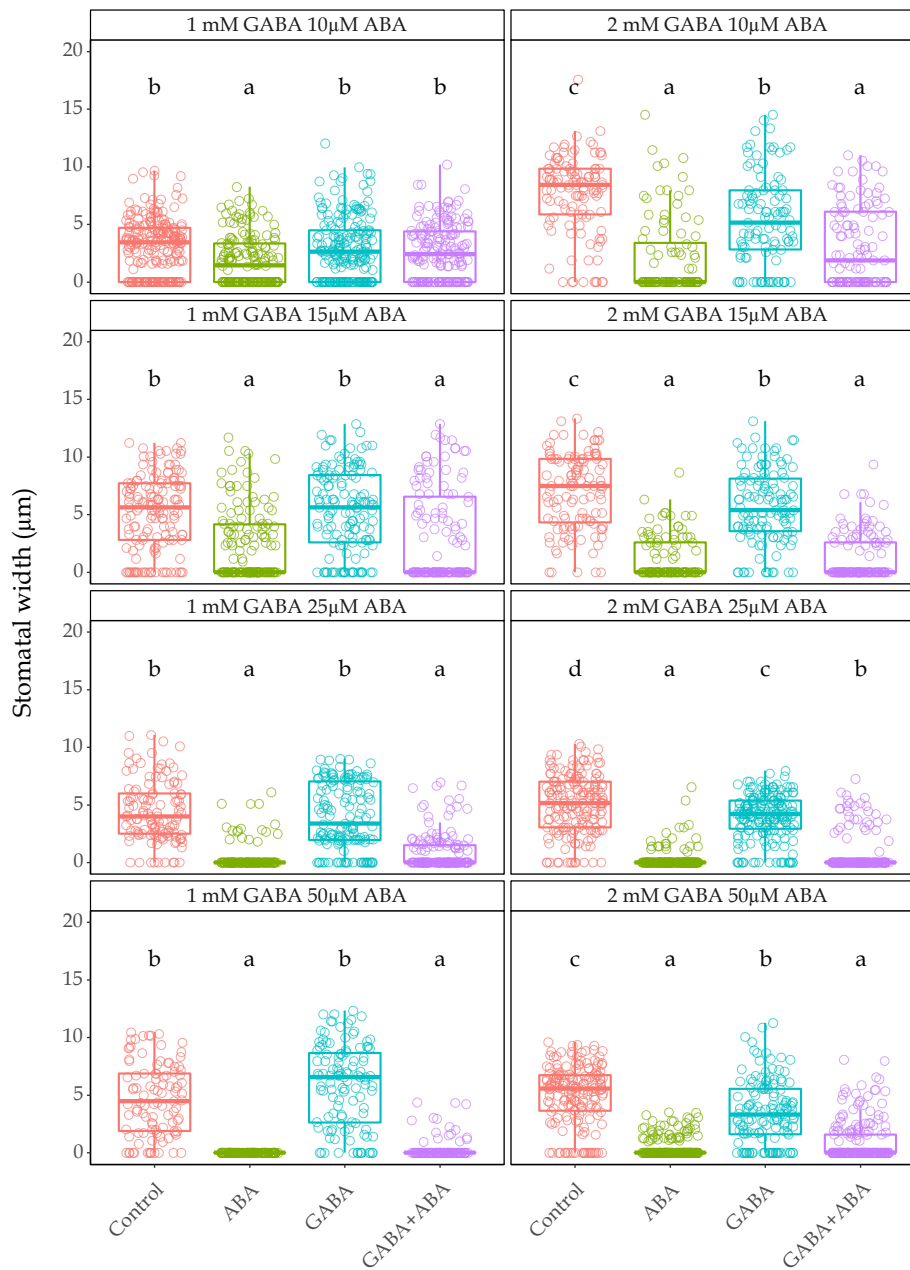


Figure B.2. Individual stomatal assay of GABA/ABA interaction. The GABA and ABA concentration combinations are 10 μM or 15 μM ABA with 1 mM GABA or 2 mM GABA. Box plots represents second quartile, median and third quartile. Over 110 stomata were measured in each group, and one-way ANOVA were performed with HSD test to determine stomatal width difference statistically; a, b, c and d represent group without significant difference, $p \leq 0.05$ per group.

Table B.2. Goodness of fit of ABA dose-response curve with GABA present

	ABA	ABA with 1 mM GABA	ABA with 2 mM GABA
EC ₅₀ (μM)	5.533	17.95	5.58
(SD)	(0.5321)	(0.6809)	(0.4142)
Degrees of Freedom	2376	1200	1162
R squared	0.3553	0.2107	0.3046
Adjusted R squared	0.3545	0.2088	0.3028
Sum of Squares	694.2	555.9	201.1
Fitting model	$Y = Bottom + (Top - Bottom)/(1 + (EC_{50}/X)^{HillSlope})$		

Note: The fitting was performed using Prism (version 9.3.0)

B.4 Individual experiments of GABA/ABA water loss assay

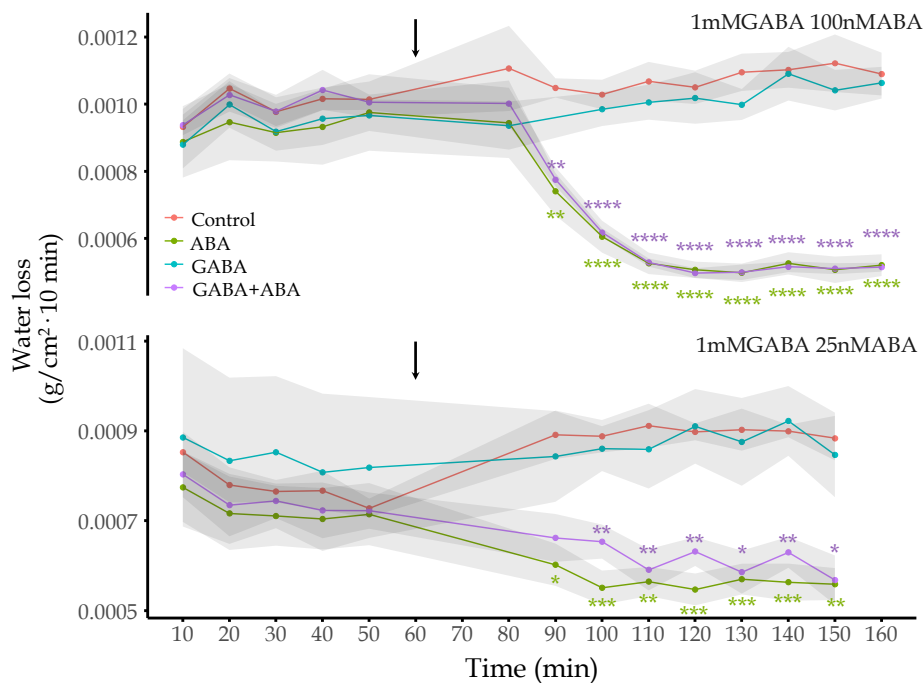


Figure B.3. Water loss assay in response to 25 nM and 100 nM ABA with 1 mM GABA. All leaf samples were weighed sequentially every 10 minutes for an hours to monitor water loss stability, then transferred to its corresponding treatment (indicated by an arrow) and continue weighting for 1.5 hours. Water loss was calculated every 10 minutes and tested with one-way ANOVA. Data represent mean \pm SE (gray ribbon). $N \geq 4$ in each group, * $p < 0.05$, ** $p < 0.01$, *** $p < 0.001$, **** $p < 0.0001$ compare to control.

B.5 ALMT protein sequence of wheat, barley and Arabidopsis

>HvALMT1 (ABQ59605) [*Hordeum vulgare*]

```

  1 MEVDHRIRVS DGDGETTAGQ GGVVAGVSFA GCWQLRSVL VGLWCWVAVF ARKVGRIARE
 61 DPRRVVHSLK VGLALTLVSV LYYVTPLFKG FGVSTMWAVL TVVVVMEYTV GGTLSKGLNR
121 AFATLVAGFI AVGAHQVANR CGAQGEPILL AIFVFFLASA ATFSRFIPEI KARYDYGVTI
181 FILTFSLVAV SSYRVEELIQ LAHQRFSTIV IGVLTCLCTT IFVFPVWAGE DLHKLTAANL
241 DKLAQFLQGL ESECFGEKAA SENLEDKAFI QVYKSVLNSK ASEDLSLNFA KWEPGHGKFG
301 FRHPWSQYQK LGALCRQCAS SMEALASYVI TLQKSQYPEA NPELTFKVRM ACGEMSSSHA
361 KALKDLSTAI RTMIVPSPAN ITMSSAIKVA KDLRNELSEI AAVLQVMHVA VTATLISDLV
421 TTIVKIAETA DNLARLGHFK NPEKTQKDVA INIAS

```

>SL19623 [*Hordeum vulgare*]

```

  1 MAAGAAGVPP AQLGSLWSTL EDQRGARGDV PLLSSAWSLP GSQAGGGDGG PKQGLLRRAG
 61 AAVAGAWGAL CDGAAEMWAF ARADPRKPVF AAKVGLALAL ISFLVFLREP RDIVSHSVWA
121 ILTVVVVFEF SIGATLSKGF NRGLGTLTAG GLALAVAELS KNLGALEEVI LIMSTFTVGF
181 MTNLAKLHPK MKPYEYGFVRV FLLTFVYVMV SGYNTGKFTD TAVSRFVLIA LGAAVSLGIN
241 IGIYPIWAGE DLHSLIAKNF AGVAKSLEGC VDGYLKCMY ERIPSKILVY QASDDPLYSG
301 YRAAVEASAQ EETLLGFIAW EPPHGPYRTR NYPWKGFTKV GGALRHCSFA VMALHGCILS
361 EIQAPPESRR VFISEIHRVG REGAKVREL GDNVKTMTKL RSSDILLEVH LAEELQKRI
421 DEKSYLLVNT ERWDTSKRAE GIKDAMNVNS AVAKENKNEV TEPTIADQTS AQHYKSFAAA
481 SFLSRYDSSA TIDGYKTLLS WPARRSFHPN LPLEDEESKT YESASALSIA TFASLLIEFV
541 ARLQNVVNAF EELSEKANFK DPVEEPVTVR VDDGGVLAKI CRSVGLKS*

```

>SL1251 [*Hordeum vulgare*]

```

  1 MACAADPSSN KNSLLILPER VKKITRIPAS WWAYAWSIGR QDQRRAIHAL KVGTAITLVS
 61 LLYILEPLFK GVGKNAMWAV MTVVVVLEFT AGATICKGLN RGFGTVIAAS LAFIIELVAV
121 RSGKVFRGFF VASSVFLIGF AATYLRFFPS IKKNYDYGVV IFLITFNLIT VSSFRQENIL
181 PLARDRLSTI AIGCAICLFM SLFVLPNWSG EDLHSCTVRK FEGLARSVEG CVNEYFGDQE
241 KHDNLLDKQT SRASIHTGYR EVLDSKSSDE SLAHYASWEP RHSMQCYSYP WQKYVKLGSV
301 LRHFAYTVAA LHGCLESEIQ TPASVRSFR NPCTRVALEV TKVLQELADS IRNHHRCDPD
361 VLCDHLHEAL QDLNSAIRSQ PRLFLGSKHG SANSRMLKEL NSSKHAASRT ALPSFKTDTI
421 SLLERKNTKA DQPSEARNERS TLGRTLKIA ITSLEFSEAL PFAAFASLLV EMVVRLELVI
481 EEVKELERAA NFKEFIQHDH LTIDITCKEK KRNGVQLSS HTVSPAEE*

```

APPENDIX B. SUPPLEMENTARY DATA OF PHYSIOLOGICAL EXPERIMENTS

>TaALMT1 (AAZ22842) [*Triticum aestivum*]

1 MDIDHGRES D GEMVGTIASC GLLLHSLLAG LGRRAAGFAR KVGGAAREDP RRVASHLKV G
61 LALALVSVVY FVTPLFNGLG VSAIWA VLT VVVMEYTVGA T LSKGLNRAL ATL VAGCIAV
121 GAHQ LAELAE RCGDQGEPI M LTVLVFFVAS AATFLRFIPE IKAKYDYGVT IFILTFGLVA
181 VSSYRVEELI QLAHQRFYTI AVGVFICLCT TVFLFPVWAG EDVHKLASGN LDKLAQFIEG
241 MEFNCFGENS VANNF GGKDF PQMHKSVLNS KATEDSLCTF AKWEPRHGQF RFRHPWSQYQ
301 KLGTLCRQCA SSMEALASYV ITTSKTQCPA AANPELSCKV RKT CGEMSLH SSKVLRDLAM
361 ATRTMTVPSP VNITMATAVK AAESLRSELA ENTALLQVMH VAVTATLLAD LVDRVKEIAE
421 CVDV LARLAH FKNPEDTKNV VVSTVSRGID EPLPDVVIL

>AtALMT9 (AEE76098) [*Arabidopsis thaliana*]

1 MAAKQGSFRH GILEKRERLL SNNGFSDFRF TDIESNDLLE NENCGRRTRL CCCSCGNLS
61 EKISGVYDDA KDVAR KAWEM GVSDPRKIVF SAKIGLALTI VALLIFYQEP NPDL SRYSVW
121 AILT VVVVFE FTIGATLSKG FN RALGTL SA GGLALGMAEL STLF GDWEEI FCTLSIFCIG
181 FLATFMKLYP SMKAYEYGF R VFL LTYCYIL ISGFRTGQFI EVAISRFLLI ALGAGVSLGV
241 NMFIYPIWAG EDLHNLVVK N FMNVATSLEG CVNGYLRCLE YERIPSKILT YQASEDPVYK
301 GYRSVESTS QEESLMSFAI WEPHPGPKS FNYPWK NYVK LSGALKHCAF TVMALHG CIL
361 SEIQAPEERR QVFRQELQRV GVEGAKLLRE LGEKVKMEK LGPVDLLFEV HLA AEELQHK
421 IDKKS YLLVN SECWEIGNRA TKESEPQELL SLEDSDPPEN HAPP IYAFKS LSEAVLEIPP
481 SWGEKNHREA LNHRPTFSKQ VSWPARLVLP PHLETTNGAS PLVETTKTYE SASALSLATF
541 ASLLIEFVAR LQNVVDAFKE LSQKANFKEP EIVTTGTDVE FSGERVGLGQ KIRRCFGM

>AtALMT12 (AEE83973) [*Arabidopsis thaliana*]

1 MSNKVHVGS L EMEEGLSKTK WMVLEPSEKI KKIPKRLWNV GKEDPRRVIH ALKVGLSLTL
61 VSLLYLMEPL FKGIGSNAIW AVMTVVVVLE FSAGATLCKG LNRGLGTLIA GSLAFFIEFV
121 ANDSGKVLRA IFIGTAVFII GAAATYIRFI PYIKKNYDYG VVIFLLTFNL ITVSSYR VDS
181 VINIAHDRFY TIAVGC GICL FMSLLVFPIW SGEDLHKTTV GKLQGLSR SI EACVDEYFEE
241 KEKEKTD SKD RIYEGYQAVL DSKSTDETLA LYANWEPRHT LRCHRFPCQQ YVKV GAVLRQ
301 FGYTVVALHG CLQTEIQTPR SVRALFKDPC VRLAGEVCKA LTELADSI SN HRHCSPEILS
361 DHLHVALQDL NSAIKSQPKL FLGSNLHRHN NKHQNGSISN NKHHQRN SSN SGKDLNGDVS
421 LQNTETGTRK ITETGSRQGG NGA VSLSSFR TDTSALMEYR RSFKNSNSEM SAAGERRMLR
481 PQLSKIAVMT SLEFSEALPF AAFASLLVEM VARLDNVIEE VEELGRIASF KEYDNKR DQT
541 ADDVRCENPA NVTISVGAAE

B.6 Hydroponic system

Table B.3. Composition of Hoagland's solution

Stock	Compound	Final concentration	Molecular weight	Amount of compound per liter	Stock concentration (mM)	Volume per liter add (mL)
A	KNO ₃	6.5 mM	101.11	82.15	812	8
	Ca(NO ₃) ₂ ·4H ₂ O	4 mM	236.16	118.08	500	
B	NH ₄ H ₂ PO ₄	0.1 mM	115.03	1.44	12.5	8
	MgSO ₄ ·7H ₂ O	2 mM	246.47	61.62	250	
C	H ₃ BO ₃	4.6 μM	61.83	0.284	4.6	1
	MnCl ₂ ·4H ₂ O	0.5 μM	197.9	0.099	0.5	
	ZnSO ₄ ·7H ₂ O	0.2 μM	287.54	0.055	0.2	
	(NH ₄) ₆ Mo ₇ O ₂₄ ·4H ₂ O	0.1 μM	1235.95	0.124	0.1	
	CuSO ₄ ·5H ₂ O	0.2 μM	249.7	0.05	0.2	
D	FeCl ₃	45 μM	162.2	36 ml of 40% w/v	45	1



**SUPPLEMENTARY DATA OF GUARD CELL ENRICHED
TRANSCRIPTIONAL RESPONSE OF GABA IN BARLEY**

C.1 R session information

R version 4.1.0 (2021-05-18)

Platform: x86_64-apple-darwin17.0 (64-bit)

Running under: macOS Big Sur 10.16

Matrix products: default

LAPACK: /Library/Frameworks/R.framework/Versions/4.1/Resources/lib/
libRlapack.dylib

locale:

[1] en_AU.UTF-8/en_AU.UTF-8/en_AU.UTF-8/C/en_AU.UTF-8/en_AU.UTF-8

attached base packages:

[1] parallel stats4 stats graphics grDevices utils
[7] datasets methods base

other attached packages:

[1] pathview_1.32.0 KEGGREST_1.32.0 scales_1.1.1
[4] annotate_1.70.0 XML_3.99-0.7 GO.db_3.13.0
[7] AnnotationDbi_1.54.1 IRanges_2.26.0 S4Vectors_0.30.0
[10] Biobase_2.52.0 BiocGenerics_0.38.0 magrittr_2.0.1
[13] forcats_0.5.1 stringr_1.4.0 dplyr_1.0.7
[16] purrr_0.3.4 readr_2.0.1 tidyr_1.1.3
[19] tibble_3.1.4 ggplot2_3.3.5 tidyverse_1.3.1
[22] edgeR_3.34.0 limma_3.48.3

loaded via a namespace (and not attached):

[1] colorspace_2.0-2 ellipsis_0.3.2 flextable_0.6.7
[4] XVector_0.32.0 base64enc_0.1-3 fs_1.5.0
[7] rstudioapi_0.13 bit64_4.0.5 fansi_0.5.0
[10] lubridate_1.7.10 xml2_1.3.2 cachem_1.0.6
[13] knitr_1.33 jsonlite_1.7.2 broom_0.7.9
[16] dbplyr_2.1.1 png_0.1-7 pheatmap_1.0.12
[19] graph_1.70.0 compiler_4.1.0 httr_1.4.2
[22] backports_1.2.1 assertthat_0.2.1 fastmap_1.1.0
[25] cli_3.0.1 htmltools_0.5.2 tools_4.1.0
[28] gtable_0.3.0 glue_1.4.2 GenomeInfoDbData_1.2.6

APPENDIX C. SUPPLEMENTARY DATA OF GUARD CELL ENRICHED
TRANSCRIPTIONAL RESPONSE OF GABA IN BARLEY

[31] reshape2_1.4.4	tinytex_0.33	Rcpp_1.0.7
[34] cellranger_1.1.0	vctr_0.3.8	Biostrings_2.60.2
[37] stargazer_5.2.2	xfun_0.25	openxlsx_4.2.4
[40] rvest_1.0.1	lifecycle_1.0.0	devEMF_4.0-2
[43] org.Hs.eg.db_3.13.0	zlibbioc_1.38.0	hms_1.1.0
[46] KEGGgraph_1.52.0	RColorBrewer_1.1-2	yaml_2.2.1
[49] export_0.3.0	memoise_2.0.0	gdtools_0.2.3
[52] stringi_1.7.4	RSQLite_2.2.8	zip_2.2.0
[55] GenomeInfoDb_1.28.2	rlang_0.4.11	pkgconfig_2.0.3
[58] systemfonts_1.0.2	bitops_1.0-7	rgl_0.107.14
[61] evaluate_0.14	lattice_0.20-44	htmlwidgets_1.5.3
[64] rvg_0.2.5	bit_4.0.4	tidyselect_1.1.1
[67] plyr_1.8.6	R6_2.5.1	generics_0.1.0
[70] DBI_1.1.1	pillar_1.6.2	haven_2.4.3
[73] withr_2.4.2	RCurl_1.98-1.4	modelr_0.1.8
[76] crayon_1.4.1	uuid_0.1-4	utf8_1.2.2
[79] tzdb_0.1.2	rmarkdown_2.10	officer_0.3.19
[82] locfit_1.5-9.4	grid_4.1.0	readxl_1.3.1
[85] data.table_1.14.0	Rgraphviz_2.36.0	blob_1.2.2
[88] reprex_2.0.1	digest_0.6.27	xtable_1.8-4
[91] munsell_0.5.0		

C.2 Data cross-validation with published data

For GCSC expression confirmation, GABA and ABA induced DE genes were compared to the Table S1 from Schäfer et al. (2018). Due to the reference genome version difference, the best hit of BLASTP alignment of Morex v2 (Camacho et al., 2009, Mascher, 2019) and barley reference assembly mentioned in Mascher et al. (2017) was used (summary in Table C.1). BLASTP result allows at most 2 top hits matched to Morex v2 protein sequence to obtain the corresponding gene ID match. Among matched genes, 1464 of ABA and 1905 of GABA induced DE genes find exactly 1 match from published dataset.

Table C.1. Amount of DE genes matched with published GCSC transcriptome data

DE genes in comparison of	Data in Chapter 4		Number of matched DE genes to Schäfer et al. (2018)
	Number of DE genes	Number of matched DE gene	
ABA vs. control	2042	1752	1885
GABA vs. control	2743	2375	2456

For ABA response cross check, ABA-induced DE genes were compared to the list of genes reported in Leonhardt et al. (2004). Because of the species difference, we link the gene id from Arabidopsis to our barley through BLASTP as mentioned above. With 151 reported ABA-induced Arabidopsis genes that has gene id, we found 24 genes matched to 38 of barley ABA-induced DE genes. All above matching data is available on GitHub (<https://github.com/CharlotteSai/BarleyGCRNASeq>).

C.3 Summary of enriched DE genes of MAPK signalling pathway

Comparison	Gene ID	logFC	Arabidopsis homologue	Araport11 description
ABA vs Control	<i>HORVU.MOREX.r2.4HG0323620</i>	3.9707	<i>AT1G07430</i>	Highly ABA-induced PP2C protein 2
	<i>HORVU.MOREX.r2.4HG0345110</i>	-3.6543	<i>AT1G09090</i>	Respiratory burst oxidase-like protein
	<i>HORVU.MOREX.r2.7HG0603990</i>	1.0007	<i>AT1G10210</i>	Mitogen-activated protein kinase 1
	<i>HORVU.MOREX.r2.1HG0045440</i>	3.2155	<i>AT1G10940</i>	SNF1-related protein kinase 2.4 (SnRK2.4)
	<i>HORVU.MOREX.r2.3HG0221890</i>	2.1568	<i>AT1G17550</i>	Homology to ABI2
	<i>HORVU.MOREX.r2.5HG0398480</i>	1.0222	<i>AT1G19230</i>	Riboflavin synthase-like superfamily protein
	<i>HORVU.MOREX.r2.6HG0477800</i>	-1.5272		
	<i>HORVU.MOREX.r2.1HG0059350</i>	1.2429	<i>AT1G64060</i>	Respiratory burst oxidase protein F
	<i>HORVU.MOREX.r2.1HG0066210</i>	2.564	<i>AT1G72770</i>	Hypersensitive to ABA1
	<i>HORVU.MOREX.r2.3HG0236180</i>	4.7953		
	<i>HORVU.MOREX.r2.4HG0328730</i>	-1.0087	<i>AT1G73500</i>	MAP kinase kinase 9
	<i>HORVU.MOREX.r2.5HG0372290</i>	1.5027	<i>AT2G25490</i>	EIN3-binding F box protein 1
	<i>HORVU.MOREX.r2.3HG0206650</i>	-2.4893	<i>AT2G26040</i>	PYR1-like 2
	<i>HORVU.MOREX.r2.4HG0318950</i>	2.4139		
	<i>HORVU.MOREX.r2.7HG0595360</i>	-2.2178	<i>AT2G29380</i>	Highly ABA-induced PP2C protein 3
	<i>HORVU.MOREX.r2.3HG0229300</i>	3.4929		
	<i>HORVU.MOREX.r2.3HG0252080</i>	2.7621		
	<i>HORVU.MOREX.r2.5HG0392330</i>	5.1048	<i>AT4G11280</i>	1-aminocyclopropane-1-carboxylic acid (acc) synthase 6
	<i>HORVU.MOREX.r2.2HG0154390</i>	1.8517		
	<i>HORVU.MOREX.r2.1HG0041310</i>	-1.2114	<i>AT4G17870</i>	Polyketide cyclase/dehydrase and lipid transport superfamily protein
<i>HORVU.MOREX.r2.7HG0555000</i>	-1.1415	<i>AT4G33720</i>	Cysteine-rich secretory proteins, Antigen 5, and Pathogenesis-related 1 protein (CAP) superfamily protein	
<i>HORVU.MOREX.r2.2HG0167340</i>	2.8554	<i>AT4G33950</i>	SNF1-related protein kinase 2.6 (SnRK2.6/OST1)	
<i>HORVU.MOREX.r2.1HG0057870</i>	-6.2532	<i>AT5G05440</i>	Polyketide cyclase/dehydrase and lipid transport superfamily protein	
<i>HORVU.MOREX.r2.2HG0089250</i>	-2.4794			
<i>HORVU.MOREX.r2.3HG0253960</i>	-4.6371			
<i>HORVU.MOREX.r2.4HG0319220</i>	-3.9479			
<i>HORVU.MOREX.r2.2HG0162190</i>	-3.1358	<i>AT5G46330</i>	Leucine-rich receptor-like protein kinase family protein	
<i>HORVU.MOREX.r2.2HG0079050</i>	6.3729	<i>AT5G51760</i>	Protein phosphatase 2C family protein	
<i>HORVU.MOREX.r2.2HG0088750</i>	1.7143	<i>AT5G62230</i>	ERECTA-like 1	
<i>HORVU.MOREX.r2.1HG0045440</i>	-2.6996	<i>AT1G10940</i>	SNF1-related protein kinase 2.4 (SnRK2.4)	
<i>HORVU.MOREX.r2.3HG0249470</i>	-1.1831			
<i>HORVU.MOREX.r2.1HG0041620</i>	1.3912	<i>AT1G32640</i>	Basic helix-loop-helix (bHLH) DNA-binding family protein	
<i>HORVU.MOREX.r2.2HG0179990</i>	-1.4213	<i>AT1G60940</i>	SNF1-related protein kinase 2.10 (SnRK2.10)	
<i>HORVU.MOREX.r2.1HG0067690</i>	1.748	<i>AT1G64060</i>	Respiratory burst oxidase protein F	
<i>HORVU.MOREX.r2.3HG0238280</i>	1.8574			
<i>HORVU.MOREX.r2.5HG0406860</i>	1.122	<i>AT1G73730</i>	Ethylene-insensitive 3-like 3	
<i>HORVU.MOREX.r2.5HG0447310</i>	-2.2584	<i>AT2G26330</i>	Leucine-rich receptor-like protein kinase family protein	
<i>HORVU.MOREX.r2.7HG0549740</i>	-1.3502			
<i>HORVU.MOREX.r2.1HG0064740</i>	2.0179	<i>AT2G32510</i>	Mitogen-activated protein kinase kinase kinase 17	

APPENDIX C. SUPPLEMENTARY DATA OF GUARD CELL ENRICHED
TRANSCRIPTIONAL RESPONSE OF GABA IN BARLEY

Continuation of Section C.3

Comparison	Gene ID	logFC	Arabidopsis homologue	Araport11 description
	<i>HORVU.MOREX.r2.1HG0064810</i>	7.2212		
	<i>HORVU.MOREX.r2.3HG0254080</i>	1.286	<i>AT2G38470</i>	WRKY DNA-binding protein 33
	<i>HORVU.MOREX.r2.1HG0043200</i>	1.9814		
	<i>HORVU.MOREX.r2.1HG0043210</i>	1.8254	<i>AT3G12500</i>	Basic chitinase
	<i>HORVU.MOREX.r2.1HG0050640</i>	-2.3435		
	<i>HORVU.MOREX.r2.5HG0431600</i>	-3.6597	<i>AT3G19690</i>	Cysteine-rich secretory proteins, Antigen 5, and Pathogenesis-related 1 protein (CAP) superfamily protein
	<i>HORVU.MOREX.r2.1HG0063880</i>	5.2978		
GABA vs Control	<i>HORVU.MOREX.r2.2HG0153890</i>	3.6695	<i>AT3G23240</i>	Ethylene response factor 1
	<i>HORVU.MOREX.r2.4HG0275980</i>	2.7159		
	<i>HORVU.MOREX.r2.1HG0012940</i>	1.3607	<i>AT3G26830</i>	Cytochrome P450 superfamily protein
	<i>HORVU.MOREX.r2.2HG0154390</i>	2.4972	<i>AT4G11280</i>	1-aminocyclopropane-1-carboxylic acid (acc) synthase 6
	<i>HORVU.MOREX.r2.7HG0555000</i>	-1.7735	<i>AT4G33720</i>	Cysteine-rich secretory proteins, Antigen 5, and Pathogenesis-related 1 protein (CAP) superfamily protein
	<i>HORVU.MOREX.r2.6HG0453490</i>	-6.6777	<i>AT4G35090</i>	Catalase 2
	<i>HORVU.MOREX.r2.4HG0341190</i>	1.4691		
	<i>HORVU.MOREX.r2.5HG0411280</i>	1.7255	<i>AT5G47910</i>	Respiratory burst oxidase protein D
	<i>HORVU.MOREX.r2.4HG0317560</i>	4.1177	<i>AT5G49480</i>	Ca ²⁺ -binding protein 1
	<i>HORVU.MOREX.r2.1HG0040530</i>	-2.431	<i>AT5G62230</i>	ERECTA-like 1

C.4 GABA induced photorespiration and carbon fixation associated genes

Comparision	GeneID	logFC	Arabidopsis Homologue	Araport11 description
GABA vs. Control	<i>HORVU.MOREX.r2.2HG0143170</i>	1.2698	<i>AT1G12900</i>	Glyceraldehyde 3-phosphate dehydrogenase A subunit 2
	<i>HORVU.MOREX.r2.3HG0258080</i>	3.4573	<i>AT1G13440</i>	Glyceraldehyde-3-phosphate dehydrogenase C2
	<i>HORVU.MOREX.r2.1HG0055260</i>	1.2234	<i>AT1G56190</i>	Phosphoglycerate kinase family protein
	<i>HORVU.MOREX.r2.1HG0029020*</i>	1.6629		
	<i>HORVU.MOREX.r2.2HG0085980*</i>	2.2066		
	<i>HORVU.MOREX.r2.2HG0086010*</i>	2.8108		
	<i>HORVU.MOREX.r2.2HG0086020*</i>	1.7642	<i>AT1G67090</i>	Ribulose biphosphate carboxylase small chain 1A
	<i>HORVU.MOREX.r2.2HG0086030*</i>	2.4883		
	<i>HORVU.MOREX.r2.2HG0086050*</i>	1.9987		
	<i>HORVU.MOREX.r2.2HG0086070*</i>	2.2942		
	<i>HORVU.MOREX.r2.2HG0086080*</i>	2.2627		
	<i>HORVU.MOREX.r2.1HG0015010</i>	2.1346		
	<i>HORVU.MOREX.r2.2HG0102880</i>	1.2286	<i>AT1G72330</i>	Alanine aminotransferase 2
	<i>HORVU.MOREX.r2.5HG0360460</i>	-1.4408		
	<i>HORVU.MOREX.r2.3HG0254340</i>	1.6395	<i>AT2G36460</i>	Aldolase superfamily protein
	<i>HORVU.MOREX.r2.3HG0258090</i>	3.369		
	<i>HORVU.MOREX.r2.6HG0490690</i>	1.5217	<i>AT3G04120</i>	Glyceraldehyde-3-phosphate dehydrogenase C subunit 1
	<i>HORVU.MOREX.r2.3HG0191310</i>	1.1187	<i>AT3G55440</i>	Triosephosphate isomerase
	<i>HORVU.MOREX.r2.4HG0325280</i>	1.5712	<i>AT4G37870</i>	Phosphoenolpyruvate carboxykinase 1
	<i>HORVU.MOREX.r2.4HG0291220</i>	1.0077	<i>AT4G38970</i>	Fructose-biphosphate aldolase 2
<i>HORVU.MOREX.r2.4HG0335670</i>	1.0438	<i>AT5G61410</i>	D-ribulose-5-phosphate-3-epimerase	

Note: * Genes are also associated to GO term photorespiration (GO:0009853) and ribulose-biphosphate carboxylase activity (GO:0016984).

References

- C. Camacho, G. Coulouris, V. Avagyan, N. Ma, J. Papadopoulos, K. Bealer, and T. L. Madden. BLAST+: architecture and applications. *BMC Bioinformatics*, 10(1):1–9, 2009.
- N. Leonhardt, J. M. Kwak, N. Robert, D. Waner, G. Leonhardt, and J. I. Schroeder. Microarray expression analyses of arabidopsis guard cells and isolation of a recessive abscisic acid hypersensitive protein phosphatase 2C mutant. *The Plant Cell*, 16(3): 596–615, 2004.
- M. Mascher. Pseudomolecules and annotation of the second version of the reference genome sequence assembly of barley cv. Morex [Morex V2], 2019.
- M. Mascher, H. Gundlach, A. Himmelbach, S. Beier, S. O. Twardziok, T. Wicker, V. Radchuk, C. Dockter, P. E. Hedley, J. Russell, M. Bayer, L. Ramsay, H. Liu, G. Haberer, X.-Q. Zhang, Q. Zhang, R. A. Barrero, L. Li, S. Taudien, M. Groth, M. Felder, A. Hastie, H. Šimková, H. Staňková, J. Vrána, S. Chan, M. Muñoz-Amatriaín, R. Ounit, S. Wanmaker, D. Bolser, C. Colmsee, T. Schmutzer, L. Aliyeva-Schnorr, S. Grasso, J. Tanskanen, A. Chailyan, D. Sampath, D. Heavens, L. Clissold, S. Cao, B. Chapman, F. Dai, Y. Han, H. Li, X. Li, C. Lin, J. K. McCooke, C. Tan, P. Wang, S. Wang, S. Yin, G. Zhou, J. A. Poland, M. I. Bellgard, L. Borisjuk, A. Houben, J. Doležel, S. Ayling, S. Lonardi, P. Kersey, P. Langridge, G. J. Muehlbauer, M. D. Clark, M. Caccamo, A. H. Schulman, K. F. X. Mayer, M. Platzer, T. J. Close, U. Scholz, M. Hansson, G. Zhang, I. Braumann, M. Spannagl, C. Li, R. Waugh, and N. Stein. A chromosome conformation capture ordered sequence of the barley genome. *Nature*, 544(7651):427–433, 2017.
- N. Schäfer, T. Maierhofer, J. Herrmann, M. E. Jørgensen, C. Lind, K. von Meyer, S. Lautner, J. Fromm, M. Felder, A. M. Hetherington, P. Ache, D. Geiger, and R. Hedrich. A tandem amino acid residue motif in guard cell SLAC1 anion channel of grasses allows for the control of stomatal aperture by nitrate. *Current Biology*, 28(9):1370 – 1379, 2018.



**SUPPLEMENTARY DATA OF TRANSCRIPTIONAL
PROFILING OF GABA DEFICIENT MUTANTS IN
*Arabidopsis thaliana***

D.1 R session information

R version 4.1.0 (2021-05-18)

Platform: x86_64-apple-darwin17.0 (64-bit)

Running under: macOS Big Sur 10.16

Matrix products: default

LAPACK: /Library/Frameworks/R.framework/Versions/4.1/Resources/lib/
libRlapack.dylib

locale:

[1] en_AU.UTF-8/en_AU.UTF-8/en_AU.UTF-8/C/en_AU.UTF-8/en_AU.UTF-8

attached base packages:

[1] stats4 parallel stats graphics grDevices utils
[7] datasets methods base

other attached packages:

[1] pathview_1.32.0	KEGGREST_1.32.0	scales_1.1.1
[4] annotate_1.70.0	XML_3.99-0.7	GO.db_3.13.0
[7] AnnotationDbi_1.54.1	IRanges_2.26.0	S4Vectors_0.30.0
[10] Biobase_2.52.0	BiocGenerics_0.38.0	magrittr_2.0.1
[13] forcats_0.5.1	stringr_1.4.0	dplyr_1.0.7
[16] purrr_0.3.4	readr_2.0.1	tidyr_1.1.3
[19] tibble_3.1.4	ggplot2_3.3.5	tidyverse_1.3.1
[22] biomaRt_2.48.3	edgeR_3.34.0	limma_3.48.3

loaded via a namespace (and not attached):

[1] colorspace_2.0-2	ellipsis_0.3.2	flextable_0.6.7
[4] XVector_0.32.0	base64enc_0.1-3	fs_1.5.0
[7] rstudioapi_0.13	bit64_4.0.5	fansi_0.5.0
[10] lubridate_1.7.10	xml2_1.3.2	cachem_1.0.6
[13] knitr_1.33	jsonlite_1.7.2	broom_0.7.9
[16] dbplyr_2.1.1	png_0.1-7	pheatmap_1.0.12
[19] graph_1.70.0	compiler_4.1.0	httr_1.4.2
[22] backports_1.2.1	assertthat_0.2.1	fastmap_1.1.0
[25] cli_3.0.1	htmltools_0.5.2	prettyunits_1.1.1
[28] tools_4.1.0	gtable_0.3.0	glue_1.4.2

APPENDIX D. SUPPLEMENTARY DATA OF TRANSCRIPTIONAL PROFILING OF GABA DEFICIENT MUTANTS IN *ARABIDOPSIS THALIANA*

[31]	GenomeInfoDbData_1.2.6	reshape2_1.4.4	rappdirs_0.3.3
[34]	tinytex_0.33	Rcpp_1.0.7	cellranger_1.1.0
[37]	vctrs_0.3.8	Biostrings_2.60.2	stargazer_5.2.2
[40]	xfun_0.25	openxlsx_4.2.4	rvest_1.0.1
[43]	lifecycle_1.0.0	devEMF_4.0-2	org.Hs.eg.db_3.13.0
[46]	zlibbioc_1.38.0	hms_1.1.0	KEGGgraph_1.52.0
[49]	RColorBrewer_1.1-2	yaml_2.2.1	curl_4.3.2
[52]	export_0.3.0	memoise_2.0.0	gdtools_0.2.3
[55]	stringi_1.7.4	RSQLite_2.2.8	filelock_1.0.2
[58]	zip_2.2.0	GenomeInfoDb_1.28.2	rlang_0.4.11
[61]	pkgconfig_2.0.3	systemfonts_1.0.2	bitops_1.0-7
[64]	rgl_0.107.14	evaluate_0.14	lattice_0.20-44
[67]	rvg_0.2.5	htmlwidgets_1.5.3	bit_4.0.4
[70]	tidyselect_1.1.1	plyr_1.8.6	R6_2.5.1
[73]	generics_0.1.0	DBI_1.1.1	pillar_1.6.2
[76]	haven_2.4.3	withr_2.4.2	RCurl_1.98-1.4
[79]	modelr_0.1.8	crayon_1.4.1	uuid_0.1-4
[82]	utf8_1.2.2	BiocFileCache_2.0.0	tzdb_0.1.2
[85]	rmarkdown_2.10	officer_0.3.19	progress_1.2.2
[88]	locfit_1.5-9.4	grid_4.1.0	readxl_1.3.1
[91]	data.table_1.14.0	Rgraphviz_2.36.0	blob_1.2.2
[94]	reprex_2.0.1	digest_0.6.27	xtable_1.8-4
[97]	munsell_0.5.0		

D.2 Summary of nutrient starvation directly related DE genes in *gad1*-Col-0 comparison with its other GO functions

Gene ID	GO terms	Description	Ontology
<i>AT1G21400</i>	GO:0003863	3-methyl-2-oxobutanoate dehydrogenase (2-methylpropanoyl-transferring) activity	MF
	GO:0005759	Mitochondrial matrix	CC
	GO:0005947	Mitochondrial alpha-ketoglutarate dehydrogenase complex	CC
	GO:0009083	Branched-chain amino acid catabolic process	BP
	GO:0009646	Response to absence of light	BP
	GO:0009744	Response to sucrose	BP
	GO:0016624	Oxidoreductase activity, acting on the aldehyde or oxo group of donors, disulfide as acceptor	MF
	GO:0043617	Cellular response to sucrose starvation	BP
	GO:0046872	Metal ion binding	MF
<i>AT1G64660</i>	GO:0004123	Cystathionine gamma-lyase activity	MF
	GO:0009970	Cellular response to sulfate starvation	BP
	GO:0018826	Methionine gamma-lyase activity	MF
	GO:0019343	Cysteine biosynthetic process via cystathionine	BP
	GO:0019346	Transsulfuration	BP
	GO:0019458	Methionine catabolic process via 2-oxobutanoate	BP
	GO:0030170	Pyridoxal phosphate binding	MF
	GO:0042631	Cellular response to water deprivation	BP
GO:0051289	Protein homotetramerization	BP	
<i>AT1G69480</i>	GO:0005802	Trans-golgi network	CC
	GO:0006817	Phosphate ion transport	BP
	GO:0015114	Phosphate ion transmembrane transporter activity	MF
	GO:0016036	Cellular response to phosphate starvation	BP
	GO:0035435	Phosphate ion transmembrane transport	BP
<i>AT1G73010</i>	GO:0004427	Inorganic diphosphatase activity	MF
	GO:0016036	Cellular response to phosphate starvation	BP
	GO:0016311	Dephosphorylation	BP
	GO:0016462	Pyrophosphatase activity	MF
	GO:0016791	Phosphatase activity	MF
	GO:0046872	Metal ion binding	MF
	GO:0051262	Protein tetramerization	BP
	GO:0071456	Cellular response to hypoxia	BP
<i>AT1G74020</i>	GO:0005774	Vacuolar membrane	CC
	GO:0009753	Response to jasmonic acid	BP
	GO:0009820	Alkaloid metabolic process	BP
	GO:0016844	Strictosidine synthase activity	MF
	GO:0051365	Cellular response to potassium ion starvation	BP
<i>AT2G02990</i>	GO:0003723	RNA binding	MF
	GO:0004518	Nuclease activity	MF
	GO:0004519	Endonuclease activity	MF
	GO:0004521	Endoribonuclease activity	MF
	GO:0006401	RNA catabolic process	BP
	GO:0009718	Anthocyanin-containing compound biosynthetic process	BP
	GO:0016036	Cellular response to phosphate starvation	BP
	GO:0033897	Ribonuclease t2 activity	MF
	GO:0090305	Nucleic acid phosphodiester bond hydrolysis	BP
	GO:0090501	RNA phosphodiester bond hydrolysis	BP
GO:0090502	RNA phosphodiester bond hydrolysis, endonucleolytic	BP	

APPENDIX D. SUPPLEMENTARY DATA OF TRANSCRIPTIONAL PROFILING OF GABA DEFICIENT MUTANTS IN *ARABIDOPSIS THALIANA*

Continuation of Section D.2

Gene ID	GO terms	Description	Ontology
<i>AT2G47190</i>	GO:0000976	Transcription regulatory region sequence-specific DNA binding	MF
	GO:0000978	RNA polymerase ii cis-regulatory region sequence-specific DNA binding	MF
	GO:0003677	DNA binding	MF
	GO:0005634	Nucleus	CC
	GO:0006355	Regulation of transcription, DNA-templated	BP
	GO:0009651	Response to salt stress	BP
	GO:0009737	Response to abscisic acid	BP
	GO:0016036	Cellular response to phosphate starvation	BP
	GO:0043565	Sequence-specific DNA binding	MF
	GO:0045893	Positive regulation of transcription, DNA-templated	BP
<i>AT2G47880</i>	GO:0005634	Nucleus	CC
	GO:0006995	Cellular response to nitrogen starvation	BP
	GO:0015035	Protein disulfide oxidoreductase activity	MF
<i>AT3G06420</i>	GO:0000421	Autophagosome membrane	CC
	GO:0005774	Vacuolar membrane	CC
	GO:0005856	Cytoskeleton	CC
	GO:0005874	Microtubule	CC
	GO:0006995	Cellular response to nitrogen starvation	BP
	GO:0015031	Protein transport	BP
<i>AT3G47340</i>	GO:0004066	Asparagine synthase (glutamine-hydrolyzing) activity	MF
	GO:0006529	Asparagine biosynthetic process	BP
	GO:0006541	Glutamine metabolic process	BP
	GO:0008652	Cellular amino acid biosynthetic process	BP
	GO:0009063	Cellular amino acid catabolic process	BP
	GO:0009646	Response to absence of light	BP
	GO:0009744	Response to sucrose	BP
	GO:0009749	Response to glucose	BP
	GO:0009750	Response to fructose	BP
	GO:0043617	Cellular response to sucrose starvation	BP
GO:0070981	L-asparagine biosynthetic process	BP	
<i>AT4G04620</i>	GO:0000421	Autophagosome membrane	CC
	GO:0005774	Vacuolar membrane	CC
	GO:0005856	Cytoskeleton	CC
	GO:0005874	Microtubule	CC
	GO:0006995	Cellular response to nitrogen starvation	BP
	GO:0015031	Protein transport	BP
<i>AT4G21980</i>	GO:0000421	Autophagosome membrane	CC
	GO:0005774	Vacuolar membrane	CC
	GO:0005776	Autophagosome	CC
	GO:0005856	Cytoskeleton	CC
	GO:0005874	Microtubule	CC
	GO:0006508	Proteolysis	BP
	GO:0006995	Cellular response to nitrogen starvation	BP
	GO:0015031	Protein transport	BP
	GO:0018215	Protein phosphopantetheinylation	BP
	GO:0019779	Atg8 activating enzyme activity	MF
	GO:0019786	Atg8-specific protease activity	MF
GO:0050832	Defense response to fungus	BP	
<i>AT5G03545</i>	GO:0006817	Phosphate ion transport	BP
	GO:0016036	Cellular response to phosphate starvation	BP

Note: Direct related gene ontology of DE genes were obtained at least 4 levels away from the root ontology categories (i.e. biological process (BP), cellular component (CC) and molecular function (MF)).

D.3 Direct related gene ontology of DE genes in *gad1245-gad2-1* comparison

Gene ID	GO terms	Description	Ontology
<i>AT1G28050</i>	GO:0046872	Metal ion binding	MF
	GO:0005634	Nucleus	CC
	GO:0008270	Zinc ion binding	MF
	GO:0006355	Regulation of transcription, DNA-templated	BP
<i>AT1G72430</i>	GO:0005634	Nucleus	CC
	GO:0009733	Response to auxin	BP
	GO:0009873	Ethylene-activated signaling pathway	BP
	GO:0071456	Cellular response to hypoxia	BP
<i>AT2G26170</i>	GO:0046872	Metal ion binding	MF
	GO:0005506	Iron ion binding	MF
	GO:0016117	Carotenoid biosynthetic process	BP
	GO:0009963	Positive regulation of flavonoid biosynthetic process	BP
	GO:0009926	Auxin polar transport	BP
	GO:0009934	Regulation of meristem structural organization	BP
<i>AT2G39920</i>	GO:0046686	Response to cadmium ion	BP
<i>AT3G09600</i>	GO:0003677	DNA binding	MF
	GO:0005634	Nucleus	CC
	GO:0006355	Regulation of transcription, DNA-templated	BP
	GO:0043565	Sequence-specific DNA binding	MF
	GO:0045944	Positive regulation of transcription by RNA polymerase II	BP
	GO:0010628	Positive regulation of gene expression	BP
	GO:0043966	Histone H3 acetylation	BP
<i>AT3G16320</i>	GO:0005634	Nucleus	CC
	GO:0016567	Protein ubiquitination	BP
	GO:0005680	Anaphase-promoting complex	CC
	GO:0031145	Anaphase-promoting complex-dependent catabolic process	BP
	GO:0007091	Metaphase/anaphase transition of mitotic cell cycle	BP
	GO:0045842	Positive regulation of mitotic metaphase/anaphase transition	BP
<i>AT3G27540</i>	GO:0003830	Beta-1,4-mannosylglycoprotein 4-beta-N-acetylglucosaminyltransferase activity	MF
	GO:0006487	Protein n-linked glycosylation	BP
	GO:0006044	N-acetylglucosamine metabolic process	BP
	GO:0018215	Protein phosphopantetheinylation	BP
<i>AT4G03400</i>	GO:0009507	Chloroplast	CC
	GO:0016881	Acid-amino acid ligase activity	MF
	GO:0009416	Response to light stimulus	BP
<i>AT4G15800</i>	GO:0019722	Calcium-mediated signaling	BP
	GO:0005179	Hormone activity	MF
	GO:0009505	Plant-type cell wall	CC
<i>AT4G26150</i>	GO:0009739	Response to gibberellin	BP
	GO:0043565	Sequence-specific DNA binding	MF
	GO:0006355	Regulation of transcription, DNA-templated	BP
	GO:0046872	Metal ion binding	MF
	GO:0003677	DNA binding	MF
	GO:0005634	Nucleus	CC
	GO:0008270	Zinc ion binding	MF
	GO:0009740	Gibberellic acid mediated signaling pathway	BP
	GO:0009736	Cytokinin-activated signaling pathway	BP
	GO:0010167	Response to nitrate	BP
	GO:0009733	Response to auxin	BP

APPENDIX D. SUPPLEMENTARY DATA OF TRANSCRIPTIONAL PROFILING OF GABA DEFICIENT MUTANTS IN *ARABIDOPSIS THALIANA*

Continuation of Section D.3

Gene ID	GO terms	Description	Ontology
<i>AT4G26150</i>	GO:0010468	Regulation of gene expression	BP
	GO:0009416	Response to light stimulus	BP
	GO:0009658	Chloroplast organization	BP
	GO:0010151	Chloroplast elongation	BP
	GO:1902326	Positive regulation of chlorophyll biosynthetic process	BP
	GO:0010380	Regulation of chlorophyll biosynthetic process	BP
	GO:0009938	Negative regulation of gibberellic acid mediated signaling pathway	BP
	GO:0010114	Response to red light	BP
	GO:0009735	Response to cytokinin	BP
	GO:0000976	Transcription regulatory region sequence-specific DNA binding	MF
<i>AT5G03380</i>	GO:0046872	Metal ion binding	MF
	GO:0030001	Metal ion transport	BP
	GO:0071456	Cellular response to hypoxia	BP
<i>AT5G37770</i>	GO:0046872	Metal ion binding	MF
	GO:0005509	Calcium ion binding	MF
	GO:0009733	Response to auxin	BP
	GO:0010038	Response to metal ion	BP
	GO:0009737	Response to abscisic acid	BP
	GO:0080164	Regulation of nitric oxide metabolic process	BP
	GO:0051592	Response to calcium ion	BP
	GO:0042542	Response to hydrogen peroxide	BP
	GO:0009646	Response to absence of light	BP
<i>AT5G39410</i>	GO:0005811	Lipid droplet	CC
	GO:0031966	Mitochondrial membrane	CC
	GO:0009247	Glycolipid biosynthetic process	BP
	GO:0005774	Vacuolar membrane	CC
	GO:0009941	Chloroplast envelope	CC
<i>AT5G60100</i>	GO:0000160	Phosphorelay signal transduction system	BP
	GO:0005634	Nucleus	CC
	GO:0032091	Negative regulation of protein binding	BP
	GO:0006355	Regulation of transcription, DNA-templated	BP
<i>AT5G65920</i>	GO:0004842	Ubiquitin-protein transferase activity	MF
	GO:0016567	Protein ubiquitination	BP

Note: Direct related gene ontology of DE genes were obtained at least 4 levels away from the root ontology categories (i.e. biological process (BP), cellular component (CC) and molecular function (MF)).

APPENDIX



SUPPLEMENTARY DATA OF SAI

E.1 Supplementary data of Average-Human/Machine Test

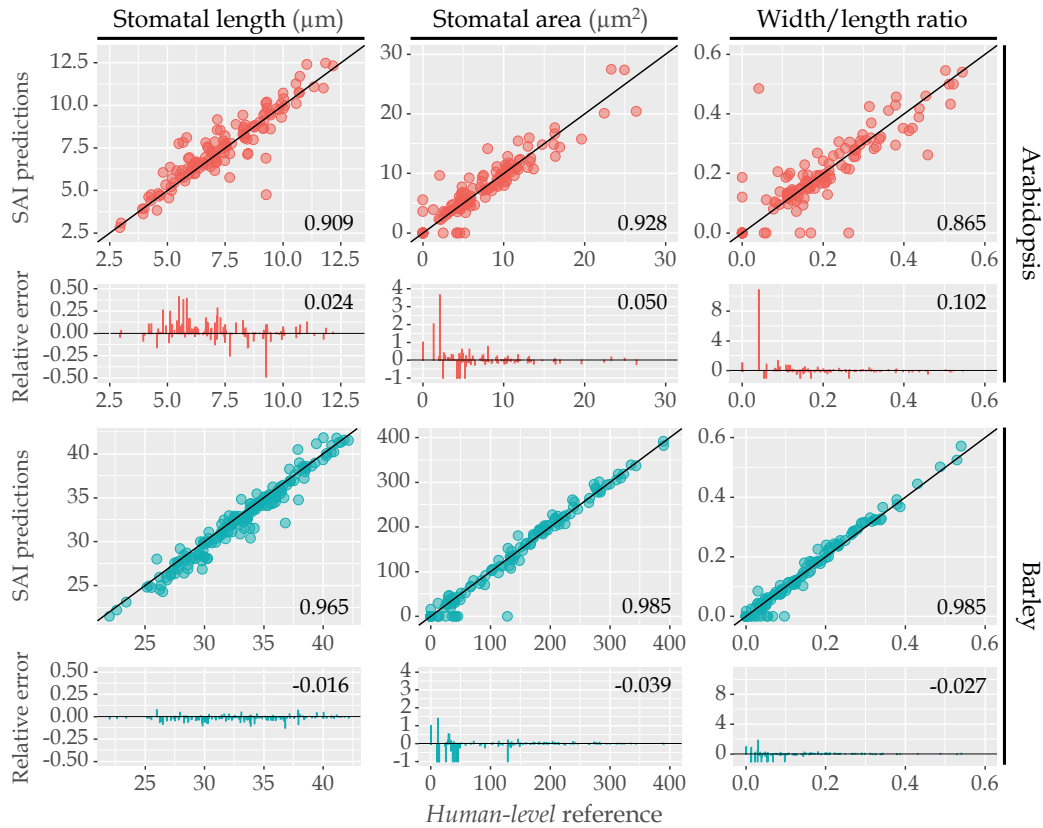
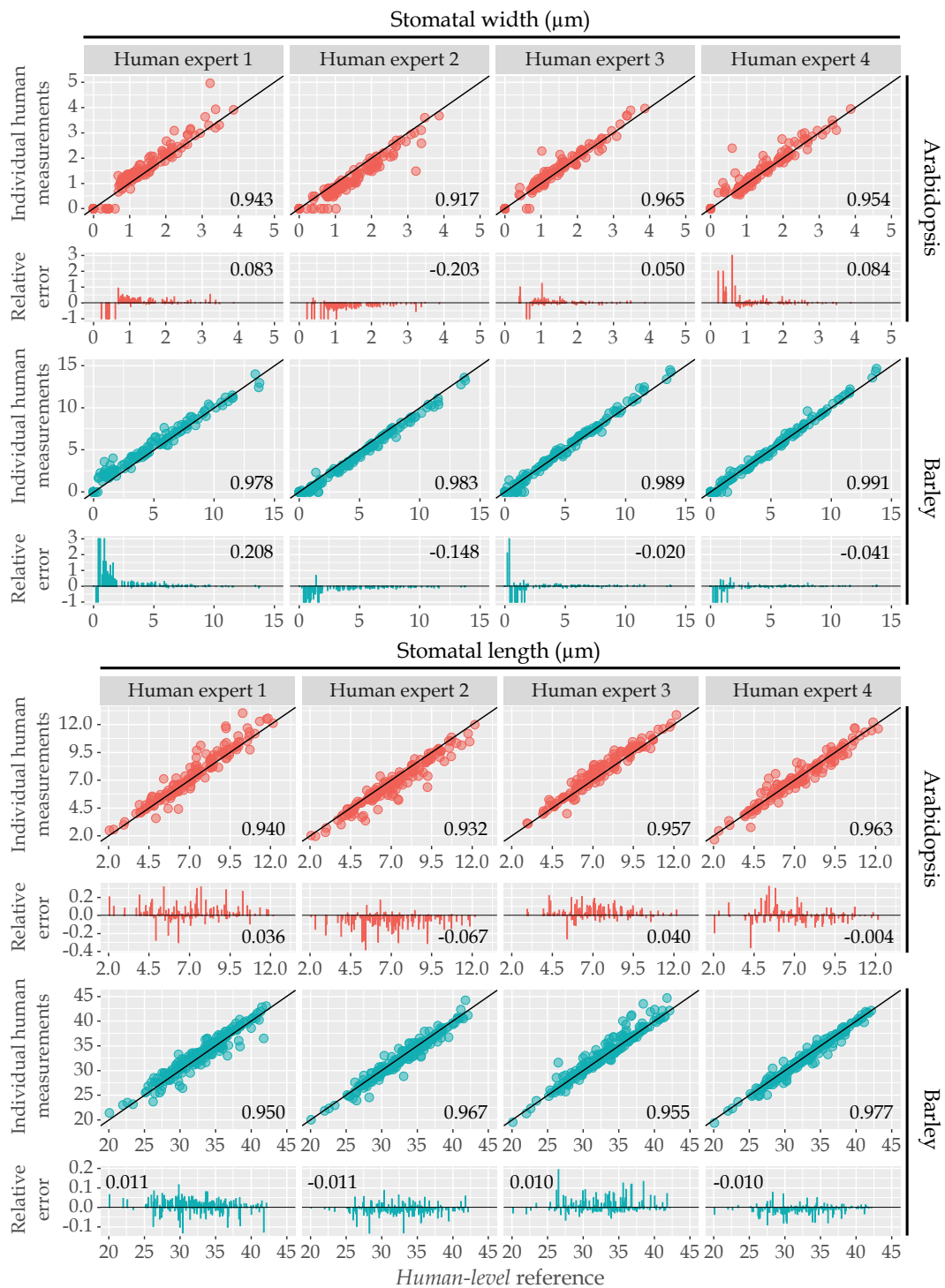


Figure E.1. SAI prediction vs human-level reference set for Arabidopsis and barley stomatal length (μm), area (μm^2) and width/length ratio. Measurements from 4 human experts on stomata morphology were collected and average length and area of each stoma were calculated as the human-level reference. SAI is compared against the reference and the concordance correlation coefficient (ranging from -1 to 1) were calculated as the determination of the accuracy performance. The corresponding relative error (RE) to human-level reference was displayed on the corresponding sub-figure with mean RE calculated. Data points are colour coded according to annotation label. (Arabidopsis: $N > 120$, barley: $N > 160$)



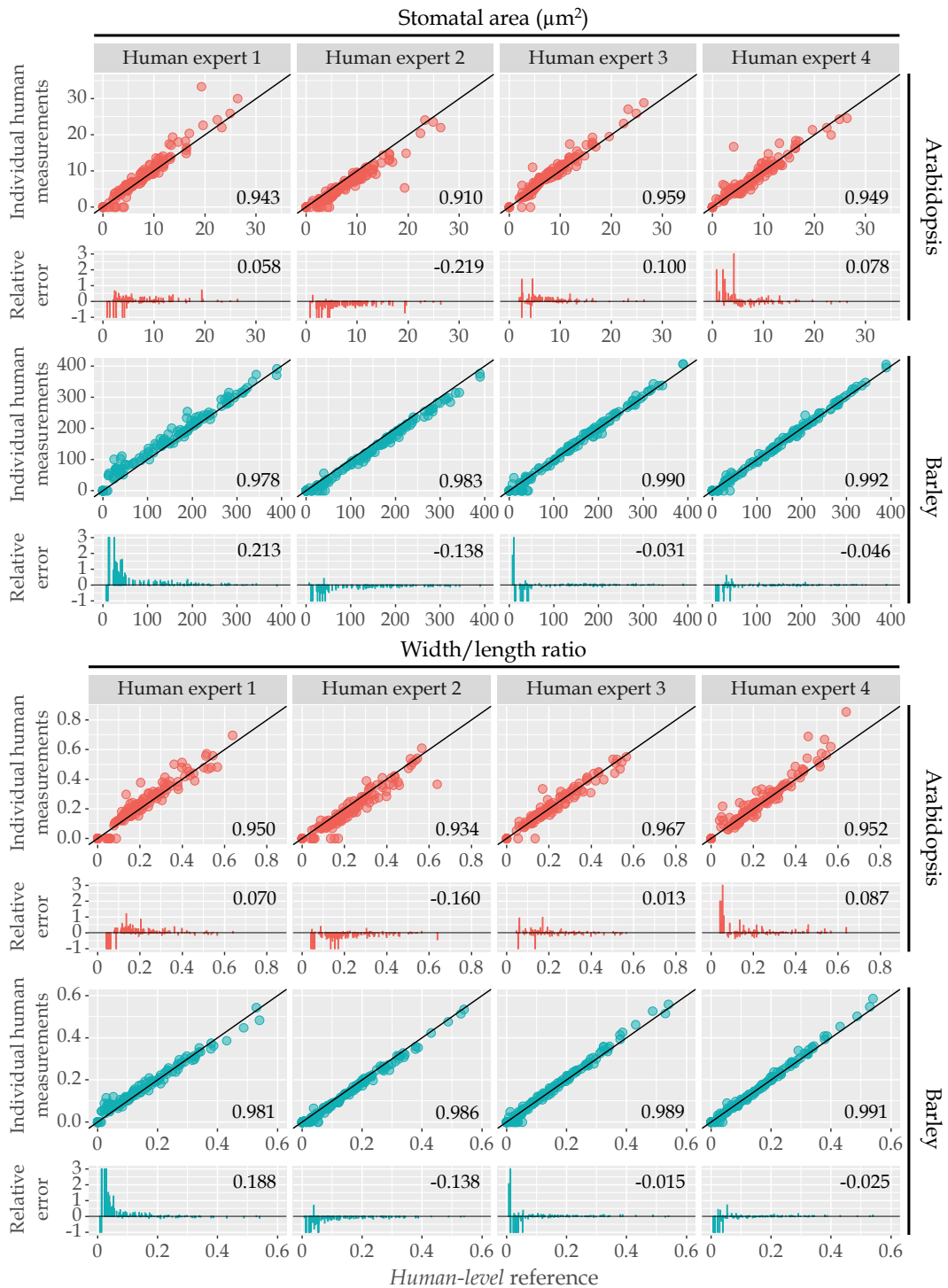


Figure E.2. Individual human measurements vs *human-level* reference set for Arabidopsis and barley with corresponding relative error of stomatal width, length, area and width/length ratio. Measurements from 4 human experts on stomata morphology are compared against the *human-level* reference (the average of human measurements) in each stoma and the concordance correlation coefficient (ranging from -1 to 1) were calculated as the determination of the accuracy performance. Stomatal width, length, area and width/length ratio from all experts were matched with human reference to calculate relative error. Mean of relative error were calculated and displayed on corresponding sub-figure. (Arabidopsis: $N > 120$, barley: $N > 160$)

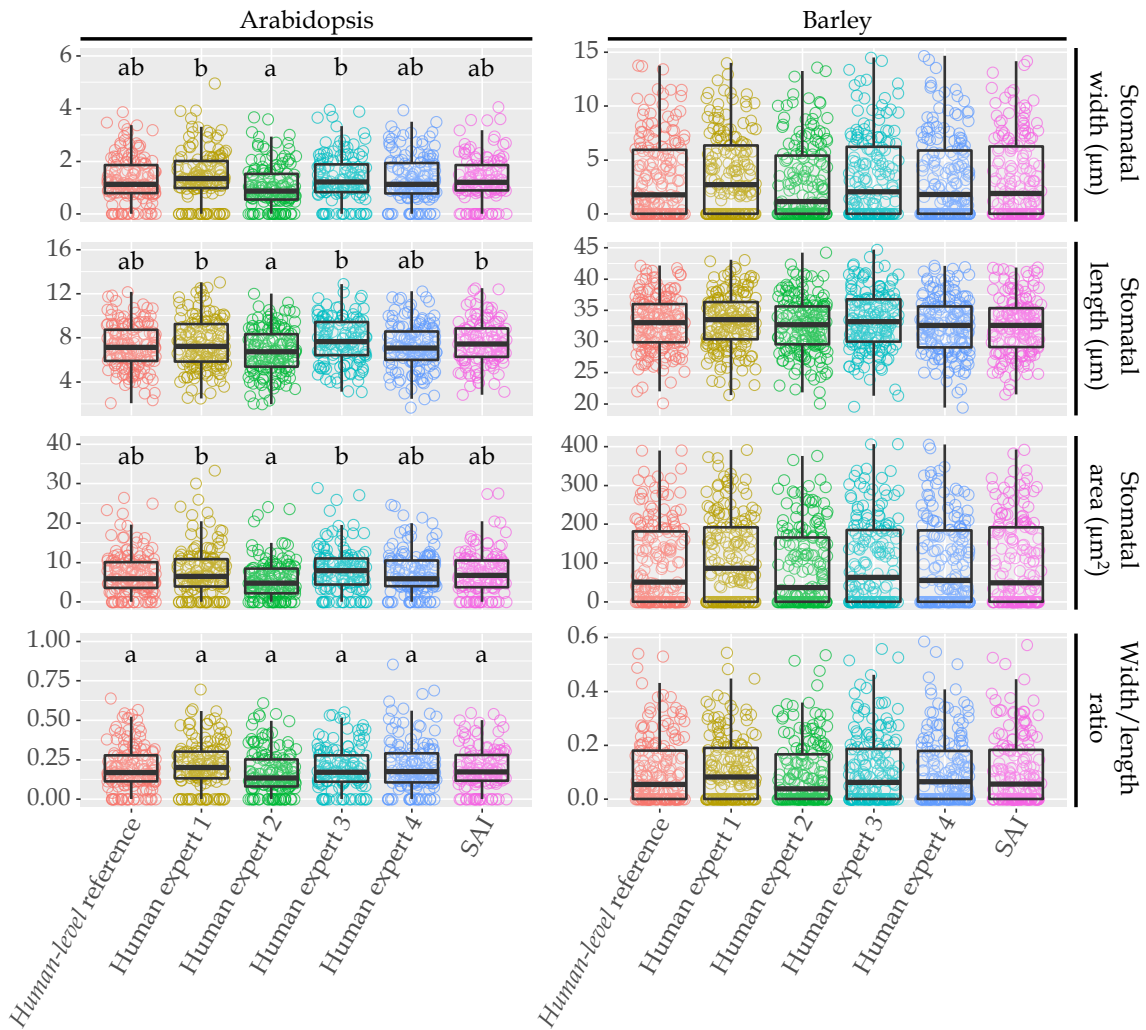


Figure E.3. Measurement comparison of stomatal width, length, area and width/length ratio in Arabidopsis and barley. Individual stomatal measurement and median visualised in box plot from *human-level* reference (the average of human measurements), 4 human experts on stomata morphology and SAI presented with one-way ANOVA with Tukey HSD Test. No differences found between source of measurements in barley, a and b represent groups without significant difference in Arabidopsis, $p \leq 0.05$ between group.

Table E.1. Summary of measured stomata in number and mean value of corresponding measuring feature.

Species	Predictor	N	Mean			
			length	width	area	width/length ratio
Arabidopsis	Human expert 1	144	7.489	1.411	7.643	0.213
	Human expert 2	149	6.770	1.028	5.547	0.169
	Human expert 3	132	7.719	1.361	8.102	0.194
	Human expert 4	139	7.225	1.322	7.200	0.209
	SAI	127	7.531	1.312	7.293	0.192
Barley	Human expert 1	175	33.232	3.657	112.002	0.112
	Human expert 2	174	32.489	2.929	88.027	0.094
	Human expert 3	172	33.203	3.416	101.689	0.109
	Human expert 4	174	32.579	3.35	100.300	0.107
	SAI	166	32.578	3.302	100.155	0.106

E.2 Supplementary data of human processed datasets

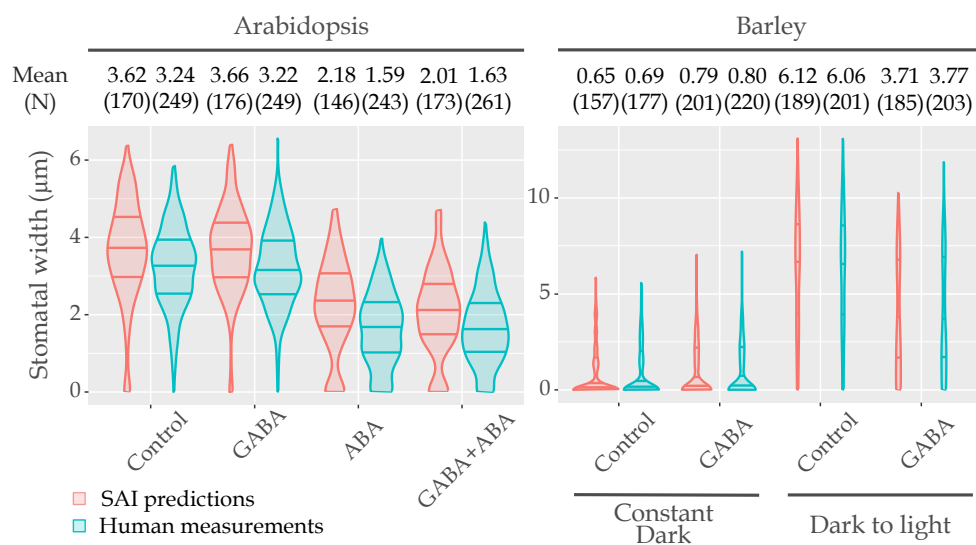


Figure E.4. Mean of stomatal width and measurement distribution illustration. The violin plot presents the distribution shape of measurements; and the interquartile range with median are marked as the line. The mean of stomatal width N were calculated in corresponding group.

E.3 Default Training Procedure

Models are trained for 90,000 iterations each. Learning rate is started at a value of 0.0006 ramping up linearly to 0.005 over the first 1,000 steps. This is then decreased by a factor of ten at 15,000 and 25,000 steps. Random cropping and horizontal flipping were employed as augmentation; adding additional variation to examples. Standard input and evaluation resolution used is 800×1333 .

E.4 Batch Size

A series of models were trained to explore the effect of input batch size on predictive power. Each model underwent the same training regime, outlined in E.3, but with a modified batch size. Evidenced by Table E.2, the number of input images during training has no impact on the learned model’s inference. Therefore, if another user wishes to train this architecture they need only have hardware capable of processing a single images at a time.

Table E.2. Model prediction scores when training with the default strategy outlined in section E.3 for various input batch sizes.

Batch Size	Bounding Box mAP%	Segmentation mAP%	Keypoints mAP %(Open, Closed)
1	82.34	60.92	71.14 (79.43, 62.86)
2	82.49	58.30	71.00 (78.55, 63.45)
4	81.30	58.59	70.59 (77.91, 63.27)
6	81.45	58.16	70.46 (78.46, 82.46)
8	80.94	59.60	71.75 (79.32, 64.19)
12	80.00	57.92	70.37 (79.12, 61.62)

E.5 Keypoint Head Complexity

Default configuration of Mask-RCNN’s keypoint detection head is tailored towards human pose estimation or identifying facial keypoints. In this case models are required to localise multiple points – either across a person or on their face. For our use case only two points need to be localised. Due to this it is argued that a reduction of complexity will not severely impact model performance on stomatal pores. Results of experiments to explore this are presented in Table E.3. Deeper and wider are said to be more complex than shallow and narrow. In Table E.3 we can see our suspicion, that keypoint head complexity can be reduced without significant impact, is supported. Bounding box and segmentation tasks are not impacted either; as should be expected. Keypoint localisation shows a slight decrease in accuracy when moving from a convolution width of 512 to 256 but only for a layer depth of 8. In all other cases differences in ability are within $\pm 1.5\%$. Motivated by these results a reduced head, with depth of 2 and width of 256, is used. This decision reduces video memory constraints for further modifications.

Table E.3. Comparison of limiting keypoint head depth and width.

Depth	Width	Bounding Box mAP%	Segmentation mAP%	Keypoints mAP% (Open, Closed)
2	256	80.17	56.38	70.01(79.42, 60.59)
	512	79.29	57.25	69.61(77.64, 61.59)
4	256	80.12	57.75	71.37(78.34, 64.41)
	512	80.19	56.73	70.53(78.53, 62.53)
8	256	79.97	56.6	70.44(78.09, 62.78)
	512	81.68	57.74	73.52(80.28, 66.77)

Note: Pooler, training and testing image resolutions are fixed at 14×14 , 320×800 and 800×1333 respectively. All models use default training strategy outlined in E.3, on the barley pore dataset.

E.6 Keypoint and Mask Head Pooler Resolution

In most cases crops containing pores generated by the region proposal network are of high resolution in comparison to poolers used by default in Mask-RCNN. A region proposal large enough to contain a cell will have dimensions of 300×200 pixels; default poolers reduce these proposals down to 14×14 for further processing. This means that prediction heads will need to make decisions about a much larger region from this considerably compressed summary. Ideally predictions would be made using a feature map with full proposal resolution but two barriers prevent this: memory consumption and uniform matrix size. To understand the benefits of increasing pooler output size a series of models were trained with different keypoint and mask head pooler resolutions, shown in Tables E.4 & E.5. A modified pooler that enables non-square dimensions is

Table E.4. Trails highlighting the impact of keypoint head pooler resolution on model performance.

Pooler Resolution	Bounding Box mAP%	Segmentation mAP%	Keypoints mAP %(Open, Closed)
14×14	80.17	56.38	70.01 (79.42, 60.59)
28×28	82.70	58.92	72.72 (81.37, 63.96)
56×56	82.41	58.78	73.73 (81.11, 66.35)
112×112	82.40	59.26	73.12 (79.68, 64.90)
14×28	82.04	57.82	72.29 (79.68, 64.90)
28×56	79.68	59.27	73.21 (81.37, 65.04)
56×112	81.07	58.84	75.33 (80.47, 70.18)

Note: All models are trained using default training procedure outlined E.3. Batch size varies across trails but has no significant impact on a model's predictive power, see Section E.4.

explored as an option in keypoint heads to better reflect closed stomatal pore crop's rectangular aspect. Evidenced by Table E.4 increasing resolution from 14×14 shows immediate benefit, however further square increase tends to only benefit prediction on closed stomatal pores. The same benefit as doubling both height and width can be achieved by using a rectangular pooler where only one dimension is increased. From example, instead of increasing from 28×28 to 56×56 , changing to 28×56 benefits a models ability to predict on closed stomatal pores more without impacting predictions made on open examples.

As masking stomatal openings is required only when a pore is open, square pooler resolutions are considered for mask heads. Table E.5 shows that an initial benefit to segmentation performance is seen in response to the pooler resolution but as higher values are used diminishing returns are observed.

Table E.5. Experiments isolating mask head pooler resolution’s effect on task performance.

Pooler Resolution	Bounding Box mAP%	Segmentation mAP%	Keypoints mAP %(Open, Closed)
14×14	79.68	59.27	73.21 (81.37, 65.04)
28×28	81.42	67.84	75.25 (81.84, 68.67)
56×56	82.22	70.03	73.71 (81.51, 65.91)

Note: All models are trained using default training procedure outlined E.3. A batch size of 2 is used and all models use a 2×256 keypoint head with pooler resolution of 26×56 .

E.7 Image Resolution

By using a smaller input resolution, the time for a model to train can be reduced. However, when a model is taught with examples at low resolution it may struggle to interpret patterns that are scaled up in a high resolution example of the same image. Ideally inference is performed at the native capture resolution of the microscopy setup. This eliminates scaling artefacts which introduce noise to samples. In Table E.6 the impact of training time resolution on inference metrics is explored. The aforementioned effect of training on small and inferring on high resolutions is observed for both pooler resolutions tested. As training resolution is increased, test time performance improves sharply and then begins to show diminishing returns. Providing a low value for the minimum crop size with an almost native maximum tends to show either no benefit or slight deficit in performance. From these trails 1200,2048 is identified as a strong candidate as a default crop size for training when inference resolution is close to capture resolution.

Table E.6. Quantifying the impact of training crop resolution on final model predictive power.

Pooler Resolution	Training Crop Size	Bounding Box mAP%	Segmentation mAP%	Keypoints mAP %(Open, Closed)
14 × 14	320, 800	54.24	25.71	39.53 (46.32, 32.74)
	800, 1200	83.41	56.54	75.44 (81.43, 69.45)
	1200, 2048	84.42	61.10	78.92 (84.66, 73.17)
	320, 2048	84.93	59.19	77.98 (85.54, 70.43)
	320, 3000	84.83	59.85	77.94 (84.55, 71.33)
28 × 56	320, 800	25.96	30.15	28.16 (10.36, 45.96)
	800, 1200	79.94	38.17	62.20 (73.55, 50.85)
	1200, 2048	83.70	58.69	77.21 (83.37, 71.17)
	320, 2048	83.84	58.40	77.60 (83.76, 71.53)
	320, 3000	84.16	60.11	76.40 (83.26, 69.54)

Note: Models with pooler resolution of 14 × 14 use keypoints heads with high complexity prediction heads, 8×512 convolutions. 28×56 used minimal complexity heads with 2×256 convolution layers. Training crop size is provided to show the minimum and maximum size of crops taken from the image that are then re-scaled to a consistent size prior to the model seeing them. All models are trained using default training procedure outlined in E.3 and evaluated at native resolution on the validation set.

E.8 Keypoint Head Complexity at Higher Resolution

Previously, it was shown that a reduction in head complexity had very little impact on final model predictive power. This conclusion is re-examined under increased training resolution. Experiments done in Appendix E.5 are repeated using 1200 – 2048 training crop sizes and evaluated at native resolution input. It is observed in Table E.7 that without significant change to mAP on open samples, closed stomata predictions can be boosted by $\approx 8\%mAP$ with increased training crop size.

Table E.7. Comparison of keypoint head depth and width with increased pooler and input resolutions.

Depth	Width	Bounding Box mAP%	Segmentation mAP%	Keypoints mAP% (Open, Closed)
2	256	85.37	70.51	73.06 (84.55, 61.57)
	512	85.15	71.4	73.9 (84.74, 63.06)
4	256	84.67	70.58	73.99 (84.48, 63.52)
	512	85.15	71.4	73.9 (84.76, 63.06)
6	256	85.47	70.47	76.18 (84.52, 67.85)
	512	-	-	-
8	256	84.94	70.15	76.44(83.68, 69.21)
	512	-	-	-

Note: All models were trained using the final strategy outlined in E.9, on the barley pore dataset. Omitted entries exceeded 32GB VRAM and therefore could not be evaluated.

E.9 Final Schema

Based on the above ablation studies the model used in comparisons to human annotation performance has a keypoint and mask pooler resolution of 56×112 and 56×56 respectively. The keypoint head's width is reduced to 256 but a depth of 8 is retained. Training random crop short edge sizes varied from 1200 to 2048 and an input batch size of two was used. Length of the learning rate warm up was increased from 1000 to 7500 to mitigate early divergence. All other learning rate, scheduling, step number and augmentation strategies remain as outlined in Appendix E.3. When training on Arabidopsis samples it was found to be beneficial to include a larger difference between the minimum and maximum crop sizes while training. These models were exposed to image crops as small as 320 and as large as their native size of 1944 pixels. The large variation present in keypoint detection on closed pores indicates any further efforts should be targeted toward this task.

E.10 Pseudocode

```
model = StomataMeasurer()
for image in images to measure do
    measurements = model(image)
    measurements = non_maximal_suppression(measurements)
    measurements = remove_detections_on_edge_of_image(measurements)
    measurements = remove_small_detections(measurements)
    for type in [width, length] do
        measurement = extract_measurement_from_keypoints(type,
measurements.keypoints)
        if is_unreasonable(measurement) then
            measurement = extract_from_polygon(type, measurements.polygons)
        end if
        measurements.type = measurement
    end for
    sample_measurements.append(measurements)
end for
sample_measurements = interquartile_range_filtering(sample_measurements)
visualisations = draw_measurements(images, sample_measurements)
save_to_file(sample_measurements, visualisations)
```